Gluconeogenesis as a System: Development of in vivo Flux Analysis of Hepatic Glucose Production in Type 2 Diabetes

By

José Orlando Alemán

B.S. Chemical Engineering
Cornell University, 2001

SUBMITTED TO THE HARVARD-MIT DIVISION OF HEALTH SCIENCES AND TECHNOLOGY IN PARTIAL FULFILLMENT OF THE REQUIREMENTS FOR THE DEGREE OF

DOCTOR OF PHILOSOPHY IN MEDICAL ENGINEERING
AT THE
MASSACHUSETTS INSTITUTE OF TECHNOLOGY
February 2008

Signature of Author_____
Harvard-MIT Division of Health Sciences and Technology
September 24, 2007

Certified by_____
Gregory Stephanopoulos, PhD
Willard Henry Dow Professor of Chemical Engineering and Biotechnology
Massachusetts Institute of Technology
Thesis Supervisor

Accepted by_____
Martha L. Gray, Ph.D.
Edward Hood Taplin Professor of Medical and Electrical Engineering
Co-Director, Harvard-MIT Division of Health Sciences and Technology

Gluconeogenesis as a System: Development of in vivo Flux Analysis of Hepatic Glucose Production in Type 2 Diabetes

by José O. Alemán

Submitted to the Division of Health Sciences and Technology on September 24, 2007 in partial fulfillment of the requirements for the degree of Doctor of Philosophy in Medical Engineering

ABSTRACT

Metabolic diseases are an increasing health concern in the developed world. Type 2 Diabetes, (T2D) affects over 100 million people worldwide and significantly contributes to chronic diseases such as atherosclerosis and kidney failure. This condition is characterized by deregulation of glucose homeostasis through the development of insulin resistance, manifested as increased glucose production in the liver. Hepatic gluconeogenesis provides *de novo* formation of glucose from three-carbon precursors such as glycerol, lactate, pyruvate and alanine. The upregulation of this pathway underlies the persistent hyperglycemia observed in diabetic patients. We have developed stable isotope tracer methods to reconstruct hepatic glucose production fluxes by infusion of $[^{13}C, {}^{2}H]$-glycerol and mass spectrometry analysis of plasma metabolites. Using this methodology we observe physiologic changes in liver cell lines and primary hepatocyte cultures in the presence of hormones insulin/glucagon and in response to gluconeogenic precursor availability. We put forth the hypothesis that in the presence of glycerol as a gluconeogenic susbtrate, glucose-6-phosphatase has an important role in modulating metabolic flux through upper gluconeogenesis. Infusion of simultaneous tracer combinations in vivo including a novel $[U-{}^{13}C,{}^{2}H_5]$-glycerol allow detailed net flux and reversibility reconstruction of upper gluconeogenesis to an unprecedented degree in a single experiment. We deployed the developed methods to probe glucose overproduction in the liver insulin receptor knockout (LIRKO) transgenic model of Type 2 Diabetes, and found unexpected similarities in the metabolic flux profile not observed by genomic, protein or metabolite measurements. Our results underscore the importance of flux measurement as a physiologic parameter akin to gene and protein expression in revealing the metabolic phenotype of cells, tissues and organisms. These methods have the potential to contribute as clinical assays to characterize excess glucose production as well as in drug development for new targets to control hepatic glucose production.

Thesis Supervisor: Gregory Stephanopoulos
Title: Willard Henry Dow Professor of Biotechnology and Chemical Engineering

Acknowledgments

Gluconeogenesis as a System: Development of in vivo Flux Analysis of Hepatic Glucose Production in Type 2 Diabetes

Table of Contents

Table of Figures

Table of Tables

List of Abbreviations

AMPK	AMP-activated Protein Kinase
AUC	Area Under the Curve
BMI	Body Mass Index
D_2O	deuterated water
DHAP	dihydroxyacetone phosphate
EMU	Elementary Metabolite Units
FBPase	fructose-1,6-bisphosphatase
G6P	glucose-6-phosphate
G6Pase	glucose-6-phosphatase
GAP	glyceraldehyde phosphate
GC-MS	Gas Chromatography-Mass Spectrometry
ggn	glucagon/glycogen
GNG	gluconeogenesis
GP	Glucose Production
GSK3	Glycogen Synthase Kinase 3
HbA1c	Hemoglobin A1c
HGP	Hepatic Glucose Production
ins	Insulin
IP	intraperitoneal (injection)
IR	Insulin Receptor
IRS	Insulin Receptor Substrate
LIRKO	Liver Insulin Receptor Knockout
MFA	Metabolic Flux Analysis
PC	Pyruvate carboxylase
PDK1	phosphoinositide-dependent protein kinase 1
PDK1	phosphatase and tensin homologue
PEPCK	phosphoenolpyruvate carboxykinase
PI3K	phosphatidylinositol-3-kinase
PIP_3	phosphatidylinositol-3,4,5-triphosphate
PKB	protein kinase B
PPARγ	Peroxisome Proliferator-Activated Receptor gamma
Pyr	pyruvate
Ra	rate of appearance of tracer
SEM	Standard Error of Measurement
STZ	streptozotocin
T2D	Type 2 Diabetes
TNFα	Tumor Necrosis Factor alpha
TZD	thiazolidenedione

CHAPTER 1: Introduction

The metabolic phenotype of a cell, tissue, organ or organism is the end product of myriad events that convert one-dimensional information as encoded in DNA and RNA, to the three dimensional level of proteins and metabolites interacting through the well-established roadmap of cellular metabolism. Both sets of information are necessary and required in cellular theory; in other words the list of parts is not sufficient to create a live system, nor is the presence of a live system without the genetic list of parts. The advent of genomics, proteomics and metabolomics enables scientists to evaluate the full set of genes, proteins and metabolites respectively, to an unprecedented degree of accuracy. Yet, the most immediate phenotype describing cellular metabolism at any given instant or flux, remains an elusive target for measurement and quantification of mammalian physiological processes in vitro and in vivo [1].

Metabolic flux will be defined throughout this thesis as the rate of interconversion between two chemical species partaking in a reaction [2]. In an analogy to transportation, flux would be the rate at which cars travel along a road as measured at a defined point. Metabolism is the union of all reactions that provide energy to living beings, and metabolic pathways are series of reactions linked by intermediaries within metabolism. The past sixty years of biochemical research have charted many of such pathways, and in our transportation analogy these can be likened to defined roads as observed in a roadmap. The overarching goal of this thesis involves reconstructing fluxes along the known metabolic pathways for glucose production in the liver. One way to achieve this goal is through the use of tracers. A *tracer* is a compound that is chemically and functionally identical to the naturally occurring compound of interest (or tracee) but is distinct in someway to allow for its unique detection [3]. Following the fate of the tracer in the body yields information regarding the

fate of the tracee compound. As a final point in our transportation analogy, this goal can be likened to reconstructing traffic flow along a major road by sending marker cars and observing their exit along the road.

Metabolism researchers have long utilized incorporation of isotopes as an important tool in elucidating metabolic routes and reconstructing the fluxes. Isotopes are variants of a chemical element with conserved number of protons (and chemical identity) but different number of neutrons causing changes in the mass of the atom in question. For example, a carbon atom has 6 protons but exists in nature with molecular masses of 12, 13 and 14 respectively. Carbon-14 is referred to as a *radioactive* isotope, meaning that the atomic nucleus is unstable and emits particles and radiation in transitioning to a *stable* carbon-13 isotope. Incorporation of radioactive isotopes from labeled substrates was one of the first techniques utilized to discover metabolic pathways such as the Krebs cycle [4] and in turn calculate metabolic flux through these pathways [5, 6]. The main advantage of this methodology involves the large signal to noise ratio obtained from radioactive decay, allowing for detection of minute amounts of incorporation into a desired pathway of interest. Its disadvantages lie in that not all reactions incorporate or release isotopes, disabling the calculation of true fluxes due to unknown specific activities of precursor pools. In the clinical realm, an important disadvantage of this technique is the established limits of exposure to radiation allowed to prevent DNA mutation and predisposition to cancer development.

Stable isotope incorporation allows for the calculation of true fluxes from the labeling patterns of metabolites of interest. With the advent of modern and powerful mass spectrometers, researchers have the ability to identify metabolites through their fragmentation signature, and in addition observe stable isotope incorporation through shifts in the mass of a given fragment. The sequentially enriched species of a defined metabolite will henceforth be called *isotopomers*. In other words, an *isotopomer* is a molecule with an isotopic tracer incorporated somewhere along the

molecule. *Positional isotopomers* are molecules with isotopic tracers incorporated at specific positions in the molecule of interest. Mass *isotopomers* refers to isotopomers that differ in their molecular weight because of incorporation of a different number of stable isotope atoms. The conjunction of mass isotopomers detected for a given compound will be called the *isotopomer spectrum*. In metabolic pathways with characterized atom transitions, mathematical models can use isotopomer spectrum incorporation data to reconstruct true metabolic fluxes given. In clinical terms, stable isotope incorporation is also desirable as radiation is no longer a concern. However, the main disadvantage of this technique involves relatively low signal to noise ratio of isotope incorporation, which in turn necessitates relatively large amounts of labeled precursor to be administered prior to obtaining a coherent signal. Through the extent of this thesis, we will utilize stable isotope incorporation into molecules of interest as the main technique from which to estimate true fluxes and evaluate their significance as markers of physiology and pathophysiology in vitro and in vivo.

The relevance of metabolic flux and control under in vivo conditions to the physiological phenotype of cells and organisms has been long realized by forward-thinking biochemists such as Reinhart Heinrich and colleagues, as early as 1973 under the guise of metabolic control theory [7-10]. I had the honor of meeting Professor Heinrich in Boston in 2003 during his sabbatical stay and collaboration with Professors Kirschner and Rapoport at Harvard Medical School. Professor Heinrich and I had a mutual acquaintance in a previous research supervisor, and we engaged in a lively conversation regarding his initial steps in biochemistry after formal training in physics, the lack of acceptance of flux analysis concepts in the greater biochemistry community and his current work utilizing these concepts to understand signaling pathways. When the conversation turned in my direction, immediately he was fascinated by my possible contribution to the field of flux analysis and metabolic engineering through the study of gluconeogenesis and hepatic glucose production. He asserted that to the best of his knowledge, there were no comprehensive studies attempting to

quantitatively reconstruct hepatic glucose production in vitro or in vivo from isotope incorporation data and that such work would be of foremost importance to himself and colleagues on his field. The vote of confidence from one of the giants in this field was simultaneously humbling and amazing, and this thesis represents the fruit of several years of work in realizing this goal described during that fortuitous meeting prior to his untimely death in 2006.

1.1 Motivation

In essence, metabolic engineering seeks to quantify metabolic fluxes and their control through analytical methodologies in order to consequently alter cellular properties for a specific goal, such as improved product yield [11]. A poignant example of this paradigm was presented by Alper and colleagues, who compared combinatorial and random strategies for metabolic space exploration in the bacterial production of lycopene. The team found that either strategy produces different sets of genes capable of optimizing lycopene production, and that the metabolic landscape shows nonlinearities and multiple local optima that difficult rational search [12]. In bacterial systems and simple eukaryotic systems such as yeast, modern molecular biology has a comprehensive arsenal of tools to modify genetic content of cellular systems and consequently allow the detailed exploration of the metabolic landscape. In mammalian systems however, limitations in genetic manipulation tools preclude genome-scale manipulation that would allow exploration of the complete metabolic landscape associated with a metabolic pathway of interest. This thesis continues the research efforts of our group to elucidate the link between genomics and physiology through metabolic flux quantification and phenotyping in mammalian systems, specifically in hepatic glucose production. Our general goal envisions flux regulation by hepatic gluconeogenesis as a single unified system. Intricate signaling networks transduce hormonal signals such as insulin and glucagon into metabolic

changes at the levels of gluconeogenesis have been described in minute detail. We show how detailed flux elucidation can yield similarly valuable information otherwise unobservable by gene, protein or metabolite measurements.

In the first part of this thesis, we developed and deployed labeling and computational tools to reconstruct hepatic metabolic fluxes and to characterize these regulatory metabolic targets of gluconeogenesis in cellular physiology, while highlighting additional relevant targets of interest for intervention at the metabolic flux level.

The second part of this thesis looks to extend the developed in vitro methodologies to the in vivo study of hepatic glucose production. The transition to in vivo setting required adapting our protocols for administration of a novel $[U-^{13}C,D_5]$-glycerol tracer to animals through the use of a subcutaneous ALZET pump, confirmation of isotopic steady state assumptions and optimization of the delivery protocols to maximize stable isotope incorporation into the glucose molecule for hepatic glucose metabolism reconstruction.

The third part of this thesis applies the methodologies derived in the previous parts to the understanding of metabolic regulation during hepatic insulin resistance in a transgenic mouse model. Through the combination of in vivo flux analysis, directed metabolite profiling and physiological testing, we explore the changes to hepatic glucose metabolism in the presence of absolute insulin resistance, and find evidence for an indirect role of insulin in decreasing gluconeogenic precursor availability to account for the moderate hyperglycemia observed in this mouse model.

Our approach integrates quantitative flux analysis data to characterize the metabolic state of liver cells and organisms and their subsequent alterations in metabolic diseases such as Type 2 Diabetes and Obesity through the following specific aims:

1.2 Thesis Objectives

Specific Aim 1: To develop stable isotope methodologies for comprehensive measurement of gluconeogenic fluxes in mammalian cell cultures for validation using parallel and combined tracer strategies. Our group has pioneered techniques for metabolic flux determination from isotopic distributions through gas chromatography-mass spectroscopy (GC-MS) in bacterial and microorganism cultures. We implemented novel methods for metabolic measurement through isotopic labeling with deuterated water (D_2O) and multiple ^{13}C and D-labeled tracers, both in parallel and simultaneously, in mouse hepatocyte cultures coupled with gas chromatography/mass spectroscopy detection that will enable detailed metabolic flux evaluation. This aim established the utility, effectiveness and robustness of the flux estimates obtained in vitro. In addition, we suggest enzymatic targets such as glucose-6-phosphatase for regulation of glucose production in the presence of glycerol as a gluconeogenic substrate.

Specific Aim 2: To apply comprehensive flux elucidation through combined multi-labeled stable isotope tracer strategies in vivo. We extended the developed methodologies for metabolic flux reconstruction of cellular glucose metabolism to hepatic glucose metabolism in vivo through infusion of simultaneous tracer combinations including a unique multi-labeled $[U-^{13}C,D_5]$-glycerol tracer in a single animal experiment. This transition involves experimental design modifications in adapting our analysis to metabolism in a live organism, and set the benchmark for exploration of physiologic validation of the developed methods. Through the use of our combined, multi-labeled tracer strategy and computational modeling of upper gluconeogenesis, we observe metabolic fluxes and reaction reversibilities in this metabolic pathway to an unprecedented degree, and observe physiological changes corresponding to feeding/fasting physiology.

Specific Aim 3: To examine perturbations in hepatic metabolic fluxes in a mouse model of experimentally-induced hepatic insulin resistance. Using the transgenic mouse model for liver insulin receptor knockout (LIRKO) as a paradigm for altered hepatic metabolism, we analyzed the hepatic glucose production flux distributions in conjunction with physiologic testing and directed metabolite profiling. We find a preserved flux distribution of upper gluconeogenesis in LIRKO, corresponding to a new steady state of glucose production despite acute effects on gluconeogenesis. These results are consistent with gluconeogenic substrate availability as a possible regulatory mechanism to preserve hepatic glucose production flux distribution intact in the LIRKO mouse when compared to its wild-type counterpart.

1.3 Approach

Our approach to reconstructing hepatic glucose metabolism from stable isotope measurements relies heavily on the use of analytical tools as mass spectrometry, coupled with data-driven computational modeling of the metabolic pathway of interest to propose and accept models for the flux distribution within statistical certainty. To this end, we applied the software application METRAN, developed by Maciek Antoniewicz [13] in recreating the flux distributions presented in this thesis. In the mammalian systems of interest to hepatic glucose production, genetic manipulation of proteins and transcription factors related is a challenging and time intensive step. At the cellular level, we induced metabolic changes in hepatocytes by modulating the availability of gluconeogenic precursors, treatment with hormones insulin and glucagon as well as therapeutic drugs such as metformin. We chose to collaborate with the Cellular and Molecular Physiology Group at the Joslin Diabetes Center directed by C. Ronald Kahn to study the liver-insulin receptor knockout model developed using Cre-LoxP technology in transgenic mice to study flux phenotype effects in hepatic glucose production of this genetic perturbation [14, 15]

1.4 Thesis Description

This thesis is divided in seven chapters representing the conceptual and experimental framework developed for in vivo flux analysis and its subsequent application to hepatic metabolism.

Chapter 1 outlines the motivation for this work, approach to the problems and describes the structure of the thesis.

Chapter 2 is a literature review of integrative physiology in current medical literature, flux analysis using mass spectrometry, metabolic diseases such as Type 2 Diabetes, the glucose production metabolic pathway and insulin signaling involved in modulating glucose production, as well as general concepts relating to the use of tracers for metabolic research.

Chapter 3 is a focused review of relevant stable isotope tracer technologies applied to hepatic glucose production that constitute the state of the art against which our developed methodologies are compared.

Chapter 4 describes our efforts to develop a methodology for integrated ^{13}C and ^{2}H flux analysis in hepatocytes, as well as the detailed use of such tools to explore flux phenotypes of primary hepatocytes in response to physiological stimuli such as insulin, glucagon, feeding and fasting.

Chapter 5 presents a novel methodology incorporating pump dosing of a novel [U-^{13}C,D$_5$] glycerol tracer for comprehensive elucidation of metabolic fluxes in vitro and in vivo.

Chapter 6 applies the in vivo flux analysis methodology developed in Chapter 5 to study metabolic alterations secondary to hepatic insulin resistance in the liver insulin receptor knockout model.

Chapter 7 summarizes the conclusions derived from this thesis work and presents recommendations for future work.

CHAPTER 2: Literature review

2.1. Integrative physiology in current medical literature and research

Physiology is the science concerned with the vital processes of organisms, especially as to how such processes **function** normally, as defined by the Stedman's Concise Medical Dictionary [16]. The word derives from the Greek roots *physis* meaning nature, and *logos* for study. The field of physiology has ancient roots that include Persian descriptions of physiological processes by Abu Bakr al Razi in the eighth century A.D. With the rediscovery of blood circulation, English anatomist William Harvey initiated the field of experimental physiology in the seventeenth century. This field contributed significantly to our understanding of bodily function and in particular changes in function that lead to disease; as such it remains central to the education of physicians in western medicine. Modern physiology is constituted by at least five sub-disciplines, including processes in the cardiovascular, brain, renal, reproductive and endocrine systems.

With the advent of molecular biology in the 1970s, attention in the medical scientific community largely shifted from physiological processes to molecular ones [17]. In recent years, there has been an attempt to recapture the importance of framing molecular questions and findings in a physiological context, giving rise to the field of integrative physiology. This renaissance in interdisciplinary physiology derives from considerable advances in the availability of genome databases, model organisms, imaging technology and genetic models [18, 19]. More recently, the development of omic technologies encompassing genomics, proteomics

and metabolomics facilitates our understanding of the intricate connections that influence the development of disease [20-22]. Many of these tools spawned significant progress in areas of biomedical science, such as cancer, heart disease, and autoimmune disease. In the area of metabolic disease, we would like to propose flux as an additional and critical readout to the integration of neurohormonal and metabolic pathways that bridge multiple organ systems including the brain, gut, skeletal muscle, cardiovascular and adipose tissues, in the development diseases of metabolism such as obesity and Type 2 Diabetes.

Much current work has deployed omic tools and analysis to the study of diabetes and obesity in leading efforts to integrate genomic, proteomic and metabolomic data into the known physiology of metabolic disease [23-27]. Given the strong heritability of the genetic traits involved in the onset of Type 2 Diabetes [28], genomic approaches are ideal for highlighting new links in our understanding of the pathophysiological changes propitiating insulin resistance and weight gain respectively. Beautiful examples of recent work integrating molecular and physiological questions include work by Mootha and colleagues in highlighting the connection between mitochondrial metabolism and insulin resistance through the action of transcriptional coactivator PGC-1α [29]. Functional gene groups were classified by nonparametric statistics to determine the significance of each gene belonging to its respective class in a tour de force of integrative genomics of disease. This study found genes that respond to transcription factor PGC-1α and are involved in oxidative phosphorylation to be coordinately downregulated in human Type 2 Diabetes. Simultaneously, PGC-1α associated with the phenotype if insulin resistance in genomic analysis in a cohort of Mexican-American patients [30].

On the other hand, the intrinsic metabolic nature of these diseases makes the analysis of metabolic flux of paramount importance in fully describing the observed pathologic phenotype.

Work by Shulman and colleagues used ^{31}P NMR highlights deficiencies in ATP metabolism that correlate with insulin resistance in human offspring of diabetic parents [31, 32]. This work contributes evidence to the theory of defective metabolic function as a corollary of muscle insulin resistance in an in vivo human context, and paves the way for measurement of fluxes as physiological markers of metabolic function in humans. In addition, Burgess and colleagues have recently shown in perfused mouse livers of serial PEPCK knockout mice through the use of ^{1}H and ^{13}C NMR how flux through PEPCK does not correlate well with gluconeogenic output, but rather correlates with TCA cycle activity in a manner reminiscent of a gatekeeper between these pathways [33]. Given the topological proximity of gluconeogenesis to mitochondrial metabolism through shared reactions, we expect the gluconeogenic gene set to show significant strength of association with the human diabetic phenotype. However, this study highlights the possibility that gluconeogenic deregulation is only one aspect of the progression to Type 2 Diabetes, and that defects in energy metabolism at the TCA cycle level may indeed run deeper and provide greater insight to the development of this growing disease. The search for integrative physiology explaining the phenotype of insulin resistance will likely require comprehensive evaluation of genome scale phenotypes to understand the pathologic sequence of events acting on the "reactome" [34]. Application of data-driven computational analysis complements genomic, proteomic and metabolomic data with metabolic fluxes establishes a framework to understand the myriad factors related to the development of Type 2 Diabetes.

2.2. Metabolic physiology and disease

2.2.1 Type 2 Diabetes and Obesity

Metabolic diseases are an increasing health concern in the developed world. It is estimated that 60% of the population of the United States is considered overweight, and 30% could be considered obese as indicated by Body Mass Index (BMI) measurements (Figure 2.1). The alarming increase in obesity prevalence has accelerated within the last 10 years, particularly in the United States of America and portions of the developed world.

Obesity Trends* Among U.S. Adults
BRFSS, 2006
(*BMI ≥30, or ~ 30 lbs. overweight for 5' 4" person)

| No Data | <10% | 10%–14% | 15%–19% | 20%–24% | 25%–29% | ≥30% |
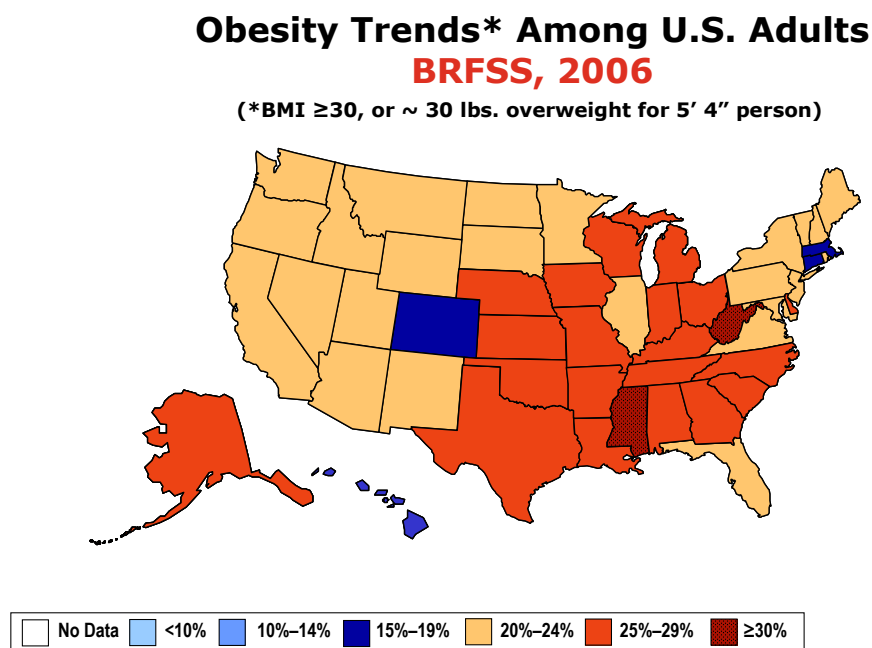
Figure 2.1: Obesity trends among U.S. Adults, 2006. Coloring scheme represents percent of the population by state with Body Mass Index (BMI) greater than or equal to 30. Figure from [35]

Regardless of the potential reasons for this increase in body mass and obesity in the population, the epidemic becomes a risk factor leading to the development of Metabolic Syndrome or Syndrome X. Metabolic syndrome is clinically diagnosed as the quartet of symptoms including abdominal (male-pattern) obesity, hyperlipidemia, hypertension and insulin resistance [36]. This quartet of symptoms is currently a topic of debate among the medical community regarding the sequence of events leading to its occurrence and its relevance in diagnostic and clinical terms. The metabolic disturbances observed in patients with this syndrome constitute the seed from which Type 2 Diabetes develops, representing the fifth leading cause of death among the US population. Indeed, the population trends of Type 2 Diabetes prevalence reflect the patterns observed in Figure 2.1 as seen in Figure 2.2.

Diabetes Trends* Among Adults in the U.S.,
(Includes Gestational Diabetes)
BRFSS 2001

| No Data ☐ | <4% ☐ | 4%-6% ☐ | 6%-8% ■ | 8%-10% ■ | >10% ☐ |
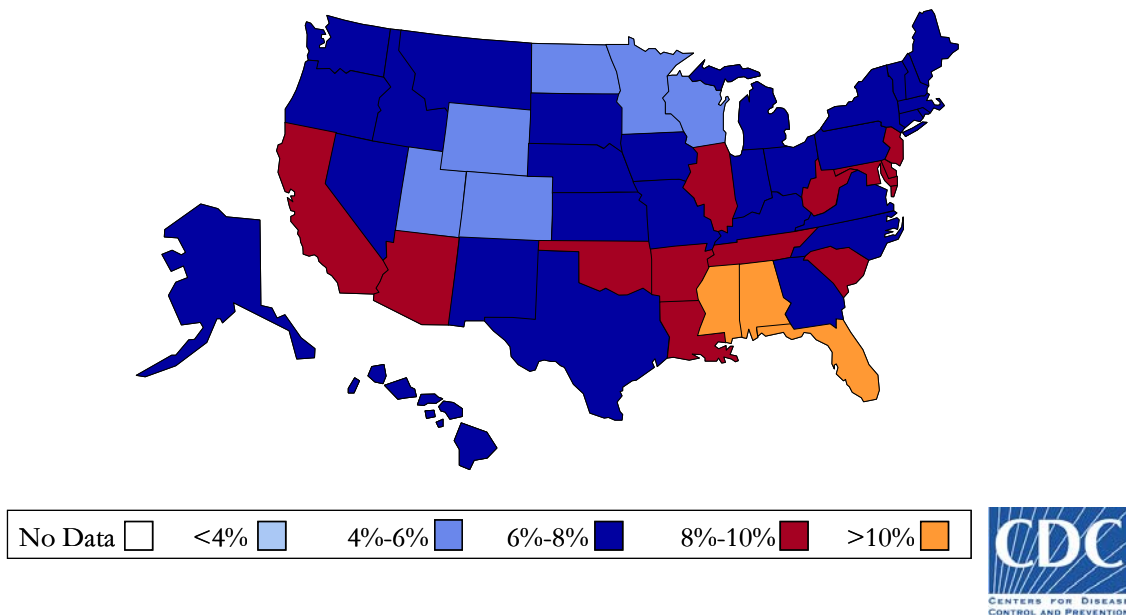
Figure 2.2: Type 2 Diabetes Trend among US Adults, 2001. Coloring represents percent of population by state meeting criteria for Type 2 Diabetes Diagnosis. Figure from [35].

Multiple epidemiological studies associate significantly increased risks of obese patients towards developing Type 2 Diabetes mellitus (T2D) [37, 38]. Diabetes mellitus is a condition characterized by elevated blood glucose levels. The word *Diabetes* comes from the Greek root meaning to siphon, referring to the frequent urination observed in patients, while the term *mellitus* stems from the Latin word for honey, referring to the sweet taste of urine in these patients [16]. The nomenclature encompasses multiple pathophysiologic processes leading to the characteristic hyperglycemia. Classification of Type 1 versus Type 2 reflects the underlying pathophysiology of the described disease. Type 1 Diabetes is an autoimmune disorder resulting in the destruction of β cells in the pancreas, the cell type responsible for production of insulin. This disease usually manifests in the first three decades of life, and is associated with symptoms such as frequent urination, weight loss, and increased plasma levels of ketone bodies and near absence of circulating insulin. Type 1 Diabetics account for 10% of the total diabetic population of nearly 18.2 million in the United States. In contrast, Type 2 Diabetics reflect insulin resistance, defined as the lack of effect to the cue of insulin in peripheral tissues such as muscle, fat and liver (Table 2.1). This disease classically manifests during middle age, but the underlying obesity epidemic is causing increases in incidence at younger ages [39]. The symptoms observed in this condition include increased frequency of urination but is otherwise asymptomatic in its early stages, and the accompanying hyperglycemia is often detected in routine clinical visits. This is the most common form of Diabetes mellitus, accounting for 90% of the diabetic population in the United States.

Diabetes is diagnosed clinically by abnormal fasting plasma glucose over 126 mg/dL , where the normal range in humans is 70-110 mg/dL [40]. Alternatively, an oral glucose tolerance test can detect Diabetes as elevated plasma glucose over 200 mg/dL two hours after administering a 75 g glucose load [41]. A longer term marker of blood glucose levels is glycated

hemoglobin A1c (HbA1c), which normally accounts for approximately 5% of circulating hemoglobin and in diabetic patients is found at 7% or greater abundance. The metabolic disturbances accompanying Type 2 Diabetes include decreased insulin-stimulated glucose uptake in fat and muscle, increased hepatic glucose production and impaired pancreatic β cell function as determined by insulin secretion [42]. Over years, hyperglycemia and hyperinsulinemia contribute to the development of the cardiovascular symptoms such as hyperlipidemia, decreased peripheral circulation, and heart disease that account for high morbidity and mortality rates among diabetic patients. As a consequence, therapy guidelines aggressively target maintaining fasting plasma glucose levels within the normal range of 70-110 mg/dL.

Therapeutic interventions for Type 2 Diabetes are aimed at reversing the deleterious effects of hyperglycemia by decreasing glucose production in the liver or increasing glucose consumption in peripheral tissues. The goal of these therapies is to maintain glucose levels as close as possible to the normal range of 70-110 mg/dL (5-7 mM) or glycated Hemoglobin A1c below 7%. Figure 2.3 summarizes currently available pharmacological therapies by their site of action. It is important to note that the single best intervention towards ameliorating insulin resistance and reversing the development of Type 2 Diabetes is improving exercise habits coupled with weight loss. Pharmacotherapy can be a significant adjuvant in this process towards normalizing glucose levels to prevent the long-term vascular complications of this disease.

Table 2.1: Features of Diabetes at Diagnosis (adapted from [39])

	Type 1 Diabetes	Type 2 Diabetes
Mechanism	Autoimmune attack on pancreatic B cells	Insulin resistance
Symptoms		
Polyuria/thirst	++	++
Weakness/Fatigue	++	++
Polyphagia with weight loss	++	-
Peripheral Neuropathy	+	++
Often asymptomatic	-	++
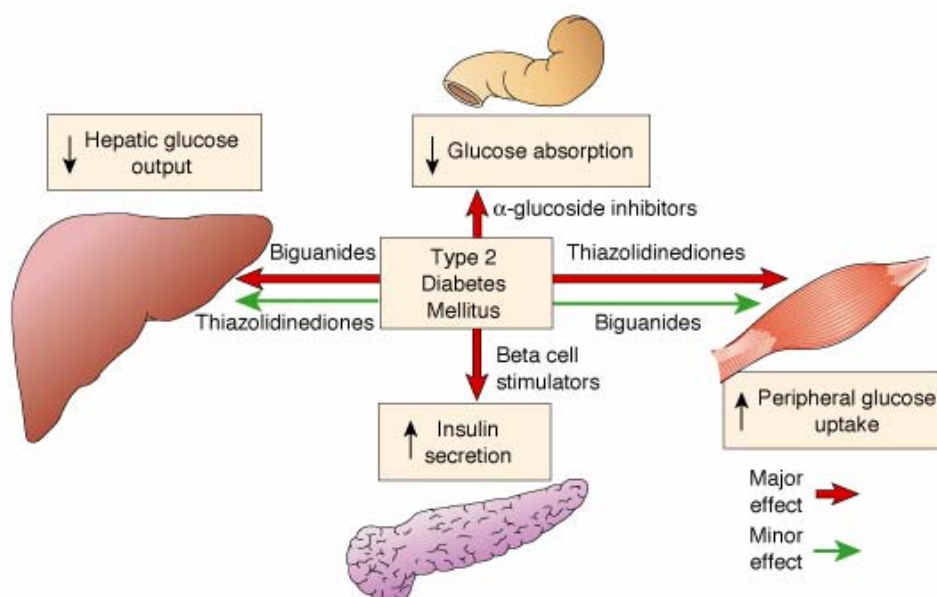
Figure 2.3: Pharmacologic treatment of Type 2 Diabetes. The treatment of Type 2 Diabetes looks to improve the consequences of hyperglycemia through multiple mechanisms. Biguanides, such as metformin, improve insulin action to lower hepatic glucose output and improve muscle glucose uptake. Beta cell stimulators such as sulfonylureas improve insulin release at the level of the pancreas through action on potassium channels. Alpha-glucosidase inhibitors decrease glucose absorption in the gut. Lastly, thiazolidenediones improve muscle glucose uptake by targeting the PPARγ nuclear receptor.

Insulin is the single therapy for Type 1 Diabetes, and is often included in management regimes of Type 2 diabetics who do not respond to other forms of pharmacotherapy. Through modification of the amino-acid sequence and additional post-translational modifications, physicians have multiple insulin preparations acting over different time scales to provide hormonal coverage in insulin deficient patients. These preparations can be described as ultra rapid acting, short acting, intermediate-acting and long acting insulin analogues. Combinations of these analogues are routinely used clinically to provide tailored plasma glucose levels.

In addition to insulin therapy, there are multiple oral agents for the treatment of hyperglycemia relevant to Type 2 Diabetes. In the gut, inhibitors of glucose absorption known as alpha-glucosidase inhibitors result in decreased plasma glucose levels but are accompanied by gastrointestinal side effects of flatulence, bloating and abdominal discomfort. A second category of drugs stimulate insulin secretion and are referred to as insulin secretagogues. Within this category, the sulfonylureas bind a receptor in the pancreatic beta cell and close the inward rectifier potassium channel $K_{ir}6.2$, depolarizing the cellular membrane and leading to calcium entry which in turn causes insulin exocytosis. However, these drugs carry an important side effect of potential hypoglycemia [39]. A third category of oral agents changes improves the effects of insulin in sensitive tissues, and are known as insulin sensitizers. Within this category, the thiazolidenedione (TZD) drug class targets nuclear receptor peroxisome proliferator-activated receptor gamma (PPARγ) to increase insulin action while developing favorable lipid profiles, decreased hepatic glucose output and increased glucose uptake from muscle and adipose tissue without causing hypoglycemia. However important side effects include liver enzyme elevation and increased risk of cardiovascular complications over long term therapy [43]. Another insulin sensitizer class is the biguanide drugs, which primarily improve insulin action in the liver leading to decreased hepatic glucose output. A member of this class,

metformin, is particularly effective in patients with insulin resistance as part of the Metabolic Syndrome. Biguanides do not cause hypoglycemia or weight gain, and carry rare side effects of lactic acidosis. Combinations of these drugs become part of the therapeutic regimes of diabetic patients. Initial therapies use lifestyle modifications and metformin as monotherapy, while patients refractory to metformin may be started on either sulfonylureas or thiazolidenediones or combinations thereof. Alpha-glucosidase inhibitors are added as third line of therapy in patients refractory to either therapy, while supplemental insulin is used when oral hypoglycemic agents fail to control blood glucose levels or when insulin levels drop as consequence of pancreatic beta cell failure.

Multiple observational studies associated increased risks of Type 2 Diabetes due to obesity [37, 38]. However, the mechanistic explanations for this sequence of events remain an issue of contention. Several hypotheses include

- signaling through beta-3 adrenergic receptors [44-46]
- pattern of fat distribution due to genetic influence [47, 48]
- deleterious effects of free fatty acids in serum [49]
- cytokine signaling through TNFα leading to a proinflammatory state [50, 51]
- dysfunctional mitochondrial metabolism [29-31]

In establishing a comprehensive metabolic flux picture of glucose production metabolism in the diabetic disease state, we will contribute to the quantitative understanding of metabolic disturbances in this chronic condition.

2.2.2 Integrative Insulin Signaling in the Liver

Understanding the phenomenon of insulin resistance requires elucidation of the sequence of events that mediate the hormone signal into action in tissues such as the liver. In Chapter 6, we study a transgenic model of hepatic insulin resistance engineered to lack the insulin receptor in its liver. The insulin receptor is a membrane tyrosine kinase which dimerizes in the presence of insulin to self-phosphorylate specific intracellular tyrosine residues [52]. This phosphorylation event triggers a protein signaling cascade that ultimately mediates the effects of insulin on multiple pathways encompassing cellular metabolism. The immediate effect of insulin receptor involves recruitment of scaffolding proteins known as the Insulin Receptor Substrates (IRS 1-4). The multiplicity of IRS proteins has recently been the subject of study in explaining the divergence of actions of insulin in different areas of metabolism. For instance, recent work in cellular and transgenic models associates IRS-1 as a regulator of glucose metabolism, whereas IRS-2 is closer to lipid and cholesterol metabolism [53]. The IRS proteins are not catalytic but rather allow interaction with other downstream effectors of insulin action, such as the phosphatidylinositol-3-kinase (PI3K).

The PI3K heterodimer consists of a regulatory and catalytic subunit, occurring in isoforms described in Figure 2.4. The regulatory subunit docks phosphorylated IRS proteins and causes the catalytic subunit to release second messenger phosphatidylinositol-3,4,5-triphosphate (PIP_3), which in turn activates further downstream signaling element phosphoinositide-dependent protein kinase 1 (PDK1). Activation of PDK1 can be downregulated by the phosphatase and tensin homologue (PTEN) protein, in turn mediating Akt/protein kinase-B (PKB) activation. Akt/PKB is a serine threonine kinase which mediates many of insulin's metabolic effects through phosphorylation of various targets including other protein kinases, transcription factors and direct enzyme targets. Most notably, Akt/PKB has

direct effects on glucose metabolism by phosphorylating glycogen synthase kinase 3 (GSK3) which in turn decreases its activity toward glycogen synthase and stimulates glycogen synthesis in the liver and muscle. Adipose and muscle glucose uptake is modulated by Akt/PKB by phosphorylating and inhibit Rab-GTPase activating protein AS160. Activation of Rab small GTPases triggers the cytoskeletal reorganization necessary for translocation of glucose transporter GLUT4, thereby increasing glucose uptake.

Suppression of hepatic gluconeogenesis by insulin is modulated in vivo through the Akt-mediated phosphorylation of transcription factor Foxo1 and its downstream inhibition of gluconeogenic enzymes PEPCK and G6Pase. [54]. Current research explains the divergent regulation of gluconeogenesis and fatty acid metabolism in the liver in response to insulin as branches of the insulin signaling pathway at the level of IRS molecules; partial IRS-1 downregulation by shRNA results in upregulation of the aforementioned gluconeogenic enzymes, while IRS-2 downregulation upregulates lipogenic enzymes SREBP-1c and fatty acid synthase [53]. The divergent functions of these signaling molecules is unified in the action of transcription factor Foxo1, which induces hepatic lipid accumulation by increased triglyceride synthesis while also inducing insulin-independent Akt expression which in turn targets G6Pase for decreased glucose production [55, 56]. The complexity of the signaling network presented can be understood in terms of critical nodes for signaling, where initial redundancy of protein component nodes leads to divergent regulation at the metabolic level. We wish to translate the complexity of this signaling network to its fundamental metabolic effects through comprehensive flux profiling, and shall use the loss of hepatic insulin receptor action as a case study for flux regulation in vivo in Chapter 6.
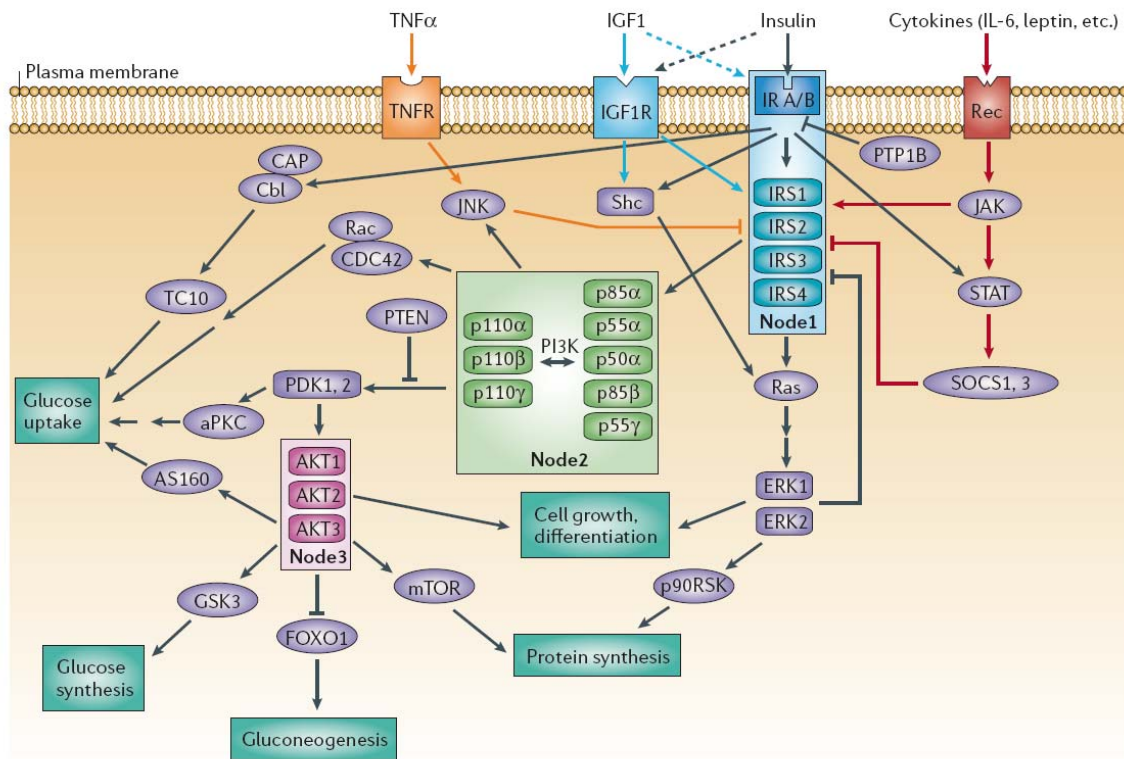
Figure 2.4: Critical nodes of insulin signaling Critical nodes form an important part of the signaling network that functions downstream of the insulin receptor (IR) (black arrows) and the insulin growth factor-1 receptor (IGF1R) (blue arrows). Signaling pathways that are activated by cytokines such as tumor necrosis factor-α (TNFα), interleukin-6 (IL-6), and leptin interfere with insulin signaling through crosstalk (orange and red arrows). Three important nodes in the insulin pathway are the IR, the IR substrates (IRS) 1–4 (light blue box), the phosphatidylinositol 3-kinase (PI3K) with its several regulatory and catalytic subunits (light green box), and the three AKT/protein kinase B (PKB) isoforms (pink box). Downstream or intermediate effectors, as well as modulators, of these critical nodes include atypical protein kinase C (aPKC), Akt substrate of 160 kDa (AS160), Cas-Br-M (murine) ecotropic retroviral transforming sequence homologue (Cbl), Cbl-associated protein (CAP), cell-division cycle 42 (CDC42), extracellular signal-regulated kinase 1 and 2 (ERK1 and ERK2), forkhead box O1 (FOXO1), glycogen synthase kinase 3 (GSK3), Janus kinase (JAK), c-Jun-N-terminal kinase (JNK), mammalian target of rapamycin (mTOR), p90 ribosomal protein S6 kinase (p90RSK), phosphoinositide-dependent kinase 1 and 2 (PDK1 and 2), phosphatase and tensin homologue (PTEN), protein tyrosine phosphatase-1B (PTP1B), Ras, Rac, Src homology-2-containing protein (Shc), suppressor of cytokine signalling (SOCS), signal transducer and activator of transcription (STAT), and Ras homologue gene family, member Q (ARHQ; also called TC10). Dashed arrows represent an activation process with less intensity. Reproduced from [54].

2.2.3 Biochemistry of glucose production: Glycogenolysis and Gluconeogenesis

Glucose metabolism is at the heart of Type 2 Diabetes, with the characteristic hyperglycemia resulting from decreased uptake in tissues that normally act as energy sinks. Glucose is consumed rapidly and selectively in a multitude of mammalian tissues (e.g., brain, medulla, red blood cells), and as such is subject to intense and specific regulation of its storage and consumption. Living organisms adapt their metabolism continuously to their nutritional environment, which may not match the immediate energetic needs of the organism at hand. There are two principal metabolic pathways that contribute to glucose production in vivo: glycogenolysis in the liver and gluconeogenesis in the liver and kidney:

Glycogenolysis

Upon ingestion of large quantities of carbohydrates, mammals suppress endogenous glucose consumption from internal stores and increased glucose uptake in skeletal muscle and the liver. This glucose in turn is formed into glycogen, a branched polymer of glucose, for eventual use during fasting. Glycogen exerts decreased osmotic pressure than the corresponding amount of glucose in plasma, and can be readily degraded. The energetic demands of the liver are primarily met by fatty acids, and its glycogen stores are reserved for release as glucose into the circulation during fasting. The contribution of glycogen to total glucose has been quantified as high as 90% and is thought to contribute up to 75% of glucose turnover during the initial stages of fasting. [42].

Several key enzymes are involved in the process of glycogen breakdown. Glycogen phosphorylase cleaves the 1,4 glycosidic bonds of in the non-reducing ends of the glycogen

chain. Debranching enzymes catalyze the removal of glucose residues at branchpoints of the glycogen polymer. Glycogen phosphorylase catalyzes the reaction which removes glucose subunits from the glycogen polymer and produces glucose-1-phosphate. Glucose-1-phosphate can then be converted to glucose-6-phosphate by the action of enzyme phosphomutase, and intersect into the glucose-6-phosphate pool prior to dephosphorylation for glucose production.

The control of glycogenolysis responds to hormonal cues due to hypoglycemia or stress. For instance, glucagon induces net glycogenolysis in a very sensitive and reproducible manner. This activation occurs in a cAMP-mediated manner causing glycogen phosphorylase activation and inhibition of glycogen synthase activity [57, 58]. Similarly, counterregulatory hormones such as epinephrine, norepinephrine, vasopressin and angiotensin positively modulate glycogenolysis [39].

Gluconeogenesis

As the transient stores of glycogen are depleted through fasting, gluconeogenesis subsequently builds glucose molecules from three-carbon intermediates from multiple metabolic sources. This unique set of reactions occurs exclusively in hepatocytes and the renal cortex. Figure 2.5 highlights the reactions that form the metabolic pathway of gluconeogenesis. Gluconeogenesis operates as the biosynthetic pathway responsible for countering glycolytic breakdown of glucose, and has often been described as the "reverse of glycolysis." Glycolysis is a highly exergonic set of reactions culminating in the production of pyruvate, ATP and NADH; several of the enzymes catalyze thermodynamically irreversible reactions. On the other hand, gluconeogenesis uses a combination of glycolytic and pathway-specific enzymes to achieve its biosynthetic end product glucose at the expense of pyruvate and ATP.

Gluconeogenic pathway enzymes are akin to their glycolytic counterparts, with exception of reaction steps that are thermodynamically unfavorable. As shown by the red arrows in Figure 2.5, pyruvate carboxylase (EC 6.4.1.1) catalyzes the synthesis of phosphoenolpyruvate from pyruvate in the first committed step of gluconeogenesis. Pyruvate carboxylase is found in liver and kidney cells, but not muscle. Phosphoenolpyruvate carboxykinase (PEPCK, EC 4.1.1.32) catalyzes the decarboxylation of cytosolic oxaloacetate into phosphoenolpyruvate, after transport from the mitochondria through the oxaloacetate-malate shuttle. As with pyruvate carboxylase, PEPCK is found in liver and kidney cells. At this point, PEP undergoes the reversible reactions of gluconeogenesis into the triose phosphate pool, condensation through aldolase and formation of fructose-1,6-bisphosphate. Fructose-1,6-bisphosphatase (EC 3.1.3.11) catalyzes the removal of the C1 phosphate and formation of fructose-6-phosphate. This enzyme is again found in the liver and kidney, and is subject to inhibition by fructose-2,6-bisphosphate and elevated levels of AMP. The last step in the metabolic pathway of gluconeogenesis is the dephosphorylation of glucose-6-phosphate through the action of glucose-6-phosphatase (EC 3.1.3.9). This enzyme is again specific to liver and kidney. These enzymes are used as markers for activity of gluconeogenesis given their unique presence in this pathway. Multiple studies support the idea that excess hepatic glucose production occurs due to dysregulation of the two key gluconeogenic enzymes, PEPCK and G6Pase [27, 59]. Insulin inhibits the expression of both of these enzymes at the transcriptional level [60] The promoters of both the PEPCK and G6Pase genes contain so called insulin responsive elements (IREs) that are essential for the effect of insulin on the regulation of those genes.

Gluconeogenesis provides roughly 25% of the glucose output necessary during the initial stages of fasting [42]. Upon depletion of glycogen stores, gluconeogenesis becomes the

principal source of glucose for the organism. The primary sources for this glucose production involve lactate from cellular respiration, alanine from protein breakdown and glycerol from triglyceride breakdown. These sources along with others will be discussed in further detail below. Mechanisms of control for gluconeogenesis have been postulated at certain bottlenecks of the reaction chain. These mechanisms include: availability of precursors and their initial conversion to the first metabolic intermediate, conversion of pyruvate to phoshoenolpyruvate (PEP) and the conversion of fructose-1,6-bisphosphate to fructose-6-phosphate [61]. The premise of these control mechanisms involve points along the metabolic pathway where alternatives for metabolite redirection exist. For instance, at the initial step conversion of the precursor to a metabolic intermediate, the metabolic alternative would involve redirecting the precursor to a different metabolic pathway. This is especially true for metabolites such as lactate and pyruvate, which can be further metabolized through the TCA cycle or redirected for amino acid biosynthesis among many pathways.
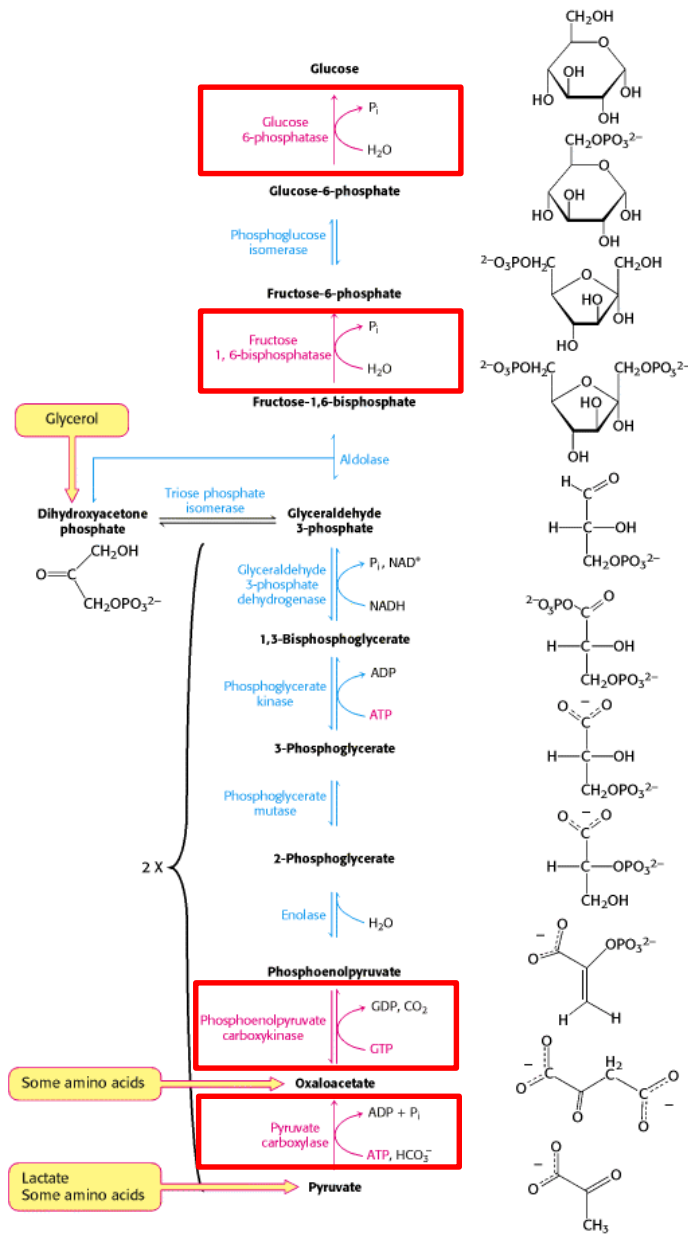
Figure 2.5: Gluconeogenesis reactions and catalyzing enzymes. Boxed reactions catalyze thermodynamically irreversible steps necessary to synthesize glucose from three-carbon precursors: Pyruvate carboxylase (PC, EC 6.4.1.1, mitochondrial), Phosphoenolpyruvate carboxykinase (PEPCK, EC 4.1.1.32, mitochondrial and cytosolic), Fructose-1,6-bisphosphatase (FBPase, EC 3.1.3.11, cytosolic), Glucose-6-phosphatase (G6Pase, EC 3.1.3.9, cytosolic). The remaining reactions are shared with glycolysis. Note, the PEPCK reaction requires the presence of the malate shuttle catalyzing transfer of mitochondrial pyruvate to cytosolic phosphoenolpyruvate. Adapted from [62].

Gluconeogenesis substrates

In designing tracer experiments to reconstruct metabolic fluxes of gluconeogenesis, we will circumscribe our reaction network to the upper portion of gluconeogenesis starting with triose phosphate isomerase. Potential tracer input points are designated in Figure 2.5 with yellow boxes, and tracer input at each point adds additional information regarding the flux distribution of metabolic steps up to that reaction. Each compound has distinct mechanisms of entry into the hepatocyte that are important considerations when deciding which compound to use as a tracer (Table 2.2), and the ultimate choice should be verified by experimental work in cellular or animal systems to confirm adequate enrichment signal.

Lactate is the principal gluconeogenic precursor under most conditions. Its circulating concentration is significant in the basal state (0.7 mM) can observe large fluctuations in the context of exercise or sepsis [42]. Much circulating lactate is the product of glycolysis from plasma glucose, and therefore its usage forms a cyclical process known as the Cori cycle. This cycle serves not only as a route to generate glucose but also as a primary mechanism to clear lactate from plasma and prevent pH disturbances. Despite the investment in energy in the Cori cycle to produce glucose from lactate, this cycle may operate to produce glucose by expending energy from fat oxidation in muscle, thereby resulting in energy transfer from adipose tissue to muscle. The resting rate of this cycle in humans has been postulated to be 15% under prolonged fasting [3]. Lactate transport in the liver occurs through the MCT family of transporters and may respond to stimuli such as starvation and acid pH, but does not limit lactate uptake under normal circumstances [63, 64].

Pyruvate is the three carbon product of glycolysis. Its circulating concentration is approximately $1/10^{th}$ that of circulating lactate (0.07 mM), and therefore usually plays a small part in contributing to gluconeogenic output. Furthermore, pyruvate can be readily absorbed

by most tissues and utilized for aerobic respiration through the TCA cycle in thermodynamically favorable reactions. These reactions limit the amount of uptake into gluconeogenesis unless concentrations are raised to superphysiological levels. Pyruvate transport is also mediated through the MCT superfamily of transporters through a proton linked mechanism, and does not limit pyruvate uptake [64]

Alanine is the major amino acid precursor for gluconeogenesis. Alanine is also the major carrier of nitrogen to the liver for deamination in the urea cycle and subsequent metabolism as glucose [62]. Thus in this way, alanine produces a metabolic cycle analogous to the Cori cycle, where there is no net glucose synthesis. In prolonged fasting and during exercise, the role of this glucose alanine cycle becomes more important as net synthesis of glucose for the consumption of the brain and red blood cells [65]. Alanine transport in the livers is mediated by specialized amino acid transporters through sodium contransport that do not limit uptake in physiological conditions [66].

Glutamine is of particular interest to metabolic researchers as a tracer given its anaplerosis into the TCA cycle, thereby contributing carbons in pathways including lipid synthesis, ketone body generation, amino acid synthesis and degradation. In terms of gluconeogenesis, glutamine contributes carbons to the formation of glucose indirectly through deamination of glucose and formation into alanine for transfer of nitrogen to the liver and subsequent deamination [67]. In the kidney, glutamine plays an important role as a gluconeogenic precursor, where it is hydrolyzed to glutamate and ammonia. The resulting glutamate is further deaminated to ammonia and alpha-oxoglutarate, which is in turn converted to glucose. When given as a gluconeogenic substrate in the liver, it suffers from similar problems as lactate and alanine due to dilution in the oxaloacetate pool from which the TCA cycle derives its carbons. Glutamine transport in liver is mediated by sodium cotransport

through specialized amino acid transporters and does not limit uptake in physiological conditions [66]. In addition, glutaminase activity as part of the urea cycle has important roles in setting glutamine metabolism throughput in the liver.

Glycerol becomes a gluconeogenic substrate under conditions of peripheral breakdown of stored triacylglycerols. Because of its late entry point into the gluconeogenic pathway at the triose phosphate isomerase reaction, glycerol is potentially an excellent gluconeogenic precursor as it enters closest to the formed product of glucose than any other three carbon substrate (Figure 2.5). Glycerol conversion to glucose is largely dictated by glycerol availability, as gluconeogenic metabolism constitutes the primary mode of glycerol clearance from plasma. Normally glycerol contributes only about 3% of the total glucose produced during fasting, but under conditions of fat mobilization such as fasting or sepsis, its contribution can increase up to 20% or more of total glucose production [68, 69]. Glycerol uptake by the liver occurs by diffusion, and glycerol kinase is thought to be the determining enzyme limiting the uptake of glycerol in vivo [70].

Fructose can be readily used to form glucose through gluconeogenesis through phosphorylation into fructose-6-phosphate by hexokinase or the preferred pathway of phosphorylation into fructose-1-phosphate by fructokinase. F1P can be broken down into DHAP and G3P and further converted into glucose through gluconeogenesis. Fructose can also be an important source of dietary carbohydrates, especially in the Western diet through sucrose consumption. However, basal use of fructose as a gluconeogenic substrate rarely occurs outside of a high fructose diet [71].

The choice of gluconeogenic substrate studied depends on the metabolic pathways of interest, the physiology studied as well as the end products to be measured. Classic biochemical work by Krebs and colleagues [70] compared the rates of gluconeogenesis perfused rat livers

for all possible gluconeogenic precursors. In this study, lactate, alanine and pyruvate were found to be the preferred substrates for gluconeogenesis with rates of 1.06, 0.66 and 1.02 μmol/min/g liver. Glycerol was found to have a production rate of 0.48 μmol/min/g and was found to preserve its glucose production rate intact whether studied in rat liver slices or perfused livers, and was hypothesized to be due to pyruvate kinase limitation given the high rates of glucose production from dihydroxyacetone and fructose. This feature of glycerol metabolism, coupled with its aggressive uptake by liver and its significance to link triglyceride breakdown to glucose metabolism were among the reasons considered in selecting it as tracer for development of our flux analysis methodologies described in this thesis.

Table 2.2: Gluconeogenic substrates and cellular entry mechanisms

Substrate	Source	Entry Mechanism	Reference
Lactate	All Tissues, Anaerobic Respiration;	Diffusion, Active Transport	[63] [64, 72]
Pyruvate	All tissues, Glycolysis	Active Transport	[64]
Alanine	Muscle, Protein Catalysis	Active Transport	[67]
Glycerol	Adipose Tissue; Triglyceride Breakdown	Diffusion, Glycerol Kinase	[73]
Glutamine	Muscle; Protein Catalysis	Active Transport	[67, 74]
Fructose	Food Intake	Active Transport, GLUT Transporters	[71, 75]

Integrated body glucose metabolism

At the endocrine level, the mobilization and storage of energy fuel for metabolism is controlled by antagonistic action of hormones glucagon and insulin, and, subsequently, the insulin/glucagon molar ratio. As shown schematically in Figure 2.6, insulin stimulates efficient storage of excess nutrients in peripheral tissues as muscle glycogen and adipose lipids upon increased intake, while suppressing mobilization of stored fuels in liver of fat. Specifically in the liver, insulin triggers a signaling cascade that stimulates glucose oxidation and storage, inhibits glucose production and stimulates fat synthesis and storage. Conversely, glucagon promotes mobilization of stored fuels through the actions of gluconeogenesis and glycogenolysis, and in turn increases glucose output from the liver. Classic biochemistry admonishes this level of control to allosteric effectors involved in modifying 'rate-limiting' enzymes of these metabolic pathways. However, the theory of metabolic control analysis would counter that regulation of metabolic flux is shared by all enzymes involved in the pathway, and that flux itself may not previous work has suggested recently how a bolus of fructose-2,6-bisphosphate had no apparent effect on overall gluconeogenic rate as measured through a combination of stable isotope tracers [76]. We propose that such contradictions can be addressed by detailed measurement and modeling of gluconeogenic flux stimulation/inhibition as part of the fasted response, in the presence of multiple gluconeogenic sources and through the action of energy-modulating drugs (metformin) or hormones such as insulin and glucagon.

As described in section 2.2, in Type 2 Diabetes insulin sensitive tissues develop resistance to hormone action, showing decreased uptake of glucose in sink tissues while increasing hepatic glucose production. Hepatic glucose output regulation remains a particularly difficult problem to understand at a systemic level. Classic work in physiology clarified the immediate

responses of the liver to increased nutrient consumption through the antagonistic action of pancreatic hormones glucagon and insulin [42]. However, the specific genetic changes triggering downstream metabolic effects and their coordinated action at the level of metabolic flux are poorly understood. This interconnection among different braches of metabolism underscores the importance of developing methods to understand cellular and organism metabolism as a unified process.

Gluconeogenesis has a key role in responding to prolonged fasting upon the depletion of glycogen reserves. The similarity of this pathway with glycolysis drew modeling interest, albeit limited. Early modeling efforts of glucose metabolism focused on the regulating role of glucokinase as the gatekeeper for metabolism in the pancreatic β cell through a minimal differential equation model [77]. These findings reflect the prevailing perspective of insulin sensing in the pancreas; where glucose metabolism greatly affects glucokinase activity, followed by hexokinase and the remaining pathway enzymes. In this work, flux control coefficient calculations quantitatively demonstrate glucokinase activity as the most sensitive parameter to the presence of glucose when compared to the activities of hexokinase and glucose transport. Through careful experimental work, Rossetti and colleagues have beautifully dissected the role of individual enzymes in a model system of liver metabolism in conscious animals through the use of the euglycemic-hyperinsulinemic clamp technique [26, 27, 78]. However, the conditions under which clamp tests are performed place considerable stress on the animals tested, and radioactive tracer use limits the flux information obtained in a given experiment. Establishing comprehensive stable isotope flux analysis tools for detailed flux elucidation of gluconeogenesis as a system will help clarify the role of the pathway constituent enzymes in regulating glucose output while elucidating potential targets for treatment of increased hepatic glucose output.
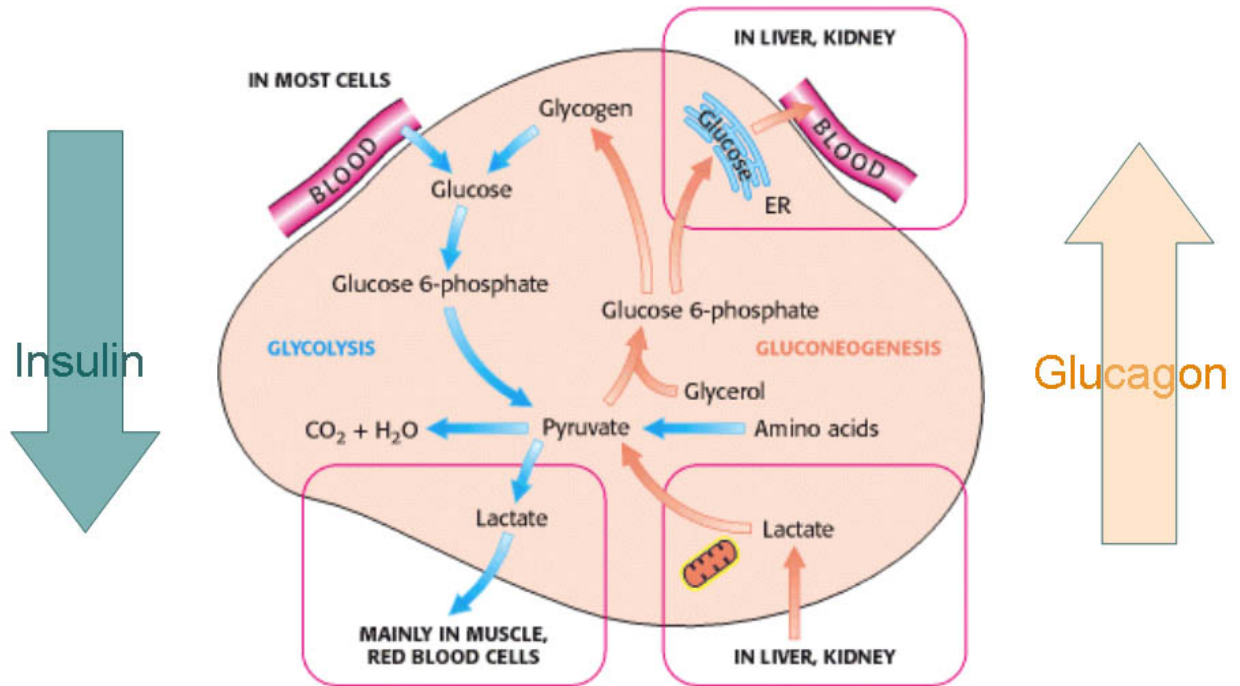
Figure 2.6: Cooperation between glycogenolysis, glycolysis and gluconeogenesis through hormonal regulation by the insulin/glucagon system. The antagonistic actions of these signals in tissue-specific manners contribute to blood glucose homeostasis. Adapted from [62].

2.3 Metabolic flux analysis using mass spectrometry

2.3.1 Metabolic Flux Analysis in Metabolic Engineering

The field of metabolic engineering has come to the limelight in reformulating concepts of control in metabolic pathways [1]. While biochemistry still praises the idea of the rate-limiting step for its conceptual importance, metabolic flux analysis has shown control of metabolite fluxes through a given pathway is shared among its constituent enzymes [9]. Several concepts and definitions are in order prior to discussing flux analysis. We defined flux in Chapter 1 as the rate of interconversion between metabolites participation in a metabolic route or pathway. A metabolite will be defined as an intermediary of a biochemical reaction.

Current methods for understanding metabolic networks rely on the framework established in metabolic flux analysis. This set of techniques has become an important method to determine the metabolic state of a cell and, consequently, the effect of genetic alterations in the metabolic phenotype in microbial systems. Metabolic engineers looks to measure quantitatively the fluxes in a defined network of interest, in order to alter the properties of the cell for a goal of interest. Cells are genetically engineered routinely to over express a particular product by upregulation or elimination of specific enzymatic reactions using molecular biology tools [1]. Often times however, single protein mutants fail to produce more desired product when compared to wild type, due in part to genetic and metabolic network interactions. Therefore, increased yield requires simultaneous modification the metabolic pathway of interest at multiple steps [10]. For instance, Alper et al. were able to engineer tolerance of *S. cerevisiae* to glucose and ethanol in a matter of weeks, by targeting epigenetic regulation of gene expression through error-prone PCR of the TATA-binding protein [79]. The realization of shared control of flux through a pathway can be used in the context of medicine to understand

the effects of a particular genetic modification or polymorphism in the metabolic phenotype of a cell or organism.

Formally, the stoichiometric conversions from substrate to product in a metabolic pathway can be expressed as a system of first order differential equations through the law of conservation of mass. As an example consider the reaction network below in Figure 2.7. The initial reaction equations are familiar (Figure 2.7A), with reversibility by the direction of the arrows. For the presented network, only reaction 3 is reversible, and we present the forward and backward reaction rates as v_{3f} and v_{3b} respectively. The atom transitions for these reactions describe the fate of individual atoms of each molecule in the reaction as shown in Figure 2.7B. For example, in reaction 2 the first atom in molecule A (represented as lowercase a) is converted to the first atom in molecule C. By the same token, the second atom in molecule A (represented by lowercase b) becomes the first atom in molecule D. The information regarding atom transitions is critical to mapping the fate of individual atoms in biochemical systems, and was collected in this thesis from textbooks as well as published literature [80-82]. From the reaction descriptions presented, we can reconstruct a metabolic network map to facilitate balances around individual metabolites. Network representations such as Figure 2.7C are particularly useful in establishing boundaries of the metabolic network studied for further characterization and for deriving species conservation equations. Lastly, the stoichiometric constraints of this model can be represented in through a matrix formalism whereby the rows of the matrix represent the metabolites involved in each reaction, and the columns represent the reactions that constitute the system as presented in figure 2.7D. This representation is commonly known as the *stoichiometric matrix* of a metabolic network, and it provides rudimentary operating conditions for a determined metabolic system laid by the law of mass conservation. Such representation does not take into account any form of kinetic behavior or

regulation, but it has found use in literature as a useful way of limiting operating conditions based on optimization of growth-based objective functions [83].

(a) Reaction Equations

$$v_1: A \rightarrow B$$

$$v_2: A+B \rightarrow C+D$$

$$v_3: B \leftrightarrow D$$

(b) Atom Transitions

$$v_1: ab \rightarrow ab$$

$$v_2: ab+AB \rightarrow aA+bB$$

$$v_3: ab \leftrightarrow ab$$
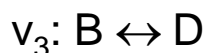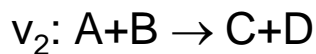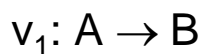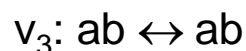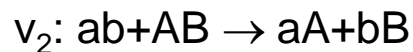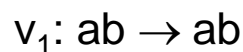
(c) Metabolic Network
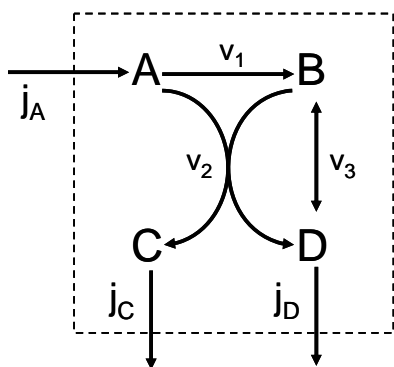
(d) Stoichiometric Matrix

$$\begin{bmatrix} -1 & -1 & 0 \\ 1 & -1 & -1 \\ 0 & 1 & 0 \\ 0 & 1 & 1 \end{bmatrix} \cdot \begin{bmatrix} v_1 \\ v_2 \\ v_3 \end{bmatrix} = \begin{bmatrix} -j_A \\ 0 \\ j_C \\ j_D \end{bmatrix}$$

Figure 2.7: Alternative representations of metabolic reaction networks. (a) Reaction Equations in simplest form. (b) Atom transitions for chemical reactions in panel. Reaction v_2 transitions atoms whereby the skeleton of the molecules reacting changes. (c) Reaction network, incorporating individual reaction velocities (v_i) and extrinsic fluxes in and out of the system represented by the dotted line (j_i). (d) Stoichiometric matrix formulation, solved by applying species conservation equations around each metabolite in the system.

The integration of each reaction into a map of the reaction network (Figure 2.7C) becomes a daunting task as the size of the network increases. Matrix notation can be especially useful in summarizing the relationships among the metabolites by conservation for each species. In matrix notation these can be represented as

$$\frac{dx}{dt} = S \cdot v \tag{2.1}$$

where S is a $m \times n$ stoichiometric matrix with m rows representing metabolites and n columns representing reactions or velocities (in the pathway), while x and v are vectors of concentrations and velocities, respectively. In situations at *metabolic steady state*, the velocities of the reaction system must reach non-trivial values that satisfy the homogenous linear system:

$$S \cdot v = 0 \tag{2.2}$$

This assumption allows the calculation of the velocity vector as a set of linear equations and solution of the reaction velocity distribution through the metabolic network. Flux is the rate at which substrate is consumed or produced in a given reaction or pathway. Thus, each reaction velocity is known as a flux, and we can calculate the overall flux of substrate through a particular pathway as a linear combination of the individual reactions that make up the network.

We will introduce stable isotope label into cellular systems in order to track the fate of individual atoms in a molecule and use this information to calculate metabolic fluxes. The simplest case under which to introduce isotopic label would involve a system at metabolic steady state, such as a chemostat bacterial culture [84]. The upper left panel of Figure 2.8 presents a curve for the concentration of metabolite in the y axis with respect to time in the x axis, where metabolite D is represented schematically by the solid green line. Introduction of label causes initial dispersion of tracer in a time scale proportional to the pool size of

metabolite D, represented by the dashed red line. Over time, the enrichment of metabolite D will not change reaching *isotopic steady state*, represented by the green shaded box. At isotopic steady state, enrichment of metabolites is not changing with respect to time, and equations for enrichment must reach non-trivial values allowing for a linear solution to the parallel homogeneous linear system. Our flux estimations assume metabolic and isotopic steady state as prerequisites to obtain meaningful flux distributions and statistical confidence intervals.

However, mammalian metabolic systems rarely meet fully the conditions for metabolic steady state [85]. Compartmentation within cells, tissue heterogeneity and rapidly changing metabolic objectives prevent intermediary metabolite concentrations from remaining constant in most conditions [86]. In order to analyze the metabolic flux distributions in such systems of importance to mammalian physiology, we must assume that metabolism is changing slowly with respect to the timescale at which we introduce isotopic label, as described by the green box in the lower left panel in Figure 2.8. Under these conditions, we can perform pseudostationary flux analysis to reconstruct metabolic fluxes. For most analysis performed in hepatoma cell lines, primary hepatocytes and in mice throughout this thesis, this condition will be the relevant paradigm for flux reconstruction.

Recent work in our group is looking to extend the work presented in this thesis to conditions where the isotopic steady state assumption may not be valid, as shown in the upper right panel of Figure 2.8. Nonstationary flux analysis utilizes transient data from stable isotope enrichment in multiple metabolites along a pathway to reconstruct the flux distribution as a function of time, and additionally provides meaningful estimates of pool sizes of the metabolites studied [87]. Lastly, metabolic systems where neither metabolic nor isotopic steady state assumptions hold require the use of dynamic modeling to recover kinetic parameter to model functional forms of concentrations [88-90]. The most successful example of dynamic

modeling in Type 2 Diabetes is the minimal model of Bergman, which enables the calculation

of insulin sensitivity parameters from a two compartment model of glucose and insulin

concentrations [91].
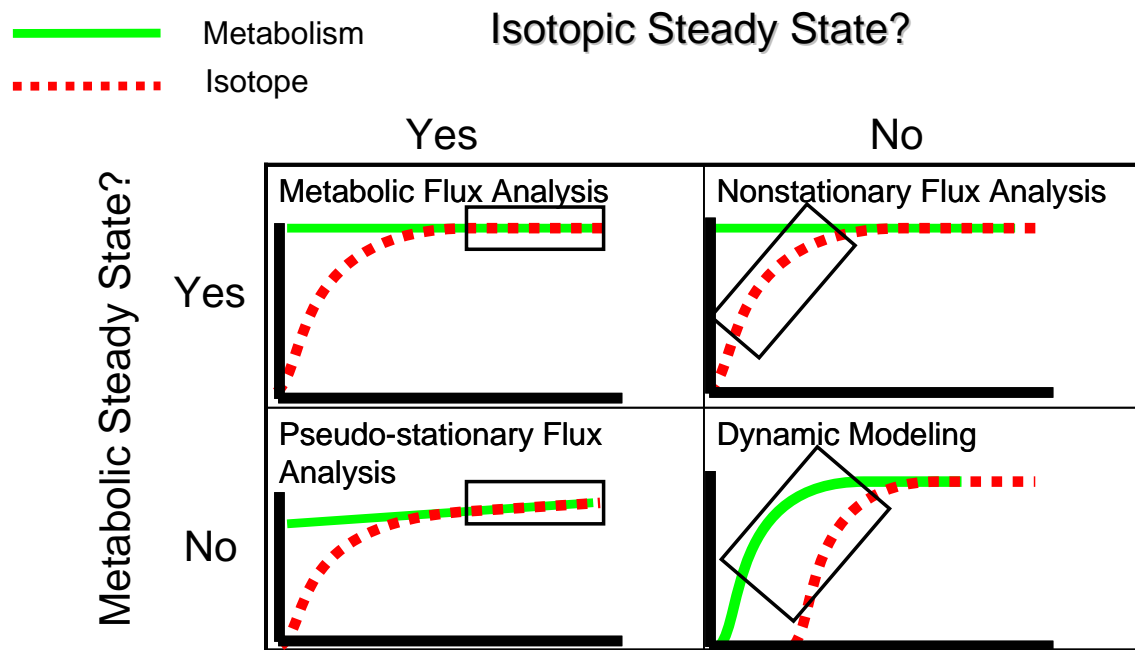
Figure 2.8: Schematic for metabolic and isotopic steady state assumptions. Under metabolic and isotopic steady state, metabolic flux analysis can be performed readily. In mammalian systems, metabolic steady state is rarely achieved and thus the relevant conditions involve pseudo-stationary flux analysis, with rapid isotopic labeling relative to metabolic changes. Recent work in our group allows the analysis of systems at metabolic steady state where isotopic labeling changes in a framework known as nonstationary flux analysis. The realm where metabolism and isotopic labeling change over similar time scales corresponds to dynamic modeling.

2.3.2 Introduction to Mass Spectrometry

In mammalian systems, the measurement of individual metabolite concentrations and fluxes in a given metabolic pathway remains a tricky endeavor, due to multiplicity of pools present in a given cell or tissue, heterogeneity of cellular phenotypes and rapidly changing metabolism. Comprehensive metabolic flux measurements rely heavily on isotope tracing methods, initially involving radioisotopes and subsequently stable isotopes. Each technique has advantages and disadvantages to be considered in the selection of one over the other for observation of labeling patterns. Radioisotope labeling experiments were among the first assays used in biochemistry for determination of spatial location of metabolic compounds in pathways such as the Calvin Cycle and the TCA cycle [4, 92]. These methods rely on intensity of particle counts for detection, and as such cannot distinguish radioisotope enrichment due to multiple labeled atoms in individual molecules or multiple labeled molecules. The ease of radioactivity measurement facilitates experiments in which short time courses (ms-min), small compound titers and spatial location of compounds are key. Recent work in our group has used radioactive tracer compounds to resolve metabolic flux distributions in microbial systems [84, 93], or as radioactive flux indicators on mammalian cell lines [94].

Stable isotope experiments, on the other hand, allow for specific determination of atom enrichment in a given molecule of interest. These labeling experiments require detection with Gas Chromatography-Mass Spectrometry (GC-MS) or Nuclear Magnetic Resonance (NMR) [95]. Given the added cost, difficulty in operation and extensive sample preparation required for the latter, our group focuses work on the former technique. Tandem GC-MS separates complex chemical samples based on affinity to a solid column and ultimately mass to charge ratio, as seen in Figure 2.9. A sample of interest is injected into the gas chromatography portion of the analytical instrument, in either gas or liquid form and is

evaporated into a gas. Many of the compounds studied in this thesis (glucose, organic acids, lipids) are not volatile in their natural form and require special chemical treatments called *derivatizations* to increase the volatility of the compound of interest for GC-MS analysis. Typical derivatizations groups include methyl esters ($R-O-CH_3$), trimethylsylil (TMS, $R-Si-(CH_3)_3$)) and *tert*-butyl dimethylsylil (TBDMS, $R-Si-(CH_2)_2-(C-(CH_3)_3)$. This volatile sample resolves into its components by affinity to a stationary phase within the chromatography column as it flows along a stream of inert mobile phase helium carrier gas. Upon exiting the gas-chromatography column, components of the sample pass to the ionization chamber in the mass spectrometer where high voltages break molecular bonds and form ions with varying masses and unit charge. Fragment ions are accelerated towards the detector of the mass spectrometer, and the distance traveled by these ions is proportional to their mass. The collection of all molecular fragments at a given retention (exit) time is known as the mass spectrum. Therefore, for every retention time where compounds exit the gas chromatography column, as seen in the middle panel of Figure 2.8, we obtain a mass spectrum for the fragment ions detected as seen in the lower panel of the same figure. The utility of mass spectrum lies in its uniqueness and reproducibility to identify a pure compound. The mass spectrum is therefore a collection of ions that can act as a fingerprint of molecules to allow for robust and simple identification within a complex mixture.

The availability of powerful mass spectrometers in research labs has facilitated the use of simultaneous detection of all small molecule metabolites present in the cell, known as the metabolome [96]. Current metabolomic analysis uses tandem liquid chromatography-mass spectrometry (LC-MS) or capillary electrophoresis-mass spectrometry (CE-MS) to analyze metabolites at high mass resolution without the need for chemical volatilization required for GC-MS [97]. Alternative metabolomic approaches using NMR exist for the study of silent

metabolic phenotypes in yeast [96]. The metabolome is a particularly interesting phenotype as it encompasses the genetic and protein expression levels to produce an immediate picture of metabolism. However, researchers have been limited in applying the use of such analysis due to compartmentation effects in cells, wide dynamic range of concentrations of metabolites and lability of the different compounds studied. Recent examples of NMR metabolomic approaches held promise as detectors of cardiovascular disease [21] but were later discredited as confounding [98]. These limitations set the stage for directed analysis of metabolic pathways through metabolic flux analysis from isotopomer data.
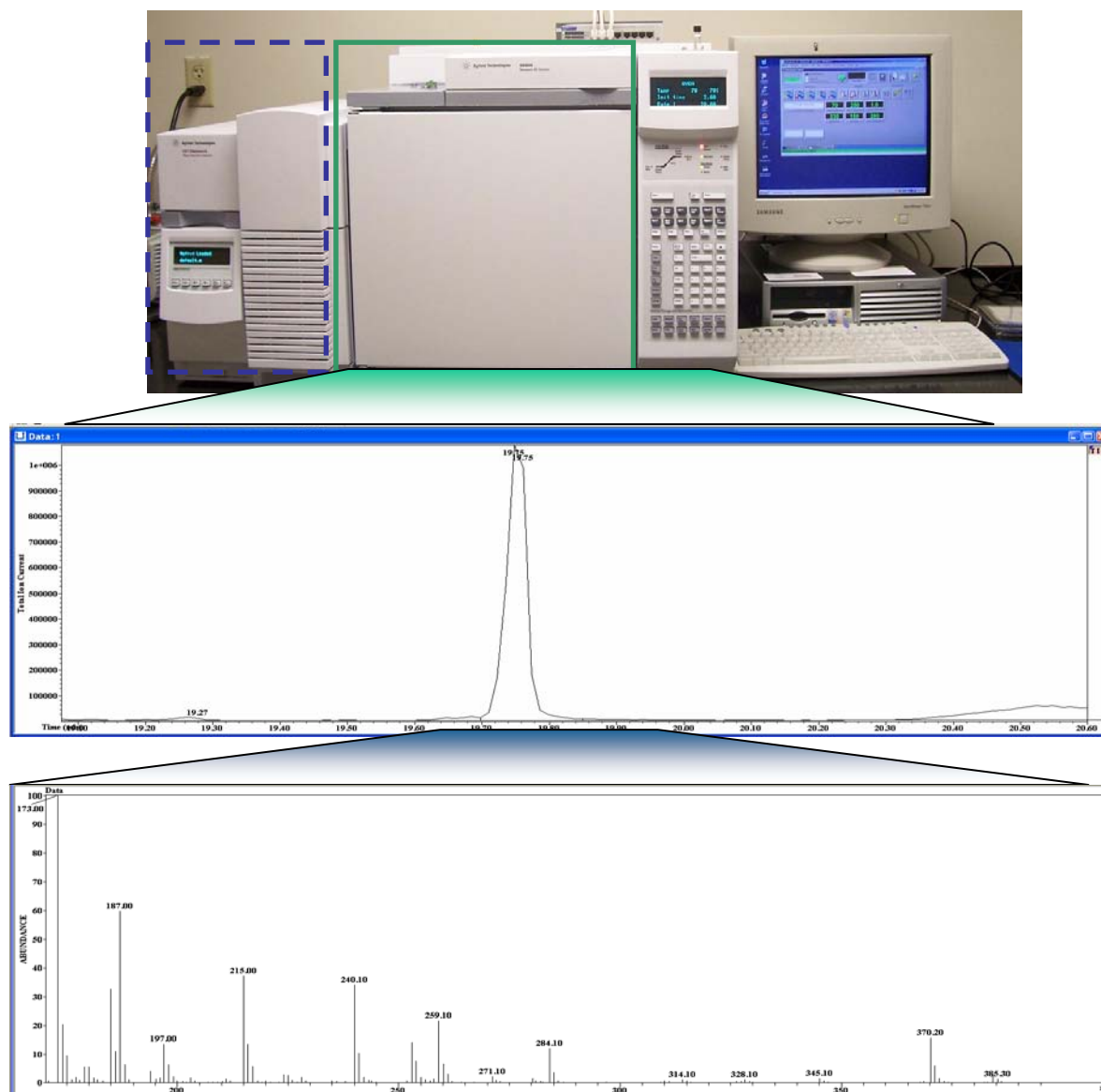
Figure 2.9: Introduction to Mass Spectrometry. A complex volatile mixture is injected into a tandem gas chromatography-mass spectrometry (GC-MS) instrument, shown in the solid box. Here, the complex mixture is separated by affinity to the solid phase in the chromatography column, and the outgoing peaks represent individual components shown in the middle panel chromatogram. The compound of interest, such as glucose, is transferred to the mass spectrometer (in the dashed box) where ionization at high voltages results in a characteristic pattern of fragments when plotted as abundance versus mass to charge ratio (m/z). This pattern is known as the mass spectrum and can be used to detect and identify molecules through comparison with reference libraries. Isotope incorporation will manifest as a rightward shift in the mass spectrum, and will be used through this thesis to reconstruct metabolic fluxes as described in Chapter 3.

2.3.3 Isotopomer and Elementary Metabolite Unit Analysis for Flux Reconstruction

Mass spectrometric methods allow researchers to simultaneously assess precisely the presence of metabolite intermediates in a pathway of interest such as gluconeogenesis. Using measurements of tracer label as proxies for atom or species concentration, we aim to express the rates at which a metabolic pathway of interest, such as gluconeogenesis, is consuming or producing a particular metabolite. Alternatively, we aim to determine the rate at which each step in gluconeogenesis occurs in wild type and pathophysiological conditions related to diabetes and obesity. This quantitative information will facilitate development of metrics that express the concrete metabolic state of cells and allow for optimum incorporation of epigenetic data from microarray studies in the gluconeogenesis pathway. Metabolic profiling studies based on MFA have been used to study hypermetabolic liver function in burn patients [99].

Metabolic flux analysis is the conceptual framework underlying the presented thesis work. As observed in Figure 2.10, we can detect labeled species of a specific 3 atom molecule through the use of mass spectrometry represented by the dark circles comprising the skeleton of each molecule. We define an *isotopomer* to be a molecule with the same chemical structure of the compound of interest, but different molecular mass due to incorporation of heavy isotopes. For the schematic presented in this figure, isotopomers correspond to each compartment separated by a dotted line, accounting for molecule incorporation 0, 1, 2 or 3 heavy atoms. If M is the molecular weight of the metabolite of interest analyzed through mass spectrometry, sequential increases in mass due to incorporation of labeled atoms will have mass M+1, M+2 and M+3. We will use the shorthand M0 to denote the original unlabeled

isotopomer M+0, and M1, M2, M3 to denote the isotopomers of the molecule in Figure 2.8. A more familiar concrete example would involve the water molecule with chemical structure H_2O. Isotopomers can occur from enrichment in different atoms in a molecule, for instance water (H_2O) has two isotopomers due to deuterium incorporation, DOH and D_2O, but only one isotopomer due to oxygen incorporation, $H_2^{18}O$. The sequential increase in molecular mass (M+0, M+1, M+2, etc) corresponds to additional labeled atoms being incorporated and is referred to as the Isotopomer Spectrum. Our group has pioneered techniques for the interpretation of isotopomer spectrum data into mathematical models for reconstruction of metabolic flux [100-102]. Growing interest in this field is evidenced by multiple groups that have implemented strategies to reconstruct metabolic fluxes from isotopomer spectra [103, 104]. Computational strategies such as isotopomer and cumomer analysis are hampered by dramatic increases in computational power necessary to track the myriad species generated by introduction of label into even simple metabolic systems. Through this thesis work, we will use the elementary unit theory for describing stable isotope incorporation for calculation of metabolic fluxes, as encoded in MATLAB software package METRAN [13].
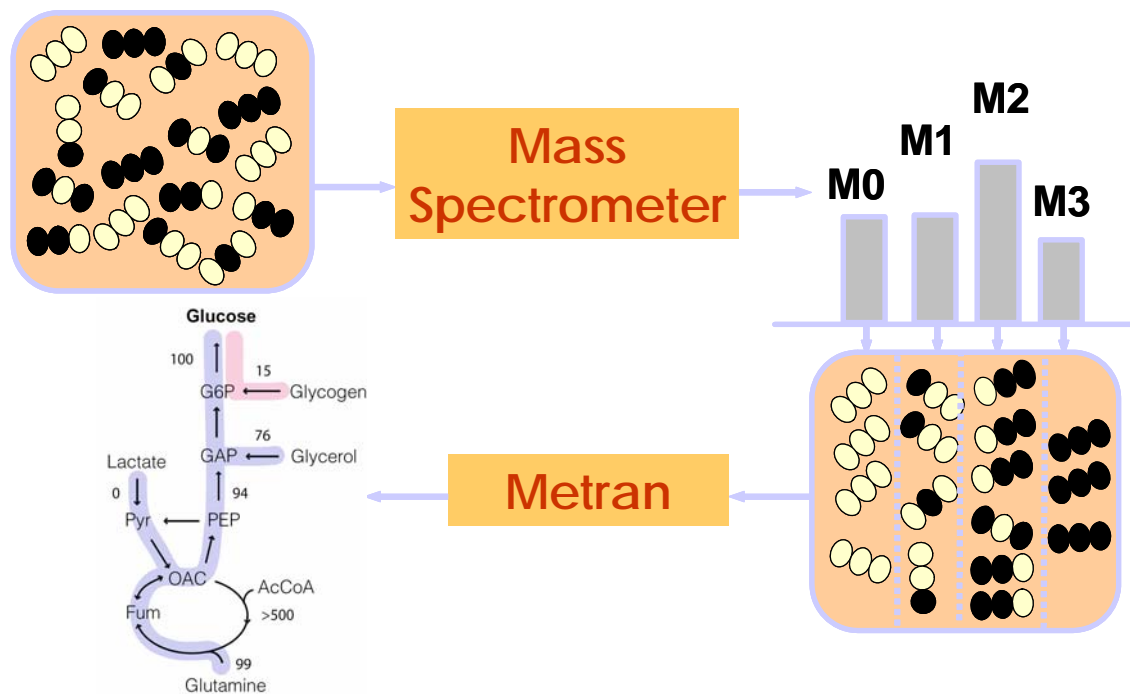
Figure 2.10: Metabolic flux analysis paradigm. Under the assumption of metabolic and isotopic steady state, NMR, GC-MS and LC-MS measurements can be converted to isotopomer distributions, and subsequently to quantitative reaction flux information through the use of MATLAB software package METRAN.

As an illustration of elementary metabolite unit theory, we can describe the metabolic network in Figure 2.7 consisting of 4 metabolites (each with 2 atom units for simplicity), 3 extracellular fluxes and 3 intracellular reactions. Reaction 3 is reversible, and we shall represent the forward flux as reaction 3f and the backward flux as reaction 3b for clarity. Each reaction can be decomposed into subsets of reactions where specific isotopomers react. Isotopomer Spectral Analysis tracks every unknown isotopomer in order to estimate the rates of appearance simultaneously at metabolic and isotopic steady state. Setting up material balances for the unknown isotopomers at metabolic and isotopic steady state, we find the reactions describing the evolution of isotopomers as follows.

Isotopomer Balances

$$0 = v_1 a_{00} + v_{3b} d_{00} - (v_{3f} + v_2) b_{00} \qquad (2.3)$$
$$0 = v_1 a_{01} + v_{3b} d_{01} - (v_{3f} + v_2) b_{01} \qquad (2.4)$$
$$0 = v_1 a_{10} + v_{3b} d_{10} - (v_{3f} + v_2) b_{10} \qquad (2.5)$$
$$0 = v_1 a_{11} + v_{3b} d_{11} - (v_{3f} + v_2) b_{11} \qquad (2.6)$$
$$0 = v_2 (a_{00} b_{00} + a_{00} b_{01} + a_{01} b_{00} + a_{01} b_{01}) - j_C c_{00} \qquad (2.7)$$
$$0 = v_2 (a_{00} b_{10} + a_{00} b_{11} + a_{01} b_{10} + a_{01} b_{11}) - j_C c_{01} \qquad (2.8)$$
$$0 = v_2 (a_{10} b_{00} + a_{10} b_{01} + a_{11} b_{00} + a_{11} b_{01}) - j_C c_{10} \qquad (2.9)$$
$$0 = v_2 (a_{10} b_{10} + a_{10} b_{11} + a_{11} b_{10} + a_{11} b_{11}) - j_C c_{00} \qquad (2.10)$$
$$0 = v_1 (a_{00} b_{00} + a_{00} b_{10} + a_{10} b_{00} + a_{10} b_{10}) + v_{3f} b_{00} - (v_{3b} + j_D) d_{00} \qquad (2.11)$$
$$0 = v_1 (a_{00} b_{01} + a_{00} b_{11} + a_{10} b_{01} + a_{10} b_{11}) + v_{3f} b_{01} - (v_{3b} + j_D) d_{01} \qquad (2.12)$$
$$0 = v_1 (a_{01} b_{00} + a_{01} b_{10} + a_{11} b_{00} + a_{11} b_{10}) + v_{3f} b_{10} - (v_{3b} + j_D) d_{10} \qquad (2.13)$$
$$0 = v_1 (a_{01} b_{01} + a_{01} b_{11} + a_{11} b_{01} + a_{11} b_{11}) + v_{3f} b_{11} - (v_{3b} + j_D) d_{11} \qquad (2.14)$$

Here a_{00} represents the isotopomer of metabolite A with no labeled atoms incorporated into its skeleton, whereas metabolite a_{11} represents the isotopomer of metabolite A incorporating two labeled atoms. Metabolites a_{10} and a_{01} denote isotopomers with different atoms labeled in their skeleton, the former includes the first atom labeled, while the latter includes the second atom labeled. We have decomposed reaction v_3 into the forward and backward fluxes for clarity and enumeration, into a forward reaction rate v_{3f} and a backward reaction v_{3b}. These equations can be solved for all unknown isotopomers given known input fluxes and fractional enrichment of the metabolites available for measurement using iterative equation solvers such as Newton's

method to provide a set of fluxes describing the metabolism in this network. However, the results obtained can be computationally expensive to determine given the size of the problem, difficulty traversing solution space and multiplicity of solutions.

Elementary metabolite unit (EMU) theory provides an algorithm to break down the computational problem into a simpler set of equations from the network presented in Figure 2.11. The first step in setting the EMU decomposition involves enumerating interacting metabolite units systematically, beginning from the measured metabolite units. *A priori*, we know we can measure the enrichment of two-atom metabolite D, and we will give tracer in the form of metabolite A labeled in its second atom. In EMU terms, these metabolite units are represented as EMU D_{12} and EMU A_2 respectively. Here, EMU D_{12} represents the two atom metabolite D with the possible enrichment in both atoms, while EMU A_2 represents the single atom labeled at position 2 of molecule A. The algorithm for EMU decomposition enumerates the interacting EMUs of size 1, namely with only one atom of enrichment, which are necessary to produce a D_{12} measurement. By inspection, we observe that only EMUs B_2 and D_2 are necessary and they interact in the network shown in Figure 2.10A. Balancing metabolite units in this network we obtain the following equations:

EMU Balances, Size 1
Balance on A_2: $0 = j_A A_2 - v_1 A_2$ (2.15)
Balance on B_2: $0 = v_1 A_2 + v_{3b} D_2 - (v_2 + v_{3f}) B_2$ (2.16)
Balance on D_2: $0 = (v_2 + v_{3f}) B_2 - (v_{3b} + j_D) D_{12}$ (2.17)

These equations can be systematically solved for the enrichment of each metabolite unit, which in turn are used to solve the EMU Size 2 network presented in Figure 2.11B. Notice that there is no metabolite unit A_1, as this portion of molecule A remains unlabeled through all atom transitions and does not impact the prediction of the labeling pattern of interest. Figure 2.10A lists the EMUs of Size 2 necessary to reconstruct the enrichment of metabolite unit D_{12}. Only EMUs A_{12} and B_{12} are necessary to reconstruct the desired enrichment of molecule D_{12}. As in

the EMU Size 1 problem, we set the interaction network among these EMUs in Figure 2.11B.

Setting up balances for the metabolite units present we obtain the following equations:

EMU Balances, Size 2

Balance on A_{12}: $0 = j_A A_{12} - v_1 A_{12}$ (2.18)

Balance on B_{12}: $0 = v_1 B_{12} + v_{3b} D_{12} - (v_2 + v_{3f}) B_{12}$ (2.19)

Balance on D_{12}: $0 = (v_{3b} + j_D) D_{12} - v_{3f} B_{12} - v_2 (A_2 \otimes B_2)$ (2.20)

Here, the term $A_2 \otimes B_2$ represents the convolution (or Cauchy product) of the vectors for enrichment of EMUs A_2 and B_2. By sequentially applying the solutions to the EMU Size 1 problem into increasingly complex EMU networks, we curb the increase in enrichment species observed with isotopomer spectral analysis. The reduction in complexity of the computational problem stems from the loss of isotopomers that do not contribute to the enrichment of the formed molecules available for measurement [13, 102]. This theory enables the analysis of complex metabolic networks such as those found in mammalian cells and organisms in a computationally tractable time.

Elementary metabolite units

A)

EMU Size 1	EMU Size 2
A_2	A_{12}
B_2	B_{12}
D_2	D_{12}
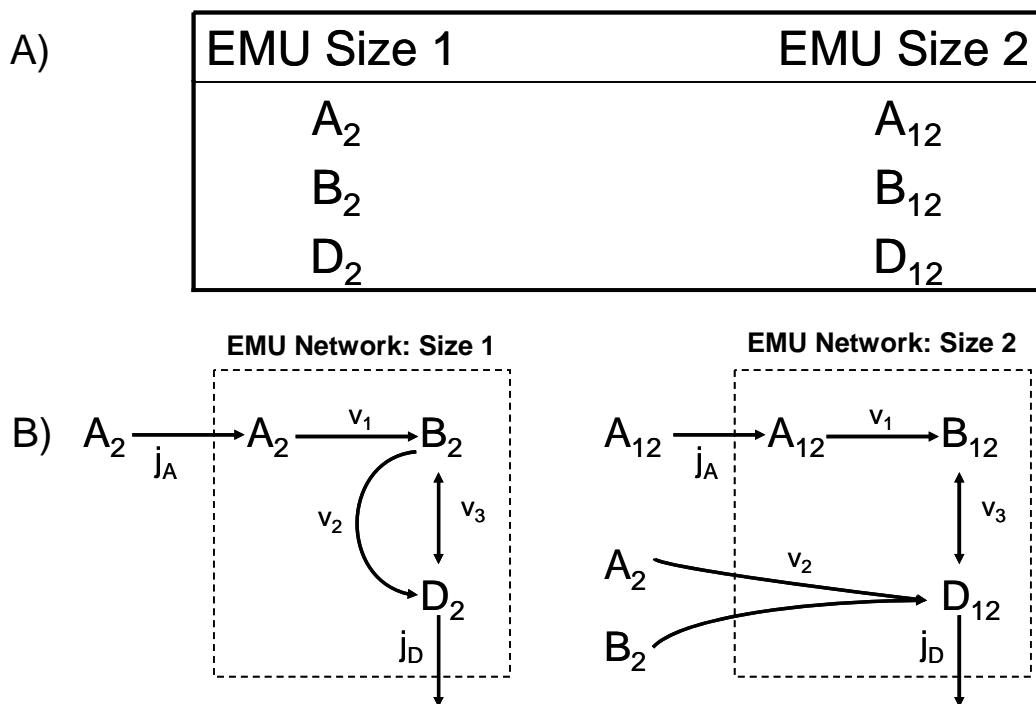
Figure 2.11: Elementary metabolite unit representation of a simple metabolic network. A) Detailed list of elementary metabolite units for metabolic network described in Figure 2.7. This network incorporates isotope tracer through elementary metabolite unit A_2 and measures D_{12} B) Elementary metabolite unit network deconstruction of simple metabolic network. The EMU network of size 1 is solved for all elementary metabolite units starting from the measured units, and is subsequently used to solve the EMU network of Size 2.

2.3.4. Mathematics of reaction flux reconstruction with isotopic label enrichment

Metabolic fluxes are determined from isotopomer data by minimizing the difference between the proposed model of the metabolic pathway of interest and the obtained measurements from isotopomer data. Therefore, flux elucidation can be framed as a parameter estimation problem for minimization through least squares as shown in Equation 2.21

$$\min \Phi = (x(u) - x^{obs})^{\mathrm{T}} \cdot \sum_x^{-1} (x(u) - x^{obs})$$
$$\text{s.t.} \quad N \cdot u \geq 0 \tag{2.21}$$

The objective function Φ represents the covariance-weighted sum of residual squares, x(u) represents the vector containing the simulated and proposed isotopomer distribution measurements, x^{obs} is the vector of experimental data containing both labeling measurements and extracellular rate measurements and Σ_x is the measurement covariance matrix with measurement variances along its diagonal. Equation 2.21 is nonlinear and requires an iterative solution scheme in the form of a quadratic programming subproblem [13]. To ensure that a global optimum was found, flux estimation was repeated four times from random initial values for all fluxes. At convergence, accurate confidence intervals were calculated by evaluating the sensitivity of the objective function with respect to individual fluxes. Sensitivities follow the F distribution function:

$$\frac{\Phi(u)|_{v_i} - \Phi(\hat{u})}{\Phi(\hat{u})/(n-p)} \sim F(1, n-p) \tag{2.22}$$

where $\Phi(u)$ is evaluated at the current flux v_i and compared to the objective function at the optimum value $\hat{u}$. The denominator of the expression represents the standard error when evaluating the objective function at the optimum value. The statistic in equation 2.22 follows

an F distribution with (1,n-p) degrees of freedom, where n is the number of measurements and p is the number of estimated fluxes.

To address the statistical certainty of the proposed model, the sum of residual squares is treated as a stochastic variable with chi-squared distribution [105]. Statistical validation of fits was accomplished by goodness-of-fit testing (i.e. chi-square test for model adequacy) and a normality test for the weighted residuals between proposed and measured isotopomers, such that:

$$\Phi(u)|_{v_i=0} \le (\Phi(\hat{u}) + \chi^2_{1-\alpha}(1)) \tag{2.23}$$

The threshold values for $\chi^2_{1-\alpha}(1)$ corresponding to 80%, 90%, 95% and 99% confidence intervals are 1.64, 2.71, 3.84, and 6.63, respectively. Thus, in order to obtain accurate confidence intervals of fluxes we need to determine the minimized sum of squared residuals as a function of the flux value. This is the value reported throughout the rest of this thesis to accept a specific fit as statistically accepted.

As described previously, mass isotopomers were simulated at each iteration through the recently introduced elementary metabolite unit modeling framework [102]. Stated formally, this method details the simplest simulation for a predetermined metabolic network based on the observed parameters determined *a priori*. Isotopic measurements are simulated through a cascade of linear subproblems of the form:

$$
\begin{aligned}
A_1(\upsilon) \cdot x_1 &= B_1(\upsilon) \cdot y_1(y_1^{in}) \\
A_2(\upsilon) \cdot x_2 &= B_2(\upsilon) \cdot y_2(y_2^{in}, X_1) \\
&\ldots \\
A_z(\upsilon) \cdot x_z &= B_z(\upsilon) \cdot y_z(y_z^{in}, X_{z-1}, \ldots, X_1)
\end{aligned}
\tag{2.24}
$$

where $A(\upsilon)$ and $B(\upsilon)$ represent isotopomer transition matrices that are strictly functions of fluxes v, x is the vector of simulated measurements and y is the vector of substrate labeling.

Previous work has shown that the EMU method will always compute a unique and stable solution for simulated measurements for a combination of metabolic fluxes, substrate labeling and proposed metabolic network [102]. It is up to the user to evaluate the obtained flux distribution for significance with regards to the experimental system obtained.

2.4 Application of isotopic tracers in metabolism research

We defined in Chapter 1 an isotope as an atom with a conserved number of electrons and chemical identity but with a different atomic mass. The aspect of conserved chemical identity is critical to the use of isotopes to reconstruct metabolism, since it allows the substitution of isotopes without perturbation of the chemical properties of a reaction network. In particular, through this thesis we combine the use of stable isotope tracer methodologies to reconstruct fluxes in cell culture and in vivo as important descriptors of metabolic health and disease.

In this section we will focus on the applications of prior tracer work to the study of metabolism in general through the use of isotope incorporation of both radioactive and stable nature. Chapter 3 lays out the details of isotopic reconstruction methods tailored for the analysis of glucose production from. Therefore, the current section only briefly covers isotope tracer methods related to glucose metabolism. Instead, we focus on concepts important to the collection, interpretation and performance of isotope tracer experiments for general metabolic flux reconstruction.

Isotopic tracers have been long used to discover metabolic pathways of varying diversity. For example, in their papers describing the path of carbon through the photosynthetic metabolic pathway, Calvin and Bassham used radioactive $^{14}CO_2$ to incorporate label into the carbohydrate compounds generated through the dark reactions of photosynthesis [92]. As the availability of stable isotopes has increased coupled with the affordability of mass spectrometers as analytical tools for common research laboratories, a strong interest has emerged in the use of stable isotope tracers. For both radioactive and stable isotopes, there are operating principles that apply to the dosing of tracers to probe metabolism regardless of the nature of the label incorporation, and we discuss several cases in the sections below.

In selecting an isotopic tracer for the study of a pathway, an important consideration is the turnover of the tracer, defined as the quantity of tracer moving through its pool per unit time [85]. Turnover of tracers is closely related to the metabolic flux through the pathway, such that the former represents the latter value normalized to the total amount of the compound present in the compartment, tissue or organ of interest. Three important aspects need to be considered when measuring the turnover rate of a metabolite [106].

- approach used to measure the kinetics of tracer incorporation
- mode of tracer administration and sampling
- choice of radioactive or stable isotope

We will describe the means by which tracers may be administered to cellular and in vivo systems, focusing on how each of the design aspects listed above impact the results and turnover measures that may be obtained from tracer administration. We illustrate key concepts through hypothetical examples followed by examples published in literature, and lastly connect the concepts to their applications presented in subsequent chapters of this thesis.

Tracer administration approach

The approach to measuring turnover parameters is largely determined by the manner of tracer administration to the metabolic system of interest, specifically whether tracer is administered through a bolus injection, constant infusion or a combination of the two methods known as the primed infusion. Figure 2.12 illustrates a hypothetical tracer enrichment curve as would be measured in plasma after dosing of a tracer. On the x axis we have the time component after tracer administration, and the y axis presents the enrichment of the measured metabolite (e.g. glucose). The shape of these curves is determined by the balance of two principal factors, namely the rate of appearance of the tracer in question and the

consumption or degradation of the tracer. Clearly, the choice of kinetic dosage strategy of tracer impacts the data obtained from the metabolic pathway of interest.
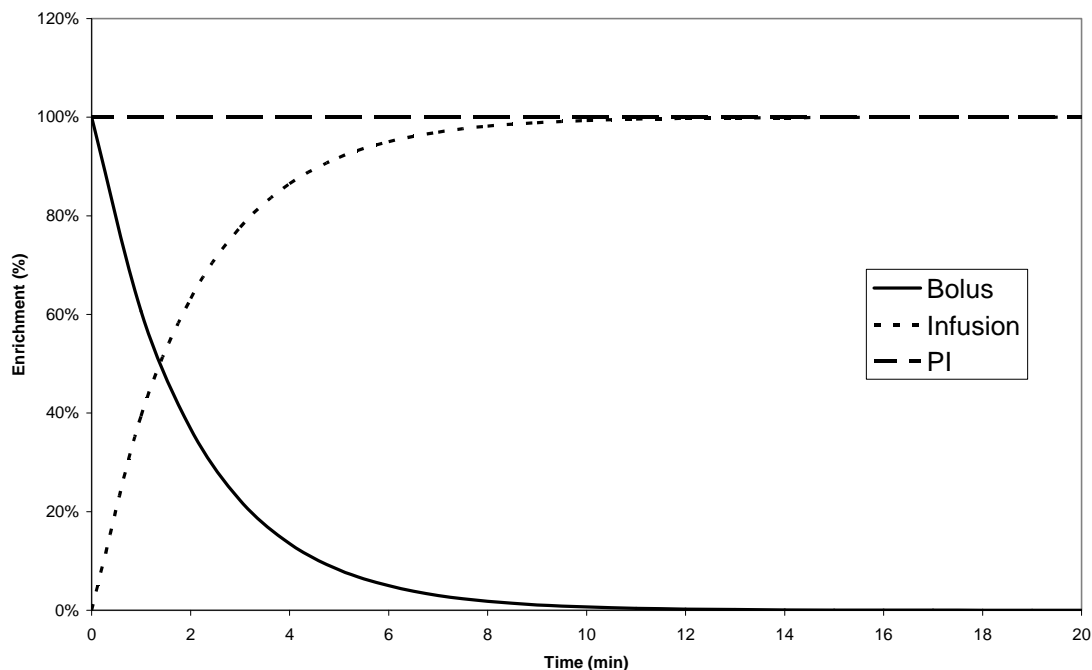
Figure 2.12: Kinetics of tracer incorporation into single metabolic pool. Solid Line = bolus infusion, dotted line = constant infusion, dashed line = primed infusion

Bolus dosing of a tracer is the simplest form of administration as it requires a single injection of the compound into the compartment of interest, usually blood. In Figure 2.12, this is represented by the solid line. In exceptional cases, the ingestion of tracer compound can be modeled as a bolus dose of tracer if the absorption kinetics are much faster than the elimination of the compound in question. There is no net rate of appearance for this compound, as direct administration will make the tracer appear at a fixed level dependent on the amount of tracee compound present. Here, we assume that there is no tracee compound present, such that the tracer is fully enriched upon appearance. The only significant term contributing to this balance is the consumption term, which can be solved analytically to yield

an exponential decay function. The analytical solution for label enrichment after a bolus dose

of tracer takes the following form

$$L(t) = L_0 e^{-kt} \tag{2.25}$$

where L(t) represents the labeling of the sampled metabolite at time t (in dpm/mol or APE),
L_0 represents the labeling of the tracee pool upon the bolus dose at time 0,
k is a constant for the elimination of the tracer from the pool of interest (in min^{-1}).

For our hypothetical example, L(t=0) = L_0. This functional form reflects exponential decay of

tracer due to uptake by the metabolic pathway. The main assumption of this methodology is

that the tracer rapidly enters the single metabolite pool and is distributed evenly throughout

this pool. Furthermore, bolus dosing heavily depends on the assumption that the metabolism

of the tracer follows first order kinetics for the disposal of the tracer. Bolus dosing has been

used extensively in model organisms and humans to reconstruct metabolic fluxes given its

simplicity. In mice, there is a report using bolus dosing of tracer to study free fatty acid

turnover using $[1\text{-}^{14}C]$-palmitate as a tracer [107]. Brunegraber and colleagues used bolus

administration of doubly labeled water ($^2H_2^{18}O$) to measure energy expenditure in mice [108].

In humans, bolus dosing of tracer has been used to study physiological aspects of white blood

cell turnover [109]. In the presented results in Chapter 6, we track the appearance of glucose

after dosing gluconeogenic precursor pyruvate as a bolus, and observe a lag in appearance of

glucose corresponding to gluconeogenic metabolism, followed by disappearance due to

glucose consumption in peripheral tissues.

In cases where the timescale of isotope incorporation invalidates the above assumption

for bolus dosing, a constant tracer infusion can be used to quantify the turnover of a

metabolite of interest as shown by the dotted line in Figure 2.12. In this manner, the tracer is

continuously infused intravenously or subcutaneously until reaching isotopic steady state,

denoted by the flat portion of the dotted enrichment curve. The analytical form of this enrichment curve is given by:

$$L(t) = L_0(1 - e^{-kt}) \qquad (2.26)$$

with variables defined as for equation 2.25. At isotopic steady state, the elimination of tracer equals the appearance of tracer assuming a single metabolic pool. In this case, the rate of appearance of the tracee can be expressed as:

$$L(t) = L_0 = \frac{F}{V \cdot C \cdot k} \qquad (2.27)$$

where F is the infusion flow rate (in APE/kg/min)
V is the volume of distribution (in mL/kg)
C is the concentration of unlabeled tracee (in APE/mL)
and k is the rate constant for elimination (in min^{-1})

We define E_p as equivalent to L_0 in the analytical form of equation 2.25. In these terms we can express the rate of appearance of the tracee as:

$$R_a = \frac{F}{E_p} \qquad (2.28)$$

where R_A is the rate of appearance of the tracer (in APE/min) and,
E_p is the enrichment plateau at steady state (in APE)

The appearance of tracer in blood has two components, dilution of tracer from the pump into the blood directly at the given infusion rate, and appearance of the tracer from metabolism at a metabolic rate of appearance to be measured. This amount of tracer must balance the tracer dosing source, with predetermined tracer enrichment and infusion rate. Rearranging the terms in equation 2.28 we obtain an analytical solution for the constant rate of appearance of tracee by dilution at isotopic steady state in the following the functional form:

$$R_a = F \times \left(\frac{E_{tracer}}{E_{blood}} - 1 \right) \qquad (2.29)$$

where R_A is the rate of appearance of the tracer (in APE/min)

E_{tracer} is the enrichment of the chosen tracer in the infusate (in APE) and,

E_{blood} is the enrichment of the sampled pool, usually blood (in APE).

This equation also denotes that the units for the rate of appearance of the tracer correspond to those of the infusion rate, either dpm/mol in the case of radioactive tracers or atomic percent excess in the case of stable isotopes. The term in parenthesis is always greater than 1 and equal to the inverse of the enrichment plateau at steady state. For most cases, we will assume $E_{tracer} = 1$ in the case of pure tracer administration. In addition, if the enrichment of tracer in blood is significantly smaller than that in the tracer solution ($E_{blood} << E_{tracer}$, such as for radioactive tracers), equation 2.29 reduces to equation 2.28. Appearance of the tracer in our experiments is linear and given by a constant rate (of infusion or pumping) and deviations in the upslope of the curve correspond to nonlinearities in the consumption of the tracer. Examples in literature where constant tracer infusions have been used include the calculation of hepatic glucose output by dilution in the tissue specific transgenic knockouts of the insulin receptor through the use of either [U-^{13}C$_6$]glucose or [3-^{3}H]-glucose respectively [14, 110]. We applied constant infusion tracing to measure hepatic glucose production using a novel doubly labeled [U-^{13}C, ^{2}H$_5$]-glycerol tracer to examine the contribution of glycerol to gluconeogenic metabolism as well as reaction reversibilities that may affect the estimation of fractional gluconeogenesis.

Lastly, the two aforementioned methods can be combined into a primed infusion, whereby the investigator administers a bolus of the isotopic tracer followed immediately by a constant infusion. The analytical solution for primed infusion dosing strategy has the following functional form:

$$L(t) = L_0 e^{-kt} + L_0(1 - e^{-kt}) \tag{2.30}$$

with the variables as defined in equation 2.25. The corresponding concentration of tracer is shown in the dashed line of Figure 2.12 is the idealized case where the uptake of tracer due to

bolus infusion is equally replaced by the appearance of tracer due to constant infusion. The cases where these rates do not match can be divided into two scenarios: disappearance of tracer from bolus dosing is faster than the rate of appearance by infusion, and the reverse case where the appearance rate from infusion is faster than disappearance due to bolus injection. In the former case, we would observe decay until reaching the isotopic steady state enrichment level and constant rate of appearance, where equation 2.29 holds. In the latter case, we would observe increase in the level of enrichment, again until reaching the isotopic steady state for a constant rate of appearance.

In essence, the primed infusion approach allows rapid achievement of isotopic steady state when compared with a bolus or constant infusion of tracer. As a consequence, the primed infusion reduces the amount of tracer necessary to dose the cell, tissue or animal involved without affecting the eventual steady state. At isotopic steady state, the rate of appearance for the traced molecule of interest calculated with equation 2.29 equals the rate at which the tracer is metabolized. This method is the preferred manner by which to administer isotopes in human clinical trials to limit the toxicity and exposure to the tracer while allowing for measurements within a reasonable amount of time. Examples of this approach include the use of deuterated water tracing by initial ingestion followed by water feeding in humans [111]. In our work presented in Chapter 5 and 6, we apply deuterated water to mice as a primed infusion, with an initial injection of intraperitoneal water to reach the desired level of enrichment (e.g., 5% total body water) followed by *ad libitum* feeding of deuterated water.

Tracer administration site and sampling site

Another important consideration regards the site of administration of the tracer compound when sampling compound from blood. In this case, not only the time course of

tracer input is critical for the interpretation of the data, but additionally the physical path the tracer takes prior to arriving at the tissue of interest can impact the interpretation of the results obtained. Ideally, the tracer should enter circulation in the same location as the tracee present in the organism of interest. For instance glycerol administered intravenously would circulate to its clearance site in the liver for gluconeogenic metabolism as glucose, while glycerol absorbed orally it would undergo partial metabolism in the gut prior to reaching the liver. Therefore, intravenous administration of tracer would underestimate the production of tracer to the extent that the liver clears the compound. In other words, should the tracer compound be cleared by a different tissue (e.g. liver) than that which releases the tracee (e.g. gut), we would observe differences in the measured rates of production as a consequence of parallel circulation when administering in the venous circulation and sampling in the arterial circulation. Of note, Katz and coworkers demonstrated that injection of labeled lactate into the arterial circulation causes significant overestimation of lactate turnover by dilution when sampling from the venous circulation [112]. Researchers with expertise in small animal surgery have successfully dosed compounds in the brain and gut circulation to demonstrate effects of brain cytokines in regulating mucosal protein turnover [113], in addition to effects of brain pyruvate metabolism in regulating liver glucose production [114].

In our studies, we applied a recently developed technique by Kurland and coworkers involving the use of miniosmotic pumps implanted in the subscapular subcutaneous space of mice [115-117]. These pumps have extensive literature documentation as effective means of administering hormones and drugs through constant infusion over extended periods of time in multiple physiological paradigms (www.alzet.com) [118]. The greatest advantage from the use of this dosing modality involves the simplicity of implantation within minutes and a minor surgical procedure that is well tolerated by animals. In principle, infusion of labeled

compounds using these pumps approximates the venous-arterial mode of tracer administration and sampling given their subcutaneous implantation, subsequent absorption into the venous circulation and eventual sampling of the tracer from the arterial circulation [115]. However, as this method is further developed, there will be important questions regarding its effect on the physiology of the systems studied, the validity of the assumptions allowing for venous-arterial dosing mode, as well as the nature of the isotopic steady state achieved.

Choice of radioactive versus stable isotopes

Lastly, the *choice of radioactive versus stable isotope* is largely dictated by the nature of the questions asked regarding metabolism, the facilities available to the investigator and the final goal regarding the methodology developed. The recent availability of stable isotope tracers from commercial vendors has greatly increased their use in research laboratories. Coupled with this observation, improvements in nuclear magnetic resonance spectroscopy and mass spectrometry techniques facilitate the measurement of the abundance of stable isotope incorporation necessary for reconstructing metabolic flux distributions. Consequently, these technical developments caused a dramatic shift away from radioisotope use and towards stable isotope use in metabolic research. Despite these general trends, at least four aspects impact the choice between radioactive and stable isotope tracers as follows:

- Radioisotope half life
- Number of measurements
- Isotope recycling
- Patient Safety

Radioisotopes are by nature unstable as discussed in Chapter 1, emitting particles that can be detected readily and decaying into stable isotopes. This rate of decay is best described by the half life, which is specific to the isotope in question. For instance, ^{14}C has a half-life of

approximately 5370 years, thereby enabling its use to date fossilized remains by abundance. On the other hand, isotopes such as ^{13}N and ^{15}O show characteristic half lives of approximately 10 and 2 minutes respectively, precluding their use as meaningful markers of metabolism. Their stable isotope counterparts, ^{15}N and ^{18}O, are generated readily and provide means to track physiologically important processes such as molecular oxygen incorporation or amino-acid metabolism.

A more subtle point regards the *number of measurements* necessary to reconstruct turnover rates from either radioactive or stable isotope incorporation. For instance, in this thesis we use labeled glycerol to monitor the production of plasma glucose. Should we choose $[U-^{14}C]$-glycerol as our tracer source, we would need two separate measurements to get meaningful enrichment values from the resulting glucose molecule; a first measurement for the concentration of glucose present and a second scintillation counting measurement for the activity of incorporated radioisotope. On the other hand, should we choose to measure glucose production through the incorporation of $[U-^{13}C]$-glycerol into glucose, we can add a separate known amount of $[^{2}H_7]$-glucose to normalize the amount measured in addition to assessing its incorporation of carbon 13. Therefore, we can obtain enrichment and concentration information simultaneously through clever use of the multiple stable isotope labeled molecules available commercially. We used these techniques to measure tracer incorporation and concentration in establishing the validity of steady state assumptions in our hepatocyte culture models [13]. In the next section, we describe the application of these stable isotope labeling strategies in literature for the elucidation of hepatic glucose production fluxes and their contribution to the development of insulin resistance.

The availability of mass spectrometric information facilitates a more thorough measurement of stable isotope label incorporation that can be used to assess tracer recycling.

For example, in tracing glucose metabolism with carbon labeled glucose, several groups including ourselves have noted the presence of enrichment patterns indicative of Cori cycling of muscle lactate [119, 120]. If a researcher chooses to measure glucose production by dilution using [U-^{14}C]-glucose, scintillation counting will measure the total activity of ^{14}C incorporated into the glucose molecule regardless of the position where the radioactive isotope lies. This in turn results in overestimation of glucose production as the Cori cycle produces glucose species incorporating 1, 2 or 3 labeled atoms in addition to the fully-labeled [U-^{14}C]-glucose contains 6 labeled atoms. When using stable isotopes with detection of label incorporation through mass spectrometry, we can directly resolve the fully labeled [U-^{13}C]-glucose molecule as an M6 isotopomer, and Cori cycling manifests as M1, M2 and M3 isotopomers. In this manner, contributing signals from Cori cycling do not interfere with the determination of body glucose production.

As the ultimate goal of these methodologies involves translation into clinical settings where metabolically relevant parameters can be assessed *in vivo*, an important consideration regards the safety of administration for the selected tracer should it come to use in the clinical setting. For both radioactive and stable isotopes, there are important considerations regarding the toxicity of the tracer molecule chosen. For non-toxic, naturally occurring molecules such as glucose or glycerol, there may be concentration dependent effects that change metabolism and should be considered accordingly with prevention strategies. Radioactive tracer use has the added disadvantage of contributing to radiation exposure to patients. While the cost-benefit analysis overwhelmingly favors usage of radioisotopes for imaging diagnostic studies, current strategies for metabolic flux determination are limited in the number of parameters determined and the clinical value they provide to guide patient management. As such, strategies utilizing stable isotopes are favored for applications involving human subject metabolic determinations,

since they are simultaneously most informative when coupled with nuclear magnetic resonance or mass spectrometry analytical techniques. In the next section, we describe the application of these stable isotope labeling strategies in literature for the elucidation of hepatic glucose production fluxes and their contribution to the development of insulin resistance.

CHAPTER 3: Stable isotope tracers in hepatic glucose production

3.1 Overview of prior isotope work related to glucose metabolism

In this chapter, we focus specifically on methodologies developed for the reconstruction of metabolite levels and fluxes related to hepatic glucose production, since this pathway forms the focus of our subsequent studies throughout this thesis. Isotopes have been used to elucidate hepatic glucose production since the early days of metabolic pathway discovery. Krebs and colleagues reported the use of radioisotope incorporation and metabolite concentration measurements in the establishment of disequilibrium of the triose phosphate isomerase system in hepatic glucose production [121]. Pilkis and colleagues assessed hormonal control of radioactive glucose synthesis from labeled [U-^{14}C]-lactate, [U-^{14}C]-DHAP and [U-^{14}C]-glycerol. In this remarkable series of studies, researchers modulated glucose production due to competing substrates and hormones in isolated rat hepatocytes, and their results confirmed the ability of glucagon to modulate pyruvate kinase activity, and, consequently inhibit glycolytic flux [122, 123]. The results from this work are consistent with previous studies examining hormonal effects of insulin, glucagon as well as substrate effects on rat hepatocyte glucose production isolated by 2-step collagenase perfusion and measured by standard enzymatic methods [124].

Simultaneously, developments in nuclear magnetic resonance (NMR) permitted the analysis of glucose production without the need for explicit separation of the glucose molecule. NMR analysis provides two types of labeling information for a given compound. First, one can determine the fractional abundance of ^{13}C at a specific carbon atom position. Determination of these fractional

enrichments is based on the fact that the ^{1}H-^{12}C interaction gives rise to a different peak in the ^{1}H-NMR spectrum than the ^{1}H-^{13}C interaction. Fractional enrichments of individual carbon atoms deconvolute as functions of isotopomer fractions. Second, adjacent nuclei of different atoms interact through spin-spin coupling to generate split peaks in characteristic patterns depending on the number of neighboring hydrogen atoms. This fine structure of NMR provides significant information regarding the labeling of individual carbon atoms in a molecule, and in addition gives positional information of the carbon atom through functions of isotopomer fractions. In this way, this technique allows for reconstruction of the isotopomer spectrum of the glucose molecule in a manner similar to that obtained through mass spectrometry.

Early work by Robert Shulman and coworkers established the utility of multidimensional nuclear magnetic resonance (NMR) in rat liver cells for measurement of the production of glucose. Using ^{31}P NMR, Shulman and colleagues reported the direct detection of a pH gradient in mitochondria of intact rat hepatocytes, as well as the detection of several sugar phosphate intermediates in the production of glucose such as glucose-6-phosphate [125]. Following this experimental demonstration of NMR measurement in intact cells, this group investigated the utilization of labeled glycerol in rat hepatocytes isolated from hyperthyroid animals by ^{13}C NMR [73]. The careful use of this spectroscopic technique permitted the researchers to not only measure the percentage label in the glucose molecule from each particular carbon as would be done in radioactive ^{14}C experiments, but additionally to reveal the distribution of labeled carbons in a single glucose molecule. Using this information, the researchers were able to measure equal contributions of the glyceraldehyde-3-phosphate and dihydroxyacetone phosphate branches of glucose metabolism. In addition, fractional enrichment loss of ^{13}C at C1 in the glucose molecule allowed estimation of pentose phosphate pathway activity in isolated rat hepatocytes. The team also detected a doubling in gluconeogenic flux from glycerol in hyperthyroid rat hepatocytes without changes in

the makeup of gluconeogenic substrate usage as measured by unchanged ratios of enrichment at C1 through C6 in the glucose molecule. In a subsequent publication, the researchers showed the equivalency of the NMR measurements to ^{14}C measurements for the purposes of gluconeogenic flux determination in the perfused mouse liver [126]. These results set a dramatic precedent to jumpstart the transition from radioactive tracer measurements to stable isotope tracer techniques. Clearly, careful determination of isotopomer labeling patterns in the glucose molecule coupled with positional information regarding isotopic enrichment can contribute additional information to reconstruct metabolic fluxes.

The next logical step in extending the use of positional enrichment information did not occur in hepatic glucose production, but rather in the study of heart metabolism. Chance and colleagues were among the first to apply the method of isotopomer analysis for time dependent evolution of ^{13}C enrichment in glutamate through nuclear magnetic spectroscopy [127]. Malloy and Sherry developed these concepts further and applied stable isotope tracers such as [2-^{13}C]-acetate, [3-^{13}C]-pyruvate, [3-^{13}C]–propionate and combinations thereof in parallel experiments to reconstruct the oxidative branches of the TCA cycle in heart metabolism through ^{13}C NMR spectra of glutamate in perfused rat hearts [128, 129]. These studies were facilitated by the commercial availability of variants with positional enrichment of the aforementioned substrates. Through the use of tracer substitutions, the authors confirmed that 88% of Acetyl-CoA during a heart perfusion is derived from exogenous substrate, with 65% of this amount provided by acetate, 30% provided by pyruvate and the remainder provided by other endogenous sources. Furthermore, the authors were able to integrate much of this data by modeling the enrichment of all 32 isotopomers of the glutamate molecule, thereby establishing a comprehensive mathematical model to indirectly calculate fluxes by fitting a proposed metabolic model to the existing isotopomer data through nonlinear least squares analysis of simultaneous differential equations. This work was motivated by a previous report by

Kalderon et al. in which the combination of NMR spectroscopy, electron impact ionization and chemical ionization GC-MS were combined to yield positional enrichment in the glucose molecule in a study of glycogen repletion metabolism in the perfused rat liver [130]. Using these techniques, the authors directly demonstrated that lactate and alanine contribute to the repletion of glycogen stores and strongly suggest that gluconeogenic activity is present even in refeeding physiology. Kalderon would go on to apply the developed technologies to the study of glycogen synthase deficiency in pediatric patients [131]. These studies showcase the rich array of information that is obtained for estimation of metabolic fluxes using ^{13}C enrichment analysis through either NMR spectroscopy or GC-MS in metabolic systems encompassing biochemical extract, cells, perfused organs and whole organisms.

We introduced the concept of isotopomers in Chapter 1 as sequentially enriched species of a given compound by incorporation of isotopic label. Quantitative analysis of cellular, tissue and organism physiology from stable isotope incorporation requires the accurate assessment of isotopomer distributions through NMR, GC-MS or a combination of these common analytical techniques. In practical terms, the use of nuclear magnetic resonance spectroscopy is limited by the expense of equipment necessary to generate the magnetic fields required to align the nuclei of interest. In addition, measurement of magnetic resonance requires concentrations of compounds in the milimollar range, further restricting the compounds which may be analyzed for isotopic enrichment through this analytical technique to abundant molecules in tissue or plasma. The greatest advantage of NMR lies in its ability to detect resonance spectra without the intrinsic need for separation of complex samples, thereby opening the possibility for potential in vivo analysis of intact tissues, organs or organisms.

In contrast, GC-MS is a relatively rapid and sensitive technique that combines separation of complex samples in the gas chromatograph with the intrinsic identification of molecules through

mass spectrometry as a means to detect changes in mass and consequently enrichment. Unlike NMR, GC-MS analysis needs processing of samples prior to injection into the separation unit, and thus requires extract preparation from the experimental system studied. Mass spectrometry therefore would best analyze biofluids that require no extensive processing prior to injection, such as cellular supernatant, plasma, urine or saliva. The most important limitations in mass spectrometric reconstruction of metabolic fluxes occur due to inaccuracies and imprecision in the measured isotopomers. Several researchers have developed techniques for the quantitative interpretation of isotopomer distributions from mass spectrometry data [132, 133]. We next examine developments in mass spectrometry techniques for the assessment of metabolic fluxes from mass spectrometric data in order to frame our MS-based approach for in vivo flux analysis within the larger literature context.

3.2 Current methodologies for metabolic flux reconstruction from mass isotopomers

3.2.1 Mass Isotopomer Distribution Analysis

The use of stable isotope tracers for metabolic flux determinations using NMR in the preceding sections motivated Katz, Lee and colleagues to ask whether similar information about fluxes from the ^{13}C enrichment of the glucose molecule could be measured through the use of GC-MS [134]. Using the precedent set by Kalderon, they set to measure gluconeogenic production and the contributions of the direct (from glucose) and indirect (from three-carbon compounds) paths to hepatic glycogen synthesis by intragastric infusion of [U-^{13}C]-glucose in rats. Careful measurement of the isotopomer spectrum of the glucose molecule harvested in the portal vein, coupled with tailored polynomial expressions to track ratios of higher mass isotopomers estimated indirect path contributions ranging from 55-65% of total glycogen deposited. This study was among the first to demonstrate the utility of isotopomer measurements in elucidating glycogen production and TCA cycle fluxes quantitatively.

The proposed mathematical expressions were further developed through mass isotopomer distribution analysis (MIDA) [133]. This methodological advance is based on the concept of envisioning biological molecules as polymers. Polymerization biosynthesis can be conceptualized as a combinatorial process whereby monomers from a precursor pool combine into the polymer of interest. After introduction of label into the monomeric pool, there are multiple types of building blocks (i.e., labeled, unlabeled) from which to assemble the polymer of interest. As a consequence, the synthesized molecules will not have uniform composition with respect to mass, but rather encompass multiple distinguishable species with varying numbers of subunits. The relative proportion of each isotopic species can then be calculated using the binomial expansion. This

framework is especially useful when analyzing macromolecules such as DNA, proteins and fatty acids, but can be just as effectively applied to smaller molecules. For instance, glucose can be envisioned as a polymer of two adjoining glycerol molecules. Using this framework, researchers have asked questions in multiple metabolic systems such as *de novo* lipogenesis in chylomicron-deficient mice [135], *de novo* lipogenesis in the presence of excess dietary carbohydrate [136] and B-cell turnover in the onset of chronic lymphocytic leukemia [109]. MIDA has been applied to assess the effects of triose phosphate enrichment in the estimation of gluconeogenic flux [120, 137].

In the context of glucose production from three carbon precursors such as glycerol, MIDA requires an important assumption regarding the existence of a single triose-phosphate pool from which glucose is formed. Initial estimates from the Hellerstein group using intravenous infusions of [3-^{13}C]-lactate, [1-^{13}C]-lactate and [2-^{13}C]-glycerol yielded estimates of fractional gluconeogenesis of 88±2, 89 ±3 and 87±2% after 48 hours of fasting in male Sprague-Dawley rats [136]. In addition, they show that after IV glucose infusion, the reduction in glucose production observed in this experimental system corresponded with decreased glycogenolysis. The authors direct experiments at testing the hypothesis of disequilibrium in the triose phosphate pool, and they argue in theoretical terms that unless disequilibrium between GAP and DHAP is severe (enrichment of 40-50% in one of the triose-P), such disequilibrium would not affect MIDA calculations. In addition, they measure the ratio of enrichment in versus C3-C6:C1-C4 in the aldonitrile pentaacetate glucose moiety after incorporation of [2-^{13}C]-glycerol, and find a value of 1.16-1.17, which impacts their synthesis calculations minimally.

The estimation of hepatic glucose production fluxes by [U-^{13}C]-glycerol incorporation through MIDA received much attention from other groups pointing out that the values obtained through this methodology consistently overestimates glucose production when compared to standard dilution methods [138 1998]. In carefully designed studies, Previs and colleagues show that

the labeling patterns obtained from glucose and analyzed by MIDA suggest multiple pools of triose phosphates present when measuring enrichment in perfused rat livers [138]. In addition, zonation of glycerol metabolism in the liver causes the underestimation observed by either depleting the dosed glycerol through first pass liver metabolism or release of unlabeled glycerol from the liver. Further work in isolated rat hepatocytes showed that the heterogeneity of glycerol metabolism can be replicated at the cellular level despite homogeneity in glycerol kinase activity, suggesting that the metabolic machinery synthesizing glucose from glycerol beyond glycerol kinase may be different in periportal versus perivenous hepatocytes [139]. In contrast, when assessing fractional synthesis of glucose from abundant serum precursors such as [U-^{13}C]-lactate in vivo, the authors note that the calculated fractional gluconeogenesis corresponds to the physiology observed without underestimation of the expected values. For example, assume that there are two pools of triose phosphate from which glucose is made in equal measure. Using glycerol as the gluconeogenic precursor, one pool is converted to glucose at five times the rate of the other, but > 90% of glucose is formed via both pools from pyruvate or lactate as the precursor. The resulting enrichment in the pools will then be fivefold different when [U-^{13}C]glycerol is administered but will differ by < 10% when [U-^{13}C]lactate is administered [140]. These data taken together suggest that MIDA requires the tracer to correspond to the dominant gluconeogenic substrate, implying that labeled lactate or pyruvate may be appropriate substrates to evaluate gluconeogenesis in vivo over glycerol.

3.2.2 Isotopomer Spectral Analysis

Isotopomer Spectral Analysis (ISA) operates under a similar conceptual framework as MIDA, utilizing combinatorial probabilities to describe the biosynthesis of macromolecules formed from a labeled monomeric precursor pool. For example and as observed in Figure 3.1, ^{13}C-labeled acetate may be dosed to hepatocytes to observe label incorporation into the sampled cellular

cholesterol pool. In order for the labeled AcetylCoA to reach this sampled cholesterol pool, the tracer molecule must initially mix with the naturally occurring AcetylCoA pool that is the precursor to the formation of cholesterol. Parameter D represents the fraction of labeled AcetylCoA present relative to the total pool of AcetylCoA present. From this mixed pool, cholesterol synthesis occurs at a specific rate given by parameter g(t). We refer to g(t) as the fractional synthesis of cholesterol relative to the natural abundance labeled cholesterol synthesized previous to the introduction of tracer. These two parameters can be solved from the polynomial expression describing the formation of individual cholesterol species through binomial expansion (Sample Equation, Figure 3.1). In this expression, the first algebraic term represents new synthesis of cholesterol after the introduction of stable isotope label, and the second algebraic term represents existing natural abundance of cholesterol.

An important difference when comparing ISA to MIDA lies in the incorporation of the dilution and fractional synthesis parameters to account for the precursor pool enrichment. In this way, a researcher can be sure that the observed increase in stable isotope incorporation to a macromolecule occurs due to an intrinsic increase in the synthesis of the molecule and not due to increased enrichment of the precursor pool. ISA has been effectively used to estimate gluconeogenesis [85], and lipogenesis [141] from glutamine versus glucose [74], among other biosynthetic products. We make use of ISA for describing the fractional synthesis of cholesterol from labeled Acetyl-CoA in hepatocytes from LIRKO mice in assessing their metabolic differences for lipid synthesis.
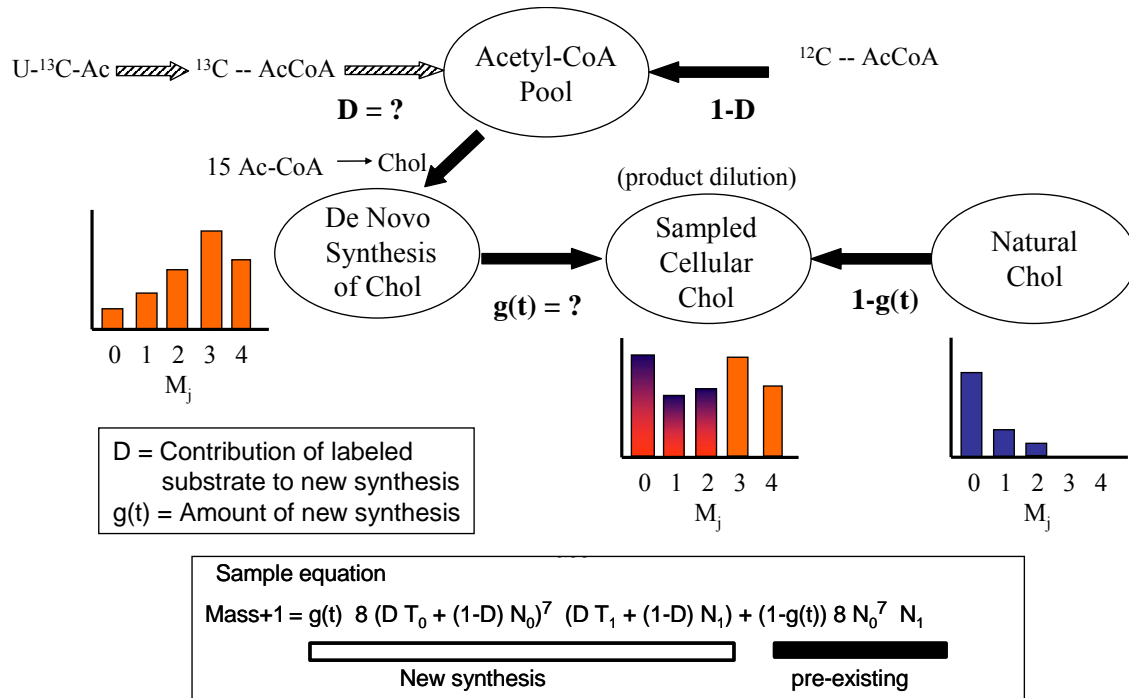
Figure 3.1: Isotopomer Spectral Analysis (ISA) estimation of lipogenic fluxes. Uniformly labeled [U-^{13}C]-acetate is fed to hepatocytes and absorbed through active transport to join the cytosolic AcetylCoA pool, where D represents the fraction of labeled to total Acetyl CoA in the cytosol. Cholesterol is in turn synthesized from this pool, forming molecules with distinct isotopomer spectrum from those existing at natural abundance in the cell. We sample cellular cholesterol to estimate parameter g(t), the fractional synthesis of labeled cholesterol to total cholesterol synthesized.

3.3. Applications to in vivo and clinical settings

The above described methods rely on the concept of a polymerization reaction to estimate gluconeogenesis. While they have generated useful results for cell culture system, they present difficulties when applied to in vivo settings, in particular due to issues of tissue heterogeneity and concentration gradients for the tracer molecule studied. We describe hereforth two methods that have gained wide acceptance for the measurement of hepatic glucose production fluxes in vivo and are considered the state of the art against which our own methodology will be compared. The first method, known as the Landau method, relies on deuterium incorporation at two different positions into the glucose molecule to estimate the fraction of gluconeogenesis contributing to hepatic glucose production using deuterated water. The second method pioneered by Malloy and Sherry, utilizes complementary information from [U-^{13}C]-propionate, [1,6-^{13}C$_2$]-glucose and deuterated water tracers through ^{13}C and ^{2}H NMR spectroscopy to measure fluxes and assess the metabolic state of perfused livers and humans directly.

3.3.1 Landau method

Deuterated water tracer is a water molecule with two deuteriums substituting the place of hydrogens for a chemical structure of ^{2}H$_2$O (or D$_2$O). In many ways, deuterated water is an ideal stable isotope tracer as it can freely traverse multiple body compartments to reach homogeneous enrichment at cellular, tissue and organ levels minimizing possible zonation effects observed with small molecule tracers [133]. Other research uses of deuterated water include serving as a solvent for aqueous samples undergoing ^{1}H NMR analysis.

In metabolic research, deuterated water has found multiple applications since its discovery and purification in 1935 by Harold Urey. Its initial use for estimation of total body water involves the application of a known quantity of deuterated water and subsequent measurement of plasma

water enrichment after isotopic equilibration. Deuterated water is also used in combination with doubly labeled water ($^2H_2^{18}O$) in the calculation of basal metabolic rate in humans [142]. Through tracking of ^2H enrichment, deuterated water has been used as a tracer to simultaneously track turnover of multiple pathways such as protein turnover, triglyceride turnover and *de novo* lipogenesis [106, 133]. We focus on the development of stable isotope methodology for assessing fractional gluconeogenesis from deuterated water.

The initial report from Landau describing determination of fractional gluconeogenesis was based on previous observations of gluconeogenesis rates using ^3H_2O [143]. Rognstad and colleagues noted that when administering tritiated water in vivo, tritium label would manifest in carbon 6 of the glucose molecule during its synthesis from pyruvate. This is due to the fact that, when ^3H_2O was administered, tritium exchanges with protons on carbon 3 of the pyruvate molecule, which in turn becomes carbon 6 of glucose through gluconeogenesis. On the other hand, tritium from ^3H_2O exchanges with carbon 2 of glucose both via gluconeogenesis and glycogenolysis. Therefore, the fraction of gluconeogenesis to total glucose production, or *fractional gluconeogenesis*, can be directly measured by the enrichment at carbon 6 of glucose given the specific activity of ^3H_2O in plasma as determined by the enrichment of carbon 2 in the glucose molecule. The use of tritiated water for measurement of fractional gluconeogenesis however was hampered by the large doses of ^3H_2O necessary to achieve sufficient incorporation into glucose for a precise measurement.

Landau initially reported the use of this stable isotope tracer deuterated water (^2H_2O, D_2O) as a means to circumvent the limitations on the radioactive dose of tritiated water necessary for gluconeogenesis measurements [111]. A critical observation regards the measurement of enrichment in carbon 6 of the glucose molecule, which underestimates gluconeogenic production from glycerol. Landau and colleagues further updated this protocol to measure the ratio of enrichment of labeled hydrogen at glucose carbon 5 as a direct measure of the contribution of gluconeogenesis with

respect to total glucose production measured by labeled hydrogen enrichment at carbon 2 [144]. From a methodological standpoint, this study required the development of derivatization techniques for the glucose molecule that conserved deuterium enrichment in carbons 5 and 2 of the intact glucose molecule. Deuterium enrichment at carbon 2 was assayed through preparation of the hexamethylenetetramine derivative of glucose, while deuterium enrichment at carbon 5 was determined by conversion of glucose to xylose and further oxidation to formaldehyde containing the enriched deuterium at carbon 5.

The main assumptions of Landau methodology involve equilibration of body water at the predetermined deuterium level. This has been demonstrated in multiple physiological settings including humans [145] In addition, important assumptions involve the equilibration of the isomerization reactions where deuterium is incorporated into the glucose molecule. As shown in Figure 3.2, deuterium enrichment at C2 is derived from the isomerization catalyzed by the phosphoglucoisomerase reaction, described by the dashed black square. There is good evidence for equilibration of this reaction rate, including their own data for deuterium enrichment of 0.5% in six human subjects, the researchers found deuterium equilibrations associated with glucose carbon 2 in the range of 0.324-0.452% after 14 hours, increasing to 0.417-0.507% after 42 hours. These values were consistently lower than the enrichments observed in urinary water for similar timepoints. Similarly, the enrichment in C5 is catalyzed by triose phosphate isomerase reaction with water at its source, and that this reaction is at equilibrium per previous research [111]. In addition, the researchers assume trivial the contribution of glucose cycling that could increase the percent of gluconeogenesis estimated since their results agree well with NMR methods measuring glycogen content that directly found this assumption to be true [146].

Using this methodology, Landau and colleagues calculated the contribution of gluconeogenesis to hepatic glucose production in healthy human subjects. Tracer was dosed in a

manner simulating a primed infusion, with initial ingestion of five ^2H_2O doses consisting of 1.0 g/kg body water, spaced in 45 minute intervals to reach a total dose of 5.0 g/kg body water and initial enrichment of 0.5%. Subsequently, patients ingested only replacement water containing 0.5% deuterium enriched water to maintain body water enrichment at the desired 0.5% level. The separation of doses is necessary to avoid side effects of deuterated water ingestion in the form of vertigo. In this context the researchers estimated the fractional gluconeogenesis contribution to total glucose production ranging from 23-42% after 24 hours fasting, and 59-84% after 42 hours fasting. These reports are consistent with previous data using NMR that measured glycogen content in the liver and showed that gluconeogenesis accounts for 65% of glucose production after a 24 hour fast in man [146]. Landau and colleagues continued using the developed methodology for the in vivo, clinical assessment of metformin effects in hepatic glucose production of diabetic patients [147] and to analyze the effects of obesity and Type 2 Diabetes in impairing gluconeogenesis and glycogenolysis response to insulin [148].
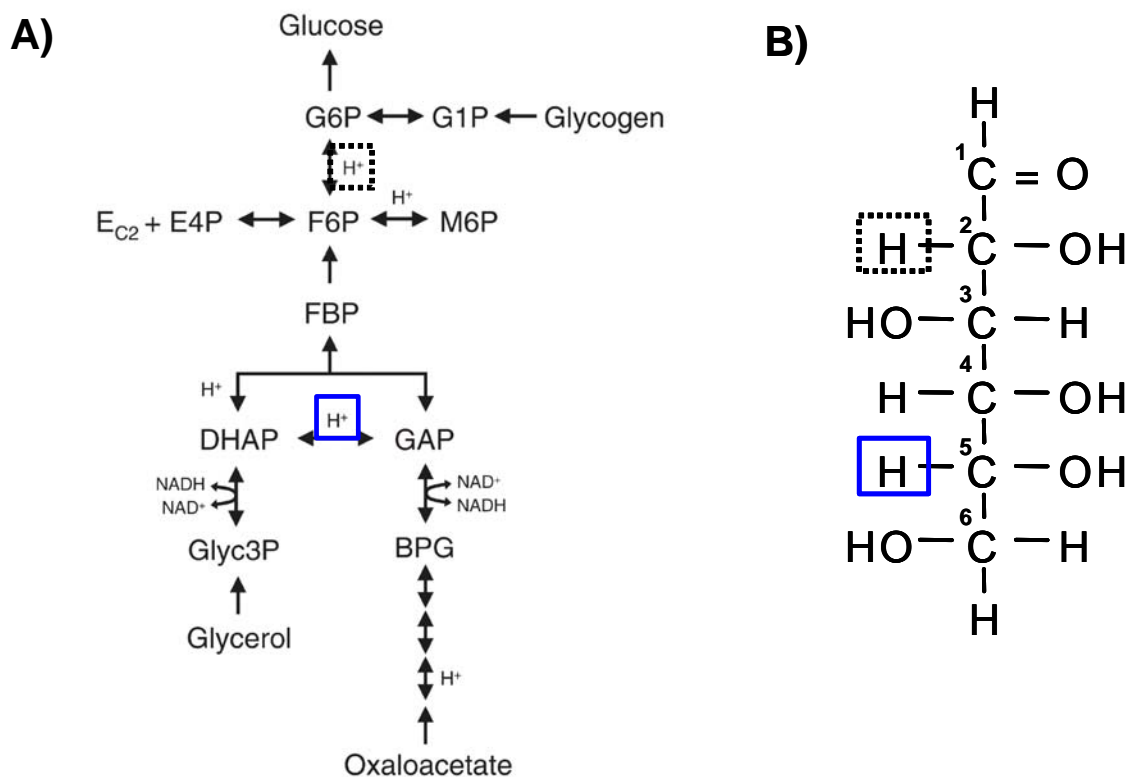
Figure 3.2: Schematic of Landau method. A) Incorporation of deuterium at the triose phosphate isomerase reaction (solid blue box) manifests as enrichment in the hydrogen atom at C5 in the resulting glucose molecule. Correspondingly, incorporation of deuterium at the phosphoglucoisomerase reaction (dashed black box) corresponds to deuterium enrichment in carbon 2 of the glucose molecule, assuming equilibrium with body water. B) Glucose molecule representation of the expected labeling patterns from gluconeogenesis and total glucose production. The ratio of deuterium enrichment in C5 over the enrichment in C2 gives the relative contribution of gluconeogenesis to total glucose production. G6P, glucose-6-phosphate; G1P, glucose-1-phosphate; E4P, erythrose-4-phosphate, F6P, fructose-6-phosphate; M6P, mannose-6-phosphate; FBP, fructose-1,6-bisphosphate; DHAP, dihydroxyacetone phosphate; GAP, glyceraldehydes-3-phosphate; Glyc3P, glycerol-3-phosphate; BPG-bisphosphoglycerate.

The most important contribution of Landau's methodology stems from its simplicity and accessibility of estimation of gluconeogenesis from plasma glucose measurements at safe, low deuterated water enrichments without the need for highly specialized equipment involving NMR. One important disadvantage of this method is that the chemical transformations needed to preserve ^{2}H enrichment at the carbons, in particular the HMT derivative of glucose, require specialized training for analytical determination of deuterium enrichment in glucose. Through this thesis, we used novel, yet simple, derivatizations of the glucose molecule in order to recover the positional information for enrichment of ^{13}C and ^{2}H experiments at every carbon and non-labile deuterium in the glucose molecule, as described in detail in Chapter 4. Therefore, we can use the information of positional deuterium enrichment at carbon 5 and carbon 2 to calculate fractional gluconeogenesis in the same manner as proposed by Landau. As such, the Landau method will form the basis for our combined multi-labeled tracer methodology through measurement of deuterium enrichment in C2 versus C5 for estimation of fractional gluconeogenesis. This measurement, in combination with [6,6-D$_2$]-glucose dilution and a unique [U-^{13}C, D$_5$] glycerol tracer enrichment enables the measurement of absolute contributions of distinct metabolic branches contributing to hepatic glucose production.

3.3.2 Integrated NMR methods

We briefly alluded to the use of NMR to measure hepatic glucose fluxes in vivo in the previous sections. This section details the current state of the art of using NMR measurements for the determination of hepatic glucose production fluxes. Following the developments in NMR by Shulman and colleagues, several groups continued expanding its use by developing techniques for multidimensional NMR analysis of metabolism including isotopes as ^{2}H, ^{13}C, ^{31}P and others. Several noteworthy examples include the aforementioned study by Rothman and colleagues in which human

patients were subject to a prolonged fast and upper gluconeogenic metabolism was assessed by simultaneous glucose production measurement by dilution of [^{3}H]-glucose, noninvasive ^{13}C NMR for hepatic glycogen content and MRI for liver volume. Using these measurements, the authors calculated fractional gluconeogenesis indirectly by subtraction of glycogenolysis from total hepatic glucose production, and obtained estimates of 64% after a 22 hour fast, 82% after a 46 hour fast and 96% percent after 64 hours fast. This tour de force combining radioactive and NMR tracer methodologies opened the door to multiple possibilities explored by these groups, including ^{31}P NMR analysis of diabetic patients and their insulin resistant offspring to demonstrate noninvasively that defects in oxidative phosphorylation metabolism are found in the condition of insulin resistance prior to the development of overt Type 2 Diabetes [31, 32, 47]. These technologies remain critical to the assessment of in vivo metabolic rates relating glucose production, but require intervention in the form of tracer injection for hepatic glucose calculation. Glycogen content measurement as described in this study is noninvasive and provides a reasonable alternative to partially reconstruct hepatic glucose production in vivo in patients.

Within the realm of integrated NMR methods, the efforts of Burgess, Malloy and Sherry stand out as attempting to integrate data obtained from parallel experiments incorporating ^{2}H and ^{13}C NMR. The foundation of this method lies in ^{13}C labeling of intermediary metabolism through the use of ^{13}C-labeled propionate as a tracer [129, 149, 150]. The administration of [1,2-^{13}C$_2$]-propionate to perfused rat livers or humans results in carbon backbone enrichment in glutamate and in the glucose molecule, which is in turn converted to gluconate for ^{13}C NMR analysis. Through the use of a simple metabolic model, the authors derived ratio expressions for the enrichment of glutamate C2 and C3, as well as gluconate C1 and C2 and subsequently glucose production [149]. This work presented a ^{13}C isotopomer analysis using a stable isotope tracer dosed orally, and was soon taken to the clinic for testing in humans.

In subsequent work, Malloy, Sherry and colleagues utilized the simultaneous dosing of oral [U-^{13}C]-propionate, ^2H_2O and [1,6-$^{13}C_2$]-glucose for calculation of a total of seven central metabolism fluxes [151]. These fluxes included hepatic glucose production, glycogenolysis, glycerol uptake to gluconeogenesis, triose phosphate uptake into gluconeogenesis, phosphoenolpyruvate carboxykinase, phosphoenolpyruvate anaplerosis and Acetyl-CoA incorporation into citrate. The calculation of the aforementioned fluxes relied on measurements of deuterium enrichment of plasma glucose in combination with ^{13}C enrichment of urinary glucuronate C5 and phenylacetylglutamine C2.

Several key assumptions underlie this method, represented schematically in the metabolic diagram in Figure 3.3. The first assumption deals with equilibration of body enrichment of water, which has been previously shown to hold for the Landau method as described in the previous section. This assumption impacts the second assumption of this method regarding incorporation of deuterium into the TCA cycle, which occurs at the isomerization reaction catalyzed by fumarase as shown by the green atom incorporating in Figure 3.3. Lastly, the authors assume that ^{13}C labeling occurs in the TCA cycle, as propionate is incorporated into succinate through propionate carboxylation as shown by the pink three carbon molecule incorporating into the succinyl-CoA pool. The [1,6-$^{13}C_2$]-glucose tracer is chosen to complement the expected carbon enrichment patterns of glucose from propionate tracing, and in turn allow calculation of endogenous glucose production by serial measurement and dilution. In this way, the researchers can normalize their relative flux values obtained through the use of deuterated water and [U-^{13}C]-propionate to absolute glucose production rates.
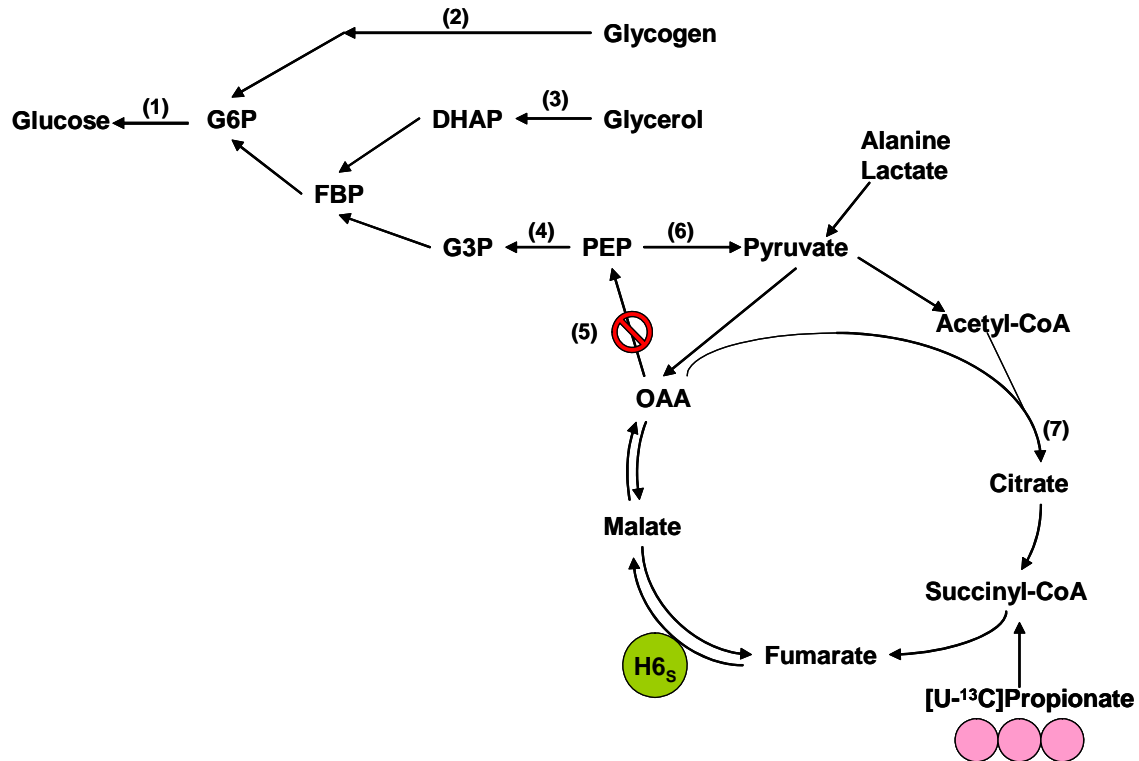
Figure 3.3: Schematic for integrated NMR methods. The reaction network presented encompasses upper gluconeogenesis, lower gluconeogenesis and the TCA cycle. The primary assumption in this method regards the separation of ^{13}C enrichment from the TCA cycle from [U-^{13}C]-propionate at the succinyl-CoA pool, along with the incorporation of deuterium in the malic enzyme reaction Figure adapted from [33, 151].

Despite the relatively simple ratio expressions utilized, the chosen fluxes provide substantial coverage of major regulatory metabolic checkpoints in central metabolism and paint a meaningful picture of the metabolic phenotype present in the tested patients (Figure 3.3). Their results confirm measurements of roughly equal contributions of gluconeogenesis and glycogenolysis to endogenous glucose production in 16 hour fasted humans [146]. Furthermore, they find evidence for zonation of the [U-^{13}C]-propionate tracer that explains obtained differences in the enrichment of hepatic glucose and glutamine produced from oxaloacetate. From the summary of the data, the authors conclude that a comprehensive metabolic profile of gluconeogenesis and the TCA cycle in humans may be obtained from the combination of three different stable isotope tracers and multidimensional NMR analysis of blood and urine samples. However, they point out that the limited sensitivity for metabolite detection in NMR required them to use at least 20 mL of plasma glucose, and suggest that improvements in sensitivity for NMR analysis are needed if this method is applied for metabolic analysis in children. This is one particular area where developing a methodology based on GC-MS can improve the available measurements for enrichment that enable comprehensive metabolic flux reconstruction of glucose production.

Utilizing the developed multinuclear NMR method, Malloy, Sherry and colleagues continued to integrate ^{2}H and ^{13}C NMR for comprehensive analysis of glucose and TCA cycle metabolism. The group showed equivalency of the estimates of fractional gluconeogenesis in humans obtained from measurements of deuterium enrichment at C5 and C2 measured by either ^{2}H NMR or GC-MS [152]. In terms of physiology, the group has carefully analyzed the metabolic effects of multiple genetic and biochemical alterations related to hepatic glucose production. For instance, a recent study shows the effects of gluconeogenic substrate availability on the observable fluxes of the TCA cycle and gluconeogenesis. In perfused mouse livers isolated from fed mice, changing the lactate/pyruvate ratio from the basal 10:1 to 1:10 increases the production in gluconeogenesis from the PEP pool

[153]. This manipulation alters the redox state of the glucose production pathway and suggests a strong metabolic flux link between TCA cycle and glucose production through PEP. In addition, the group has characterized several transgenic strains of animals that show defects in their gluconeogenic phenotype. Additionally, recent analysis of the PGC-1α -/- knockout mouse showed reduced gluconeogenic flux from PEP despite expressing normal levels of gluconeogenic enzyme transcripts by RT-PCR. The mice also showed reduced flux through the TCA cycle and mitochondrial fatty acid β oxidation with corresponding decreases in the expression of TCA cycle and fatty acid oxidation genes. Collectively, these results suggest that the decrease in gluconeogenesis on the PGC-1α -/- mouse result secondary to decreases in fatty acid oxidation and TCA cycle flux. Another example of this analysis involves the sequential analysis of decreased hepatic levels of PEPCK in perfused livers of multiple transgenic mice, as shown by the stop sign in Figure 3.3 [33]. Using the combined, multinuclear NMR strategy described previously, the researchers correlate the level of PEPCK enzyme expression with flux estimates of gluconeogenesis from a series of mice with 100, 80, 30, 10 and 0% PEPCK protein content, and show non-linear decrease in PEPCK flux. Intriguingly, their analysis suggests that PEPCK does not control gluconeogenic flux as determined by flux control coefficient calculations. The integrated NMR methods presented in this section provide an array of opportunities for detailed metabolic characterization of hepatic glucose metabolism, and represent the state of the art regarding non-invasive reconstruction of intermediary metabolism.

3.4 Objectives from current work

Given the previous background in the use of stable isotope tracer work for reconstruction of hepatic glucose metabolism, we would like to frame the developed methodologies in this thesis in perspective with the relevant literature cited earlier. The objectives of this thesis can be stated directly as follows:

- Integrated use of ^{13}C and ^{2}H tracer enrichment using GC-MS
- Gluconeogenic flux modulation from glycerol by glucose-6-phosphatase in vitro
- Combination of [U-^{13}C, D$_5$]-glycerol, [6,6-D$_2$] glucose and deuterated water as tracers for in vivo flux analysis of glucose production.
- Metabolic flux analysis in vivo without catheterization of mice
- Preserved gluconeogenic flux distribution in a transgenic model of hepatic insulin resistance

First, our developed methodologies make use of simultaneous administration of multiple isotopic tracers combining both ^{13}C and ^{2}H enrichment for calculation of key fluxes though an integrated data-driven model. Several definitions are at hand with regards to the use of multiple tracers. *Parallel* tracers will be hereforth used to describe tracers utilized in different instances of the same experimental condition. Results from parallel tracer experiments provide complementary metabolic information about the metabolic system studied, and are *integrated* computationally into a proposed metabolic model through software platforms such as METRAN. *Combined* tracers will be defined as the use of multiple tracers within the same experimental condition. The presented integrated NMR methods in Section 3.3.2 are examples of combined tracer use resulting in ^{13}C, ^{2}H labeled glucose subsequently analyzed through multinuclear NMR. Lastly, we define *multi-labeled tracers* as the inclusion of multiple stable isotopes within a single tracer molecule, for example in the case of [U-^{13}C,D$_5$]-glycerol. We expand these concepts in Chapter 5 in presenting our own developed methodology in detail.

In order to develop our tracer methodology for in vivo flux analysis of glucose production, we first tested our ability to reconstruct hepatic glucose production fluxes in vitro. We performed extensive studies in primary mouse hepatocytes that led to the selection of glycerol and water as the tracers of choice to reconstruct hepatic glucose metabolism [13]. In these preliminary experiments, we prepared a gluconeogenic precursor-rich medium and performed parallel tracer experiments with cultured mouse hepatocytes for 8 hours in order to observe incorporation of label onto the glucose molecule through gluconeogenesis. We substituted the precursor of interest with its stable isotope-labeled counterpart as shown in Figure 3.4, which included [U-^{13}C]-acetate, [U-^{13}C]-glutamine, [U-^{13}C]-glycerol, [D$_5$]-glycerol and D$_2$O. We present the isotopomer spectrum obtained for secreted glucose in the aldonitrile pentaacetate derivative fragment at m/z 287 in the side panels, with the control condition for unlabeled glucose in the lower left-hand panel and the schematic metabolic network for upper gluconeogenesis studied in the center panel.

In this system, [U-^{13}C]-acetate is a poor gluconeogenic precursor, as shown by the absence of enrichment over natural abundance in the upper left-hand panel of Figure 3.4. The lack of incorporation of acetate into glucose can be explained since mouse hepatocytes, like human hepatocytes, lack the ability to reduce Acetyl-CoA back to pyruvate through enzyme pyruvate synthase. [U-^{13}C]-glutamine as a gluconeogenic tracer causes deviation from natural abundance enrichment consistent with incorporation into the glucose molecule as shown in the left middle panel of Figure 3.4. However, this tracer does not reach isotopic steady state in the time scale of the experiment performed, and would be an inconvenient tracer from which to assess multiple conditions of glucose production modulation. [U-^{13}C]-glycerol as a tracer shows a distinctive pattern of incorporation, in which we observe significant enrichment in the M3 and M6 isotopomers of the glucose molecule consistent with incorporation of 1 or 2 glycerol subunits into the backbone of the resulting glucose molecule. As shown in the right top panel of Figure 3.4, these enrichment

signatures constitute the basis for the algebraic expressions for which MIDA and ISA calculate parameter *f*, for fractional gluconeogenesis [136]. [D_5]-glycerol on the other hand, shows significant enrichment over that of natural abundance, but the glucose enrichment patterns are not clear in the same way as those for [U-^{13}C]-glycerol. Here, computational integration from a comprehensive model such as METRAN becomes an invaluable tool in which to reconstruct metabolic fluxes. Lastly, deuterated water at 10% enrichment causes significant incorporation of deuterium in the resulting glucose molecule which requires detailed understanding of the deuterium transitions inherent in the metabolic network studied. This experiment allowed us probe the effects of using multiple tracers to integrate isotopomer data generated from ^{13}C and ^{2}H tracers incorporation computationally using GC-MS analysis of glucose enrichment.

Furthermore, this experiment motivated us to consider the use of glycerol as a potential tracer to elucidate detailed gluconeogenic fluxes in vitro. Glycerol as a gluconeogenic tracer shows excellent uptake by mouse hepatocytes, and the atom transitions in each of the reactions in this pathway are well documented in textbooks and literature [82]. In addition, administering glycerol as a tracer permits the careful estimation of this compound's contribution to hepatic glucose production which can be used to estimate for the contribution of lipolysis to gluconeogenesis. Glycerol has been estimated to contribute 10-30% to glucose production in special circumstances in vivo [144]. However, the use of glycerol as tracer for estimation of gluconeogenesis through MIDA has been questioned for its ability to overestimate gluconeogenesis [138, 139]. We circumvent these difficulties by estimating fractional gluconeogenesis from deuterated water as described in section 3.3.1, and strictly using the information obtained from glycerol to elucidate its contribution to glucose production and reaction reversibilities that exchange deuterium with the glucose molecule.
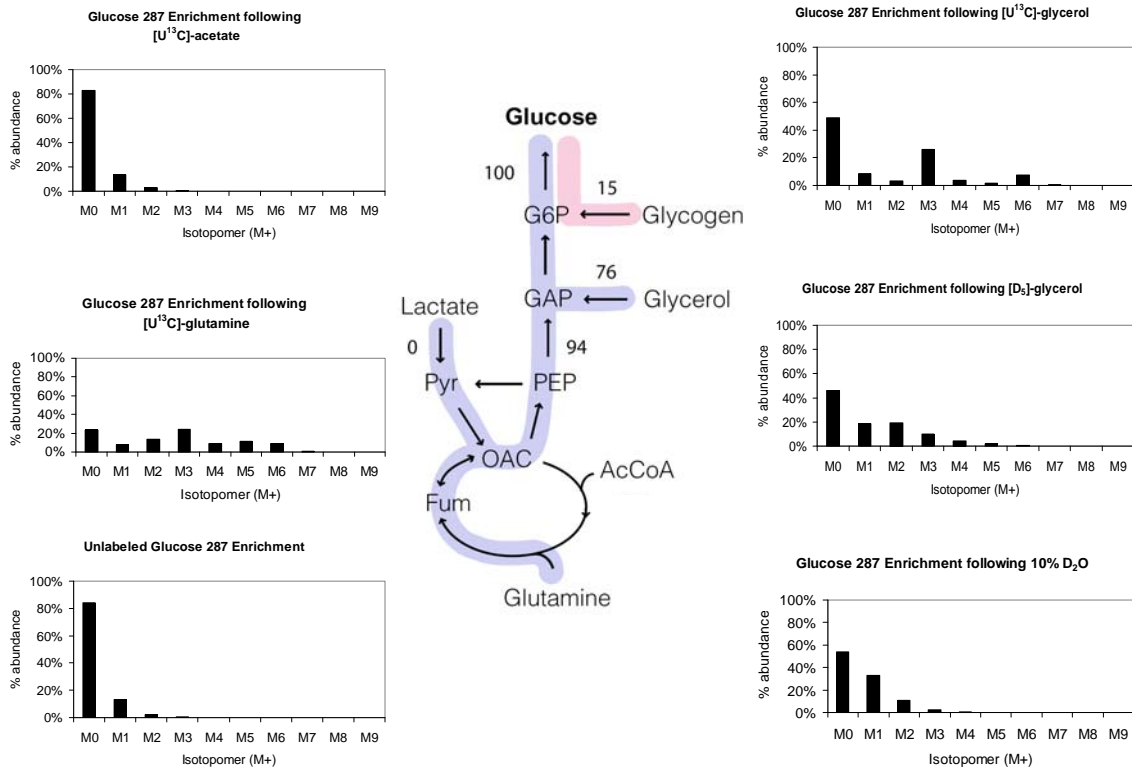
Figure 3.4: Tracer selection for glycerol and deuterated water. Primary mouse hepatocytes were isolated from a single BL6 mouse, attached in collagen coated plates and incubated overnight prior to addition of tracers in chemically identical, gluconeogenic precursor-rich medium. Blue represents glucose production from gluconeogenesis, pink represents glucose production from glycogenolysis.

The choice of glycerol as a tracer for measuring gluconeogenesis is controversial. There are several reasons for this choice from theoretical, experimental and practical considerations. The first reason deals with the size of the plasma pools of each metabolite necessary to reach a predetermined enrichment level in vivo. Plasma lactate circulating concentration in mice is approximately 1 mM, plasma pyruvate concentration is approximately 0.1 mM and plasma glycerol concentration is approximately 0.3 mM [139] Therefore, in order to reach a determined enrichment of lactate in plasma, infusion rates for the tracer species need to be three times as high as those of glycerol given similar uptake rates by peripheral tissues. Since the enrichment of the precursor molecule determined the resulting concentration of the enriched species to be detected, this aspect is critical in determining signal to be detected in plasma. Furthermore, concentrations of plasma lactate are subject to large variations due to anaerobic respiration by muscle. In addition, comparative analysis of for rate of appearance from glucose [2-^{13}C] glycerol versus [3-^{13}C]-lactate or [1-^{13}C]-lactate found glycerol to be a more efficient tracer with which to label glucose from the triose phosphate pool [136] Pyruvate on the other hand, would be an ideal substrate in which to analyze gluconeogenesis in terms of the size of the circulating pool in plasma. However, pyruvate is the common metabolite for tissues for generation of ATP via the TCA cycle, and body uptake of pyruvate by muscle is significantly greater than glycerol uptake, therefore limiting the amount of circulating pyruvate available for liver uptake and gluconeogenesis. When using MIDA for estimation of gluconeogenesis, both lactate and pyruvate have been shown to correctly estimate gluconeogenesis over glycerol substrates [139]. In spite of these limitations, we opted to continue working with glycerol as a tracer given its favorable uptake properties in hepatocytes, well known atom transition biochemistry, and physiological significance with regards to lipolytic conditions.

In our in vitro work described in Chapter 4, we used parallel dosing of deuterated water, [U-^{13}C]-glycerol and [D$_5$]-glycerol in cellular systems capable of *de novo* glucose production, to assert the

metabolic flux distribution of upper gluconeogenesis. In this way, we found significant metabolic differences between the cellular models, specifically H4IIEC3 cells, primary mouse hepatocytes and primary rat hepatocytes. In addition, we used an array of perturbations known to affect glucose production in vivo in order to examine their effects towards upper gluconeogenesis flux redistribution. One set of perturbations involved the presence of hormones insulin and glucagon, shown in section 2.2.3 to affect glucose production by regulating specific enzymes of hepatic glucose production. The second set of perturbations involved the presence and absence of glycerol as a gluconeogenic substrate, which is preferentially utilized by hepatocytes as a gluconeogenic substrate unaffected by PEPCK activity. In this setting, we find our results reveal several principles of the glucose bioreaction network with respect to flux distribution. First, in all cellular systems studied gluconeogenesis dominated the relative flux distribution of hepatocyte glucose production. Second, we observed physiologic changes in fractional gluconeogenesis when modulating glucose production through the action of hormones insulin and glucagon. Third, in the presence of glycerol as a gluconeogenic substrate, G6Pase was identified as the enzyme controlling the glucose production phenotype, whereas PEPCK had a secondary role in determining glucose production.

We adapted the stable isotope tracer methods developed to in vivo glucose production of upper gluconeogenesis in Chapter 5. The motivation of this transition involves the assessment of hepatic physiology and the effects of tissue interactions that would be absent from our in vitro systems. In order to maximize the amount of enrichment information obtained by dosing glycerol as a gluconeogenic precursor, we custom ordered a novel [U-^{13}C, D$_5$]-glycerol tracer that would allow higher mass isotopomers to contribute to the analysis of glucose backbone biosynthesis as well as reversibilities of reactions that exchange hydrogen with body water, as shown in Figure 3.5B. Our in vivo flux analysis method described in Chapter 5 is based on the combination and simultaneous application of this unique [U-^{13}C, D$_5$]-glycerol tracer in combination with [6,6-D$_2$] glucose and

deuterated water as shown in Figure 3.5A, where the entry points for ^{13}C label are shown in red boxes and the entry points for deuterium labeling are shown in blue boxes. This combination of tracers has not been described in literature previously, although the use of the second and third tracers is common individually [110, 144]. We used [6,6-D$_2$]-glucose (Figure 3.5B, bottom) to calculate hepatic glucose production by a standard dilution method, which in turn will normalizes the relative fluxes obtained from ^{13}C and ^{2}H tracing of glucose, as shown in the schematic metabolic network of upper gluconeogenesis in Figure 3.5A. The logic of using this tracer is similar to the use of [1,2-^{13}C$_2$]-glucose by Jones and colleagues in their integrated ^{13}C, ^{2}H flux analysis strategy using NMR. Lastly, the incorporation of deuterated water into the glucose molecule can be used to calculate fractional gluconeogenesis by the Landau method, as shown by the solid and dashed boxes in Figure 3.5C. Our collection of unique glucose fragments for the glucose molecule allows positional analysis to distinguish deuterium enrichment occurring from [6,6-D$_2$] glucose or deuterated water enrichment in the same glucose molecule shown in Figure 3.5C. In this way, different deuterium tracers provide complementary information regarding the fate of multiple biochemical processes that contribute to the production of glucose. We were thus able to reconstruct upper gluconeogenic fluxes in greater detail than reported previously, while simultaneously measuring the total contribution of hepatic glucose production, fractional gluconeogenesis and glycerol contribution to glucose production.
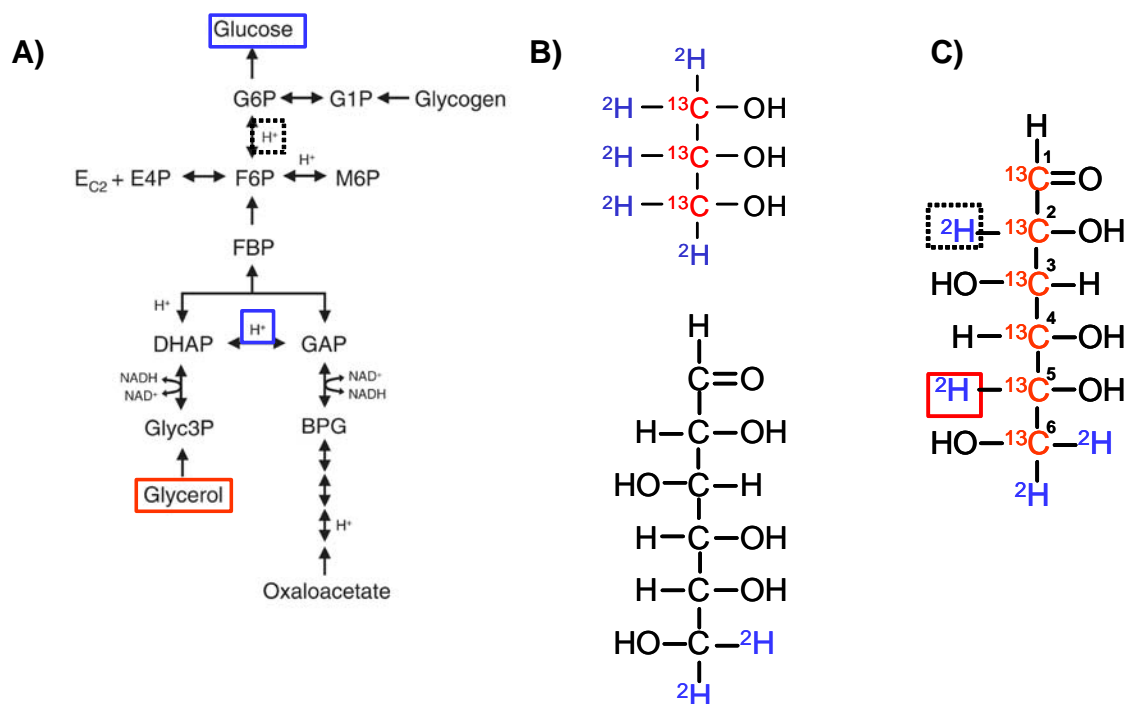
Figure 3.5: Combined, multi-tracer GC-MS method developed in this thesis. We simultaneously dose glycerol, deuterated water and glucose as sources of ^{13}C and deuterium respectively. A) Entry points in upper gluconeogenic metabolism of the aforementioned tracers B) Chemical Structure of [U-^{13}C,D$_5$]-glycerol and [6,6-D$_2$]-glucose, with red indicating ^{13}C label and blue indicating ^{2}H label C) Resulting glucose molecule, incorporating ^{13}C labeling in its carbon skeleton, deuterium labeling from D$_2$O at C2 and C5, and deuterium labeling from glucose at C6.

There are inherent assumptions in using any tracer methodology in vivo to elucidate glucose production fluxes, and our methodology is no exception. Our assumptions can be stated directly as follows

- Pseudo-metabolic steady state
- Isotopic steady state
- Deuterated water labeling constant
- No scrambling of glycerol tracer
- No TCA cycle usage of tracer signal

We address these assumptions through experimental design, mass spectrometric inspection of plasma glucose and glycerol enrichment as well as additional biochemical tests, and revisit them in detail in Chapter 5 as part of the development of in vivo flux analysis of hepatic glucose production.

Infusion of the novel $[U-^{13}C, D_5]$-glycerol and $[6,6-D_2]$ glucose was accomplished by adapting the use of a miniosmotic pump procedure to administer glycerol over extended periods of time without the need for indwelling catheter implantation in animals [115]. This method is advantageous as it does not require extensive small animal surgery expertise for catheterization, and is well tolerated by mice. In recent publications, this method has been used to study gluconeogenic metabolism in transgenic mouse models deficient in PPARα [115], Pten [154] and lipin [154]. This method simulates a constant infusion of glycerol tracer and pumps achieve steady state flow rates within 3-6 hours of implantation, thereby allowing for observation of turnover in metabolic pools in the range of minutes to hours such as hepatic glycogen.

We tested the response of metabolic fluxes to physiological and pathophysiological perturbations in the metabolic pathway of glucose production in Chapters 5 and 6 respectively. These studies serve a twofold purpose. First, they allow verification of the estimated metabolic parameters such as hepatic glucose production, fractional gluconeogenesis and glycerol contribution to glucose with previous reports in literature. In Chapter 5, we are most interested in the effects of

normal perturbations known to affect glucose fluxes substantially, such as the presence of energy regulating hormones insulin and glucagon, feeding and fasting physiology as well as the availability of gluconeogenic precursors in the form of glycerol. Second, these studies provide flux responses as the integration of genetic, protein and metabolite level information [155, 156].

We present in Chapter 6 the in vivo flux analysis of the liver-insulin receptor knockout (LIRKO) mouse as a paradigm of the metabolic flux effects of hepatic insulin resistance in the development of Type 2 Diabetes. The LIRKO mouse is a transient tissue-specific model of hepatic insulin resistance, which displays marked hyperinsulinemia, glucose intolerance and the inability to suppress hepatic glucose production in the context of a euglycemic-hyperinsulinemic clamp. At the same time, these mice are nearly normoglycemic and preserve their hepatic glucose production flux nearby the level of their wild-type counterparts despite markedly increased levels of gluconeogenic enzymes expressed in their livers. Our in vivo metabolic flux analysis of this transgenic mouse shows decreased hepatic glucose production with respect to the wild-type mouse, but also preserved relative flux distribution and usage of gluconeogenic substrates. These similarities demonstrate the remarkable ability of this transgenic mouse to adapt their glucose metabolic demand by modulating glucose uptake in muscle, and additionally points to mechanisms such as gluconeogenic substrate availability and glucose-6-phosphatase modulation of metabolite levels for indirect and direct effects of insulin action that would be unobservable through genetic or proteomic assessment.

In summary, we introduced the current methodologies for flux analysis of hepatic glucose production using stable isotope tracers, including combinatorial methodologies such as MIDA, ISA, Landau and NMR methods to assess isotopomer distributions and describe the basis for our developed combined, multi-labeled method for in vivo flux analysis. These methodologies provide a rich array of tools from which to probe hepatic physiology, both in the normal state and in abnormal states induced by genetic or environmental manipulations. In addition, we set the stage for

the comparison of the results presented in the upcoming chapters. In the next section, we present the initial in vitro studies reporting the use of parallel use of glycerol and deuterated water tracers for the estimation of upper gluconeogenic fluxes. Through the integrated use of deuterium and carbon-13 tracers, we reconstruct upper gluconeogenesis fluxes and reversibility in cellular systems capable of de novo glucose production. Using metabolic flux as a marker of cellular physiology, we analyze metabolic perturbations relating to hormones insulin and glucagon as well as substrate availability and put forth a hypothesis for flux regulation by glucose-6-phosphatase in the presence of glycerol.

CHAPTER 4: Integrated ^{13}C, ^{2}H flux analysis using multiple isotopic tracers: Application to determination of primary hepatocyte glucose production from glycerol measured by mass spectrometry

4.1 Introduction

The liver plays a critical role in regulating glucose homeostasis through modulation of *de novo* glucose synthesis and glycogen storage to balance daily changes in nutritional and hormone status. In a post absorptive physiology scenario, both hepatic glycogenolysis and gluconeogenesis contribute to endogenous glucose production (GP) and homeostasis [144, 146]. Gluconeogenesis is the pathway responsible for *de novo* production of glucose from 3-carbon intermediates, as well as the target metabolic pathway of action for antidiabetic therapy [147]. The physiologic role of this pathway emerges during a prolonged fast, when tissues such as the brain and red blood cells preferentially require glucose to meet their metabolic demands. After liver glycogen is depleted, gluconeogenesis increases dramatically in the presence of glucagon as well as counterregulatory hormones such as epinephrine [42]. The substrates for gluconeogenesis include alanine and glutamate from protein breakdown, lactate from muscle anaerobic respiration and glycerol from triglyceride breakdown. The major source of carbons for gluconeogenesis is the common pool of oxaloacetate via the TCA cycle, contributing approximately 50% of the glucose carbons in the fed state and nearly all carbons after a prolonged fast [146]. Glycerol can provide a source of carbon in lipolytic conditions, accounting for 3-5% of total glucose production in the postabsorptive state and

increasing to over 20% in a prolonged fast or during parenteral nutrition with liposomes [139, 157]. The demand for these potential carbon sources is closely linked to metabolic pathways such as AcetylCoA oxidation via the TCA cycle and energy generation, and exquisitely regulated through the integrated action of hormones such as insulin and glucagon [39].

Measurement of endogenous glucose production is performed indirectly through static measurements of gene, transcript, protein or metabolite levels along the molecular cascade leading to changes in glucose production. In the fasted state, glucagon acts through its receptor and stimulates the production of second messenger cAMP and propagation of signal to increase the transcription of gluconeogenic enzyme genes. In the fed state, insulin initiates a signaling cascade in hepatocytes by autophosphorylation of the insulin receptor, recruiting of IRS-1, PI3K, Akt, ultimately inhibiting the Foxo1 transcription factor that activates the transcription of gluconeogenic enzyme genes *g6pc, fbp1* and *pck1* [54]. Static measurements include gene expression, protein amount and activity of the three enzymes that catalyze thermodynamically committed reactions: glucose-6-phosphatase (G6Pase), fructose 6-bisphosphatase (FBPase) and phosphoenolpyruvate carboxykinase (PEPCK) [82].

While useful as initial markers, static measurements do not represent the functional cellular operation and are insufficient to assess network component interactions and emergent properties [155]. On the other hand, direct measurements of glucose production involve measurement of carbon or deuterium flux through this pathway. Through the combination of endogenous glucose production measurements with isotope dilution and specific tracer signals, researchers get increasingly complete pictures of the metabolic state of endogenous glucose production and its connection to other energy metabolic pathways, thereby establishing a central carbon metabolism network. Examples includes the measurement of fractional gluconeogenesis through deuterium enrichment from ^2H_2O, which in combination with [6,6-^{2}H]-glucose can estimate absolute rates of

gluconegenesis [144], and the combination of ^{2}H and ^{13}C NMR analysis of plasma glucose and glutamate from simultaneous [U-^{13}C]-propionate, [1,2-^{13}C$_2$]-glucose and ^{2}H$_2$O administration allowed for detailed reconstruction of seven fluxes in central carbon metabolism linking hepatic glucose production and TCA cycle metabolism [151] as described in detail in Chapter 3. Other researchers have utilized [3-^{13}C]-lactate, or [U-^{13}C]-glucose for assessment of endogenous glucose production; however neither of these tracers differentiates glucose produced from glycogen, glycerol or the TCA cycle [158, 159]. These methods remain limited in the number of fluxes described from the gluconeogenic pathway, in particular the contribution of specific gluconeogenic precursors to the total glucose output.

In the present study, we applied multiple stable isotope tracers in parallel, combining ^{13}C and ^{2}H enrichment in an integrated manner to elucidate detailed fluxes of the glucose production pathway in cellular systems capable of *de novo* glucose production. As defined in chapter 3, we will use the word parallel to describe tracers utilized in different instances of the same experimental condition, and integrated computationally. The purpose of the study is to establish a complete picture of upper gluconeogenic metabolism through comprehensive analysis of ^{13}C and ^{2}H enrichment of secreted glucose molecules measured by mass spectrometry. We have applied new computational methods to calculate the fluxes that contribute to total glucose output in the liver in addition to the relative contribution of glycogenolysis to gluconeogenesis, in a framework called Integrated Carbon-Deuterium Flux Analysis (ICDFA) [102, 105, 160]. In particular we asked the question, how do fluxes beyond the glucose-6 phosphatase junction (where the gluconeogenic and glycogenolysis fluxes merge) change due to hormonal regulators of gluconeogenesis such as insulin and glucagon with glycerol as a gluconeogenic substrate? We observe the glucose-6-phosphate reaction as a critical branchpoint for the regulation of gluconeogenic flux in the presence of glycerol and juxtaposing the established view of transcriptional suppression of gluconeogenesis via PEPCK

downregulation. Our experiments establish a comprehensive framework by which to measure gluconeogenic fluxes at a fine resolution to characterize potentially silent metabolic phenotypes that may be contributing to the development of Type 2 Diabetes in the liver.

In our in vitro work described hereforth, we use parallel dosing of deuterated water, [U-^{13}C]-glycerol, [D$_5$]-glycerol and deuterated water in cellular systems capable of *de novo* glucose production, to assert the metabolic flux distribution of upper gluconeogenesis. In order to establish metabolic homogeneity in the cellular systems studied and to propitiate glucose production, we designed our assays to be rich in gluconeogenic precursors. In this way, we found significant metabolic differences between the cellular models studied, specifically H4IIEC3 cells, primary mouse hepatocytes and primary rat hepatocytes. In addition, we used an array of perturbations known to affect glucose production in vivo in order to examine their effects regarding upper gluconeogenesis flux redistribution. The first set of perturbations involved the presence of hormones insulin and glucagon, shown in section 2.2.3 to affect glucose production by regulating specific enzymes of hepatic glucose production. We find H4IIEC3 cells and rat hepatomas to remain sensitive to insulin, as shown by significant decreases in absolute glucose production, by modulating fluxes in upper gluconeogenesis. On the other hand, mouse hepatocytes show relative insensitivity to action of this hormone. The second set of perturbations involved the presence and absence of glycerol as a gluconeogenic substrate, which is preferentially utilized by hepatocytes as a gluconeogenic substrate unaffected by PEPCK activity. In this setting, we find our results reveal several principles of the glucose bioreaction network with respect to flux distribution. First, in all cellular systems studied gluconeogenesis dominated the relative flux distribution of hepatocyte glucose production. Second, in the presence of glycerol, G6Pase was identified as the enzyme controlling the glucose production phenotype, whereas PEPCK had a secondary role in determining glucose production. These results establish the importance of flux determination in vitro to fully characterize the metabolic phenotype

of glucose production, and have potential as assays to uncover therapeutic targets to control excess glucose production in Type 2 Diabetes.

4.2 Materials

Bovine insulin, dexamethasone, glucagon, Dulbecco's modified Eagle's medium powder (DMEM), fetal bovine serum (FBS), and other cell culture reagents were purchased from Sigma (St. Louis, MO). Biochemicals were obtained from Sigma Chemicals (St. Louis, MO) unless otherwise specified. [U-^{13}C$_3$]-glycerol was obtained from Cambridge Isotope Laboratories (Andover, MA). [^{2}H$_5$]glycerol was obtained from Isotec (Miamisburg, OH). Hepatocyte Medium Base was DMEM powder (Sigma) supplemented as described by Block [161]. Hepatocyte Attachment Medium consists of Hepatocyte Medium Base supplemented with 5 nM insulin, 100 nM dexamethasone and 20 mM glucose. Hepatocyte Growth Medium (HGM) consists of Hepatocyte Medium Base supplemented with 1 nM insulin, 100 nM dexamethasone and 20 mM glucose. Medium containing gluconeogenic precursors includes the following substrates: 1 mM pyruvate, 10 mM lactate, 5 mM glutamine, 2 mM acetate and 1 mM glycerol. Hormones, glucose, and fetal bovine serum were added to this base medium as specified.

Antibodies for Western Blotting were provided by New England Biolabs (Ipswich, MA).

Animals - Male C57BL/6 mice were obtained from Taconic (Germantown, NY). Animals were housed in a facility approved by the American Association for Accreditation of Laboratory Animal Care. All animals received humane care in compliance with institutional guidelines. Mice had free access to water and chow *ad libitum* before the study. Mice were between 7 and 12 weeks old and 25-32 g body weight at their time of hepatocyte isolation.

4.3 Experimental Methods

4.3.1 H4IIEC3 Glucose Production Assay

H4IIEC3 cells were purchased from ATCC (Manassas, VA). Our protocol followed that of Fukuhara et al. [162], with the following modifications: H4IIEC3 cells in 12-well plates were preincubated in Dulbecco's Modified Eagle Medium (DMEM) with 5 mM glucose, 10 % fetal bovine serum (FCS), 50 nM cAMP and 100 nM dexamethasone for 24 hours as outlined in Figure 4.1 Cells were washed twice with PBS, and stimulated in gluconeogenesis buffer (glucose-free DMEM-base, 4 mM glutamine, 1 mM sodium pyruvate, 50 μM cAMP and 100 nM dexamethasone) with 1 mM [D_5] glycerol as a label source and any other indicated reagents. After further incubation for 24 hours, we determined the amounts of glucose released into the medium from H4IIEC3 cells. RNA was prepared from cultured cells using an RNEasy Mini-kit (Qiagen) and adjusted to quantitate 100 ng of total RNA. RT-PCR was performed on gluconeogenic genes *g6pc*, *fbp1*, *pck1* and control *actb* using the iScript One-Step RT-PCR kit with SYBR green (BioRad, CA). The primers utilized were as follows: Glucose-6-phosphatase, *g6pc*, anti:5'-CCAGTCCTGGAGTCTTCGTAATT-3' sense: 5'-ATGGAGGAAAGAATGAACGTGCT-3'; PEP carboxykinase, *pck1*, anti: 5'-TTCCTCACTTCCTGGGGCAG-3' sense: 5'-TGCCTCCTCAGCTTGCATATTG-3'; Fructose-1,6-bisphosphatase, *fbp1* anti: 5'-TTCAGCAGCTGGGTCATCTCGC-3' sense: 5'-ATGGTGGACCATGCGCCCTT-3' Actin B, *actb* anti: 5'-CCATCACACCCTGGTCCCTA-3' sense: 5'-ATGGATGACGATATCGCTGCG-3.'

A)

-24 hr   0 hr   Tracer: 1 mM [D$_5$]-glycerol   24 hr

Modulation Media
- DMEM Base
- 5 mM glucose
- 10%FBS, 1% PS
- 50 nM cAMP
- 100 nM Dex

GNG Buffer
- DMEM Base
- 0 mM glucose
- 4 mM Gln, 1 mM pyr
- 50 μM cAMP
- 100 nM Dex

B)

HGM Maintenance
- 5 nM insulin
- 100 nM Dex
- 20 mM glucose
- 7%FBS

HGM Glucose Assay
- 0 mM glucose
- 100 nM Dex
- +/- ins, ggn, dbcAMP
- 10% D$_2$O

-48 hr   -24 hr   0 hr   1 hr   3 hr

Surgery Perfusion   Attach

1 mM pyruvate
10 mM lactate

HAM
- 1 nM insulin
- 100 nM Dex
- 5 mM glucose
- 7% FBS

HGM Modulation
- 1 nM insulin
- 100 nM Dex
- 5 mM glucose
- 7% FBS

Tracers:
- **1 mM [U-^{13}C$_3$]-glycerol**
- **10% ^{2}H$_2$O**

Figure 4.1: Glucose Production Assay Protocols on Adherent Cells. A) Timeline schematic of H4IIEC3 glucose production assay B) Timeline schematic of rat/mouse glucose production assay.

4.3.2 Rat Hepatocyte Experiments

Rat hepatocytes were kindly donated by Linda Griffith at MIT, and isolated by 2-step collagenase perfusion for *in-situ* isolation of rat hepatocytes, based on the method described by Friend [163, 164]. Our attached hepatocyte experiments follow the manner of Block et al. [161], whereby purified cells were suspended in Hepatocyte Attachment Medium (HAM) and seeded in 12-well plates ($6.1x10^5$ cells/well) for 90 minutes at 37°C. Attached cells were washed once with PBS and cultured overnight in Hepatocyte Growth Medium (HGM). After 24 hr incubation at 37°C and 5% CO_2 we washed the attached hepatocytes once with PBS, and subsequently cultured in glucose-free HGM for the purposes of glucose production assays. Concentrations of glucose and lactate were determined by analysis with YSI 2700 Stat Plus glucose/lactate analyzer (YSI Inc., Yellow Springs, OH).

4.3.3 Mouse Hepatocyte Experiments

Mouse hepatocyte isolation - Our hepatocyte isolation protocol is based on Block et al [161] and further developed by Wong [156]. Briefly, the mouse is anesthetized with tribromoethanol (250 mg/kg IP) for the duration of the procedure. The surgeon exposes the intraperitoneal abdominal contents including the liver, portal vein and inferior vena cava. The portal vein is cannulated with a 24.5G catheter, and the liver perfused for 15 minutes at a rate of 7 mL/min with calcium-free perfusion buffer to remove blood from the fibrous liver sac. Mouse euthanasia follows exsanguinations after cutting the inferior vena cava to complete the perfusion circuit. The blanched liver is perfused with collagenase solution (200U/mL) for 10 minutes at 7 mL/min to release hepatocytes from the

extracellular matrix. The digested liver is excised and placed in preservation buffer, where the digested cells are gently scraped from the liver sac, washed and purified with Percoll to remove dead cells and enrich the hepatocyte fraction. At this point cells are counted and viability assessed by Trypan Blue exclusion. Typical viabilities are between 85-90%, with cell yields of 1.0-1.5x10^6 cells/g mouse (25-40x10^6 cells). Isolated hepatocytes were suspended in Hepatocyte Growth Medium (HM) and prepared accordingly for attachment or experiments as described below.

Mouse hepatocyte attached experiments - Our cultured hepatocyte experiments follow the manner of Block et al. [161] with the following modifications. Primary mouse hepatocytes were seeded onto Type I collagen-coated tissue culture plates (BD Biosciences, Bedford, MA) in Attachment medium (Hepatocyte Medium Base supplemented with 1 nM insulin, 100 nM dexamethasone, 7% FBS, and 10 mM glucose). Glucose production experiments used 12-well plates with a density of 6.1 ×10^5 cells/well in 600 μl of Attachment medium. The cells were allowed to attach for 1 hour at 37°C in a humidified atmosphere containing 5% CO_2. Cell were then washed with PBS and cultured in Hepatocyte Maintenance Medium. After 24 hours, cells were washed with PBS and given Preincubation medium with volumes identical to those given for Maintenance medium. After overnight incubation, the cells were again washed with PBS to remove excess glucose and cultured with HGM Glucose Assay medium (100 nM dexamethasone, 0 mM glucose, 10% D_2O) for 1 hr at 37ºC. Depending on the experimental condition, each well was stimulated with 25 nM insulin, 10 nM glucagon, 50 μM dibutyril-cyclic AMP or no hormones (basal). At this point, each well was spiked with a 100x stock of gluconeogenic precursors lactate and pyruvate to a final concentration of 10 mM lactate: 1 mM pyruvate. Again depending on the experimental condition, we spiked [U-^{13}C] glycerol from 100X stock solution to a final concentration of 1 mM. The cells were cultured for the following 2 hours at 37ºC and the supernatants collected and frozen to -80ºC for further

analysis. Concentrations of glucose and lactate were determined by analysis with YSI 2300 Stat Plus glucose/lactate analyzer (YSI Inc., Yellow Springs, OH). The term "insulin sensitivity" was used during comparisons between treatments with insulin in the Assay medium. A change in sensitivity was considered significant if the difference between the glucose produced in the two insulin treatments was significant ($p < 0.05$).

Mouse hepatocyte suspension experiments - Mouse hepatocytes were prepared for primary culture by nonrecirculating 2-step collagenase perfusion, as adapted from Seglen [165] based on the method by Berry [163, 164]. After isolation, cells were washed once with PBS and immediately cultured in glucose-free HGM containing insulin or glucagon at concentrations of 1 nM, 10 nM ,100 nM, 1 μM and 10 μM, in medium containing 10% deuterated water (D_2O) or 1 mM [U-^{13}C]-glycerol as a tracer source and gluconeogenic precursors supplemented as follows: 1mM pyruvate, 10 mM lactate, 5 mM glutamine, 2 mM acetate and 1 mM glycerol. The medium was chemically identical in all conditions, with the labeled counterpart substituted for the indicated gluconeogenic precursor at the time of incubation with tracer. Cells were cultured for 2 hr at 37C in a 5% CO_2 atmosphere, at this time cells were centrifuged for 1 min at 10,000 RPM to remove the cell pellet and freeze the supernatant at -80C.

Western Blots - The integrity of the insulin signaling pathway in mouse hepatocytes was evaluated by Western Blotting for presence and phosphorylation state of key intermediary signaling proteins. Isolated primary cells were attached overnight in Advanced DMEM (GIBCO) with 10% FBS, and serum-starved for the next 6 hours. At this time, the cells were stimulated with 125U insulin (Roche) for 1 hr. Stimulated cells were lysed with lysis buffer and the ensuing cell extract was frozen at -80°C for further analysis. Blots were performed in a Bio-Rad mini Protean system.

4.3.4 Derivatization of glucose

Glucose labeling patterns were determined by GC/MS analysis of aldonitrile pentapropionate, methyloxime pentapropionate and di-O-isopropylidene propionate derivatives of glucose [166]. The fragmentation pattern of these derivatives in the intact glucose molecule is presented in Figure 4.2. For each derivatization 100 µL of sample was deproteinized by addition of 500 µL of acetone (~4°C). The mixture was centrifuged and the supernatant evaporated to dryness under air flow. For aldonitrile pentapropionate derivatization, 50 µL of 2 wt% hydroxylamine hydrochloride in pyridine was added to the dry residue and the sample heated at 90°C for 60 min. This was followed by addition of 100 µL of propionic anhydride and heating at 60°C for additional 30 min. The sample was then evaporated to dryness, dissolved in 100 µL of ethyl acetate and transferred into an injection vial. Methyloxime pentapropionate derivatization deviated slightly from the previous protocol in using methoxyamine hydrochloride instead of aldonitrile hydrochloride. For di-O-isopropylidene propionate derivatization, 500 µL of 0.38 M sulfuric acid in acetone was added to the dry residue and the sample incubated at room temperature for 60 min. 400 µL of 0.44 M sodium carbonate was added to neutralize the reaction, followed by addition of 1 mL of saturated sodium chloride. Di-O-isopropylidene derivatives were extracted by partitioning with 1 mL of ethyl acetate. The upper, organic layer was evaporated to dryness, followed by addition of 150 µL of propionic anhydride in pyridine (2:1 v/v) and heating at 60°C for 30 min. The sample was then evaporated to dryness, dissolved in 100 µL of ethyl acetate and transferred into an injection vial. The fragmentation patterns produced by the union of these methods gives positional information on the labeling of individual carbon and hydrogen atoms in the glucose molecule as seen in Figure 4.2. The

isotopomer distribution of each fragment thus provides a rich data set for the calculation of fluxes contributing to overall glucose output.
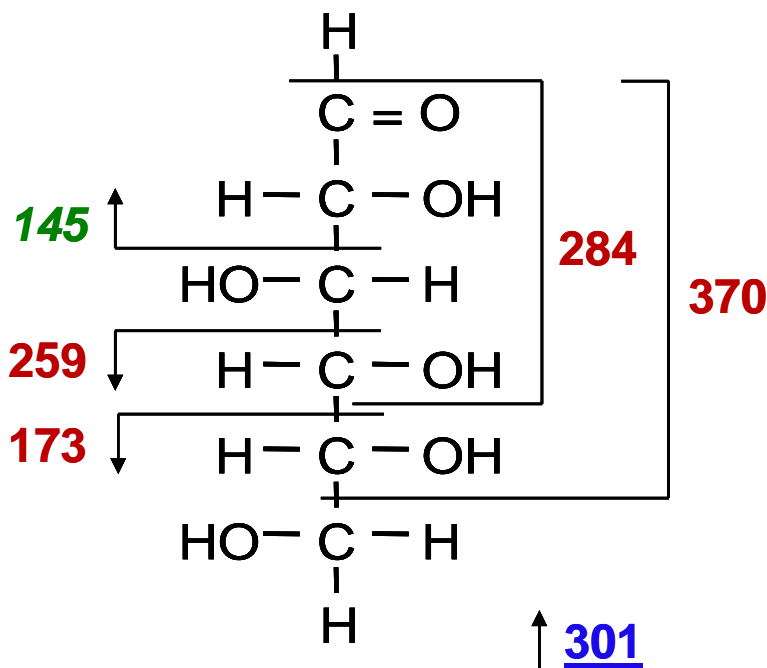
Aldonitrile pentapropionate

Methyloxime pentapropionate

<u>Di-O-isopropylidene propionate</u>

Figure 4.2: Glucose Fragmentation Patterns. The aldonitrile pentapropionate derivative of glucose produces fragments with m/z 173, 259, 284 and 370. The methyloxime pentapropionate derivative of glucose produces a fragment with m/z 145 (italics). The Di-O-isopropyledene propionate fragment of glucose produces a fragment with m/z 301 (underline).

4.3.5 Isotopomer Enrichment Analysis

Gas Chromatography-Mass Spectrometry (GC/MS) analysis for isotopomer enrichment was performed using HP 5890 Series II GC (Gas Chromatograph) equipped with a DB-1701 [30 m x 0.25 mm (inner diameter) x 0.25 μm] capillary column, connected to HP 5971 MSD (Mass Selective Detector) operating under ionization by electron impact (EI) at 70 eV. The mass spectrometer was calibrated using the 'Max Sensitivity Autotune' setting. Helium flow was maintained at 0.737 mL/min by electronic control. The temperatures of the injector and the detector were kept at 250°C and 300°C, respectively. The temperature of the column was started at 80°C for 1 min, increased to 280°C at 20°C/min, and held for 4 min. For analysis of aldonitrile pentapropionate glucose, mass spectra were recorded in the mass range 172-182, 258-268 and 369-379 at 50 scans/sec. The fragment at m/z 173 ($C_{13}H_{16}O_8N$) retains the C5-C6 carbon and hydrogen atoms of glucose, the fragment at m/z 259 retains the C4-C6 carbon and hydrogen atoms of glucose and the fragment at m/z 370 retains C1-C5 carbon and hydrogen atoms of glucose. For the analysis of methyloxime pentapropionate glucose ion intensities were recorded at m/z 145-149 at 50 scans/sec. The fragment at m/z 145 ($C_{13}H_{19}O_7$) retained C1-C2 carbon and hydrogen atoms of glucose. For the analysis of di-O-isopropylidene propionate glucose, mass spectra were recorded in the mass range 301-313 at 50 scans/sec. The fragment at m/z 301 ($C_{13}H_{19}O_7$) retained all six carbon atoms and all seven carbon-bound hydrogen atoms of glucose. Measured intensities were corrected for the contribution of noise (baseline correction), and mass isotopomer distributions were obtained by integration. All mass isotopomer values were expressed as fractional abundances, whereby the sum of all mass isotopomers equals one. All aforementioned fragments were utilized in the integrated analysis of mass spectra for flux analysis in each treatment condition unless otherwise noted.

4.3.6 Computation methods

Metabolic fluxes and their confidence intervals were determined by fitting mass isotopomer abundances of glucose fragments to a detailed gluconeogenesis metabolic network model. The generalized algorithm for MFA was incorporated into our flux analysis tool METRAN. In short, METRAN estimates fluxes by minimizing the difference between the observed and simulated measurements using an iterative least-squares minimization procedure as described in Section 2.3.4 [13]. Briefly, the objective of this routine is to evaluate a set of feasible fluxes that best accounts for the observed isotopomer measurements. At convergence, nonlinear statistical techniques were applied to obtain accurate 95% confidence intervals of fluxes by evaluating the sensitivity of the objective function with respect to fluxes using elementary metabolite unit theory as described previously [13, 102]. Flux validation was accomplished by a statistical test for the goodness-of-fit based on chi-square test for model adequacy, and a normality test for the weighted residuals [105]. To ensure that a global optimum was found, flux estimation was repeated at least four times starting with random initial values. Sensitivity analysis was employed to determine the most important measurements in the estimation of individual fluxes as described previously [13]. All computations were performed with Matlab 6.5 and Matlab Optimization Toolbox (Mathworks, Natick, MA). Flux data are presented as mean ± standard deviations (or 68% confidence interval), unless otherwise noted.

The metabolic network model of upper gluconeogenesis incorporates the reactions listed in Table 4.1. The network model contains two potential gluconeogenic precursors, oxaloacetate and glycerol as seen in Figure 4.3. Oxaloacetate represents a common pool where gluconeogenic precursors lactate, pyruvate and alanine converge. Oxaloacetate is in turn converted to phosphoenolyruvate through an irreversible reaction catalyzed by gluconeogenic enzyme phosphoenolpyruvate carboxykinase (PEPCK). Therefore, the PEPCK flux in our model represents

combined input from precursors lactate, pyruvate, alanine, glutamine and related amino acids and organic acids involved in the tricarboxylic acid cycle. Glycerol enters the pathway through the irreversible reaction catalyzed by glycerol kinase, and is incorporated into the metabolic route via dihydroxyacetone phosphate (DHAP). Glycerol contribution is measured explicitly as part of modeling stable isotope incorporation from glycerol into glucose. Previous work suggests glycerol contributed 3-6% of overall gluconeogenic flux in humans [167]. Reaction reversibility and stereochemistry were assigned based on current knowledge [80, 82] and listed in Table 4.1. For example, it is known that phosphoglucose isomerase (PGI) transfers specifically the pro-R hydrogen at C1 of fructose 6-phosphate (F6P) to the C2 position of glucose 6-phosphate (G6P). Hydrogen exchange with the solvent was also observed for PGI [80, 81, 168]. Malaisse et al. (1990, 1991) reported for a single passage in the direction F6P→G6P, 65% intramolecular hydrogen transfer and 35% hydrogen exchange, and for a single passage in the direction G6P→F6P, 72% intramolecular hydrogen transfer and 28% hydrogen exchange. It is also known that triose phosphate isomerase (TPI) has the same stereochemistry as PGI. Phosphomannose isomerase (PMI), on the other hand, has the opposite stereochemistry, i.e. PMI specifically abstracts the pro-S hydrogen of F6P and exchanges it with the solvent. No intramolecular hydrogen transfer was observed for this reaction, i.e. the hydrogen at C2 of mannose 6-phosphate (M6P) always originates from the solvent. The last five reactions in the model (reactions 17-21) account for hydrogen incorporation/metabolism of oxaloacetate and NADH. Oxaloacetate may incorporate hydrogen atoms at C3 from the solvent in reactions of the tricarboxylic acid cycle, e.g. fumarase, or via alanine aminotransferase. Reactions 17-18 describe hydrogen exchange of the pro-S and pro-R hydrogen atoms, respectively. Our model further includes three explicit sources for NADH hydrogen, i.e. 1,3-biphosphoglycerate via GAPDH (reaction 11), hydrogen exchange with the solvent (reaction 19), and from unlabeled endogenous sources (reaction 20). In this model, all fluxes are expressed as percentages of the glucose output

flux, which was fixed at 100. There are 17 unknown independent fluxes in this model: flux of glycerol and oxaloacetate to glucose (reactions 10 and 16), hydrogen exchange of pro-S and pro-R hydrogen atoms of oxaloacetate with the solvent (reactions 17-18), fractional contribution of the solvent and unlabeled endogenous sources to NADH (reactions 19-20), and 11 reversible reactions.

4.3.7 Statistics

All data were analyzed using a Student's t test (Microsoft Excel) for single comparisons between means from experimental groups. $P < 0.05$ was considered statistically significant. In cases where multiple groups were all compared to a single group, the Dunnett's test for multiple comparisons was applied [169]. $P < 0.05$ was considered statistically significant. Data are presented as means ± standard error unless otherwise noted.
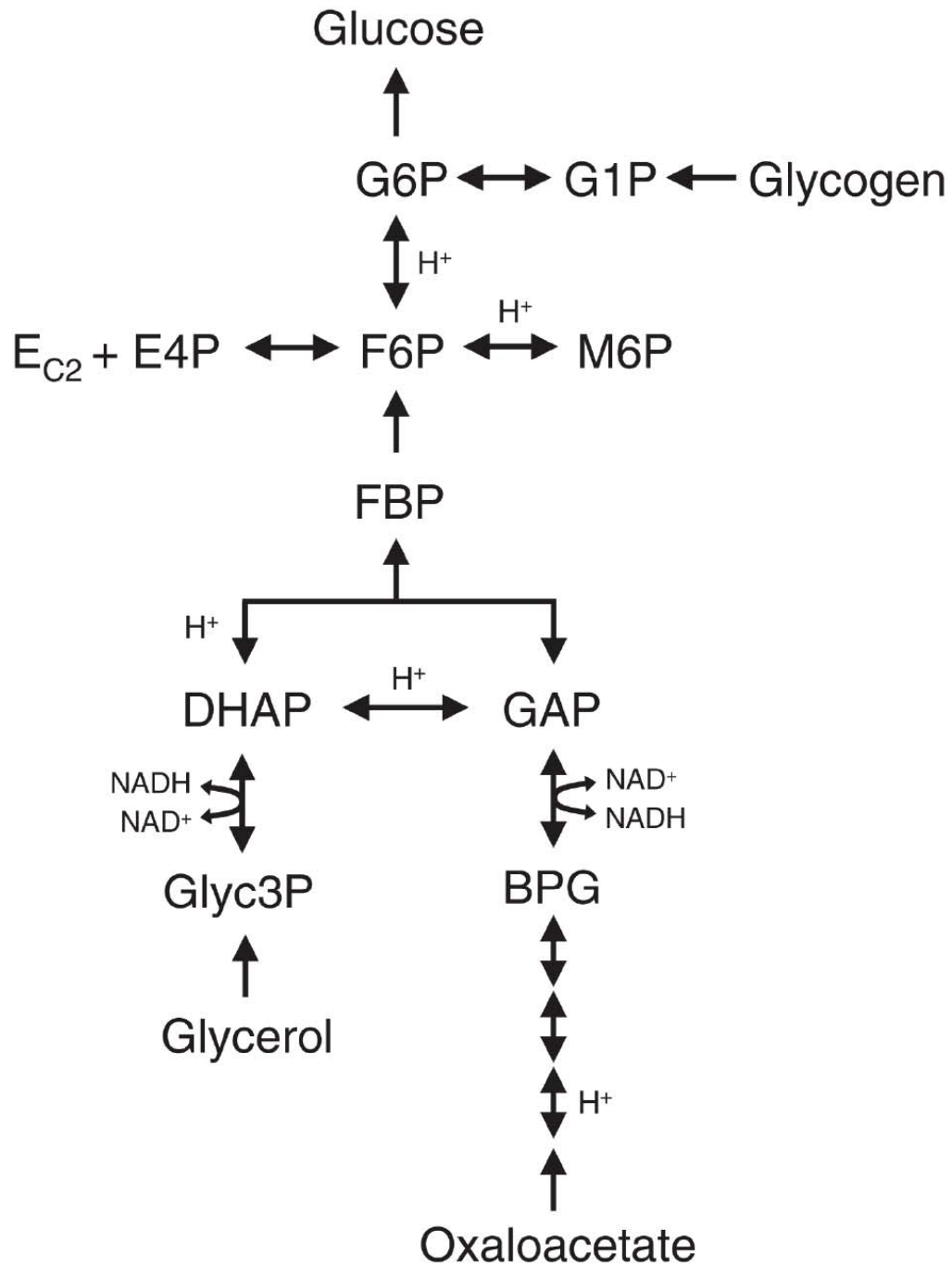
Figure 4.3: Upper gluconeogenesis metabolic network utilized for flux calculations. The corresponding reaction stoichiometry and atomic transitions for network reactions are given in Table 4.1.

Table 4.1: Stoichiometry and atom transformations for gluconeogenesis model incorporated into METRAN

No.	Enzyme	Stoichiometry	Atom transformations*
Upper gluconeogenesis			
1	glucose 6-phosphatase	G6P → Gluc	abcdef → abcdef
2	phosphoglucose isomerase	F6P + 0.3 H ↔ G6P + 0.3 H	abcdef ↔ abcdef
			(70%) C1-H^{proR} ↔ C2-H
			(30%) C1-H^{proR} + H ↔ H + C2-H
3	fructose 1,6-bisphosphatase	FBP → F6P	abcdef → abcdef
4	aldolase	DHAP + GAP ↔ FBP + H	abc + def ↔ cbadef
			(DHAP)C1-H^{proS} ↔ H
5	triose phosphate isomerase	DHAP + 0.3 H ↔ GAP + 0.3 H	abc ↔ abc
			(70%) C1-H^{proR} ↔ C2-H
			(30%) C1-H^{proR} + H ↔ H + C2-H
6	phosphomannose isomerase	F6P + H ↔ M6P + H	abcdef ↔ abcdef
			C1-H^{proS} + H ↔ H + C2-H
7	transketolase	F6P ↔ E-C2 + E4P	abcdef ↔ ab + cdef
Glycogenolysis			
8	phosphorylase	Glycogen → G1P	abcdef → abcdef
9	phosphoglucomutase	G1P ↔ G6P	abcdef ↔ abcdef

* For each compound carbon atoms are identified using lower case letters to represent successive carbon atoms of each compound.

Table 4.1 Continued. Stoichiometry and atom transformations for gluconeogenesis model incorporated into METRAN

No.	Enzyme	Stoichiometry	Atom transformations*
Glycerol metabolism			
10	glycerol kinase	Glyc → Glyc3P	abc → abc
11	glycerol 3-phosphate dehydrogenase	Glyc3P ↔ DHAP + NADH	abc ↔ abc
			C2-H ↔ NADH
Lower gluconeogenesis			
12	glyceraldehyde 3-phosphate dehydrogenase	BPG + NADH ↔ GAP	abc ↔ abc
			NADH ↔ C1-H
13	phosphoglycerate kinase	3PG ↔ BPG	abc ↔ abc
14	phosphoglycerate mutase	2PG ↔ 3PG	abc ↔ abc
15	enolase	PEP + H ↔ 2PG	abc ↔ abc
			H ↔ C2-H
16	phosphoenolpyruvate carboxykinase	OAC → PEP + CO2	abcd → abc + d
Hydrogen incorporation into oxaloacetate and NADH from endogenous sources			
17		OAC + H → OAC + H	abcd → abcd
			C3-H^{proS} + H ↔ H + C3-H^{proS}
18		OAC + H → OAC + H	abcd → abcd
			C3-H^{proR} + H ↔ H + C3-H^{proR}
19		H → NADH	H → NADH
20		unlabeled → NADH	H^{unlabeled} → NADH
21		NADH → other	NADH → H^{other}

* For each compound carbon atoms are identified using lower case letters to represent successive carbon atoms of each compound.

4.4 Results

4.4.1 H4IIEC3 flux distribution shows altered glucose metabolism, insulin sensitivity

H4IIEC3 hepatomas conserve regulation of expression of gluconeogenic enzymes, the insulin receptor and its signaling pathway, thus allowing suppression of cellular glucose production by insulin and survival in glucose-free medium [170, 171]. Our glucose production assay for H4IIEC3 cells was based on that of Fukuhara, [162] as seen schematically in Figure 4.4A. The goal of this study was to replicate the suppression of glucose production by physiologic amounts of insulin in a cell line assay. Cells were cultured in a preincubation medium for 24 hours to stimulate transcription of gluconeogenic genes by the prevailing low glucose environment as well as the presence of glucagon second messenger analog dibutyril-cyclic AMP. The primary gluconeogenic substrates in this medium include amino acids in trace concentrations, 4 mM glutamine and 1 mM pyruvate, which were maintained constant through both preincubation and labeling periods. During the isotopic labeling period, cells were grown in the presence of gluconeogenic stimulator cAMP and labeled gluconeogenic precursor 1 mM $[D_5]$-glycerol over 24 hours. Even in these conditions, the maximum production of glucose from these cells is minimal and of the order of 80 nmol/million cells/day, suggesting metabolic redirection into glycogen and subsequent consumption for energy metabolism.

The suppression of glucose production by insulin is shown in Figure 4.4A. We observe significant decreases in glucose production at insulin concentrations as low as 0.03 nM, while suppression saturates after treatment with 0.1 nM insulin. Stimulation with similar concentrations of glucagon did not produce significant changes in glucose production, acting as controls since these cells lack the glucagon receptor [171]. In order to maximize the metabolic effect of insulin in

suppressing glucose production, we chose to study further the untreated condition as well as the maximum 1 nM insulin treatment. RT PCR-analysis of gluconeogenic genes under these conditions showed a significant 99.8% suppression of the *g6pc* transcript relative to expression of the *actb* gene, while the levels of *fbpc* and *pck1* remain unchanged as seen in Figure 4.4B. Therefore, the measurement of glucose release suggests suppression of gluconeogenesis consistent with the observed decrease in accumulated glucose.

In order to compare the effects of insulin suppression on gluconeogenic fluxes, we performed metabolic flux analysis through administration of 1 mM $[D_5]$-glycerol as tracer during the hormonal stimulation phase. *A priori*, we expected glycerol to contribute significant proportion of gluconeogenesis carbon, and contribute as a gluconeogenic substrate in addition to glutamate and pyruvate present in the incubation medium. Fractional gluconeogenesis (i.e., the fraction of HGP contributed to gluconeogenesis) has been estimated using deuterium labeled glycerol tracer in perfused livers, which additionally revealed release of glycerol molecules from the liver [138]. Glucose release in the basal condition was modest despite the presence of superphysiological pyruvate and glutamate, we opted to dose excess gluconeogenic substrate in the form of $[D_5]$-glycerol in order to obtain measurable deuterium enrichment in the glucose molecule. The isotopic enrichment of the secreted glucose molecule in this experiment yields reaction fluxes assuming isotopic steady state through computational analysis of the enrichment patterns of fragments with m/z 173, 259, 284 and 370, presented in Appendix 4.A. The resulting relative fluxes were adjusted to the absolute amounts of glucose production in untreated condition (Figure 4.5). Net reaction fluxes are presented as percent relative to glucose output in the basal untreated condition. The simulation and flux estimation results in a sum of squares of residuals of 12.9, indicating an accepted fit for the glucose model proposed with respect to the presented data.

In the basal condition, we observe that glycogenolysis contributes 89% of total glucose output. Gluconeogenesis in turn contributes 11% of flux to the production of glucose, a small amount that would be consistent with a small amount of glucose production in this cellular assay. We found interesting that the pattern of labeling in the secreted glucose suggests selective uptake of [^{2}H$_5$]-glycerol over substrates in the oxaloacetate pool, even in the presence of superphysiological amounts of both substrates. We observed similar preference for glycerol uptake in glucose production in mouse and rat hepatocytes under all conditions tested. Glycerol contributes almost all of the carbon flux to provide deuterium enrichment to the triose phosphate pool.

Insulin treatment of H4IIEC3 hepatomas results in a significant 70% decrease (p<.05) in glucose production from baseline, as shown in Figure 4.5. As in the untreated case, glucose flux is mostly derived from glycogenolysis. The relative flux from glycogenolysis in both treated and untreated conditions shows this metabolic branch to have a sizable contribution to the overall glucose production in this system. In the untreated case, 89% of total glucose produced comes from glycogenolysis, while the scaled counterpart in the insulin-treated condition represents only 24% of total glucose production in the untreated condition. We observe a significant change in the percent contribution of gluconeogenesis to glucose production in the presence of insulin, decreasing from 11% to 5% in the insulin-treated cells and corresponding to the expected effects observed through gene transcript experiments. In relative terms however, this difference does not manifest a change in fractional gluconeogenesis, which in the untreated condition contributes approximately 10% to the total glucose flux, while in the insulin-treated condition fractional gluconeogenesis represents a 17% contribution to the total glucose output. In both treatment cases, glycerol is a major substrate for glucose production in H4IIEC3 cells, whereas lactate, pyruvate and amino acids do not contribute significantly to the cellular production of glucose in vitro. Glycerol could potentially blunt fractional

gluconeogenesis differences observable in the absence of mass effects, and we explore these possibilities further in our rat hepatocytes experiments.

Despite the obvious metabolic differences with liver physiology, the H4IIEC3 glucose release assay could become a convenient screen for drugs or compounds that alter liver glucose output, as well as an analysis tool to dissect the genomic and flux effects of antidiabetic agents that target this pathway [170] From the obtained flux distribution through [^{2}H$_5$]-glycerol uptake, the metabolism in these cells resembles that of the PEPCK knockout phenotype in the preferential use of glycerol as a gluconeogenic substrate [172]. The limitations of this assay include the lack of liver cell lines that conserve the necessary machinery to produce glucose and to modulate this production. There are also experimental considerations in maintaining the gluconeogenic phenotype of these cells over extended culture times, and indeed we observed loss of glucose production after subsequent passages of the cellular population. The lack of a functional glucagon receptor precludes the study of increased glucose production that would be present in a diabetic patient unless stimulatory intermediates are used. In order to assess flux effects of both insulin and glucagon in a single cellular system, we pursued using primary rat and mouse hepatocytes as model cellular systems of *de novo* glucose production.
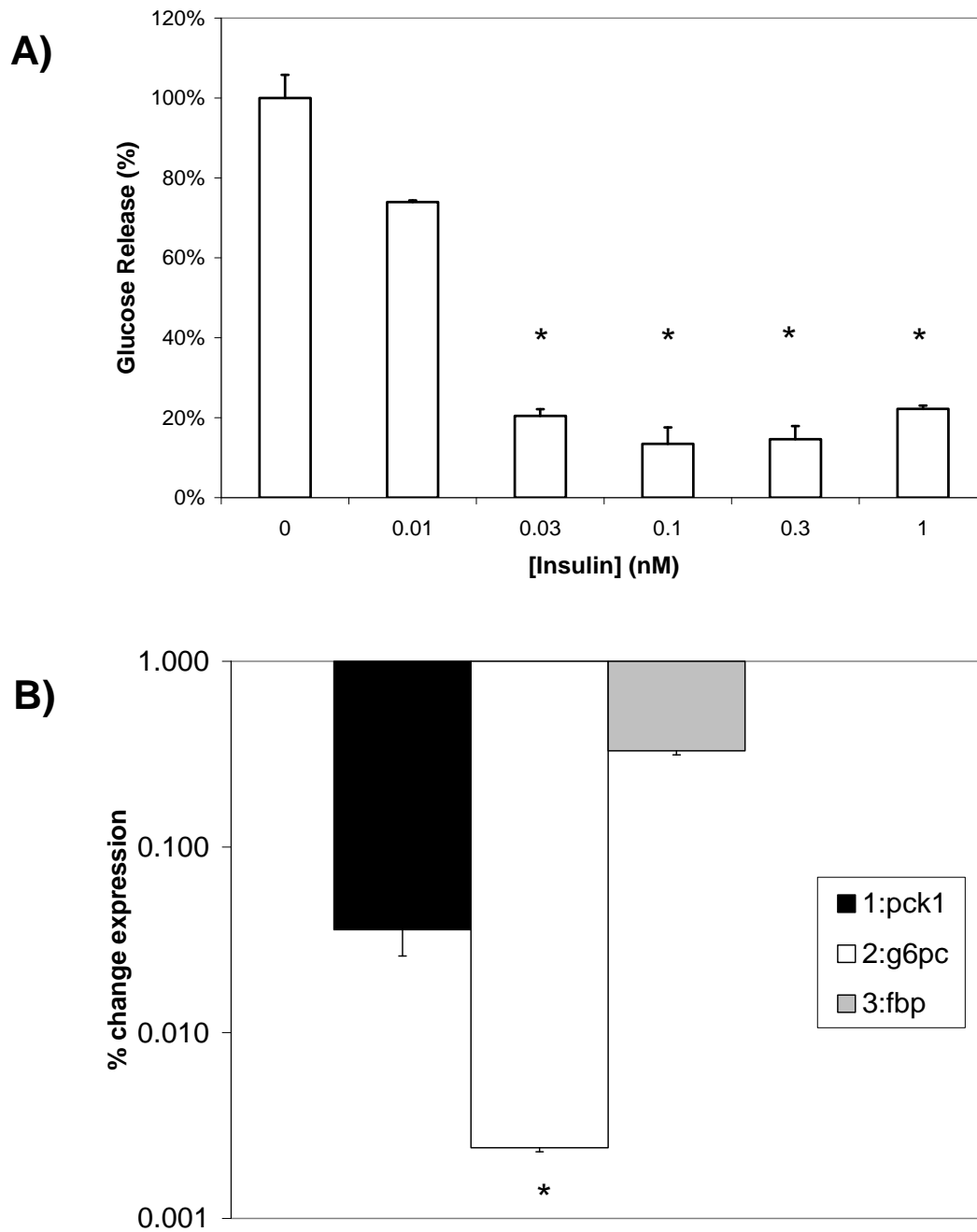
Figure 4.4: Insulin downregulates glucose production in H4IIEC3 hepatomas. A) Insulin dose response for glucose release in H4IIEC3 cells (n=2-4. * = p<.05). B) RT-PCR analysis of gluconeogenic gene expression, expression changes expressed as ratio of treated (1 nM insulin) versus untreated condition, normalized to *actb* expression (n=3, * = p<0.05).
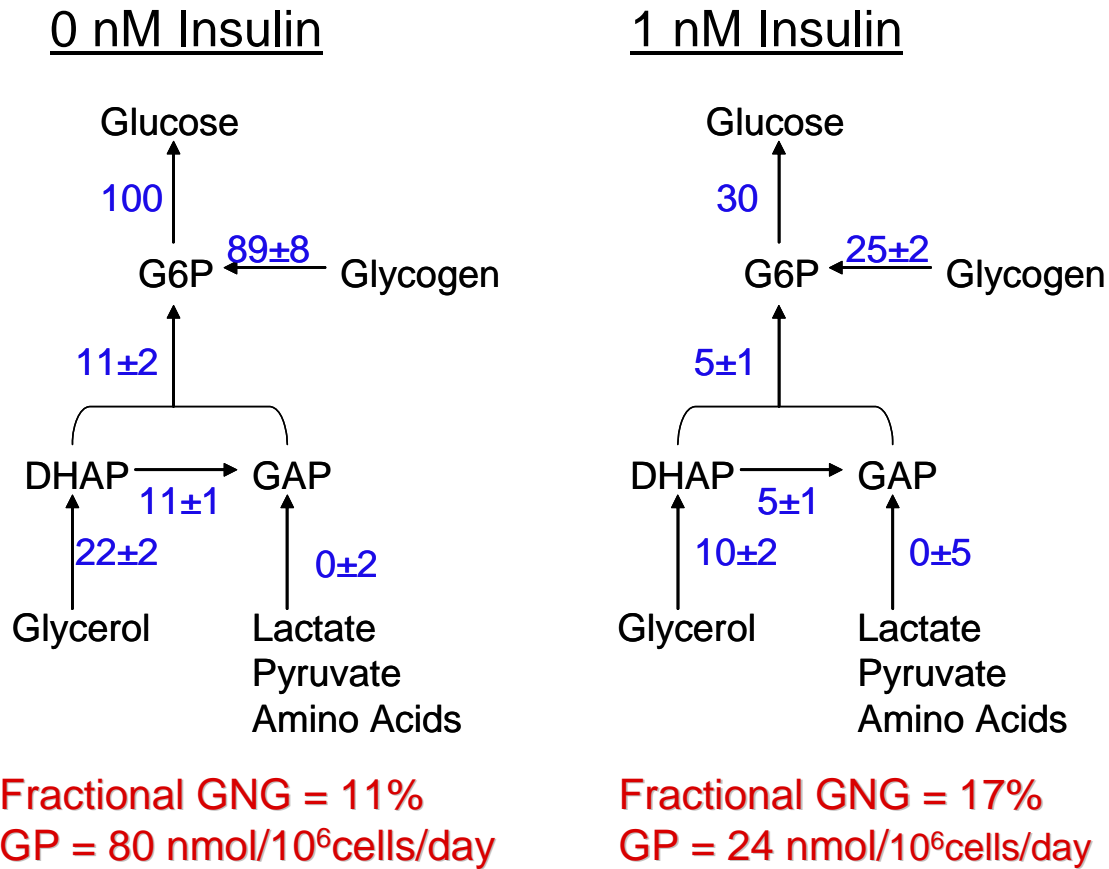
Figure 4.5: Metabolic flux analysis of H4IIEC3 hepatomas reveals upper gluconeogenesis regulation at glucose-6 phosphate junction. Net fluxes are presented normalized to glucose output in the untreated condition at their adjoining reactions with 68% confidence intervals. Fractional gluconeogenesis is calculated as the ratio of gluconeogenesis flux over total glucose production. The accepted fit combines glucose fragments with m/z 173, 259, 284 and 370. GP = glucose production, G6P = glucose-6-phosphatase, DHAP = dihydroxyacetone phosphate, GAP = glyceraldehyde phosphate.

4.4.2 Primary rat hepatocytes modulate gluconeogenic flux physiologically by redistributing fluxes around glucose-6-phosphate

In light of H4IIEC3 glucose production data, we sought to investigate glucose production in rat hepatocytes, as they remain the most accepted cellular model for studying liver physiology [164]. Rat hepatocytes were attached in collagen-coated plates to promote their survival and recovery from perfusion and reconstitute their metabolism distinctly from a stress response. We designed an attached hepatocyte experiment to test the production of glucose over a 2 hour period in the presence of stable isotope 10% deuterated water or 1 mM [U-^{13}C]-glycerol after addition of gluconeogenic substrates lactate/pyruvate at 10:1 ratio, shown in Figure 4.1B. Unlike the previous experimental design, the short term nature of exposure to gluconeogenic substrate in the form of lactate and pyruvate is expected to drive gluconeogenesis without significant transcription of gluconeogenic enzymes. The lactate/pyruvate ratio of 10:1 is meant to emulate the proportion of these substrates in plasma; however the total concentration of the lactate pool in our experiment is approximately tenfold that of plasma concentration. Preliminary experiments showed these cells to be remarkably metabolically active in culture, and we observed glucose production rates of approximately 10 nmol/million cell/hour, consistent with production rates studied previously [164]. High concentrations of gluconeogenic substrates were necessary to operate in a metabolic regime where lactate and pyruvate were present through the duration of the experiment and avoid significant usage of labeled glucose as a substrate for energy generation. Other researchers have adapted perfusion apparatuses to administer physiological amounts of substrates in vitro in order to maintain metabolic steady state [139].

We were most interested in assessing hormonal effects of insulin and glucagon on flux distributions through upper gluconeogenesis in a metabolic system more reflective of liver

physiology. Hormonal treatment was dosed over an acute period of three hours after changing medium to a glucose-free environment. In addition, pyruvate and lactate were spiked after 1 hour in the glucose free-medium and in the presence of hormonal modulators to permit glucagon-mediated activation of gluconeogenesis through second messenger cAMP and insulin-mediated suppression of glucose production through increased glycogen deposition [124]. These conditions do not reflect physiology, but allow for the absolute determination of glucose output rates from the cultured cell population. In addition, previous work with primary hepatocytes had shown that the uptake of glycerol tracer and production of glucose in glucose free-medium result in linear concentration time courses, thus indicating that a metabolic steady state is reached [13]. Under these culture conditions, we observed a distinct response from rat hepatocytes to suppress their glucose production by 81% (p<.05) in the presence of 25 nM insulin, while the same cells increased their total glucose output by 241% in the presence of 10 nM glucagon from the untreated condition (Figure 4.6).

The first brachpoint for modulation of glucose production occurs at the glucose-6-phosphatase junction, where glycogenolysis and gluconeogenesis meet. The isotopomer spectrum of glucose secreted by these cells is presented in Appendix 4.A and was used to estimate the relative gluconeogenic flux as shown in Figure 4.7. The metabolic reconstruction utilized to obtain these fluxes combined glucose fragments at m/z 173, 259, 284 and 370. Comparing the insulin, basal and glucagon-treated hepatocytes, we note a trend in the amount of glycogen utilized by the cells whereby the fractional contribution of gluconeogenesis increases steadily from 35 to 55 to 76%. These changes agree with prior results on primary rat hepatocytes on the modulation of gluconeogenesis by insulin and glucagon due to direct effects on gluconeogenic enzymatic activity [123]. Rat hepatocytes increase their utilization of available substrates to produce glucose as expected from classic liver physiology, but the extent to which the gluconeogenic flux increases with hormonal stimuli in the presence of glycerol in primary hepatocytes is undocumented.

Next, we asked whether availability of uncommon gluconeogenic substrates would affect the hormonal response observed in rat hepatocytes. In particular, glycerol was selected as a substrate for two reasons: methodologies for flux reconstruction have often used glycerol as a chosen substrate given its significant uptake into glucose [120], and glycerol by itself would be present in lipolytic conditions where gluconeogenesis would be expected to be active in the absence of insulin. The addition of glycerol to glucose-free culture medium significantly increased the production of glucose under all treatment conditions ($p<0.05$) as observed in Figure 4.6. Glycerol concentration in plasma is approximately 0.1 mM, thereby we used superphysiological concentration of this substrate following the above logic regarding potential depletion. Hormonal response trends are conserved in the presence of glycerol, such that insulin treatment decreases glucose production by 22% from basal and glucagon increases net production by 27%. In net terms however, these increases show similar magnitude to the changes observed in glycerol-free culture medium, corresponding to a decrease in the production rate by 16.4 nmol/10^6 cells/hr in the presence of insulin and an increase of 19.1 nmol/10^6 cells/hr in the presence of 25 nM glucagon. The magnitude of these changes in glucose production lowers the statistical significance of the trend observed, however without eliminating the physiological trends for glucose production modulation by insulin and glucagon.

In order to identify the substrate sources that contribute to the aforementioned changes of gluconeogenesis in the presence and absence of glycerol, we can inspect the detailed flux distributions obtained through ^2H_2O incorporation as shown in Figure 4.7. Here, net fluxes are presented normalized with respect to the basal production of glucose using 10% deuterated water as a tracer. The net fluxes of gluconeogenesis modulate nonlinearly in the absence of glycerol, from 7% to 55% to 259% when comparing insulin-treated, basal and glucagon treated flux distributions. In the absence of glycerol, rat hepatocytes derive all their carbons from the oxaloacetate pool represented by pyruvate in this model. Glycogenolysis in the absence of glycerol is stoichiometrically

fixed by gluconeogenic output, and consequently reflects the nonlinear increase in glucose production observed. Therefore, hormonal influence over glucose production flux propagates in a geometric manner throughout the network as set by glucose-6-phosphatase demand. This manner of flux demand regulation can have significant implications for the ability of hepatocytes to accommodate gluconeogenic substrate bolus demand.

In the presence of glycerol, we observe a different pattern in the flux distributions that contribute to glucose production in Figure 4.8. As shown by the bold numbers in each treatment condition, percent gluconeogenic flux increases linearly from 69% to 93% to 116% when comparing insulin-treated, basal and glucagon treated flux distributions. Remarkably, the most striking effect of glycerol availability is to maintain glycogen deposition and contribution at relatively low levels between 7-10% of basal glucose production relative to the untreated condition. Relative to the glycerol free conditions, this represents a significant repression of glycogenolysis flux, in particular in the basal and glucagon treated conditions. When glycerol is present, it becomes the primary source for gluconeogenic carbon, similar to results obtained from radioactive studies in isolated rat hepatocytes [123]. This increased usage of glycerol comes at the expense of metabolite usage in the oxaloacetate pool, despite an overall increased glucose output when comparing insulin treated versus glucagon-treated hepatocytes. Modulation of gluconeogenesis without significant changes in glycogenolysis flux in the presence of glycerol is suggestive of flux modulation at the upper portions of gluconeogenesis, in particular at the glucose 6-phosphatase junction of gluconeogenesis. This indicates absence of PEPCK regulation in controlling the overall gluconeogenic flux. Lower gluconeogenesis at the PEPCK branch plays only a secondary role in supplying carbon for glucose production, the latter being driven predominantly by G6Pase activity.

We also performed exploratory experiments in this experimental setup to assess the effects of pharmacologic agents in the glucose production phenotype, in the hope of elucidating potential

targets that modulate glucose production flux. Treatment with gluconeogenic inhibitor metformin did not change hepatocyte glucose production *per se*. Addition of 1 mM oleic acid to induce hepatocyte insulin resistance caused a significant increase in glucose production. Mayo-Johnson et al. observed inhibition of gluconeogenesis from lactate after octanoate addition to suspended rat hepatocytes [124]. When oleic acid treatment was combined with treatment with biguanide metformin rescued the normal sensitive levels. Interestingly, treatment with glipizide, a sulfonylurea whose main action site is thought to be in the pancreas, caused even more drastic increase in overall glucose production Previous research with glipizide in rat hepatocytes has observed decreases in glucose production from gluconeogenesis, while other groups have observed a slight increase in glucose production attributable to increased activity of glycogen phosphorylase [173, 174]. Metformin is known to act through AMP kinase, which inhibits the transcription of gluconeogenic enzymes PEPCK and G6Pase in an insulin independent manner [175]. The presence of glycerol in our glucose production assay forces control of gluconeogenesis to glucose-6-phosphatase, implying that regulation of glucose production in the presence of glycerol occurs through modulation of glucose-6-phosphatase activity. These results, in conjunction with those presented in Figure 4.7, indicate that glycerol availability determines glucose production through the activity of glucose-6-phosphatase such that known inhibitors of gluconeogenesis can normalize glucose production levels in vitro.

The rat hepatocyte model provides a glimpse into a healthy liver system, and the obtained pattern of flux changes corresponds to the established physiology of liver glucose production. Insulin not only dramatically reduces fractional gluconeogenesis by rat hepatocytes, but does so in a manner that minimizes the contribution of substrates from the lactate/pyruvate/amino acid pool. Concomitantly, the use of glycogen fraction of glucose output supplied from increases in the presence of insulin and decreases in the presence of glucagon. The presence of glycerol alters this

picture by blunting the hormonal effects of the aforementioned branchpoints, and skewing the uptake of glycerol as the preferred substrate for glucose production. It will be interesting to assess which flux corresponds closest to the total glucose output of cells in the various conditions; previous results in primary hepatocytes suggest the gluconeogenic flux calculated from isotopomer distributions to correlate well with total glucose production measured enzymatically in mouse hepatocytes [156].
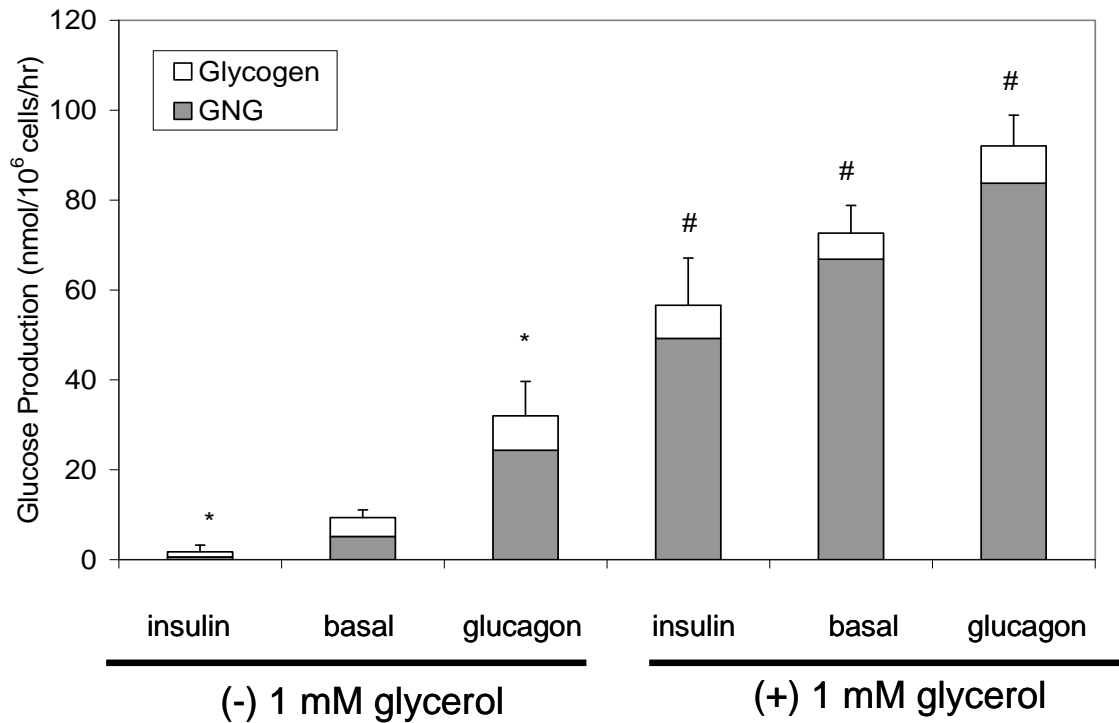
Figure 4.6: Hormone response for glucose release in primary rat hepatocytes. (-) glycerol experiments use 10% deuterated water as tracers, while (+) glycerol experiments use [U-^{13}C]-glycerol as tracer (* = p<.05 vs basal, # = p <.05 vs glycerol-free). Gray bars indicate the contribution of gluconeogenic flux to hepatocyte glucose output, while white bars indicate the contribution of glycogenolysis to hepatocyte glucose output. Data are presented as mean ± SEM

Insulin

Glucose

19

G6P ←12±1 GGN

7±1

DHAP ←6±1 GAP

0   13±2

Glyc   Pyr

Basal

Glucose

100

G6P ←45±5 GGN

55±5

DHAP ←55±1 GAP

0   110±10

Glycerol   Pyr

Glucagon

Glucose

341

G6P ←82±7 GGN

259±20

DHAP ←259±23 GAP

0   521±50

Glyc   Pyr
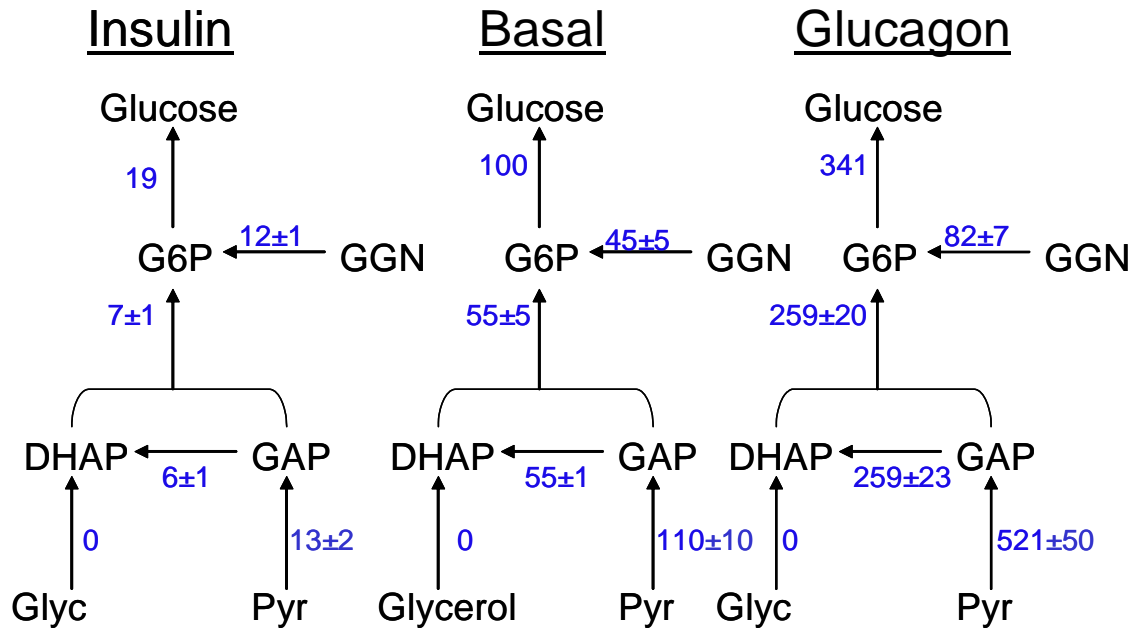
Figure 4.7: Metabolic flux analysis of hepatocyte glucose production in the absence of glycerol. Numbers represent net fluxes in the absence of glycerol, using 10% deuterated water as tracer. Fluxes are normalized with respect to the glucose output in the basal condition and presented with their 68% confidence interval. Treatment with 25 nM insulin (left flux map) decreases gluconeogenic flux in the presence and absence of glycerol. Similarly, treatment with 10 nM glucagon (right panel) effects increased gluconeogenic flux in a geometric manner. G6P = glucose-6-phosphatase, GGN = glycogen, DHAP = dihydroxyacetone phosphate, GAP = glyceraldehyde phosphate, Glyc = glycerol, Pyr = pyruvate.
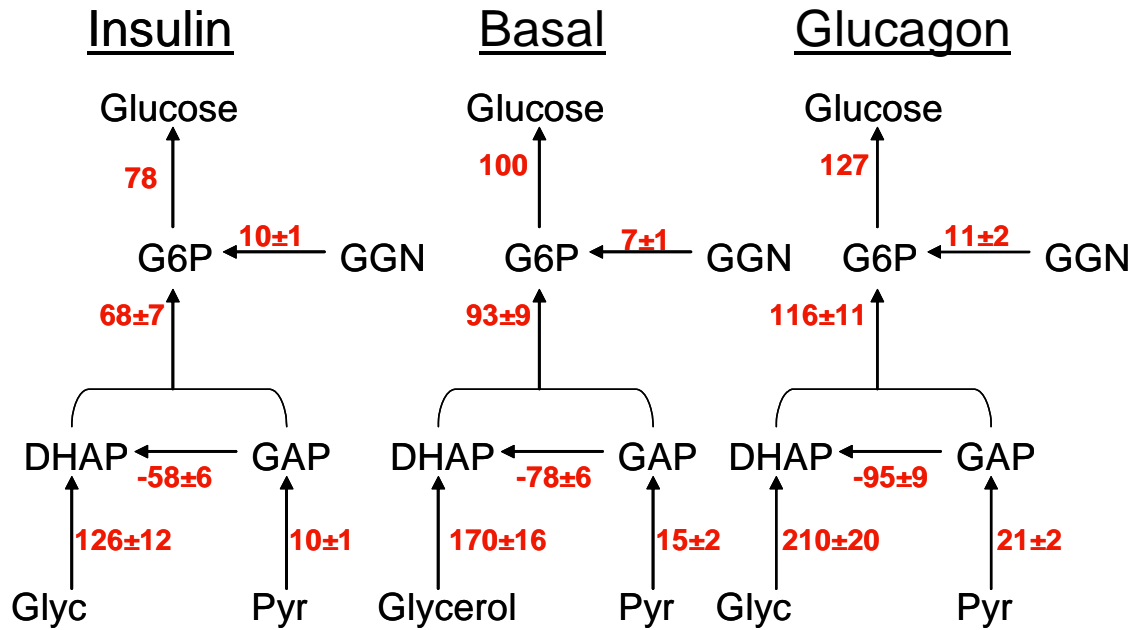
Figure 4.8: Glycerol availability redistributes fluxes around glucose-6-phosphate in the presence of glycerol in rat hepatocytes. Numbers represent net fluxes in the presence of 1 mM [D$_5$]-glycerol as tracer. Fluxes are normalized with respect to the glucose output in the basal condition and presented with their 68% confidence interval. Treatment with 25 nM insulin (left flux map) decreases gluconeogenic flux in the presence and absence of glycerol. Similarly, treatment with 10 nM glucagon (right panel) effects increased gluconeogenic flux in a linear manner. G6P = glucose-6-phosphatase, GGN = glycogen, DHAP = dihydroxyacetone phosphate, GAP = glyceraldehyde phosphate, Glyc = glycerol, Pyr = pyruvate.
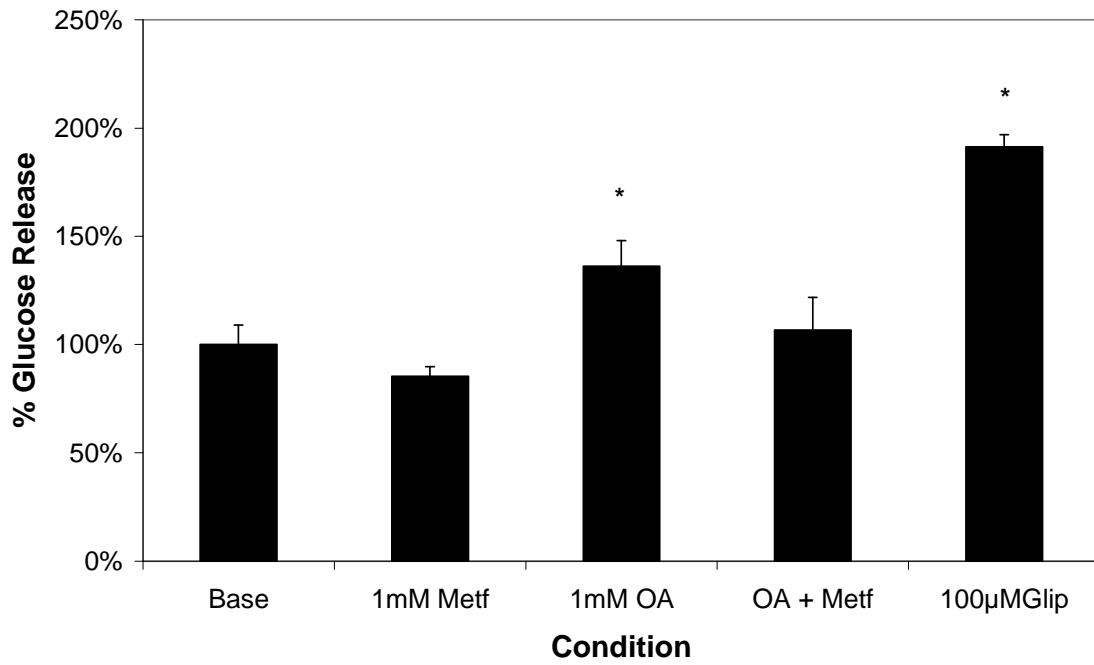
Figure 4.9: Effect of pharmacologic modulators of gluconeogenesis on glucose release. Metf = 1 mM metformin treatment. OA = 1 mM oleic acid treatment, OA+Metf = oleic acid + metformin treatment. Glip = 100 μM glipizide treatment. (n=3-5, * = p<0.05)

4.4.3 Primary mouse hepatocytes redistribute flux around glucose-6-phosphate despite partial insulin resistance.

Our goal of developing in vivo metabolic flux analysis in mice motivated the examination of flux distributions of gluconeogenesis in mouse hepatocytes. Transgenic manipulation of gluconeogenic enzymes [33], transcription factors such as PPARα[116] and hormonal signals as the insulin receptor [14] in mice results in abnormal glucose production phenotypes by genomic or proteomic measurements. The physiological characterization of these phenotypes remains a challenging endeavor that can be complemented by detailed elucidation of hepatic gluconeogenic fluxes, revealing critical aspects of metabolism such as total glucose output, fractional gluconeogenesis and substrate usage. In our in vitro system, we replicated the culture conditions in the attached rat hepatocyte experiments described previously to assess the effects of acute gluconeogenic substrate and glycerol availability on mouse hepatocyte glucose production. Unlike rat hepatocytes, mouse hepatocytes did not show any effect of glycerol in stimulating glucose production. The main effect was that of glucagon in stimulating glucose output as shown in Figure 4.9A. As for rat hepatocytes, we also calculated flux distributions in the upper gluconeogenic pathway from isotopomer analysis of secreted glucose fragments with m/z 173, 259 and 370. In the basal state, mouse hepatocytes were significantly more active in converting gluconeogenic substrates to glucose, with production rates of approximately 90 nmol/million cells/hour and within physiological range [164]. The relative flux distributions are rigid at the G6P branchpoint, showing glycerol to be a secondary substrate in favor of lactate and pyruvate (Figure 4.9B). Notably, we observe total substitution of the gluconeogenic precursor flux in the presence of glycerol to recapitulate the results observed previously regarding substrate availability effects on gluconeogenic flux; namely glycerol becomes a preferred substrate of gluconeogenesis when present as part of the nutritional milieu. Unlike rat hepatocytes, the distribution of substrate usage remains balanced

between glycerol and the oxaloacetate pool, with roughly equal contributions from both branches of metabolism.

Interestingly, attached mouse hepatocytes show decreased modulation of glucose production in the presence of hormones glucagon and insulin, with only 30-40% reduction in rate of glucose production between insulin and glucagon treatment, in comparison to the several fold reduction observed in primary rat hepatocytes. This effect suggests that the mouse hepatocyte model may express partial insulin resistance in the model studied, and results obtained from this cellular model should be interpreted carefully. In mouse hepatocytes, the resulting metabolic flux reconstructions suggest a pattern whereby within a given gluconeogenic substrate environment, the lower gluconeogenesis flux through oxaloacetate closely corresponds with glucose production. However, across different substrate availabilities (i.e., glycerol-free vs. glycerol), the lower gluconeogenesis flux as measured from the oxaloacetate pool changes drastically without affecting the glucose production phenotype, as shown in Figure 4.10B. This behavior suggests that the fluxes from glycerol and lower gluconeogenesis are coordinated to fulfill the demand for gluconeogenic substrates to produce the key intermediate glucose-6-phosphate. This demand is driven by enzymes upstream of G6P, notably, G6Pase.

A)

B)
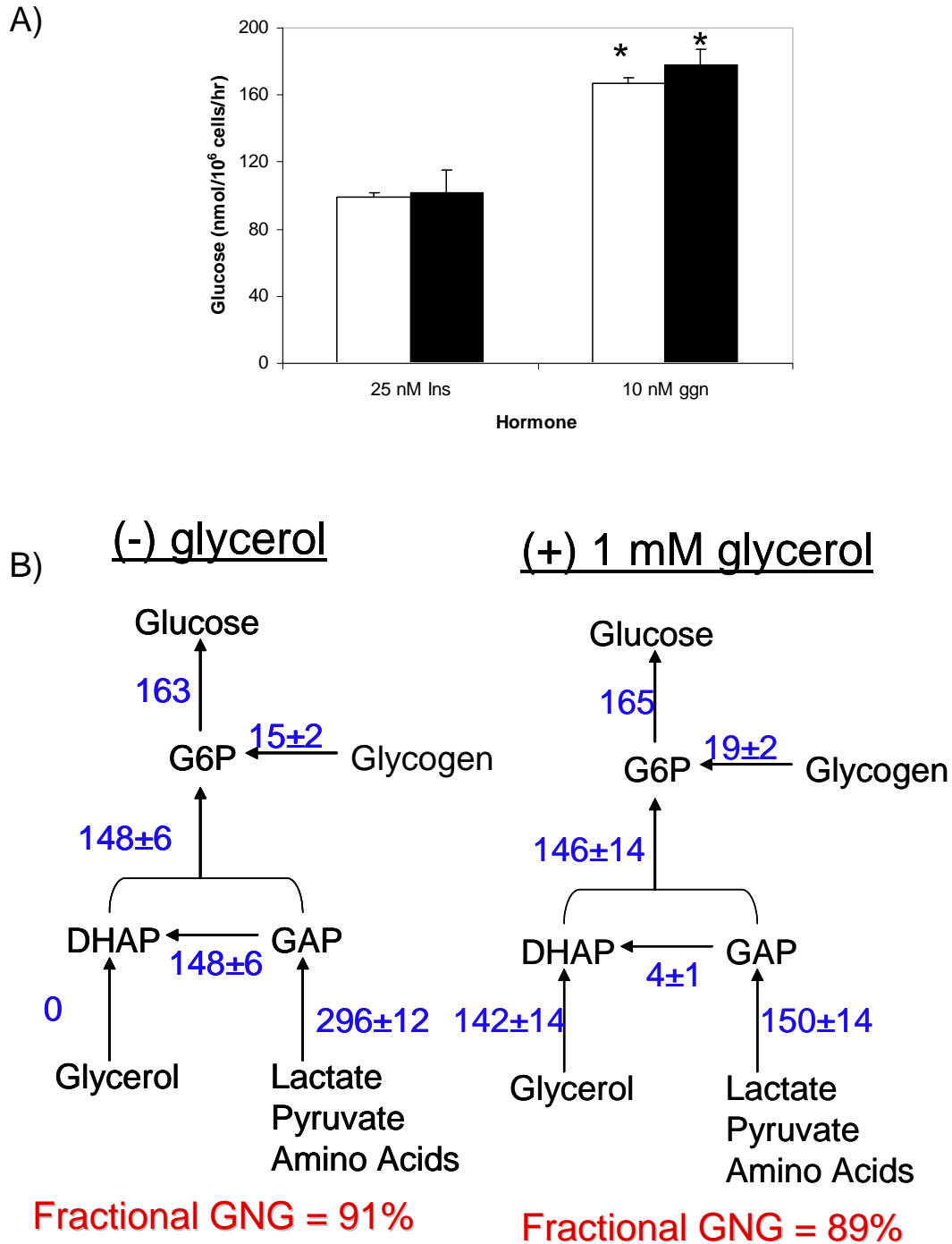
Figure 4.10: Mouse hepatocytes redistribute gluconeogenic flux in the presence of glycerol. A) Hormone response for glucose release in the absence (white bars) and presence (black bars) of 1 mM glycerol. (ins = insulin, ggn = glucagon, n=3, * = p< 0.05).B) Flux distribution of glucose production in the absence and presence of 1 mM glycerol under glucagon treatment. Fluxes are presented as nmol/10^6 cells/h ± 68% confidence interval. G6P = glucose-6-phosphatase, GGN = glycogen, DHAP = dihydroxyacetone phosphate, GAP = glyceraldehyde phosphate.

In order to understand the extent of insulin resistance in mouse hepatocytes, we next investigated hepatocyte glucose production in fresh suspended mouse hepatocyte experiments. Fresh cells provide a more physiologically active model of glucose production compared to attached mouse hepatocytes, since the attachment process in collagen-coated plates may influence the glucose production phenotype. Suspended hepatocytes were cultured over 2 hours with 10% deuterated water, and we performed a hormonal dose response curve for these cells in the presence of insulin immediately after isolation when they are most productive of glucose and measured percent glucose release relative to the untreated condition As observed previously [176], in these experiments too, mouse hepatocytes marginally changed their production of glucose with physiologic hormonal stimuli, needing micromolar concentrations of either insulin or glucagon to obtain statistically significant changes. The observed insulin resistance in this cellular model could be a factor in explaining the redistribution of substrate usage while maintaining total glucose production fixed; if the demand for glucose-6phosphate is set and irresponsive to hormonal cues, the lower gluconeogenic substrates would redistribute accordingly to meet the set demand for G6P.

Through deuterated water incorporation, we reconstructed upper gluconeogenesis fluxes relative to the untreated condition (Figure 4.11B) as in the H4IIEC3 results shown previously. Specifically, we notice that mouse hepatocytes primarily utilize the lower entering substrates of the gluconeogenic pathway, glycerol and the pools of lactate/pyruvate/amino acids, to produce secreted glucose, in roughly equal proportions. There is little to no contribution from glycogenolysis, consistent with the 24 hour fast that the animal was subjected prior to hepatocyte isolation. On the other hand, the insulin treated condition shows a 7% decrease in glucose production from the basal condition, and a 13% increase in glycogenolysis contributing to total glucose output. In addition, the insulin treated-cells preferentially utilize the lactate/pyruvate/amino acid pool as their substrate for

gluconeogenesis, while decreasing the uptake of glycerol. The glucose-6-phosphate branchpoint in this case shows decreased percentage of gluconeogenic flux utilized for total hepatocyte glucose production from 100% to 86%, contrary to the observed results in H4IIEC3 and rat hepatocyte experiments. Insulin treatment under these experimental conditions changes the utilization of gluconeogenic substrates, increasing the oxaloacetate pool uptake to 123% from a basal 105% of glucose output. Interestingly, the decrease in gluconeogenesis flux (basal 93%, insulin-treated 80%) is primarily accounted for by decreased glycerol uptake (basal 95%, insulin treated, 36%). This pattern is unlike the previously observed gluconeogenesis substrate usage patterns in primary rat hepatocytes.

A)

B) 0 nM Insulin   1 μM Insulin
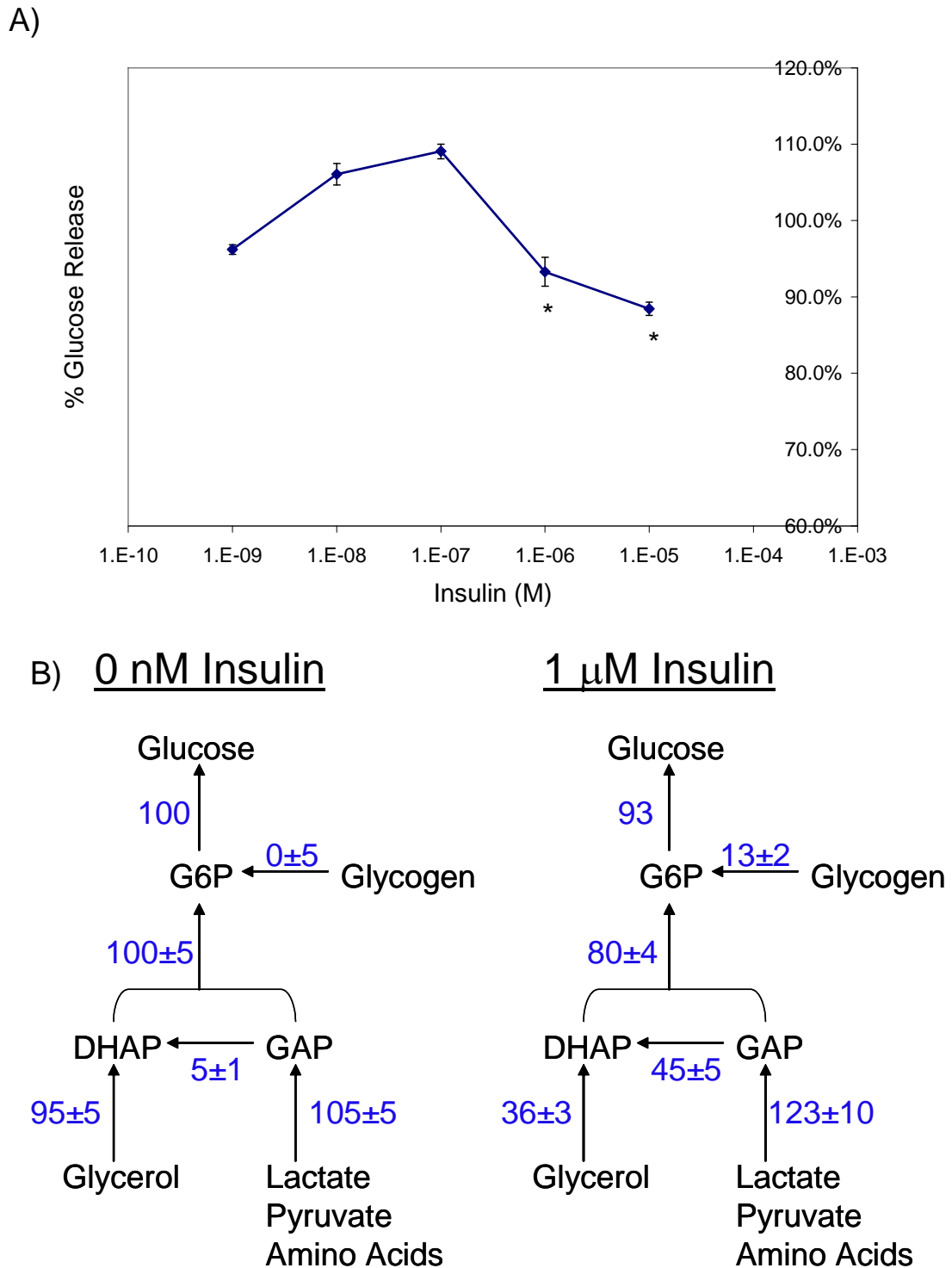
Figure 4.11: Mouse hepatocyte dose response experiment with pharmacologic concentrations of insulin. A) Insulin dose response for glucose release in primary mouse hepatocytes. Data are mean±SEM (n=3-5, * = p<.05 vs basal) B) Flux analysis of basal and insulin treated (1μM) glucose production in mouse hepatocytes. Fluxes are normalized to glucose production in the basal condition and presented with their 68% confidence interval.

Decreased suppression of glucose production behavior was partially explained by changes in insulin signaling as shown in Figure 4.12. Here, our isolated mouse hepatocytes were compared to liver lysates stimulated with 125U insulin over 1 hour prior to processing for presence and phosphorylation of insulin signaling intermediates such as the insulin receptor (IR), IRS-1, Akt, and ERK. The results presented in Figure 4.12 comparing four experimental conditions: primary hepatocytes and liver lysates as mentioned above, and the presence and absence of insulin. The insulin signaling intermediates insulin receptor and IRS-1 are shown in Figure 4.12A. First, we observe presence of the aforementioned signaling proteins in all experimental conditions, as expected for the normal phenotype of the cells and animals studied and confirming an intact insulin signaling pathway. Second, we observe that for the liver lysate controls, there is increased presence and phosphorylation for IR and IRS-1 in the presence of insulin, as expected for this positive control. Third, for primary hepatocytes, we observe large bands corresponding to the presence and phosphorylation of IR and IRS-1, in the presence or absence of insulin, when compared to liver lysates. This enrichment reflects the isolation of the hepatocyte fraction when compared to the normal fraction of hepatocytes in the intact liver. When comparing phosphorylation in IR and IRS-1, there is a relative decrease in the intensity of the phosphorylation band in the absence of insulin in primary hepatocytes. However, even in the control for insulin treatment, there is significant basal phosphorylation of IR and IRS-1 suggestive of insulin resistance. We interpret these results to mean that the insulin signaling cascade at the level of IR and IRS-1 in primary hepatocytes is intact and active, and significantly more active over that observed in liver lysates in the absence of insulin. This basal activation is unexpected and reflects partial insulin resistance that is consistent with the decreased effects of insulin to suppress glucose production observed in mouse hepatocytes.

The lower signaling proteins of the insulin signaling cascade reflect similar patterns to those described for IR and IRS-1. We examined presence and phosphorylation of Akt as well as ERK to

assess whether a blockage in the downstream effectors of the IR could be causing the observed insulin resistance. As shown in Figure 4.12, we compare the same four experimental conditions of primary hepatocytes and liver lysates, in the presence or absence of insulin. As for IR and IRS-1, we observe enrichment in the primary hepatocyte lanes due to enrichment in the hepatocyte fraction where the signaling molecules are present. We also replicate the phosphorylation of the first and second tyrosine residues as well as ERK in liver lysates in the presence of insulin. Lastly, we observe significant basal phosphorylation of pAkt and pERK in the absence of insulin, despite a relative decrease in the intensity of the bands in the absence of insulin. Therefore, we cannot point to a specific point in the insulin signaling cascade where defects in signal transduction would inhibit the downstream effect of suppressing glucose production. Our results suggest that the mouse hepatocyte model indeed reflects partial insulin resistance as shown by phosphorylation of insulin signaling intermediates, therefore explaining the lack of gluconeogenesis suppression observed in our biochemical assays and flux analysis assays.
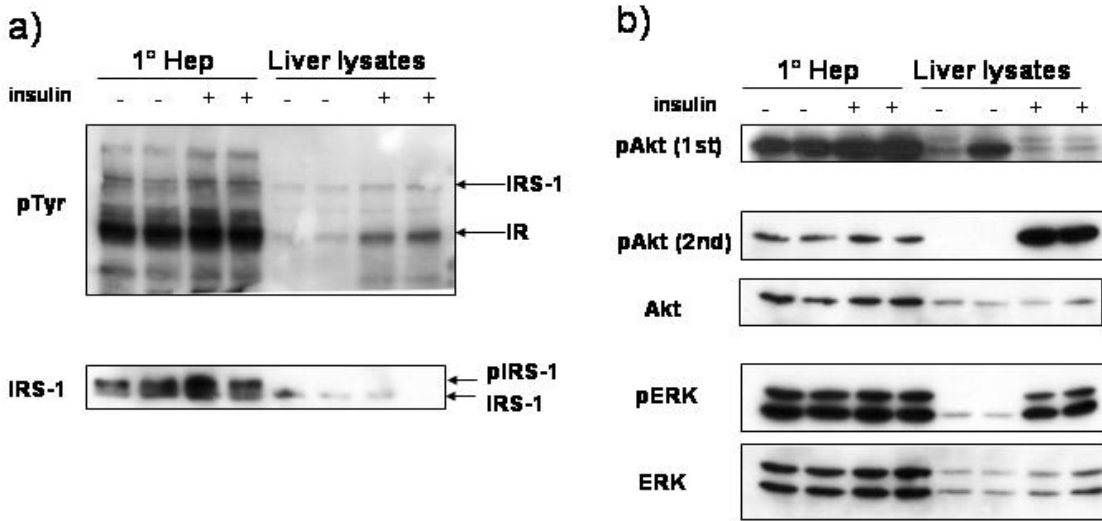
Figure 4.12: Western blot analysis of insulin signaling in primary C57BL/6 hepatocytes. Primary murine hepatocytes were attached to 12-well plates and cultured overnight in Advanced DMEM (Gibco), serum starved for 6 hours and induced with 125U insulin for 1 hr. Advanced DMEM was found to contain trace amounts of insulin. a) Phosphotyrosine Western Blots for upper insulin signaling molecules insulin receptor (IR) and insulin receptor substrate 1 (IRS-1) comparing primary C57BL6 hepatocytes +/- insulin stimulation versus C57 BL6 liver lysates +/- insulin stimulation. Both phosphorylated and unphosphorylated counterparts are present in hepatocytes. b) Western Blots for downstream insulin signaling effectors Akt and ERK with their respective phosphorylation residues.

4.5 Discussion

Methodological Considerations - In the previous results, we demonstrate the feasibility and relevance of flux analysis in cellular models of glucose production such as primary liver cells. Flux analysis has seen significant progress in microbial systems where the assumptions of metabolic and isotopic steady state can be readily attained in chemostat experiments. In mammalian cells, factors discussed in Chapter 3 hinder metabolic reconstruction given compartmentation effects, heterogeneity of metabolite pools and undefined metabolic pathways. We assumed a pseudo-stationary flux analysis paradigm such that the timescale of isotopic incorporation is much faster than changes in metabolite concentrations, in order to apply steady state computational methods to the analysis of the resulting isotopomer data of glucose secreted to the extracellular medium. Recent efforts to characterize *de novo* adipogenesis biology through flux partitioning of secreted metabolites applied a similar paradigm to observe reorganization of metabolic pathways consistent with a lipid loading phenotype [177].

We have limited our analysis to the enrichment of positional isotopomers of the glucose molecule as would be accessible from plasma *in vivo*. This contrasts previous work in cellular systems where scientists systematically assess isotopomer enrichment of multiple metabolic intermediates [74, 178].The positional isotopomer information presented in this work makes use of novel glucose derivative fragments for the accurate assessment of mass isotopomer enrichment of the glucose molecule [13]. Positional isotopomer enrichment information can be assessed through analytical techniques such as NMR and GC-MS. The former technique is of particular relevance in the analysis of abundant compounds in biofluids or measurement of in vivo enrichment patterns, as it does not require disruption of the cellular system. On the other hand, GC-MS analysis presents advantages for analytical measurement of isotopomers given that analysis of complex samples is relatively rapid, and instruments are more readily accessible to investigators. We chose to perform our analysis for

glucose enrichment in a standard GC-MS platform that maximizes the degree of positional information through novel derivatization strategies customized for accuracy and precision necessary in isotopomer and metabolic flux analysis.

Few studies integrated the use of ^{13}C and ^{2}H enrichment for metabolic reconstruction, and the most successful examples do so by astute analysis of enrichment patterns derived in multiple plasma and urine metabolites, coupled with parallel multidimensional NMR [149, 151]. Carbon based tracers are the most frequently used probes to assess hepatic glucose metabolism [117, 119, 123]. Deuterium enrichment has been applied for in vivo studies of gluconeogenesis through the methodology developed by Landau and colleagues using deuterated water (D$_2$O) labeling. Through our methodology, we elucidated upper gluconeogenic fluxes from the measurement of multiple fragments of a single glucose molecule using a formal metabolic reconstruction algorithm. The potential for application of this integrated, simultaneous analysis in humans is considerable in light that deuterated water, [6,6-D$_2$]-glucose and glycerol can be administered orally to reach measurable ^{13}C and ^{2}H enrichment in plasma glucose.

We have previously shown that tracer choice is critical to the determination of such fluxes, as the most informative tracer may not be the most obvious choice given the physiology of the system [13]. In preliminary studies in the mouse hepatocyte glucose release assay, we studied the uptake of multiple tracers in parallel to elucidate reaction fluxes in the gluconeogenic pathway, and reached the conclusion that deuterated water and labeled glycerol were most informative for the system studied given the nature of the reaction network as well as the uptake and residence time of label in the network [13]. Comparing possible substrates of gluconeogenesis, glutamine takes the longest time to traverse the reaction network to glucose, followed by acetate, lactate, alanine, glycerol and deuterated water in decreasing order. From a physiologic standpoint, lactate and alanine are known to be the major substrates of gluconeogenesis in vivo, and are ideal compounds to trace metabolism that

avoid underestimation effects due effects of precursor pool enrichment when using combinatorial methodologies to describe glucose synthesis using MIDA [138, 139, 146].

There are limitations in our design pertinent to the analysis of these experiments. The choice of glycerol for the measurement of glucose production remains controversial. Compared to pyruvate and lactate, glycerol shows uptake rates about 50% of the natural precursors of gluconeogenesis, and comparable to important amino acid substrates such as alanine in the perfused rat liver [70]. In addition, due to its location for incorporation into gluconeogenesis at the triose phosphate isomerase reaction through DHAP, glycerol is less likely to dilute with metabolites in the oxaloacetate pool. In our hands, glycerol was readily converted to glucose over short-term experiments in which we sought to analyze the effects of physiologic modulators on the metabolic flux distribution. Improvements to the experiments presented here would involve the use of $[U-^{13}C]$-lactate and $[U-^{13}C]$-pyruvate in order to better resolve fluxes related to TCA cycle activity as well as uptake into gluconeogenesis from the oxaloacetate pool. These tracers carry additional constraints in terms of determining the intracellular pyruvate enrichment in order to determined the dilution of tracer by unlabeled pools of the precursor in hepatocytes [61]

An additional limitation involves the amounts and enrichment of both glycerol and deuterated water used in our experiments, which are higher than those reported for similar in vitro and in vivo experiments. These amounts are an important consideration to modify the developed methods in translating to an in vivo context [111, 139]. Specifically, deuterated water enrichments of 0.5% or less would be desirable to avoid side effects in a clinical setting. Plasma glycerol levels are approximately 0.1 mM, but consumption in peripheral sinks such as adipose tissue may necessitate higher glycerol concentrations to increase the rates of infusion to account for 20-30% of circulating plasma glycerol necessary to ensure significant enrichment into glucose. Carbon labeled glycerol tracers have been used extensively in literature, but tracer choices are limited due to difficulty in

interpretation of the resulting isotopomer data [134]. Thus, in these experiments we selected glycerol in order to increase glucose production and facilitate isotopomer analysis, but *a priori* we could not predict how the presence of this specific substrate would alter the flux in the metabolic network, as evidenced by the drastic changes induced by the presence of glycerol in Figure 4.6. The ideal tracer does not affect the metabolic pathway of interest such that trace pool is processed normally, and this could be an area of exploration in future experiments using the developed model with different ^{13}C and ^{2}H tracers in the form of alanine, pyruvate and lactate.

The presented methodological approach for integrated ^{13}C, ^{2}H analysis of glucose production fluxes is not limited to in vitro reconstruction of gluconeogenic flux. Furthermore, this computational reconstruction of upper gluconeogenesis metabolism could be readily adapted to analyze the contributions of gluconeogenic substrates to this metabolic pathway in whole animals and humans with the platform developed for flux analysis using multiple stable isotope tracer incorporation [102] We hope these studies will provide the motivation to biological researchers to pursue flux measurements as an integral part of the characterization of metabolic disease phenotypes, in what could make clinical fluxomics a reality.

Physiological considerations – In the presented results, we examined the effects of several perturbations on the metabolic flux distributions of upper gluconeogenesis in multiple cellular systems capable of de novo glucose production. The first variation in the glucose production phenotype was observed across the cellular model studies, namely H4IIEC3 hepatomas, primary rat and primary mouse hepatocytes. The basal glucose production phenotypes examined by flux distributions across these cellular systems are revealing, in that they point out physiologic differences to be considered when analyzing metabolic perturbations in each system. H4IIEC3 hepatomas showed striking differences with respect to their usage of gluconeogenesis with fractional gluconeogenesis values among the

lowest observed in literature. These results point to the usage of glycogen as their primary source of glucose, in turn allowing them to survive in glucose free medium. Fractional glycogenolysis described through our flux analysis can respond to either glycogen deposition per se, or glucose cycling through glycogen. In comparison, rat hepatocytes in their basal state showed remarkable uptake of glycerol and fractional gluconeogenesis of 55% in the basal state, consistent with in vitro work in rat hepatocytes using radioactive tracers [130]. The measured changes in fractional gluconeogenesis and glucose output are consistent with reported effects of insulin and glucagon on glycogen synthesis and overall glucose production in rat hepatocytes [124]. However, both rats and mice show fast basal metabolic rates suggestive of higher fractional gluconeogenesis, with rates observed as high as 80-90% after a 24 hour fast immediately prior to isolation [139]. The lower fractional gluconeogenesis may correspond to differences in metabolism due to attachment and continued culture of these cells. Lastly, mouse hepatocytes in their basal state show high rates of fractional gluconeogenesis and glucose release when compared to rat hepatocytes, corresponding to the values observed in literature [136, 139]. The metabolic rate of mice is higher in mice than in rats, is proportional to the mass of the animal, and the tenfold difference in weight between rats and mice may partially account for the difference in depletion of glycogen sources that contributes the observed changes in fractional gluconeogenesis.

The second perturbation dealt with the presence and absence of hormones, specifically the presence of insulin and glucagon that are known to modulate the production of glucose in vivo and in vitro. As expected from the For the H4IIEC3 system, we observe significant suppression of glucose release in the presence of physiological amounts of insulin, which manifests in decreases in both branches of hepatic glucose production gluconeogenesis and glycogenolysis. This decrease is driven primarily by decrease in metabolic flux from glycogen, as expected from the largely glycogen-driven metabolic flux distribution [170, 171]. On the other hand, stimulation via insulin and

glucagon in rat hepatocytes demonstrates dramatic fold changes in glucose release in absolute terms, with concomitant changes in fractional gluconeogenesis measured. These results suggest a geometric manner of propagation of gluconeogenic flux in response to glucose-6-phosphatase demand. Previous research has noted the ability of the liver to accommodate large boluses of gluconeogenic substrate (alanine and glycerol) without stimulating glucose production, which would require the observed changes in gluconeogenic flux in order to modulate glucose production at a constant level [179]. A geometric change in glucose production over the short time scale of glucose production observed in our experimental setup is suggestive of substrate-enzyme interactions that modulate glucose production in the absence of transcriptional changes to regulate enzyme production or degradation. Furthermore, a geometric change in glucose production is suggestive of regulation at two different points in the metabolic network presented, suggestive of combined effects of PEPCK and G6Pase to modulate glucose production in the absence of glycerol.

The third perturbation studied was the presence or absence of glycerol as a gluconeogenic substrate. Along the lines of this perturbation, we observed the effects of glycerol presence to increase hepatocyte glucose production in rat hepatocytes even with high concentrations of lactate and pyruvate present (Figure 4.6) suggestive of preferential use in de novo glucose production. This effect corresponded to a tenfold difference in the glycerol uptake metabolic flux, irrespective of hormonal treatment. Mouse hepatocytes on the other hand, show balanced usage of glycerol compared to the metabolites in the oxaloacetate pool per our flux analysis results and did not increase their glucose output significantly in the presence of glycerol. These results suggest a particular regulatory structure in light of the preserved glucose output for mouse hepatocytes: within a given substrate availability condition (+/- glycerol) the lower gluconeogenesis flux from the oxaloacetate pool is determined by the joint action of PEPCK and G6Pase. However, across different substrate availabilities and in the presence of glycerol, the role of G6Pase sets the demand

for gluconeogenic output, and the lower gluconeogenesis flux regulated by PEPCK accommodates the uptake of substrates in the oxaloacetate pool to meet this demand [156]. Glycerol is incorporated by diffusion into cells and its rate of uptake is modulated by glycerol kinase [73]. This phosphorylation reaction is incorporated into our modeling approach, but not actively observed through the flux calculations obtained from glucose isotopomer data. Glycerol kinase is evenly distributed in the liver and does not contribute to the differences in precursor pool enrichment that cause fractional gluconeogenesis underestimation, with only 10% variation in activity across the liver lobule [139]. An interesting extension of this work would be to combine gene expression, phosphorylation or activity information of glycerol kinase into the observed calculations to distinguish between glucose output demand set by glucose-6-phosphatase and supply provided by glycerol kinase.

The observed partial insulin resistance in mouse hepatocytes was surprising. Few reports compare glucose production between mouse and rat hepatocytes, and the overwhelming majority of literature in the field of liver glucose metabolism uses rat hepatocyte preparations given the number of cells obtained from a single isolation ($\sim$300x10^6) versus mouse ($\sim$30x10^6) allow for a much larger number of experimental conditions. Of the few studies that look at mouse hepatocyte glucose production, only Greenaway et al. [176] has documented the rate of production from gluconeogenic precursor [U^{14}C]-lactate to decrease from 209 to 123 nmol/10^6 cells/30 min upon stimulation with 1 µM insulin (70% decrease) from the basal state in primary mouse hepatocytes suspension. The comparable reductions in glucose production by insulin stimulation from Mayo-Johnson et al. [124] establish a 10% decrease in the amount of glucose production over 2 hours from basal state, and a maximal 30% decrease from cells stimulated with 40 µM cAMP in primary rat hepatocytes in suspension. We postulate that there are intrinsic differences in how mouse hepatocytes survive the isolation procedure, as the volume of liver perfused at the chosen perfusion flow rate (7 mL/min)

would correspond to higher shear rates that could disturb the integrity of the received cells and subsequently damage component of the insulin signaling pathway.

Our flux analysis studies suggest that in the presence of glycerol, gluconeogenic flux is modulated through glucose-6-phosphatase to accommodate demand for glucose. The data supporting this conclusion include the observation of decreased substrate usage from the oxaloacetate pool in the presence of glycerol, where PEPCK would be active in modulating glucose production output. Recently, several studies debated the importance of different gluconeogenesis enzymatic targets with regards to the development of therapeutic strategies to control the increased glucose output observed in Type 2 diabetics. Brain-liver connections through the vagus nerve specifically target the *g6pc* gene for upregulation of hepatic glucose production with concomitant increases in gluconeogenesis and hepatic glucose output during clamp studies after intracerebroventricular injection of glucose or lactate in rats [114]. This finding stands in contrast to the known effects of downregulating glucose-6-phosphatase activity; genetically manifested as glycogen storage deficiency I (von Gierke's disease) or chemically by the administration of chlorogenic acid derivative S4048 [180]. In both cases, glucose fluxes are redirected to glycogen synthesis with mild reductions in plasma glucose levels in the basal state. From a metabolic network design standpoint, regulation of throughput through a metabolic pathway is most effectively achieved by modulation at the beginning or end of the defined metabolic route [2], supporting the notion of glucose-6-phosphatase being a critical regulator of hepatic glucose output. Fructose-1,6-bisphosphatase inhibitors have appeared recently as viable options for reducing excess hepatic glucose metabolism, but their effects are moderate compared to those of standard therapy with metformin [181]. This difference may be due to the aforementioned effects of metformin to reduce both PEPCK and G6Pase activity through AMPK. Lower in the gluconeogenic pathway, PEPCK inhibitors include metformin and mercaptopicolinic acid, the former of which is used as first line

therapy for treatment of Type 2 Diabetes while the latter is not available for pharmacotherapy given chemical instability and unwarranted side effects from similarities with chelator picolinic acid. This inhibition is predicated on insulin regulation to decrease PEPCK transcription in liver and hepatoma cells [182]. Intriguing analysis of partial liver PEPCK knockdown in transgenic mice shows the flux control coefficient of PEPCK to be approximately 0.18, contrasting the notion of PEPCK as the regulating enzyme of gluconeogenesis [33]. It is not clear how the modulation of these enzyme levels by genetic, chemical or other means extrapolates to the physiological phenotype of hepatic glucose production, and such analysis will require a systems approach such as the one presented here for the measurement of gluconeogenic fluxes and integration of the resulting data into our understanding of hepatic glucose output regulation.

Hyperglycemia is a principal characteristic of Type 2 Diabetes mellitus that stems from insulin resistance. It also contributes to disease pathogenesis by impairing both insulin sensitivity and insulin secretion [183-186]. Thus, hyperglycemia is not only a symptom of diabetes, but also a driving force that can sustain or worsen the diabetic state. Elucidation of the pathophysiology of liver insulin resistance in Type 2 Diabetes is essential to the development of potential treatment strategies. We presented evidence supporting the biochemical hypothesis that under the presence of glycerol as a gluconeogenic substrate, the glucose-6-phosphate branchpoint becomes a critical regulation point of primary hepatocyte glucose output in relatively insulin resistant mouse hepatocytes. Glycerol bypasses an important checkpoint of gluconeogenesis through PEPCK, thus making it an interesting substrate to investigate the flux regulation of hepatocyte glucose production through the fructose-1,6-bisphosphatase and glucose-6-phosphatate junction points individually and relative to each other. In our flux analysis experiments, the role of the glucose-6-phosphatase flux is critical in modulating overall glucose output given the structure of the biochemical pathway of gluconeogenesis, thus supporting research noting the importance if this enzyme in regulation in the

context of local metabolite regulation of G6P levels through the pentose phosphate pathway [26] and of a brain-liver connection in the regulation of glucose production [114]. It would be interesting to compare the combination of available antagonists of glucose-6-phosphatase [180] and fructose-1,6-bisphosphatase [181] in our model to compare a possible reduction of primary hepatocyte glucose output without concomitant redirection of flux into the hepatic glycogen pool.

In conclusion, we used an integrated carbon-13, deuterium flux analysis platform to reconstruct metabolic flux distributions in cellular systems capable of *de novo* glucose production. In this manner, we showed that the presence of glycerol as tracer and gluconeogenic substrate impacts the metabolic flux distribution in a twofold manner, by increasing glucose production from gluconeogenesis and by making the available glycerol the preferred substrate over other possible carbon sources at the oxaloacetate pool. This preference is conserved even in insulin resistant cells, despite their inability to accommodate large changes in glucose production due to substrate availability. In addition, this preference may reflect a metabolic flux regulatory strategy for glucose-6-phosphatase when glycerol is present as gluconeogenic substrate. Furthermore, we have shown that comprehensive analysis of hepatic glucose production can be achieved by integrated ^{13}C, ^{2}H labeling of the glucose molecule and analysis through GC-MS, thereby allowing a practical method for measuring gluconeogenesis within a single study through data-driven reconstruction of hepatic glucose metabolism. These studies open the possibility for the application of a combined labeling strategy in plasma glucose in vivo through mass spectrometry, offering the possibility of non-invasive metabolic examination of transgenic mouse models and human patients.

Appendix 4.A: Representative uncorrected mass isotopomer distributions of glucose fragments utilized for metabolic reconstruction.
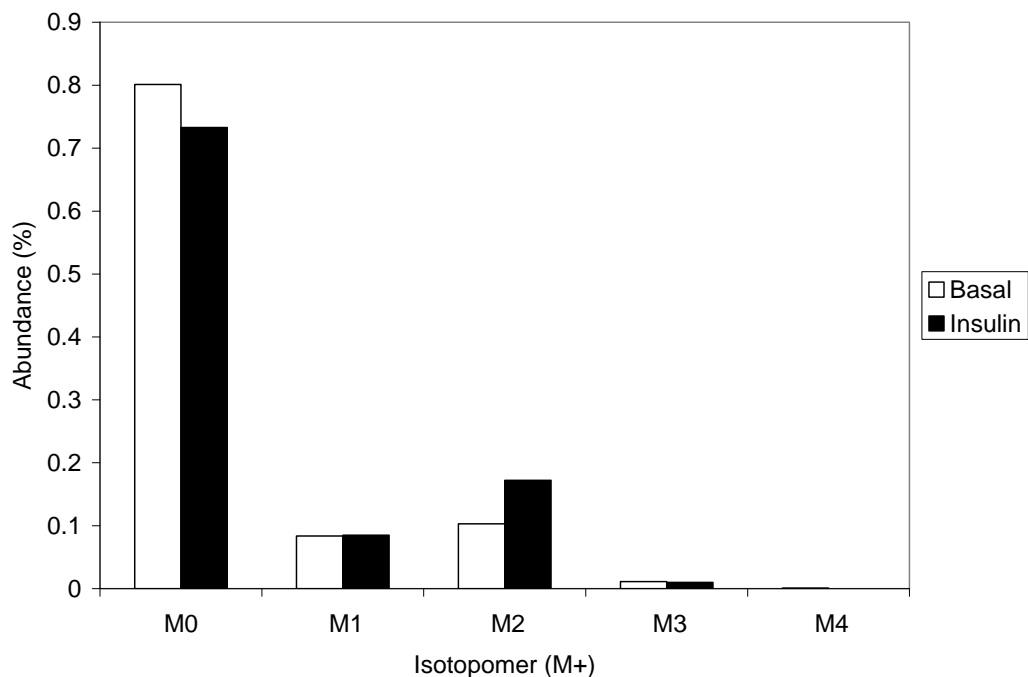
Figure 4.A.1: Glucose Fragment 173 Mass Isotopomer Distribution for H4IIEC3 hepatoma experiment.
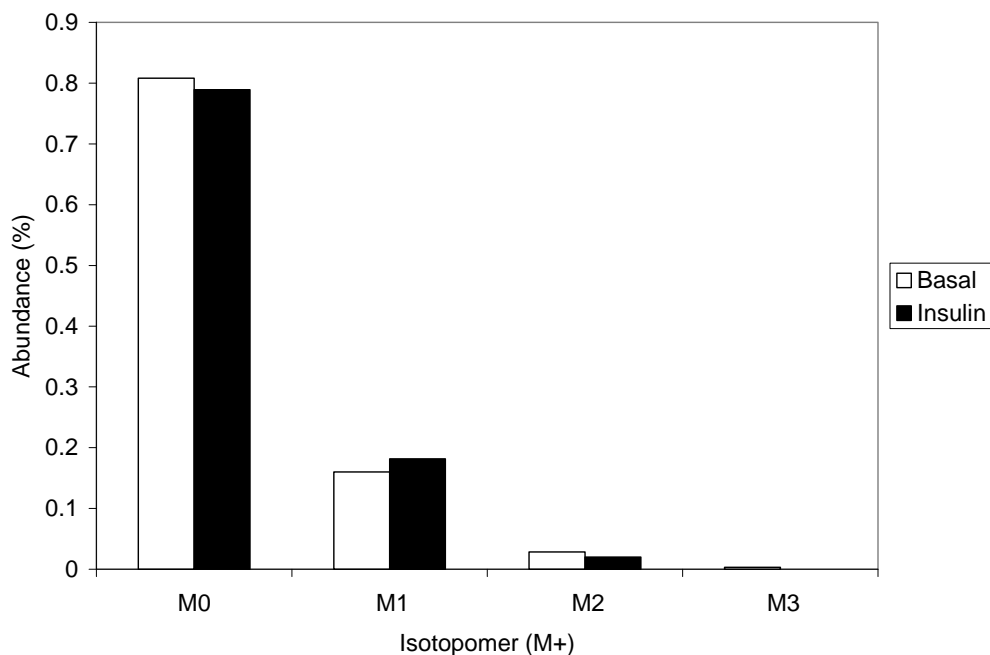
Figure 4.A.2: Glucose Fragment 370 Mass Isotopomer Distribution for H4IIEC3 hepatoma experiment.
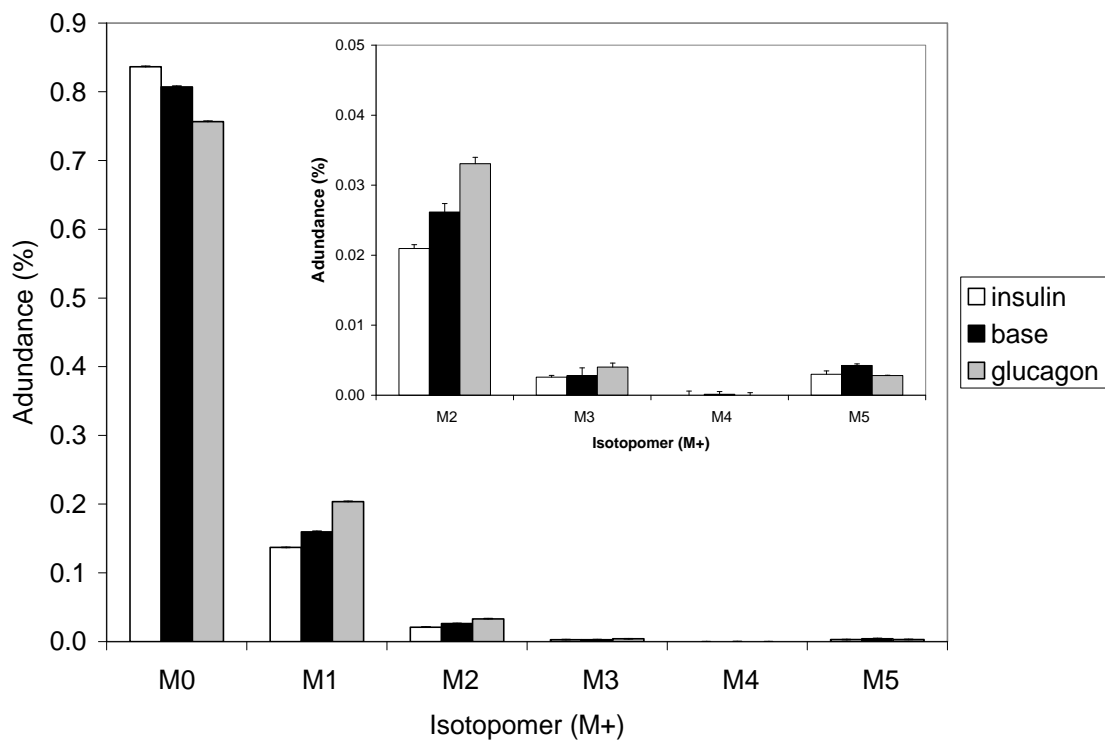
Figure 4.A.3: Glucose Fragment 173 Mass Isotopomer Distribution for rat hepatocyte experiment. Culture conditions in the absence of glycerol.
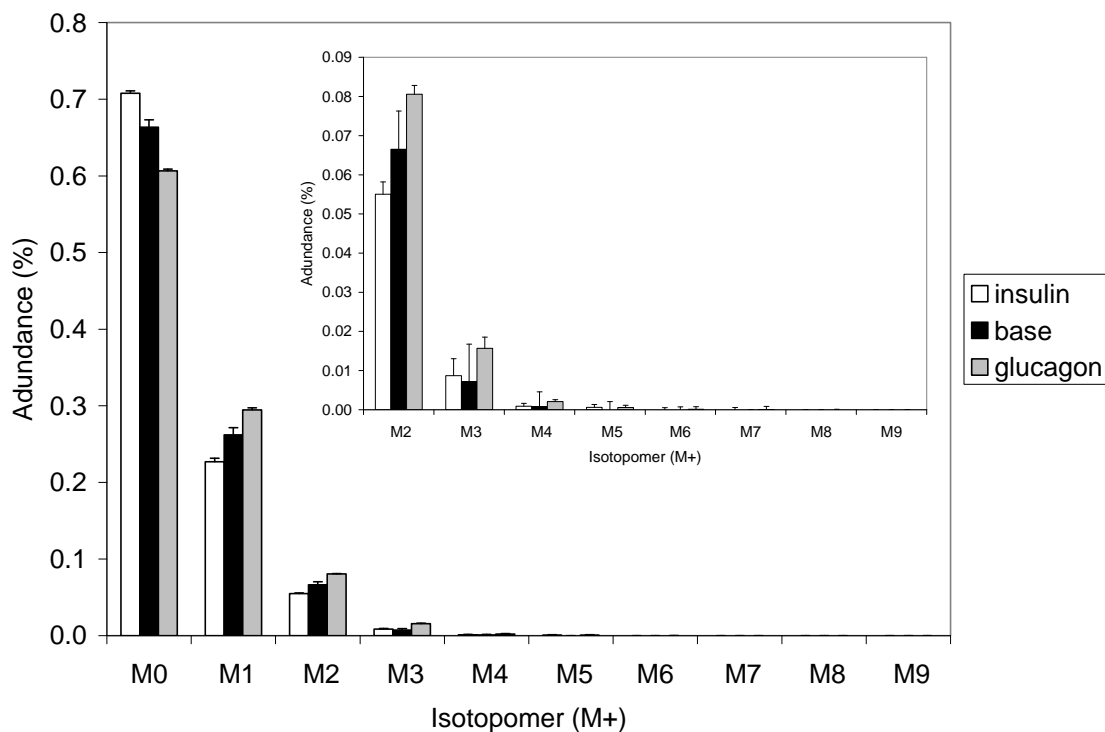
Figure 4.A.4: Glucose Fragment 370 Mass Isotopomer Distribution for rat hepatocyte experiment: Culture conditions in the absence of glycerol.
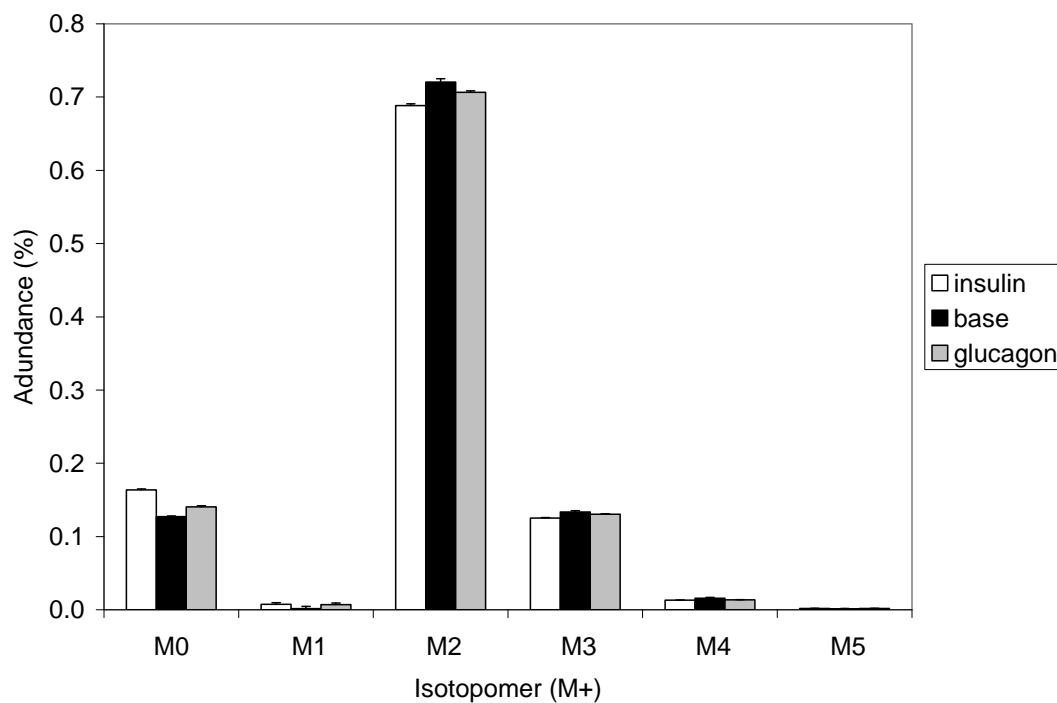
Figure 4.A.5: Glucose Fragment 173 Mass Isotopomer Distribution for rat hepatocyte experiment. Culture conditions in the presence of glycerol.
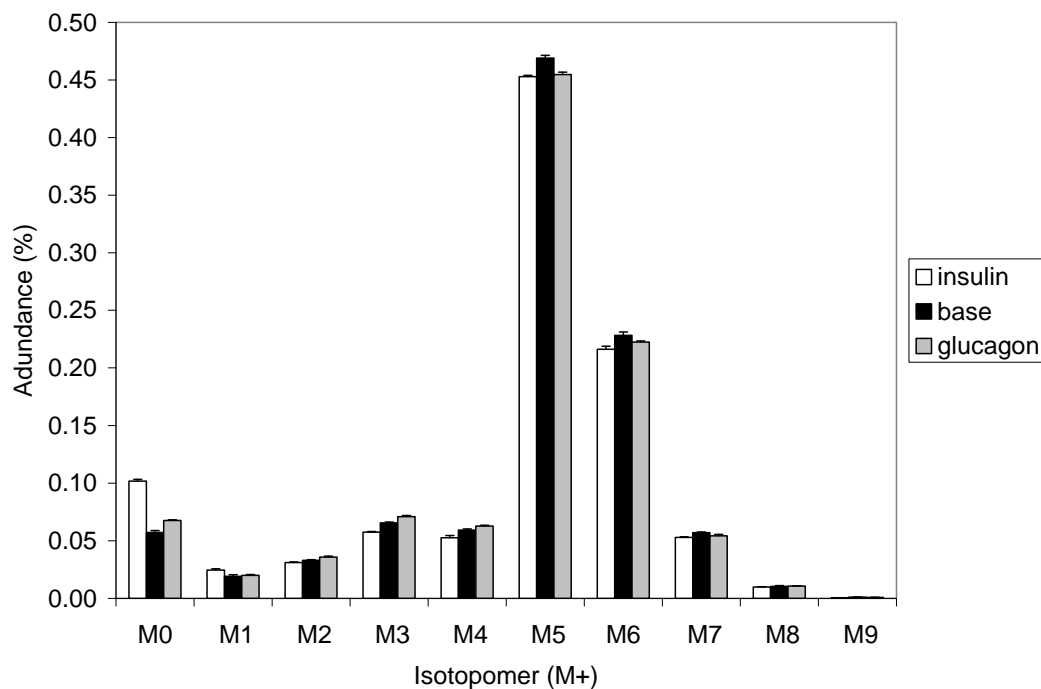
Figure 4.A.6: Glucose Fragment 370 Mass Isotopomer Distribution for rat hepatocyte experiment: Culture conditions in the presence of glycerol.

CHAPTER 5: Development of in vivo flux analysis of gluconeogenesis using [U-^{13}C, D$_5$]-glycerol and mass spectrometry

5.1 Introduction

In the previous chapter we described exploration of stable isotope tracing techniques to reconstruct gluconeogenesis fluxes in vitro, by single tracer estimation of key gluconeogenic fluxes and computational integration of complementary tracer data in cellular experiments. Our computational framework permitted the accurate estimation of upper gluconeogenic fluxes in vitro and the postulation of an increased role for G6Pase regulation of gluconeogenesis in the presence of glycerol as a gluconeogenic substrate. In this section we introduce parallel labeling of tracers defined as the use of individual stable isotope tracers in different experiments run in parallel whose results are analyzed simultaneously and as part of the same dataset to ascertain specific aspects of metabolism. An example of this technique is the work presented in Chapter 4, where [U-^{13}C]-glycerol, [D$_5$]-glycerol and deuterated water were used to probe independently the same experimental system (primary hepatocytes) to computationally reconstruct upper gluconeogenic metabolism. Parallel tracer labeling constitutes the bulk of the current stable isotope published literature in mammalian metabolism with established precedents [73], and have been successfully applied in limited cases in vivo through the use of dilution estimation, Mass Isotopomer Distribution Analysis or Isotopomer Spectral Analysis [136, 148]. Other examples of using parallel stable isotope labeling in the reconstruction of metabolic fluxes include the use of either single tracers in multiple in vivo experimental conditions [116, 117] or multiple tracers to resolve individual

fluxes within a larger metabolic map [33]. In cellular systems or perfused organs, parallel labeling strategies are justified under the assumption of reproducible cellular behavior under similar physiological conditions. These approaches are valid given the lack of interaction with other peripheral tissues through blood. In organisms however, the information afforded by parallel stable isotope tracers labeling limits the readout of individual markers of metabolism as the number of subjects studied decreases due to the complexity of animal or human studies. In this context, the computational strategies for metabolic flux reconstruction presented previously accomplish a posteriori integration of parallel labeling results in vivo or in human studies.

An alternative to parallel tracer labeling is labeling from the use of combined stable isotope tracers, where careful examination of enrichment patterns in metabolic intermediates selectively highlights pathways of interest in vivo. We define the combined use of multiple tracers as the integration within a single experimental system of multiple precursors with stable isotope label. These precursors may have different chemical identity (glycerol vs. water), may include the same stable isotope (e.g. [D$_5$]-glycerol and D$_2$O) or different stable isotopes (e.g. [U-^{13}C]-glycerol vs. [D$_5$]-glycerol). There are multiple examples of the combined use of stable isotope tracers in literature. For instance, Jones et al used the combination of [U-^{13}C]-propionate, ^{2}H$_2$O and [1,6-^{13}C$_2$]-glucose tracing to reconstruct key fluxes in the TCA cycle and gluconeogenic metabolic pathway through multi-dimensional NMR [151]. Landau and colleagues simultaneously applied ^{2}H$_2$O tracing with [6,6-D$_2$]-glucose tracing to measure absolute gluconeogenic output in diabetic patients treated with metformin [147]. Previous reports made use of computational analysis for the elucidation of [U-^{13}C]-glutamate fluxes in vivo in reconstructing central carbon metabolism in the heart, in particular to model the concentrations of all glutamate isotopomer species by mass action kinetics [127, 187]. The advantages of combined tracer methods include the analysis of multiple metabolic parameters in a single metabolic system, thereby minimizing the need for control conditions and reducing the

number of experiments necessary to ascertain metabolic fluxes. On the other hand, this very same ability makes the analysis of the resulting enrichment data more complicated, thus requiring sophisticated analysis to track the potential species generated by the multiple labels introduced into the metabolic pool of interest, such as our developed computational platform METRAN.

Further developing these ideas, there is evidence that providing multiple stable isotope labels within a single tracer molecule can augment the information gathered in experiments with limited experimental subjects. We define a multi-labeled tracer a precursor molecule containing multiple stable isotopes within its chemical structure, such that each tracer provides different and perhaps complementary information regarding the fate of the labeled atoms. The concept of multi-labeled isotope tracers exists in literature, where nutrition researchers utilized ^{13}C,^{15}N labeled amino acids to track protein synthesis rates as well as for structure determination of proteins [188, 189]. Positron Emission Tomography can use selective labeling of multi-labeled tracer molecules to augment the information obtained by positron emission of secondary ions involved in glucose or amino-acid metabolism [48, 190]. Multidimensional NMR techniques parse through the different sources of label by inspecting specific resonances of either ^{1}H, ^{2}H, ^{13}C ^{31}P or other paramagnetic nuclei individually [189]. Mass spectrometry on the other hand, can only detect changes in mass within a given molecular fragment, and cannot distinguish between sources of label per se. The use of multi-labeled tracers incorporating ^{13}C and ^{2}H for mass spectrometric analysis of intermediary metabolism is seldom reported in literature, in particular due to the lability of deuterium which requires detailed understanding of hydrogen transitions along a metabolic route. In this chapter, we report the use of a unique [U-^{13}C, D$_5$]-glycerol tracer custom-designed to analyze reversible and net fluxes in upper gluconeogenesis in vivo through mass spectrometry analysis of the glucose molecule.

The motivation for pursuing a combined, multi-labeled stable isotope strategy is that it facilitates the comprehensive estimation of metabolic fluxes contributing to hepatic glucose production in

vivo. In order to achieve comprehensive flux measurements in vivo, researchers will face a paradigm shift from estimation of individual fluxes by dilution as described in Section 2.4 to the simultaneous evaluation of enrichment in multiple metabolic pools. Multiple metabolic pools can be accessed by either broad spectrum metabolite enrichment measurements through mass spectrometry, or alternatively by combined, multi-tracer label incorporation into a single molecule. We have chosen the latter option as a means to limit the amount of sample needed for detection in a given sample of clinical value, such as a small animal organ or a human clinical sample. Comprehensive flux analysis measurements through combined, multi-labeled tracer incorporation will help elicit system properties of central carbon metabolism such as modularity and flexibility of flux redistribution, as well as reaction reversibilities that would otherwise requires specific tailored experimental design.

We define reaction reversibility as the ratio of the actual exchange flux to the maximum flux (forward plus exchange flux) where the forward flux is by definition 100. Reversibilities are expressed in percent of the forward flux, with minimum value of 0% for no exchange flux in irreversible reactions, or 100% for a fully reversible reaction. Reaction reversibility measurement requires careful design of labeled hydrogen tracers that exchange label with environment water or intervening metabolites. For example, Malaisse et al analyzed the use of deuterium incorporation from water by yeast phosphoglucoisomerase through NMR and radioisotopic methods, and found evidence for intramolecular reaction transfer of deuterium to the C2 of glucose in 72% of reactions in the direction from G6P to F6P [80, 81]. This intermolecular reaction changes the expected enrichment patterns of deuterium in C2 of the produced glucose molecule, and must be taken into account when modeling upper gluconeogenesis. In order to achieve accurate reconstructions of net fluxes and reversibilities, computational modeling of metabolic fluxes needs complete knowledge of carbon and deuterium tracer atom transitions in the pathways of interest, and computational power required to track all potential enriched species generated. Data-driven comprehensive flux

measurement could be potentially integrated with genomic, proteomic and metabolomic data becoming increasingly available to researchers.

Additional constraints in developing in vivo metabolic reconstruction methodologies include:

- Safety of tracer administration
- Perturbations to the biochemical status of the individual by the chosen tracer
- Nature of the sample to be analyzed
- Nature and amount of the compounds to be analyzed
- Signal to noise ratio for isotopic enrichment

Safety of tracer administration is of paramount importance in medical research. The chosen tracers should be possible to readily administer to patients preferably in non-invasive fashion, hence the importance of deuterated water administered orally in estimating total body water, fractional gluconeogenesis and multiple biosynthetic rates [144, 191]. The route of administration impacts how quickly the patient may reach isotopic steady state, the overall circulating concentration of the chosen tracer and consequently the metabolic fluxes observed. The nature of the sample analyzed also determines the number of metabolites observed, their respective concentrations and the overall enrichment present. For instance, glucose enrichment is observable in plasma samples from a normal patient, but nearly impossible to observe in urine unless pathology is present. Lastly, the interacting pathways leading to the observed labeling pattern need to be carefully and systematically considered to limit the ability of the model to overfit the data presented.

Recently, our group estimated statistically satisfactory flux distributions from combined ([U-^{13}C]-glucose + [1-^{13}C]-glucose) tracers through computational reconstruction of metabolic fluxes from amino acid isotopomer data in microbial systems, under conditions where amino-acid metabolism may be changing slowly with respect to the timescale of isotope incorporation into the system [160]. This progress motivated us to question whether we could apply similar comprehensive tools for metabolic flux elucidation in vivo in a well-studied metabolic route such as hepatic glucose production, which has clinical importance as a contributor to the hyperglycemia observed in patients

with Type 2 Diabetes. We considered the aforementioned constraints in designing a combined multi-labeled tracer strategy to analyze the metabolic flux distribution of hepatic glucose production in as detailed degree as possible with our current mass spectrometric technologies. These specifications led us to use multiple stable isotope tracers simultaneously within a single experiment, to maximize the amount of information observed from readily accessible plasma glucose. Our methodology builds on Landau's deuterated water method with the addition of a distinct [U-^{13}C,D$_5$]-glycerol tracer. These tracers are dosed simultaneously, and we rely on measurement of ^{2}H and ^{13}C enrichment in the glucose molecule. We measured enrichment of six different glucose fragments using recently introduced methods [13]. These data collective define an overdetermined data set with 25 redundant measurements from which accurate metabolic fluxes and their respective confidence intervals are estimated. This is in contrast to current strategies in perfused livers integrating ^{13}C and ^{2}H NMR to calculate mutually exclusive fluxes [33, 153]. We report on the development of this labeling strategy that uses a doubly-labeled [U-^{13}C,D$_5$]-glycerol tracer, coupled with [6,6-D$_2$] glucose and ^{2}H$_2$O that elucidates detailed metabolic flux distributions of glucose production in vitro and in vivo. This work facilitates comprehensive flux determination as physiological markers aiding the understanding of metabolic disease as Type 2 Diabetes and Obesity.

5.2 Materials

Bovine insulin, dexamethasone, glucagon, Dulbecco's modified Eagle's medium powder (DMEM), fetal bovine serum (FBS), and other cell culture reagents were purchased from Sigma (St. Louis, MO). Biochemicals were obtained from Sigma Chemicals (St. Louis, MO) unless otherwise specified. [U-^{13}C]glycerol was obtained from Cambridge Isotope Laboratories (Andover, MA). [^{2}H$_5$]-glycerol was obtained from Isotec (Miamisburg, OH). The custom synthesized glycerol tracer [U-^{13}C, D$_5$]glycerol (99+ At% 13C, 98+ At% 2H) was purchased from Omicron Biochemicals (South Bend,

IN). The isotopic purity was of the tracer validated by GC/MS analysis. Hepatocyte Medium Base was DMEM powder (Sigma) supplemented as described by Block [161]. Hepatocyte Attachment Medium consists of Hepatocyte Medium Base supplemented with 5 nM insulin, 100 nM dexamethasone and 20 mM glucose. Hepatocyte Growth Medium (HGM) consists of Hepatocyte Medium Base supplemented with 1 nM insulin, 100 nM dexamethasone and 20 mM glucose. Medium containing gluconeogenic precursors includes the following substrates: 1 mM pyruvate, 10 mM lactate, 5 mM glutamine, 2 mM acetate and 1 mM glycerol. Hormones, glucose, and fetal bovine serum were added to this base medium as specified. We used ALZET Pumps model 2001D (Durect, CA) as described previously [115].

5.2.1 Animals

Male C57BL/6 mice were obtained from Taconic (Germantown, NY). Animals were housed in a facility approved by the American Association for Accreditation of Laboratory Animal Care. All animals received humane care in compliance with institutional guidelines. Mice had free access to water and chow *ad libitum* before the study. Mice were between 7 and 12 weeks old and 25-32 g body weight at their time of sacrifice.

5.3 Experimental Methods

5.3.1 Hepatocyte Isolation and Experiment

Our hepatocyte isolation protocol is based on Block et al [161] and further developed by Wong [156] and described previously (Chapter 4). For glucose production experiments, isolated hepatocytes were suspended in Hepatocyte Growth Medium (HM) and cultured in 6-well plates (10^6

cells/well) for 30 minutes at 37°C. After this time we collected the cell suspension, centrifuged for 1 min at 50g and 4C and collected the supernatant for glucose enrichment analysis.

5.3.2 ALZET Pump Implant

ALZET Pump model 2001D was implanted in 7-12 week-old mice as recommended by the manufacturer. The site of implantation is the dorsal space slightly posterior to the scapulae; once implanted the contents of the pump are delivered into the local subcutaneous space, and absorption of the compound by local capillaries results in systemic administration similar to arteriovenous administration [115, 116]. We anesthetized each animal with tribromoethanol (250 mg/kg IP) as general anesthetic and buprenorphine preoperatively (0.1 mg/kg IP, 0.08 mL) as analgesic. Animals usually recovered readily from the implantation procedure within hours, and fasted through the extent of the infusion.

The pump cargo included 2M [U-^{13}C, D$_5$]-glycerol, 2M [6,6-D$_2$]-glucose dissolved in saline solution. These concentrations were sufficient to administer tracer through the extent of the experiment (Table 5.1). Each mouse was simultaneously injected a bolus of deuterated water saline solution to reach 5% total body water enrichment, and fed 5% deuterated water *ad libitum*. Mice were fasted through the extent of the experiment, and sacrificed at 6 hr post-pump implant for plasma and tissue collection.

For mass spectrometric assumption validation, several variants of the aforementioned protocol were employed. For time course experiments evaluating glycerol enrichment, mice (n=2) were fitted with pumps including only 2M [U-^{13}C, D$_5$]-glycerol in 200 mL of saline solution. Mice were allowed to recover from surgery at predetermined times of 3, 6, 12 and 24 hours fasting, after which plasma and liver tissues were collected and snap frozen at -80C.

For tracer substitution experiments, mice (n=2) were fitted with pumps including either 2M [6,6-D$_2$]-glucose, 2M [U-^{13}C, D$_5$]-glycerol or 2M [U-^{13}C, D$_5$]-glycerol in 200 mL of saline solution. Mice were allowed to recover from surgery for 6 hr fasting, after which plasma and liver tissues were collected and snap frozen at -80C.

5.3.3 Derivatization of glucose, glycerol

Glucose labeling patterns were determined by GC/MS analysis of aldonitrile pentapropionate, methyloxime pentapropionate and di-O-isopropylidene propionate derivatives of glucose [166] as described previously (Chapter 4). Glycerol labeling patterns were determined from the glycerol aldonitrile propionate derivative at m/z 173 in the same GC-MS run as the derivatized glucose.

5.3.4 Isotopomer Enrichment Analysis

Gas Chromatography-Mass Spectrometry (GC/MS) analysis for isotopomer enrichment was as described previously (Chapter 4). Measured intensities were corrected for the contribution of noise (baseline correction), and mass isotopomer distributions were obtained by integration. All mass isotopomer values were expressed as fractional abundances, whereby the sum of all mass isotopomers equals one. All aforementioned fragments were utilized in the integrated analysis of mass spectra for flux analysis in each treatment condition unless otherwise noted.

5.3.5 Computation methods

The generalized algorithm for MFA was incorporated into Matlab based-flux analysis package METRAN as described in section 2.3.4. Briefly, at convergence, nonlinear statistical techniques were

applied to obtain accurate 95% confidence intervals of fluxes by evaluating the sensitivity of the objective function with respect to fluxes using elementary metabolite unit theory as described previously [13, 102]. Flux validation was accomplished by a statistical test for the goodness-of-fit based on chi-square test for model adequacy, and a normality test for the weighted residuals [105]. To ensure that a global optimum was found, flux estimation was repeated at least four times starting with random initial values to residual sum of squares accepting the proposed model with the 95% confidence interval. Sensitivity analysis was employed to determine the most important measurements for estimation of individual fluxes as described previously [13]. All computations were performed with Matlab 6.5 and Matlab Optimization Toolbox (Mathworks, Natick, MA).

The gluconeogenesis network model used for flux calculations was described previously (see Chapter 4, Figure 4.3 and Table 4.1). In short, the network model is comprised of 24 reactions utilizing 26 metabolites, with 5 substrates (oxaloacetate, glycerol, glycogen, water, and NADH from endogenous sources), 3 products (glucose, CO2, and a metabolic sink for NADH), and 18 balanced intracellular metabolites. Stereospecific atom transitions were assigned for all reactions in the model based on current knowledge.

5.3.6 Statistics

Data were analyzed using a Student's t test (Microsoft Excel) for single comparisons between means from experimental groups. $P < 0.05$ was considered statistically significant. In cases where multiple groups were all compared to a single group, the Dunnett's test for multiple comparisons was applied [192]. $P < 0.05$ was considered statistically significant.

5.4 Results

5.4.1 Computational reconstruction of upper gluconeogenesis by combined, multi-labeled tracer infusion.

We established the utility of using multiple tracers within a single experiment (combined tracer approach) during in vitro experiments with primary hepatocytes capable of glucose production. Based on our previous cellular work (Chapter 4), we selected glycerol as tracer due to its aggressive uptake for the production of glucose by the liver relative to traditional tracers such as alanine, pyruvate and glutamine. There is evidence that glycerol can act as an effective tracer for measurement of rate of appearance of hepatic glucose [136], while others point out that glycerol as a gluconeogenic tracer may be problematic when calculating fractional synthesis rates by polymerization, in that it consistently underestimates the desired rates of synthesis [138, 139]. Our method does not make use of combinatorial mathematics, and our previous work with mouse hepatocytes as well as computational modeling [13] suggests that a custom-designed, multi-labeled [U-^{13}C,D$_5$]-glycerol tracer can overcome dilution limitations due to tissue heterogeneity given its inclusion of ^{13}C on its skeleton.

A key consideration in the design of these *in vivo* experiments is how to provide the tracer in vivo. We adopted the use of mini-osmotic pumps in mice described in literature for the continued dosing of tracer in the form of gluconeogenic precursor glycerol [115, 116]. With the exception of deuterated water, gluconeogenesis precursors undergo partial metabolism in peripheral tissues that may confound the spectrometric measurements of the glucose molecule. In addition, partial consumption of these metabolites through portal circulation necessitates their continued dosing to ensure significant presence and enrichment of the end molecule glucose while maintaining pseudostationary metabolic steady state. Furthermore, a constant rate of infusion allows for gradual

adjustment of the hepatic metabolic program whereas a bolus infusion would perturb the synthetic rates associated with the metabolic fluxes to be determined. Instationary flux analysis techniques may permit the development of flux analysis strategies in the transient period before reaching isotopic steady state, which would additionally provide information regarding active pool sizes of metabolites [87].

We next considered the amounts of tracer that need be present in order to obtain measurable enrichment signal in plasma glucose. Glycerol concentrations in murine blood are approximately 0.05-0.3 mM, with a total circulating amount in the micromolar range. The fixed pumping rates afforded by the miniosmotic pumps allowed us to determine the rate at which compound was being delivered to the subcutaneous space. From preliminary cellular experiments, we estimated that approximately 20-30% of the total glycerol present must be enriched in order to have significant label uptake into the glucose molecule to allow reliable metabolic flux reconstruction. Titration of glycerol pumping rates from 0.0075 mg/hr to 1.5 mg/hr resulted in a non linear uptake of glycerol into circulating glucose. At 1.5 mg/hr glycerol we reached 30% enrichment as determined by mass spectrometric measurements. At this pumping rate, circulating glycerol can be expected to turn over in a timescale of minutes (Table 5.1) thereby enabling a pseudo-stationary analysis of metabolism. An important disadvantage of high glycerol concentrations in vivo is the non-physiological nature of this tracer in contributing to gluconeogenesis.

Our methodology does not rely on glycerol condensation into glucose to describe gluconeogenesis, but instead utilizes the fractional gluconeogenesis estimation method from deuterium enrichment in C5/C2 as proposed by Landau [144]. Deuterium C5/C2 enrichment afforded accurate estimation of fractional gluconeogenesis in fasted murine hepatocytes, but overestimation of fractional gluconeogenesis in fed mouse hepatocytes, due to observed disequilibrium of PGI under our culture conditions in abundance of gluconeogenic substrates [13].

Using 10% deuterated water tracer in vivo in fasted mouse implanted with a sham pump, we replicated the ability to estimate fractional gluconeogenesis from deuterium enrichment in C2 of glucose versus deuterium enrichment in C5 of glucose. We incorporated isotopomer data from aldonitrile pentapropionate glucose fragments at m/z 173 and 370, methyloxime pentapropionate glucose fragment at m/z 145, and di-O-isopropyledene propionate glucose fragment at m/z 301 into our metabolic model and obtained statistically acceptable fit at SSRES of 2.3. Qualitatively, M1 enrichment in aldonitrile pentapropionate fragment m/z 173 corresponds to deuterium enrichment at carbon C5, M2 enrichment at fragment m/z 370 corresponds to deuterium enrichment in both C2 and C5, while M1 enrichment at methyloxime pentapropionate fragment m/z 145 corresponds to deuterium enrichment at C2. Figure 5.1 presents the isotopomer spectrum for one such glucose fragment at m/z 370, for both uncorrected abundance (5.1A) and the corrected counterparts (5.1B). We use this information to separate the contributions of deuterated water from multi-labeled glycerol tracer in our in vivo flux analysis methodology. In this way, our methodology circumvents the limitations regarding triose phosphate disequilibrium stated by Previs et al. for fractional gluconeogenesis calculation from through MIDA [139].

The combination of isotopic tracers in vivo serves to augment the resolution of upper gluconeogenesis fluxes. The simplest measurement of glucose production metabolism involves using deuterated water in vivo, where a single tracer provides accurate determination of fractional gluconeogenesis. We measured fractional gluconeogenesis in vivo in a fasted mouse through positional deuterium enrichment only shows gluconeogenesis contribution to total glucose production of 100±5% as seen in the left hand panel of Figure 5.2. The blue numbers in this figure represent net fluxes for the outlined reaction, with the bounding interval presented where fluxes cannot be reliably estimated. The fractional contribution of glycogenolysis cannot be determined directly by this approach but is estimated indirectly through balance at the G6P junction. Glycogen

is seen to contribute minimally to the production of glucose in this model. Deuterated water enrichment of plasma glucose gives only coarse estimates of the contributions of glycerol compared to the oxaloacetate, with the majority of flux towards glucose deriving from the oxaloacetate pool of metabolites including lactate, pyruvate and alanine. As each experiment was performed individually in a single mouse, the confidence intervals presented in Figure 5.2 correspond to estimation of error of the proposed metabolic model to describe the observed enrichment patterns in the glucose molecule. They do not represent standard error of multiple experiments, but rather our confidence in the ability to estimate the flux of interest from the data present. Factors that affect this interval include but are not limited to: quality of the isotopomer data, number of isotopomers or glucose fragments present for analysis and number of reactions in the proposed metabolic model [105]. We conclude that fluxes determined from deuterated water analysis are characterized by tight confidence around the G6P branchpoint, but are rather poorly suited to describe the contribution of different substrates to gluconeogenesis in particular when glycerol is present as a gluconeogenic substrate.

We next considered the possibility of augmenting the available enrichment information in the glucose molecule by the addition of glycerol tracers. In particular, we used a unique multi-labeled [U-^{13}C,D$_5$]glycerol tracer as source of enrichment of higher mass isotopomer of glucose that would permit the usage of the M1 isotopomers in the aldonitrile glucose fragment at m/z 173 and 370 for the exclusive analysis of enrichment by water. One disadvantage of using this tracer is that isotopomer data cannot be corrected for natural abundance as both ^{13}C and ^{2}H enrichment can be expected in the resulting glucose molecule. Therefore, proposed isotopomer distributions must be computationally simulated based on the metabolic model of interest. We performed each simulation from four different starting points in order to insure convergence of the flux estimates obtained from data-driven computation. We present below uncorrected isotopomer data in order to reflect the raw data presented in Appendix 1.

As shown in Figure 5.1A, the addition of [U-^{13}C, D$_5$]-glycerol individually increases qualitative and mol percent enrichment of the glucose molecule in mouse plasma. The source of this enrichment could be deuterium, carbon-13 or a combination of these. We incorporated isotopomer data from aldonitrile pentapropionate glucose fragments at m/z 173, 259 and 370, methyloxime pentapropionate glucose fragment at m/z 145, and di-O-isopropyledene propionate glucose fragment at m/z 301 into our metabolic model presented in Chapter 4, obtaining statistically accepted fit at SSRES of 24.3. The aldonitrile pentapropionate glucose fragment at m/z 284 was not included in this analysis due to poor data quality. The set of glucose fragments presented in Chapter 4 and used here reconstructs the positional carbon and deuterium enrichment of the glucose molecule and in turn the fate of atoms that contribute to the production of this molecule.

As shown in Fig. 5.2 (middle column), flux estimation with [U-^{13}C, D$_5$]-glycerol accurately reconstructs the glycerol branch of upper gluconeogenesis contributing 52% of glucose production, by dilution of the glycerol tracer in plasma as well as inspection of carbon-13 incorporation into the resulting glucose molecule. As shown in Figure 5.1, the source of this increase in confidence stems from increased enrichment in higher mass isotopomers of glucose, and is appreciated directly visually in either uncorrected isotopomer data (Figure 5.1A) or corrected isotopomer data (Figure 5.1B). However, fractional total gluconeogenesis cannot be resolved within statistical certainty when using this tracer individually, and the only bounds for this flux can be estimated (interval [65-100]). The uncertainty in this flux stems from the inability to estimate the contribution of the OAA pool to the production of hepatic glucose, as shown by the bounded interval [76-150]. Thus, [U-^{13}C, D$_5$] glycerol is ideally suited to elucidate glycerol contribution to gluconeogenesis, but by itself is not a solution for comprehensive flux analysis of upper gluconeogenesis.

Simultaneous use of deuterated water and multi-labeled [U-^{13}C,D$_5$]-glycerol resolves both fractional gluconeogenesis and detailed reversibilities in the metabolic pathway of *de novo* synthesis of

glucose. We incorporated isotopomer data of glucose fragments from labeling with both D$_2$0 and the previous glycerol tracer and obtained statistically accepted fit at SSRES of 21.1. As observed in Figure 5.1, there is appreciable enrichment over the observed patterns when using [U-^{13}C, D$_5$]-glycerol individually in particular at higher mass isotopomers. M1 enrichment reflects that of deuterated water treatment, while M2 denotes increased enrichment over that of [U-^{13}C, D$_5$] glycerol treatment. Furthermore, the improvement in statistical confidence for substrate usage allows discernment of glycerol uptake relative to gluconeogenic substrates in the oxaloacetate pool (lactate, pyruvate, alanine). As shown in Figure 5.2 (right column), we confirm the fraction of glycerol at 52$\pm$4% with very tight confidence intervals. In this case, the contribution of gluconeogenic substrates through the oxaloacetate pool is better estimated at 137$\pm$4% of total glucose output. It is interesting to note that glycerol contributes a significant amount of flux to glucose production when present, consistent with earlier literature in primary rat hepatocytes, perfused livers and in vivo [73, 136]. On the other hand, glycerol is not considered a physiological source of glucose production as discussed in Chapters 2 and 4. Thus it is possible that the observed flux distributions in the presence of glycerol are different than those observed in an unperturbed system.

In this section, we presented evidence that combined, multi-labeled [U-^{13}C,D$_5$]-glycerol tracing of the glucose molecule augments the information obtained from plasma glucose enrichment in order to computationally reconstruct upper gluconeogenic metabolism. The encouraging flux results are enabled by redundancy in glucose isotopomer measurements due to multiple glucose isotopomer fragments from a family of derivatizations methods. Next, we sought to test the possibilities for reconstructing metabolic flux distributions in conditions where fluxes would be expected to change, such as feeding and fasting.

Uncorrected m/z 370

A)

Corrected m/z 370

B)
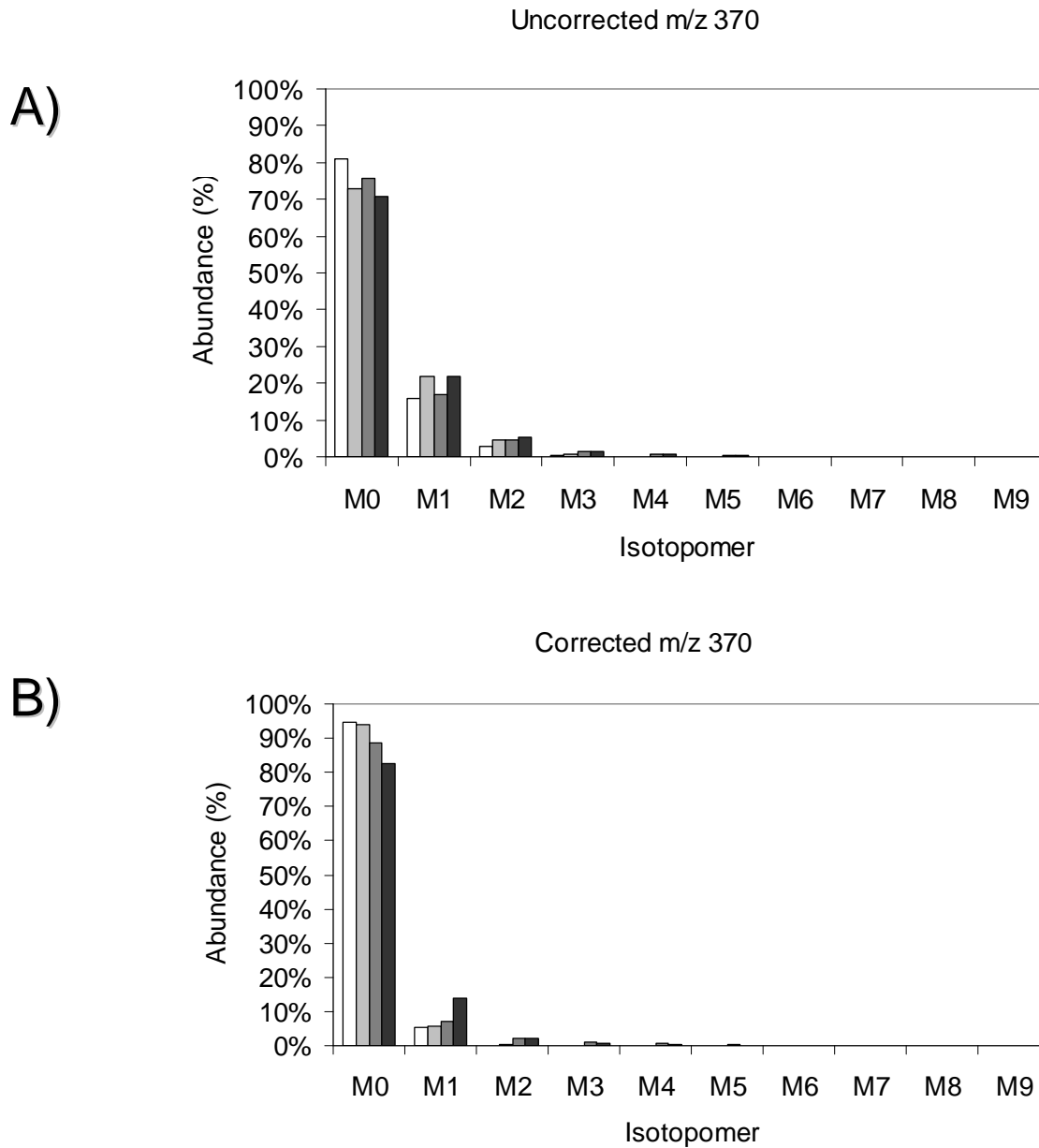
Figure 5.1: Aldonitrile pentapropionate glucose fragment 370 isotopomer spectra for pilot experiment demonstrating increased label incorporation in plasma glucose when using tracer [U-^{13}C, D$_5$]-glycerol alone or in combination with deuterated water. White bar = natural abundance, Light Gray = 10% Deuterated Water. Dark Gray = [U-^{13}C, D$_5$]-glycerol, Black bar = [U-^{13}C, D$_5$]-glycerol +10% Deuterated Water. A) Uncorrected mass isotopomer spectrum for aldonitrile pentapropionate glucose fragment with m/z 370. B) Simulated corrected isotopomer spectrum of aldonitrile pentapropionate glucose fragment with m/z = 370.
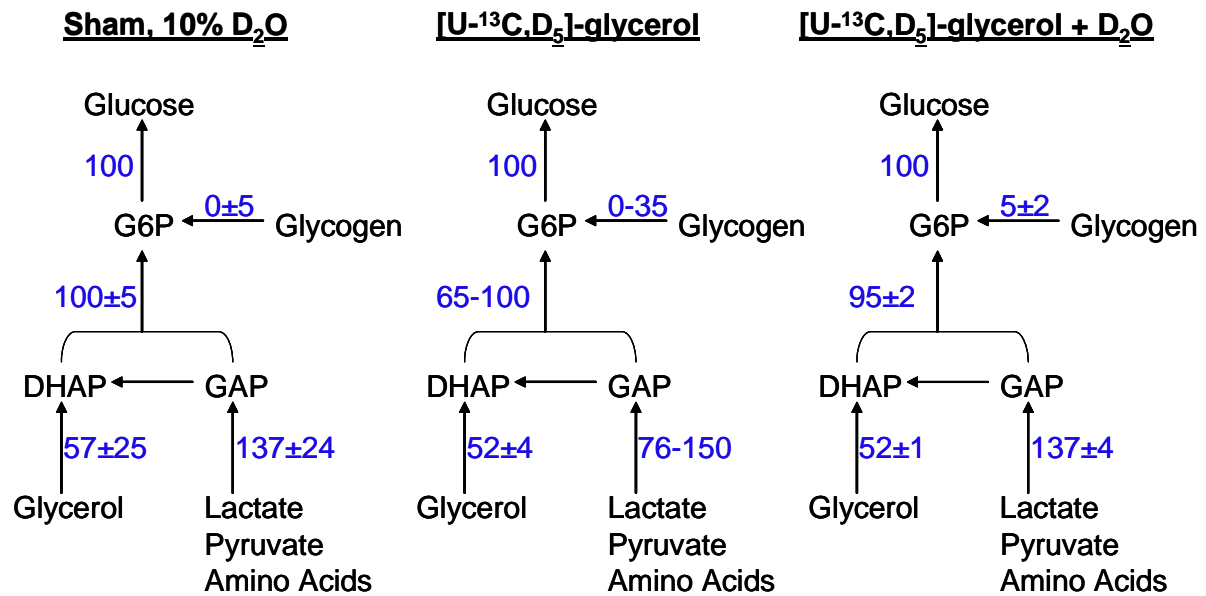
Figure 5.2: Increased resolution of flux determination via tracer combination in vivo for upper gluconeogenesis in mice. Pilot study comparing determined fluxes in individual mouse infusion experiments. Mice were surgically implanted miniosmotic ALZET pumps containing either saline (sham) or 2M [U-^{13}C, D$_5$]-glycerol, and injected via IP bolus deuterated water to reach 10% total body water enrichment (TBW = BW*0.6). After 24 hours, plasma was collected for glucose enrichment measurement through mass spectrometry. Mass spectrometric data were analyzed by METRAN. Fluxes are presented as percent total glucose production for each animal, +/- 68% confidence interval. Where confidence intervals cannot be calculated exactly, the interval bounding the estimated flux is presented.

5.4.2 Physiologic validation of comprehensive in vivo metabolic flux analysis of upper gluconeogenesis.

<u>Study of fed vs. fasted hepatocytes</u>

The computational validation of the flux estimates obtained constitutes a marked improvement in realizing comprehensive flux estimation of upper gluconeogenesis. However, care must be exercised to ensure that the flux estimates thus obtained are reasonable in the context of various physiological paradigms one wishes to study. As a physiological check of the validity of the estimated fluxes in the context of hepatic glucose production, we sought to determine the contribution of gluconeogenesis to hepatocyte glucose production in a feeding situation. A significant body of work has documented the changes in this ratio in the absence of glycerol, where gluconeogenesis may contribute 40-60% of the total glucose output of a fed liver, compared to a 80-100% of total glucose production in a fasted liver [42, 193]. To this end, we isolated hepatocytes from ad libitum fed C57BL/6 mice in tandem with hepatocytes of a 24 hour fasted mouse, and measured glucose production enzymatically and through stable isotope incorporation into the glucose molecule over a 30 minute incubation where the contribution of glycogen breakdown would also be present. Our method assumes that glycogen breakdown contributes only unlabeled glucose to the total pool of produced glucose. A representative sample of the obtained isotopomer fractions of glucose fragments at m/z 301, 145 and 370 representing three different derivatizations procedures is shown in Figure 5.3. The left hand panel presents data utilizing 10% deuterated water as the source of ^{2}H label, while the right hand panel presents data utilizing a combination of 25% [U-^{13}C, D$_5$] glycerol and 10% deuterated water. We present data as uncorrected isotopomer spectra since, as mentioned earlier, the presence of ^{13}C and ^{2}H within a single product glucose molecule precludes the correction procedure based on known abundances of the aforementioned isotopes.

Several patterns emerge just from visual inspection of glucose enrichment data in the feeding and fasting experiment in Figure 5.3. Glucose isotopomer enrichment measurements are highly reproducible, unlike amount or concentration measurements that depend on sources and sinks contributing to the circulating plasma pool. Triplicate analysis confirmed biological variation in enrichment to be relatively small and at all times less than 0.3 mol%. Thus, the isotopomer signature both in vitro and in vivo provides a reliable means to reconstruct metabolism independent of metabolite concentrations, provided the metabolite of interest is present in sufficient amount for accurate measurement of the isotopomer envelope. Secondly, we observe significant differences in the isotopomer spectra obtained under feeding and fasting physiologies, as well as different from natural abundance of plasma glucose. Qualitatively we observe that fasting hepatocytes yield more enrichment of higher isotopomers than their feeding counterparts. The notable exception to this trend is m/z 145, which encompasses the C5 and C6 carbons of the glucose molecule and the corresponding deuterium at C5. We utilized the complement of glucose fragments at m/z 145, 173, 259, 284, 301 and 370 to computationally reconstruct upper gluconeogenic fluxes, with statistically accepted SSRES of 13.0 and 21.1 for the correspondence between proposed and simulated glucose isotopomer measurements.

The resulting metabolic reconstructions of upper gluconeogenesis from MS glucose fragments are shown in Figure 5.4. As before, we present only net fluxes in blue for clarity. We note that fed hepatocytes are significantly more active than fasted mouse hepatocytes in their glucose production (GP), with net glucose production values of 318±12 nmol/10^6 cells/hr when compared to fasted hepatocytes producing 142±17 nmol/10^6 cells/hr ($p<0.05$). The most important result in this experiment relates to changes in fractional gluconeogenesis. Specifically, fractional GNG accounts for 42% of total glucose output in fed hepatocytes compared to 95% of total glucose production in fasted hepatocytes. This result compares well with measurements in fasting

gluconeogenesis in mouse hepatocytes, as well as refed mice fitted with subcutaneous ALZET pumps [115]. The most striking change in fluxes occurs for the glycogenolysis flux, increasing from values of 5%±2 in fasted hepatocytes to 58%±2 in fed hepatocytes. This flux may reflect the increased availability of glycogen in fed hepatocytes as well as the increased activity of glycogenolytic enzymes such as glycogen phosphorylase. The tenfold increase in glycogenolysis flux contrasts the change observed in fractional gluconeogenesis, from 42%±2 in fed hepatocytes to 95%±2 in fasted hepatocytes. On a normalized scale, glycerol and oxaloacetate consumption rise in the fasted state to accommodate the demand on glucose-6-phosphate due to increased gluconeogenesis. The usage of glycerol by fed and fasted hepatocytes is significant and consistent with values observed in Chapter 4. In addition, we observe that fasted cells preferentially increase their substrate usage fluxes from the oxaloacetate pool over the glycerol pool, as the triose phosphate usage of oxaloacetate increases from 55/84 to 137/190 from fasted to fed hepatocytes. This pattern is suggestive of increased demand on the oxaloacetate pool of metabolites by PEPCK in fasting conditions, unlike the results observed in Chapter 4 for glycerol fed-hepatocytes.

In addition, fractional equilibration for the following four reactions was estimated precisely: 63%±5 equilibration for PGI, 72%±4 equilibration for TPI, 8%±3 equilibration for transketolase, and 18%±6 equilibration for the combined activity of PMI and G6PDH reactions. The estimated reaction reversibilities were identical for fasted and fed hepatocytes, suggesting that these fluxes are not affected by changes in nutrient availability from feeding to fasting conditions in the conditions studied for hepatocyte glucose production. To our best knowledge, this is the first method that allows the estimation of reaction reversibilities in the gluconeogenesis pathway in vitro without specific tracer design.
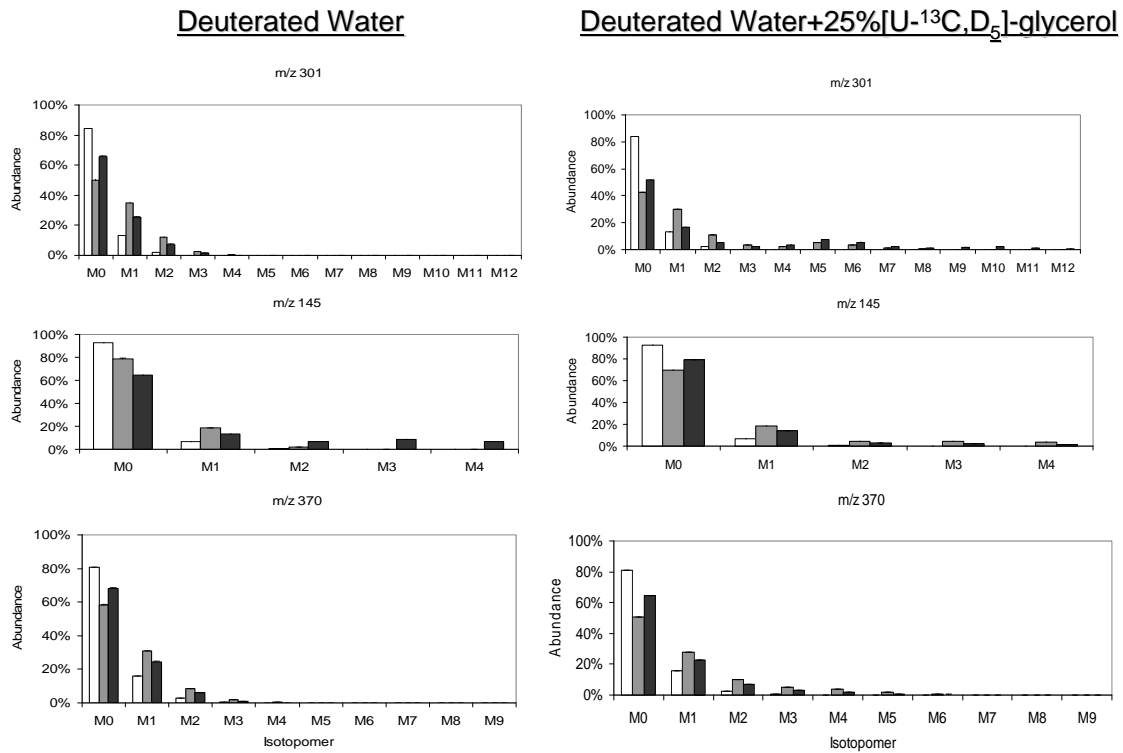
Figure 5.3: Glucose Isotopomer Spectra for production under fasting (gray) or feeding (black) condition in primary mouse hepatocytes. White bars correspond to natural abundance. Tracer is 10% deuterated water in the left panels, and a combination of 25% [U-^{13}C, D$_5$ glycerol] and deuterated water in the right hand panels. Data presented are uncorrected mass isotopomer spectra for 3 different derivatizations methods. Data are mean ± SEM (n=3).

A) **Fed**   B) **Fasted**

Glucose   Glucose

100   100

G6P ← 58±2 Glycogen   G6P ← 5±2 Glycogen

42±2   95±2

DHAP ← GAP   DHAP ← GAP

29±1   55±2   52±1   137±4

Glycerol   Lactate   Glycerol   Lactate
           Pyruvate   Pyruvate
           Amino Acids   Amino Acids

GP = 318±12   GP = 142±17
nmol/10^6 cells/hr   nmol/10^6 cells/hr
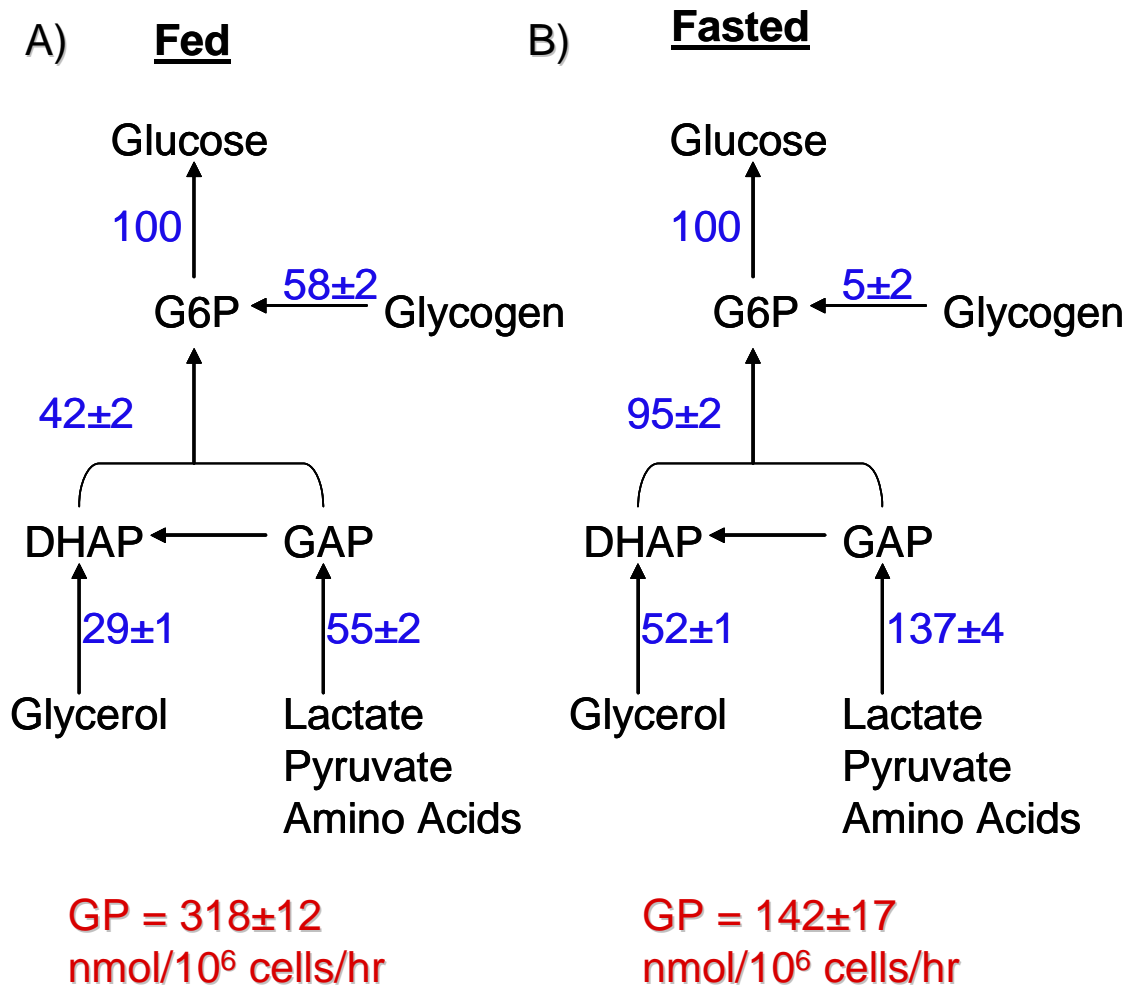
Figure 5.4: Tracer combination reconstructs feeding-fasting hepatic glucose metabolism. A) Hepatocytes from *ad-lib* fed or 24 hour fasted mice were isolated and cultured in the presence of 25% [U-^{13}C, D$_5$]-glycerol (1 mM) and 10% deuterated water for 30 minutes (n=3). We collected supernatant and analyzed medium glucose for stable isotope enrichment through mass spectrometry and integrated data using METRAN. Fluxes are presented as percent total glucose production for each animal, +/- 68% confidence interval. GP = glucose production, data are mean ± SEM.

In vivo physiological validation of fasting hepatic glucose metabolism

Next, we applied the combined, multi-labeled tracer approach to the study of fluxes in fasted mice. These experiments served several objectives. First, they sought to reconstruct metabolic fluxes in vivo from glucose isotopomer enrichment data using our proposed combined-multi labeled-tracer strategy as designed by the previous experiments in hepatocytes. Second, we chose to perform 6 hour infusions for in vivo flux determination. This interval was selected such that, on the one hand, it would allow sufficient incorporation from glycerol into glucose and limit potential effects of tracer recycling. In vivo flux analysis was performed in fasted C57BL6 mice (n=2) fitted with subcutaneous ALZET pumps. Cargo included a combination of 2M [U-^{13}C,D$_5$]-glycerol, 2M [6,6-D$_2$]-glucose, while deuterated water was injected intraperitoneally to reach 5% total body water enrichment and fed subsequently *ad libitum*. We measured the enrichment of glucose through aldonitrile pentapropionate fragments at m/z 173, 259, 284 and 370, with methyloxime pentapropionate fragment at m/z 145 and di-isopropyledene propionate fragment at m/z 301. The resulting isotopomer spectra were used in flux reconstruction using METRAN with accepted SSRES of 41.8 and 20.9 respectively.

Results of flux distributions are shown in Figure 5.5 normalized to 100% of total glucose output flux. For this experimental setup the presence of [6,6-D$_2$] glucose enables the calculation of hepatic glucose production (HGP) at 32.5 mg/kg/min from the enrichment of isotopomer M2 in the glucose spectrum by dilution and therefore anchor relative fluxes to an absolute scale. The reported HGP value of 32.5 mg/kg/min is higher than hepatic glucose output rates in IV infused rats (14±1) [136] and even mice (22±3) [15] Possible reasons for discrepancies between our values and those reported in literature include stimulation of glucose production by the administered glycerol. At the same time, the enrichment in higher isotopomers allows detailed flux elucidation of

hepatic glucose production, fractional gluconeogenesis and percent contribution of multiple substrates to gluconeogenic flux.

In our in vivo flux analysis of hepatic glucose production, gluconeogenesis contributes 79±7% of flux to hepatic glucose production as determined by deuterium enrichment in C5 over C2. This result is lower than our previous estimations in fasting mouse hepatocytes (95±2%, Figure 5.4B), rat hepatocytes (76±8%, Chapter 4) but higher than fractional gluconeogenesis of 51±7% reported in fasting rats after 6 hours and closer to fractional gluconeogenesis observed in fasted rats after 11 hours (79±8%) [136]. Estimates for fractional gluconeogenesis as high as 95% under fasting conditions can be a consequence of the fast metabolic rate of mice. (Chapter 4) [124]. Discrepancies may be due to food residues in mouse cage, incomplete depletion of glycogen stores after a 6 hour fast and timing of the surgical intervention for ALZET pump implant. As observed in Figure 5.5 for the in vivo metabolic flux distribution, the liver draws primarily from the oxaloacetate pool to meet its physiological demand for glucose. Glycerol contributes only 12% of total carbon flux, in accord with the smaller circulating pool of this substrate in a physiological context compared to alanine, pyruvate and lactate. This result was surprising, especially when comparing the uptake observed for in vitro glucose production in the presence of glycerol (Chapter 4). These results indicate that the metabolic regime operating during in vivo flux analysis is substantially different from that in vitro, with moderate usage of glycerol substrates compared to the gluconeogenic substrates in the oxaloacetate pool. The proportions of glycerol:pyruvate:lactate concentrations are conserved as 1:1:10 in all experiments, but the absolute amounts in cellular experiments are approximately tenfold those in vivo.

Hydrogen labeling from [U-^{13}C,D$_5$]-glycerol glycerol permitted the estimation of reaction reversibilities as defined in the equation inset of Figure 5.5, as a ratio of the exchange flux relative to the maximum forward flux of 100. Exchange fluxes are defined as the minimum of the forward and

reverse fluxes of a reversible reaction. Computational reconstruction of upper gluconeogenesis metabolism suggests the presence of transketolase and phosphomannose isomerase activities, shown by the reaction reversibilities of 21±5% and 24±12% respectively. Cohen and colleagues reported transketolase activity of 10% in fasted rat hepatocytes through ^{13}C NMR incorporation from [2-^{13}C]-glycerol [73]. Our results denote a significantly higher presence of transketolase activity. Reaction reversibility analysis obtained from deuterium labeling also confirms that phosphoglucose isomerase and triose phosphate isomerase have reversibilities close the maximum allowable value of 100%, as assumed by the Landau method.

Glucose

100

G6P $\xleftarrow{21\pm2}$ Glycogen

79±7

DHAP $\xleftarrow{67\pm7}$ GAP

12±0.4

146±10

Glycerol   Lactate
                Pyruvate
                Amino Acids
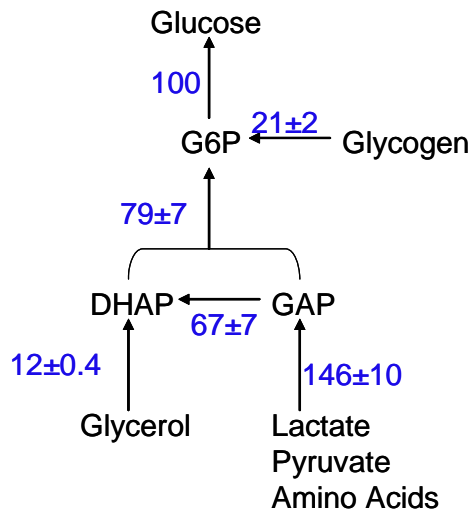
- HGP = 32.5 ± 0.5 mg/kg/min
- Reaction Reversibilities
  - PGI: 74±7
  - TPI: 83±5
  - TK: 21±5
  - PMI: 24±12

$$\% equil = \frac{v_{exch}}{v_{exch} + 100} \times 100$$

$$v_{exch} = \min\left(v_f, v_r\right)$$

Figure 5.5: In vivo flux distribution for hepatic glucose metabolism after 6 hour infusion. Fasted C57BL6 mice (n=2) were infused a combination of tracers through miniosmotic ALZET pump including 2M [6,6-D$_2$]-glucose, 2M [U-^{13}C, D$_5$]-glycerol, and 5% deuterated water (intraperitoneal and fed) over 6 hours, at which time plasma was collected. Absolute hepatic glucose production is calculated by dilution Fluxes are presented as percent total glucose production for each animal, +/- 68% confidence interval. Reaction reversibilities are presented as percent and defined as in the equation inset, where exchange flux v_{exch} is the minimum of the forward flux (v_f) and the reverse flux (v_f). PGI = phosphoglucose isomerase, TPI = triosephosphate isomerase, TK = transketolase, PMI = phosphomannose isomerase.

5.4.3 Assumptions of in vivo flux determination

Several assumptions are key to our ability to reconstruct metabolic fluxes from mass spectra.

They are:

- Pseudo-metabolic steady state
- Isotopic steady state
- Deuterated water labeling constant
- No scrambling of glycerol tracer
- No TCA cycle usage of tracer signal

Metabolic Pseudo-Steady State

The first assumption deals with metabolic steady state, the condition whereby metabolic intermediary concentrations remain constant through the time period over which fluxes are evaluated. True metabolic steady state, as discussed in Chapter 2, is not achievable in vivo due to lability of the metabolic pools studied, compartmentation of metabolites or active regulation of metabolite concentrations by hormonal influences. The concept of a physiological steady state involves a homogenous pool in which mixing of the tracer occurs rapidly [61]. We can perform flux calculations under the assumption of a pseudo-metabolic steady state such that isotope enrichment of metabolite pools of interest occurs on a faster time scale than that over which metabolite concentration pools change. In the case Table 5.1 highlights the relevant design specifications for the pump characteristics used for tracer infusion. Glycogen stores in mouse liver are estimated to have a turnover time of 3 hrs in the postprandial state from analysis in fed mouse hepatocytes [164]. Based on this estimate of the size of the metabolic pool of glucose in the liver, we designed our infusion strategy such as to maintain a pseudo-metabolic steady state over a time period of 4-6 hours, the timescale over which liver glycogen stores turn over completely. For the substrate flow rates in Table 5.1, plasma glycerol turns over in minutes due to its small circulating concentration, whereas glucose turns over in minutes to hours. Providing both substrates at a constant infusion

over multiple hours at high concentrations abolishes potential metabolic gradients known to occur in the liver due to periportal and perivenous metabolic differences, but opens the possibility for substrate accumulation. From an experimental time point, we kept animals in a prolonged fast throughout the duration of the experiment in order to maintain the underlying hepatic physiology constant. Other groups subjected mice to 17h fasting infusions followed by 5h refeeding period, and observed metabolic changes in hepatic glucose production consistent with a fasting to feeding transition such as decreased fractional gluconeogenesis [115]. In addition, we designed time course experiments and delayed infusion experiments to be discussed below (Figures 5.7, 5.8) that confirm a pseudo-metabolic steady state at each 6 hour time period. Several researchers pointed to metabolic inequalities at the cellular level of hepatocytes in terms of the triose phosphate content when using [U-^{13}C]-glycerol as a tracer [139]. Calculation of reaction reversibilities can provide indication to the extent which the metabolic pathway for glucose production is perturbed due to the presence of the infused tracer or underlying metabolic changes. In our results presented in Figure 5.5, TPI and PGI reversibilities confirmed at 83% and 74% respectively. A severely perturbed metabolic system would be expected to reflect altered reversibilities due to mass action effects on the intervening enzymatic rates, and this is not the case from our computational evidence in vivo.

Table 5.1: Relevant ALZET pump specifications

- Model: 2001D
- Lifetime: 24 hr
- Pumping rate: 8 μl/hr

- Glycerol
    - Pump Concentration = 2M
    - Pump Amount = 400 μmol = 36.8 mg
    - Glycerol Flow Rate = 1.5 mg/hr
      = 24.6 μg/min
    - Plasma Concentration = 50-300 μM
    - Circulating glycerol
      = (300 nM/mL)*(1mL)
      = 300 nmol = 27.6 μg
    - Pool Turnover Time = 27.6 μg/24.6 μg/min = 1.1 min

- Glucose
    - Pump Concentration = 2M
    - Pump Amount = 400 μmol = 72.0 mg
    - Glucose Flow Rate = 2.9 mg/hr
      = 48 μg/min
    - Plasma Concentration = 5-7 mM
    - Circulating glucose
      = (5.6 μmol/mL)*(1mL)
      = 5.6 μmol = 1 mg
    - Pool Turnover Time = 1000 μg/48 μg/min
      = 20.7 min

Isotopic Steady State

The second assumption involves the presence of isotopic steady state during the tracer infusion under in vivo conditions. In physiological systems, isotopic steady state can be independently achieved from metabolic steady state in conditions such as exercise [61] The isotopic steady state assumption has several important implications that stem from the need to maintain a balance between introducing label at sufficient amounts to yield observable levels of glucose isotopomers and minimizing the perturbation of the metabolic system with the tracer in question. Deuterated water can be expected to equilibrate rapidly across body compartments in a span of hours when given as a primed infusion [145]. This is not necessarily the case with our additional tracers of [U-^{13}C, D$_5$]-glycerol and [6,6-D$_2$]-glucose, which we administered through constant infusion and have significant plasma pools to incorporate. To this end, we optimized infusion time in order to achieve maximum enrichment of plasma glucose due to [U-^{13}C, D$_5$]-glycerol. Animals were fitted with subcutaneous ALZET pumps for 3, 6, 12 and 24 hours using only [U-^{13}C,D$_8$] glycerol as a tracer, after which time plasma glucose was collected for enrichment analysis by GC-MS. Calculations in Table 5.1 suggest that 30 minutes of infusion time at the rates of the pump should be theoretically sufficient to replace the plasma glucose and glycerol pools with infused substrate. In reality, this time scale is extended due to stabilization of the pumping rate over the first hours of infusion as well as interaction with the pools of glycerol present in adipose tissue as well as preexisting glucose in the form of liver glycogen.

As observed in Figure 5.6A, the 3 hour isotopomer spectrum corresponds to natural abundance of plasma glucose fragment of mass 370, thus indicating presence of a transient regime for glycerol pumping into peripheral tissues as well as stabilization of the pumping rate. At the 6 hour infusion we observe increased corrected enrichment of 10% and decreased abundance of the base isotopomer in the presence of the [U-^{13}C,D$_5$]-glycerol. Stable isotope enrichment increases

monotonically at 12 hours to 19% and 24 hours to 36%, with maximum glucose enrichment achieved after 24 hours of infusion length under our experimental conditions. As evidenced by Figure 5.6B, longer infusion times than even 24 hours may be needed to achieve isotopic steady state from glycerol infusion and asymptotically reach a maximum isotopic enrichment. We can extrapolate the exponential decay constant for enrichment in Figure 5.6B as 0.17/hr assuming an exponential process in a single metabolic pool of glucose. Using this value, 95% enrichment is reached at 18 hours post implant, therefore suggesting that longer infusions in the order of 18-24 hours using glycerol as a tracer would be necessary to achieve isotopic steady state as observed in human infusions [61]. Comparing flux estimates for upper gluconeogenesis obtained from the complement of glucose fragments at 6 and 24 hours, we observe similar fasting physiologic responses with respect to fractional gluconeogenesis of 79% at 6 hours and 72% at 24 hours, with similar contributions from the glycerol and oxaloacetate pools to the production of glucose under the same physiological conditions of fasting. These metabolic reconstructions suggest that isotopic steady state can be achieved despite lacking a controlled metabolic system with slowly changing enrichment.
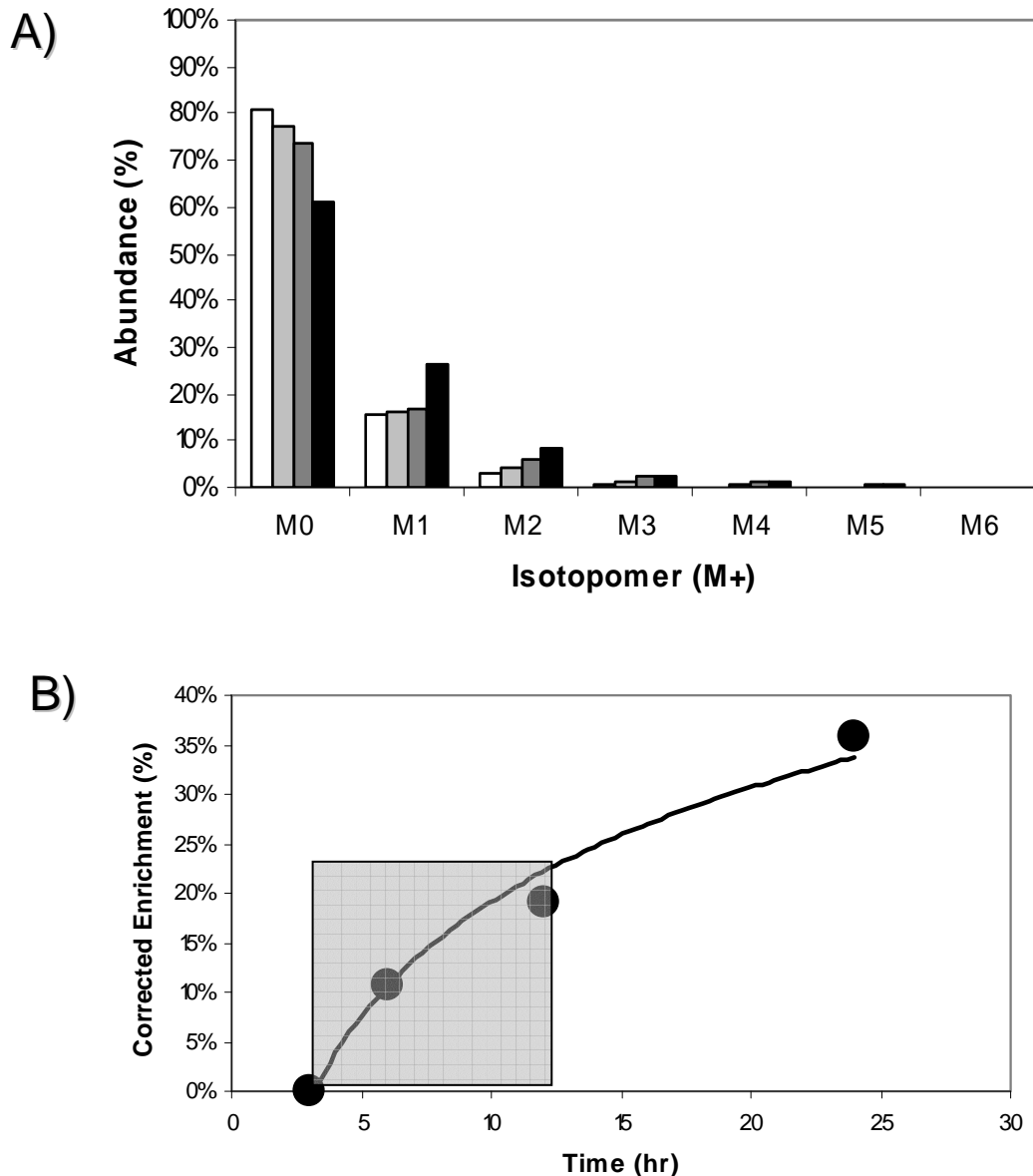
Figure 5.6: Longer tracer exposure increases plasma glucose enrichment in vivo. Mice (n=2) were infused 2M [U-^{13}C, D$_5$]-glycerol tracers through miniosmotic ALZET pumps over varying time lengths. A) Uncorrected isotopomer spectrum of plasma glucose enrichment for m/z 370 [C5H5] at 3 hr (white), 6 hr (light gray), 12 hr (dark gray) and 24 hr (black). B) Corrected enrichment for the aldonitrile pentapropionate glucose fragment with m/z 370 over time. Zero percent enrichment signifies natural abundance, and the shaded box indicates the ideal enrichment range for preventing tracer recycling.

Constant Content of Deuterated Water

The third assumption regards the enrichment of water being constant over the time scale of the experiment. We dosed water as a bolus and fed *ad libitum* to simulate a primed infusion of tracer as described by equation 2.29. Deuterated water as a tracer has been shown to distribute evenly across body compartments after 5 hours of dosing [145]. However, it is also possible to find lower than expected enrichments of plasma deuterated water as measured by deuterium exchange with acetone, pointing to possible tracer loss or disequilibrium in the exchange rates among compartments and plasma. At the relatively high concentrations of deuterated water utilized in this study, we did not observe differences in the endpoint enrichment with the average plasma water enrichment after 24 hours of 4.35±0.05% for the in vivo flux analysis experiment by deuterium exchange with acetone.

Intact glycerol enters the liver

Similarly we assume that glycerol enters the liver with the same labeling pattern as dosed by the miniosmotic pump. Specifically, we sought to confirm that administered [U-^{13}C,D$_5$]-glycerol reached the gluconeogenic site (i.e. liver) without significant changes in its labeling patterns. Subcutaneous dosing of glycerol tracer over an extended period of time maximized stable isotope incorporation from glycerol into the glucose molecule. Using an infusion length of 6 hours, we designed chemically identical pump cargos containing 2M glycerol and 2M glucose, and systematically substituted the substrates dosed with their labeled counterparts [6,6-D$_2$]-glucose, [U-^{13}C]-glycerol and [U-^{13}C,D$_5$]-glycerol. As observed in Figure 5.7, plasma glycerol enrichment in the presence of [6,6-D$_2$]-glucose remains at natural abundance, i.e., it is not affected by the presence of labeled glucose. This suggests that no reverse flux from glucose to glycerol takes place in vivo. Introducing [U-^{13}C]-glycerol in this system shifts the mass of plasma glycerol fragment 173 containing [C2,H3] 2

amu towards higher mass, while [U-^{13}C,D$_5$]-glycerol shifts the mass spectrum 5 units towards higher masses. The abundance of M+2 and M+5 fragments is 30% suggesting that the administered [U-^{13}C,D$_5$]-glycerol constitutes approximately 30% of the total circulating glycerol, in line with the 25% labeled glycerol administered for hepatocyte flux estimation. Most importantly, the plasma glycerol results confirm that either fully labeled glycerol or unlabeled glycerol is present in vivo. In the context of the data in Table 5.1, we could expect glycerol content to account for over 50% of plasma glycerol after 6 hours, thus there must be extrahepatic consumption of glycerol causing losses in addition to those from glucose production. Potential tissues accounting for this consumption would most likely include kidney and heart.
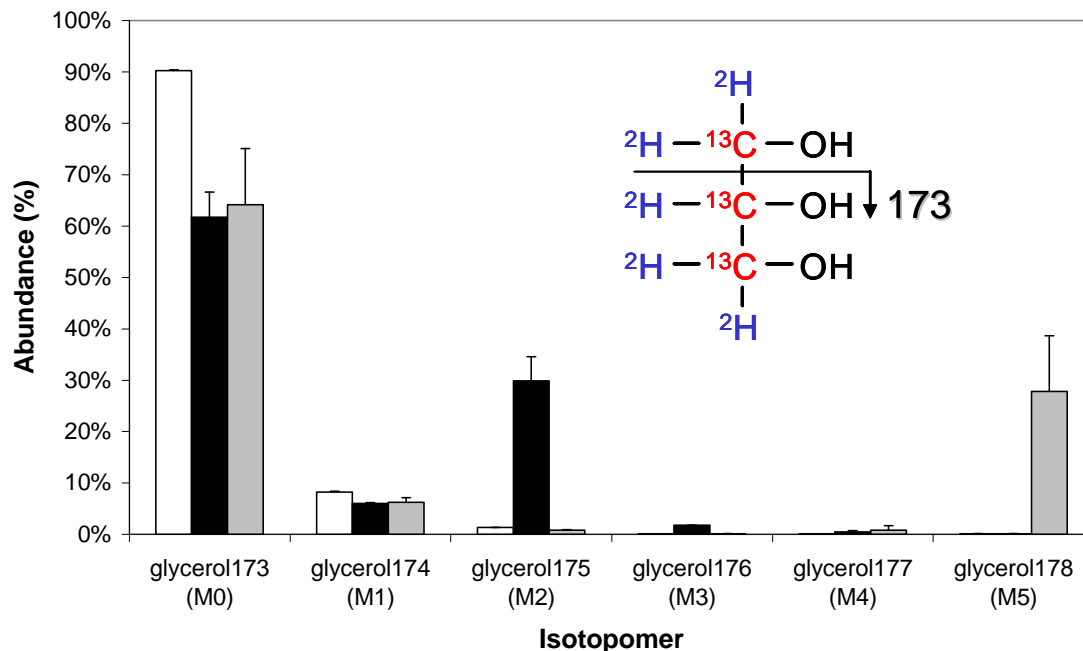
Figure 5.7: Plasma glycerol enrichment reflects [U-^{13}C, D$_5$]-glycerol enrichment in vivo. Mice (n=2) were infused glycerol over 6 hours in three chemically identical pump conditions: [6,6-D$_2$]-glucose (white), [U-^{13}C]-glycerol (black) and [U-^{13}C, D$_5$]-glycerol (gray), all at 2M. Data are presented uncorrected isotopomers of the aldonitrile propionate glycerol fragment at m/z 173. Data are mean±SEM (n=3).

To further address potential tracer recycling in our experimental measurements, we designed an alternate glycerol infusion strategy, whereby a lynch coil catheter of predetermined length was fitted to the miniosmotic pumps to permit saline priming over 8 hours. At this time, glycerol infusion started as in the previous protocol without transient changes in pumping rate. The resulting enrichment in plasma glucose is presented in aldonitrile pentapropionate glucose fragment at m/z 173 in Figure 5.8. Interestingly, the glucose labeling pattern observed by this delayed protocol is consistent with higher enrichment than either 6 or 12 hour infusion lengths. We cannot rule out that glycerol may have escaped the pump at an earlier time due to mechanical device failure from this data; such analysis would require a time course experiment on the same animal over the expected infusion time. However these results raise the possibility that changes in metabolism over the course of 14 hours post implant are contributing to produce differences in glucose enrichment observed.
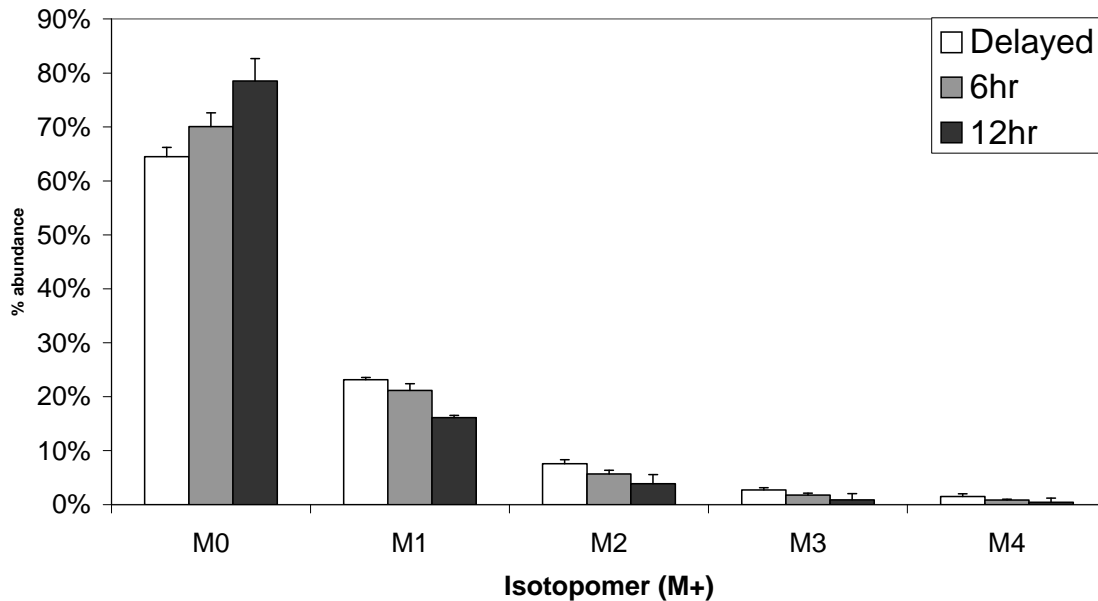
Figure 5.8: Delayed infusion protocol results in higher glucose enrichment. Isotopomer spectrum for aldonitrile pentapropionate glucose fragment at m/z 173. Mice (n=3) were infused a combination of tracers through miniosmotic ALZET pumps including 2M [6,6-D$_2$]-glucose, 2M [U-^{13}C, D$_5$]-glycerol, and 5% deuterated water (IP and fed). Glucose and glycerol infusion was delayed for 8 hours by fitting a lynch coil catheter filled with a predetermined volume of saline to miniosmotic pump. Data are presented as mean±SEM (n=2).

Tracer is not Consumed in Reactions of the TCA Cycle

Our modeling approach focused on the reactions that comprise upper gluconeogenesis, in particular commencing at the triose phosphate isomerase junction for metabolites in the oxaloacetate pool, and glycerol kinase for glycerol, as detailed in Chapter 4. We do not include the TCA cycle in our proposed metabolic model in Chapter 4, which is an important source of tracer scrambling that increases the complexity of the analysis of glucose enrichment. By using glycerol as our primary tracer, we circumvented the formation of secondary tracers in vivo from the TCA cycle due to its preferential usage in gluconeogenesis over lactate and pyruvate. These latter tracers need precursor pool enrichment measurements of the oxaloacetate pool in order to estimate true rates of appearance of glucose through gluconeogenesis [61]. Under normal physiology, glycerol is not expected to interact with the oxaloacetate pool [61]. The only relevant dilution preceding the production of glucose from glycerol would be expected from glycogenolysis, precisely one of the fluxes of interest in the calculations presented, which is measured independently through the use of deuterated water in our combined-tracer methodology.

From the obtained measurements of plasma glucose and plasma glycerol enrichment, we can only infer whether [U-^{13}C,D$_5$] glycerol tracer is consumed in the TCA cycle. One possible way to assess this effect would be to observe significant M2 enrichment in the glucose molecule formed from metabolism of the carbon backbone of glycerol into DHAP, pyruvate and again into glucose. We did not observe significant M2 enrichment in glucose beyond experimental error compared to [U-^{13}C]-glycerol as shown as shown in Figure 5.9B and Figure 5.10. These values can be explained by the presence of transketolase in our metabolic model. In addition, in previous cellular experiments using [U-^{13}C] glycerol as a tracer, we did not observe significant lactate enrichment, which is consistent with absence of cycling between glycerol and the TCA cycle [13]. We interpreted this finding to mean that there was residual transketolase activity in hepatocytes producing

formation of any M1 and M2 fragments in the presence of [U-^{13}C]-glycerol. Direct determination of TCA cycle scrambling could be achieved in this system by sampling the enrichment in the oxaloacetate pool in the liver through the extent of the infusion. One way of assessing this would be to infuse a precursor of pyruvate (alanine or lactate) and measuring the enrichment of pyruvate in the hepatic vein. In addition, should there be detected enrichment in the oxaloacetate pool observed; the additional problem arises for how to measure the dilution of label in the oxaloacetate pool due to TCA cycle activity. The production of oxaloacetate from the TCA cycle could be accounted for by tracking the fate of individual carbon enrichment in the glucose molecule, which is possible using the complement of glucose fragments described previously [13, 61]. In this case, we would extend our modeling approach to include the reactions in the TCA cycle in greater detail providing greater degrees of freedom from which to fit observed labeling patterns in glucose.

Liver glycogen remains unlabeled

Our modeling also assumes that glycogen remains an unlabeled source of glucose through the extent of the experiment. We inspected this assumption by measuring decreased glycogen deposition in the livers of animals undergoing glycerol infusion of 0.44±0.03 mg/g wet liver after ethanol precipitation. These values are consistent with those found after 24 hour fast in mice and decreased from those found in fed BL6 mice [194]. We expected this result as the mice fasted throughout the extent of the infusion protocol, and thus would be expected to deplete glycogen stores within 3 hours of removal of food [164]. In addition, we tested the obtained glycogen for the possibility of observing stable isotope enrichment in the resulting digested glucose. The trace glycogen present in the liver showed unnatural enrichment after amyloglucosidase digestion and GC-MS analysis, but the amounts were small enough to be considered contamination from plasma glucose.

Qualitative interpretation of glucose enrichment

Direct inspection of glucose enrichment gave insight to the potential information to be gained in a combination experiment with multi-labeled glycerol tracer. Theoretically, M1 enrichment would reflect enrichment primarily from deuterated water, M2 enrichment would reflect primarily enrichment from dosed [6,6-D$_2$]-glucose for hepatic glucose output calculation, and higher isotopomers describe the formation of glycerol units from the carbon skeleton as well as hydrogen transitions in the intervening reactions. As observed in Figure 5.9A, the enrichment in the M2 isotopomer corresponding to [6,6-D$_2$]-glucose condition indicates approximately 6% enrichment of total plasma glucose, correlating to a glucose production rate of 32 mg/kg/min. This value overestimates basal hepatic glucose production in the context of clamp experiments [15] but is similar to enrichment achieved in similar ALZET pump dosing experiments [115]. Dosing with [U-^{13}C]-glycerol shows enrichment in the M3 and M6 isotopomers through union of two glycerol molecules into the carbon skeleton of glucose, as observed in our previous experiments in primary hepatocytes. In comparison, treatment with [U-^{13}C,D$_5$]-glycerol causes appreciable enrichment in the M4 isotopomer of aldonitrile pentapropionate glucose fragment 173 as shown in Figure 5.9A, as well as observable enrichment in the M4, M5 and M6 isotopomers of aldonitrile pentapropionate glucose fragment 370 in Figure 5.9B and Figure 5.10. Enrichment at higher mass isotopomers implies higher signal to noise ratio and further ability to predict fluxes by constraining the estimation problem to the existing isotopomer distributions (Figure 5.9B, inset Figure 5.10). Our ability to detect such small changes in enrichment is enhanced by the fact that biological variability in enrichment is considerably smaller than variability in amounts of compound detected by GC-MS. The combination of isotopomer distributions from multiple glucose fragments provides the basis for the data-driven modeling approach encoded in METRAN to reconstruct hepatic glucose metabolism.
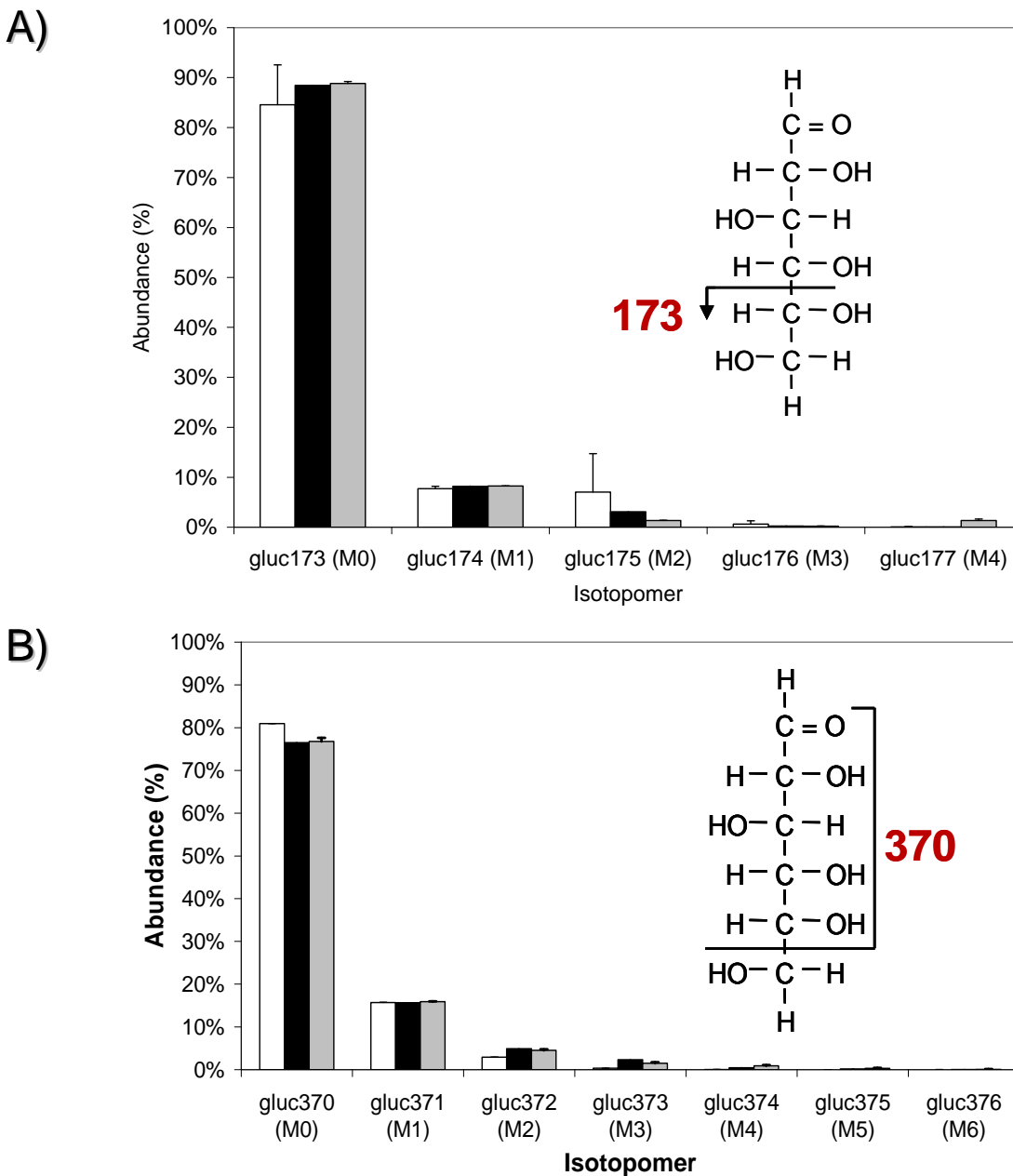
Figure 5.9: Plasma glucose enrichment augmented by incorporation of [U-^{13}C, D$_5$]-glycerol in vivo. Mice (n=2) were infused with glycerol over 6 hours in three chemically identical pump conditions: [6,6-D$_2$]-glucose (white), [U-^{13}C]-glycerol (black) and [U-^{13}C, D$_5$]-glycerol (gray), all at 2M. A) Uncorrected isotopomer spectrum of plasma glucose enrichment for m/z 173 [C$_2$H$_3$]. B) Uncorrected isotopomer spectrum of plasma glucose enrichment for m/z 370 [C$_5$H$_5$]. Enrichment of glucose fragments with m/z 370 in the [6,6-D$_2$] glucose condition coincides with natural abundance within 0.1% experimental error. Data are presented as mean±SEM.
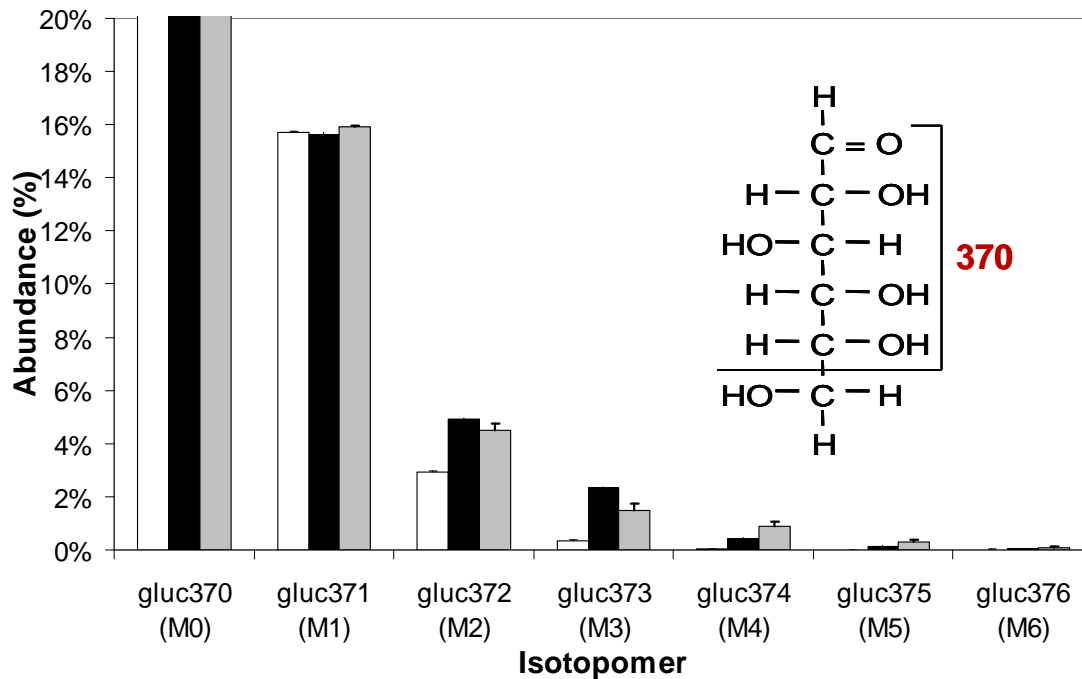
Figure 5.10: Detail of uncorrected glucose isotopomers M1-M6 by incorporation of [U-^{13}C, D$_5$]-glycerol in vivo after 6 hour infusion. Note the enrichment of isotopomers M3-M6 is significantly increased during infusion with [U-^{13}C, D$_5$]-glycerol. Infusion conditions: [6,6-D$_2$]-glucose (white), [U-^{13}C]-glycerol (black) and [U-^{13}C, D$_5$]-glycerol (gray), all at 2M. Data are presented as mean±SEM.

5.5 Discussion

In the previous chapter we showed how net and exchange fluxes of the upper gluconeogenic pathway associated with glucose production can be estimated through combination of ^{13}C and ^{2}H tracing in substrates including [U-^{13}C]-glycerol, [D$_5$]-glycerol and ^{2}H$_2$O [13] (Chapter 4). Furthermore, we showed how fluxes determined through computational integration of parallel tracer labeling are incorporated into coherent models of glucose production metabolism. In this chapter, we adapted the use of a unique three-tracer strategy for the accurate estimation of gluconeogenesis fluxes from a single in vivo experiment. Quantitative analysis of plasma glucose mass isotopomer distributions from incorporation of [U-^{13}C,D$_5$]-glycerol into glucose required the use of elementary metabolite unit framework described in Chapter 2 and in literature [87]. This algorithm simplified the computational problem of isotopic species simulation from over 42,000 isotopomers to approximately 200, by selectively eliminating isotopomer species that do not contribute to the formation of the observed metabolic species by mass spectrometry. With detailed understanding of atom transitions in the gluconeogenic metabolic route, we could perform a similar type of analysis when using single tracers as source of ^{13}C or ^{2}H label. The use of ^{13}C and ^{2}H stable isotopes in a *combined, multi-tracer labeling strategy* provided additional degrees of freedom and *redundancy* from which to fit a proposed flux distribution to the observed mass isotopomer spectra within predetermined statistical degree of confidence as determined by a chi-squared test.

The significance of the obtained results lies in the completeness of the flux estimates obtained with a single measurement technology. Previous work has utilized tandem measurements from multi-dimensional NMR to gain complementary information regarding enrichment of different molecules and moieties related to central carbon metabolism [33, 127]. Here, we are utilizing a single detection technology, mass spectrometry, to assess enrichment by combining derivatizations of the glucose molecule that enable positional enrichment measurements. ^{13}C labeling of the glucose

backbone permits independent measures of glucose biosynthesis, whereas ^{2}H enrichment provides estimates of fractional gluconeogenesis and reaction reversibilities. As end product of our analysis, we not only obtain net fluxes corresponding to ^{13}C-based flux analysis, but also gain insight regarding reaction reversibilities that underlie critical assumptions in simpler methodologies utilizing individual tracers. For instance, transketolase activity measurement through non-tracer methods would require enzyme concentration/activity measures, or thiamine cofactor level assessment. We find evidence suggesting the activity of TK is present in hepatic glucose production in vivo despite no *a priori* evidence to suggest that this enzyme would be active (Figure 5.5) . This result implies that modeling efforts for glucose production should consider pentose phosphate pathway activity as a potential source of tracer loss. In addition, we find good agreement with phosphoglucose isomerase and triose phosphate isomerase reversibilities of 83 and 74% respectively, indicating that both reactions are close, but not quite at equilibrium, as assumed and measured previously [111, 144]. Our method is amenable for use in the context of small animals where plasma glucose amounts are limited, and in clinical setting where the number of glucose samples obtained is reduced due to subject availability.

Integrative flux analysis of hepatic glucose metabolism sheds light on the functional biochemistry of the cell or organism in ways that reductionist experimental analysis would not capture interactions[155]. Reductionist biochemistry successfully elucidated the full complement of reactions possibly present in the cellular machinery. However, functional conversion of metabolites through a metabolic pathway such as upper gluconeogenesis is often limited to a core set of reactions that comprise metabolic system behavior. Our results underscore the importance of assessing the contribution of different gluconeogenic substrates in the measurement of fractional gluconeogenesis, in particular when the addition of a particular tracer may change its metabolite concentration of plasma. Extensions of this work would entail the use of [^{13}C]-pyruvate and [^{13}C]-

lactate variants that would better simulate physiologic plasma concentrations of gluconeogenic precursors [139]. These tracers would permit the analysis of interactions with lower gluconeogenesis and the TCA cycle, which would entail collection of hepatic metabolic intermediates of the TCA cycle. In addition, this analysis could contribute to dissection of the role of gluconeogenesis as gatekeeper for TCA cycle flux [33].

Selection of tissue specific metabolic biomarkers is a critical aspect of in vivo comprehensive flux analysis that determines the extent of reconstruction possible as well as the confidence of the produced results. We chose glucose production as a model pathway in part due to its tissue specificities (liver, kidney), presence of the product metabolite in plasma, and well characterized carbon and deuterium atom transitions. The choice of glycerol tracer is aided by tissue colocalization of glycerol kinase in the liver [195, 196], thereby permitting synthesis of glucose from glycerol without intervening transport across tissues in plasma. In adapting combined, multi-tracer labeling strategies for metabolic pathways present in other tissues, researchers must exert care to analyze the pathways of interest with respect to their input sources, biochemical knowledge of carbon-13 and deuterium transitions among constituent reactions, as well as potential products carrying label off the pathway to other tissues. For instance, in designing a tracer strategy to reconstruct triglyceride synthesis in adipose tissue, glycerol tracers as well as acetate tracer would permit the reconstitution of the trigyceride molecule synthetic rate. Since triglyceride secretion is limited by lipoprotein transport, we would consider harvesting adipose tissue for enrichment analysis of fatty acid and triglyceride intermediate pools present, as well as potentially analyzing plasma triglyceride content. Forward simulation experiments for the expected isotopomer distributions in vivo are helpful in framing the questions and fluxes to be ascertained as well as the best tracer strategy to be used.

There are several limitations to the methodology proposed. ALZET pumps provide a convenient alternative for tracer infusion in settings where mouse catheter placement is unavailable

or unreliable [115-117, 154]. Delivering stable isotope tracer through miniosmotic pumps permits chronic administration of gluconeogenic precursor, which in turn complements the acute nature of established catheterized infusion protocols such as the euglycemic-hyperinsulinemic clamp. However, these pumps require an initial period to reach steady state of tracer infusion after drawing water by osmotic gradients from their surroundings. In this context the experimental procedure could by priming animals with [U-^{13}C,D$_5$]-glycerol and [6,6-D$_2$]-glucose such as to overlap with the increasing flow rate of the pump over the initial hour of infusion. The choice of glycerol as a tracer for gluconeogenic flux reconstruction is also controversial, in particular when using condensation polymerization reactions to describe the production of glucose [138, 139]. Our method does not use condensation polymerization for gluconeogenic calculations, and questions regarding tissue heterogeneity of metabolic function were addressed computationally by fitting dilution parameters for partial glycerol usage, as well as experimentally by providing high concentrations of glycerol over extended infusion periods [13]. However, further examination of the combined multi-labeled tracer methodology under isotopic steady state in vivo could help clarify these claims. At the other end of the spectrum, longer infusion times create the potential for recycling of tracer into unknown or incompletely described metabolic pathways, therefore hindering the statistical analysis of the generated isotopomer data.

We envision the application of these methodologies in several directions. First, the use of combined multi-labeled tracer strategies have the potential of limiting the amount of interventions necessary to reconstruct hepatic metabolism in vivo, thus making these methodologies ideal for their use in a clinical research setting. The presented combined, multi-labeled tracer strategy and data-driven analysis can be readily incorporated into euglycemic-hyperinsulinemic clamp methodology to provide detailed functional insight to the changing nature of hepatic glucose fluxes in the presence of insulin [197]. Deuterated water, and [6,6-D$_2$]-glucose are routinely used in clinical research

separately or in combination, and the administration of labeled glycerol could be incorporated to intravenous tracer regimes. Glycerol is rapidly absorbed orally, but undergoes degradation in the gut such that intravenous injection would be the preferred method of administration [198]. Second, one important factor limiting the widespread use of stable isotope labeling strategies for metabolic phenotyping in the clinical setting include the cost of supplying [U-^{13}C, D$_5$]-glycerol in sufficient amounts to achieve 30% plasma enrichment as shown in Figure 5.7A. In this respect, instationary flux analysis methodologies that incorporate isotopic transients under metabolic steady state would be the next logical step to extend in vivo metabolic flux analysis [87]. These analytical technologies would limit the amount of time and/or tracer necessary to estimate metabolic fluxes, or alternatively could provide indirect information regarding the active metabolite pools present in the tissue of interest and their relative sizes.

Metabolic fluxes have a unique role in the development of metabolic diseases, such as Obesity and Type 2 Diabetes. The fundamental phenotype in these conditions is metabolic deregulation in the form of increased deposition of lipids into adipose tissue in the former, and decreased muscle glucose uptake with increased liver glucose output in the latter. As such, genomic, proteomic and metabolomic data can only partially describe the metabolic phenotype in these diseases, and comprehensive analysis of these conditions requires functional information in the form of reaction rates for their comprehensive depiction. In addition to metabolic diseases with high prevalence such as Type 2 Diabetes and Obesity, the analysis of detailed fluxes and reversibility could play a major role in elucidating novel treatment strategies for rare diseases of intermediary or specialized metabolism. For example, glycogen storage disease type II (Pompe's disease) is known to be caused by a deficiency of enzyme alpha-1,4-glucosidase, whose function in terms of overall glycogen breakdown remains in question. The isolated enzyme appears to be catalytically active, and thus the defect likely occurs in the production, breakdown or network interactions of the protein

[199]. This disease could be studied in detail by designing specific glucose tracers incorporating deuterium selectively to highlight the functional junctions blocking glycogen breakdown in the corresponding animal model or in vivo. Another interesting pathway would involve reconstruction of fructose metabolism in the context of a high fructose diet, to understand the metabolic deregulations that accompany this common scenario in a quantitative fashion.

In conclusion, our data support the use of a combined, multi-labeled glycerol tracer strategy for the comprehensive estimation of upper gluconeogenic metabolic fluxes encompassing net and reversible rates. This methodology is unique in its use of a novel [U-13C,D5]-glycerol tracer not reported in literature, estimation of reaction reversibilities, the combination of multiple tracers within a miniosmotic pump, and the computational reconstruction of flux distributions with corresponding statistical confidence based on measurement redundancy. We are the first group to report such comprehensive computational reconstruction of metabolism in vivo, paving the way for development of fluxomic assessment of metabolism. Challenges remain to further optimize these methods and assess their validity in other physiological contexts. In the next chapter, we address one of these challenges by deploying the developed combined, multi-labeled tracer methodology in a transgenic model of insulin resistance, and provide insight to the metabolic disturbances that accompany Type 2 Diabetes in the liver

CHAPTER 6: Flux analysis of liver metabolism in the LIRKO model of insulin resistance

In the previous chapter, we demonstrated the use of in vivo metabolic flux analysis through the development of a combined, multi-labeled tracer strategy incorporating a unique [U-^{13}C,D$_5$]-glycerol tracer, [6,6-D$_2$] glucose and deuterated water, and we developed this method against physiological paradigms such as feeding and fasting in order optimize and elucidate its potential for comprehensive metabolic flux analysis in vivo. In this chapter, we will apply the developed methodology for in vivo flux analysis to a specific model of hepatic metabolic deregulation in the form of liver insulin resistance.

6.1 Introduction

Insulin is the hormone which orchestrates the storage of nutrients and energy in the fed state. The hormone is released from the pancreas in response to increased nutrient availability, and stimulates the liver via portal circulation to adapt its metabolic program for increased glucose and lipid deposition [42]. The specific hepatic metabolic processes directly targeted by insulin include stimulation of glycogen synthesis and deposition, suppression of glucose production by gluconeogenesis/glycogenolysis and increased fatty acid triacylglycerol synthesis with VLDL secretion [42]. Insulin also has extrahepatic, or indirect effects that impinge on the liver's ability to produce glucose, by reducing the availability of gluconeogenic substrate release from muscle and adipose tissue (e.g. lactate, alanine, glycerol) as well as lowering free fatty acid

concentrations that would provide NADH for glucose biosynthesis [200, 201]. The direct effects of insulin to suppress hepatic glucose production are mediated through the insulin signaling cascade starting with the insulin receptor, IRS proteins, PI3K, Akt, and the FOXO transcription factor and converge to the decreased transcription of gluconeogenic enzymes pyruvate carboxylase (PC, EC 6.4.1.1), phosphoenolpyruvate carboxykinase (PEPCK, EC 4.1.1.32), fructose-1,6-bisphosphatase (FBPase, EC 3.1.3.11) and glucose-6-phosphatase (G6Pase, EC 3.1.3.9) [54]. These enzymes catalyze thermodynamically irreversible steps of de novo glucose synthesis, and their amounts of gene and protein expression are used as surrogate static markers of gluconeogenic activity. The balance of direct and indirect effects of insulin action has been studied extensively in normal physiology and Type 2 Diabetes, where hepatic glucose production is increased through gluconeogenesis and the resulting hyperglycemia further augments the indirect effects of insulin [201, 202]. Insulin resistance is the hallmark feature of Type 2 Diabetes, and failure of insulin action manifests as excess glucose production by the liver, which is targeted therapeutically by biguanide drug metformin.

The liver insulin receptor knockout (LIRKO) mouse is a tissue-specific model of Type 2 Diabetes engineered to reflect complete hepatic insulin resistance through Cre-LoxP recombination of the liver insulin receptor [14]. These animals are viable and characterized by dramatic hyperinsulinemia which has been hypothesized to occur in part due to pancreatic beta cell hyperplasia and decreased hepatic insulin clearance due to loss of insulin receptor-mediated uptake in the liver [203]. LIRKO mice exhibit modest hyperglycemia in the fasted state which is exacerbated by feeding. When subject to glucose and insulin tolerance tests, the transgenic mice show glucose intolerance and insulin resistance. Complete hepatic and partial peripheral insulin resistance are also evident in this model given the inability of insulin to suppress hepatic glucose production and increased glucose turnover in the presence of high

insulin levels during the euglycemic-hyperinsulinemic clamp [15, 203]. Treatment of this transgenic mouse with streptozotocin to ameliorate hyperinsulinemia results in mildly reduced hepatic glucose production (HGP) and increased glucose turnover compared to untreated LIRKO [15]. These effects have been postulated to indicate the presence of direct effects of insulin suppression through increased gluconeogenic enzyme levels, and indirect effects of insulin suppression of HGP through decreased levels of free fatty acids [203].

We were interested in studying the LIRKO mouse as its complete hepatic insulin resistance causes a liver gene expression profile consistent with increased gluconeogenesis, as measured through increased expression of G6Pase and PEPCK mRNA, and decreased expression of pyruvate kinase [14]. The transcription of PEPCK mRNA is suppressed in the presence of insulin through the insulin signaling cascade, and is dominant over the effects of cAMP, glucagon and dexamethasone [204]. Glucose-6-phosphatase gene expression has been shown to be regulated by insulin and glucose levels independently of insulin [27, 205] Decreased glycogen deposition in the LIRKO liver has been observed by histological Periodic acid Schiff-staining, and is expected due to the lack of insulin-mediated inactivation of glycogen synthase kinase 3 (GSK3) [54] in addition to unopposed glucagon action on glycogen phosphorylase A through cAMP signaling [62]. In light of the above described changes, this transgenic model has been hypothesized to rely entirely on gluconeogenesis for its glucose production [206]. However, the functional physiologic studies described found slightly lower glucose production by LIRKO mice in the basal state with respect to the wild type. We posit that a reason for this apparent paradox in terms of functional glucose production could be explained by further elucidating the flux distribution of hepatic glucose production in the LIRKO liver. In this way, we could observe functional metabolic regulatory mechanisms such as decreased gluconeogenic substrate availability or preserved glucose demand that would directly distill

from metabolic flux analysis and would otherwise be obviated through genomic, proteomic or even metabolomic screening of this transgenic model.

The developed tools for in vivo flux analysis in Chapter 5 give researchers powerful methods to characterize and reconstruct metabolism in vitro and in vivo in a data-driven manner from enrichment data in stable isotope incorporation experiments. Our goal in developing this methodology is to enable detailed metabolic flux analysis to integrate liver metabolism and its defects in the development of Type 2 Diabetes. Our in vivo flux analysis methodology allows us to probe not only the contribution of gluconeogenesis to hepatic glucose production, but most importantly allows reconstruction of substrate usage fluxes contributing to increased glucose production in liver insulin resistance. This method dissects the contribution of gluconeogenic precursors such as glycerol that contribute to insulin's indirect effects of substrate availability, effecting increased hepatic glucose production.

In this chapter, we adapt our demonstrated protocol for in vivo flux analysis of hepatic glucose production to a cohort of LIRKO and IRlox animals under fasting conditions to reconstruct hepatic metabolic fluxes of upper gluconeogenesis. Using a combined, multi-labeled tracer strategy, we are able to accurately measure parameters such as hepatic glucose production, fractional gluconeogenesis and contribution of glycerol to glucose production without the need for catheterizing animals. Interestingly, our results show a preserved fasting flux distribution with respect to hepatic glucose production, whereby the LIRKO liver metabolizes glucose in a manner similar to the fasted liver of its normal counterparts. Physiologic testing in the form of a pyruvate tolerance test unmasks the gluconeogenic phenotype of the LIRKO mice, and directed liver metabolite profiling reveals unchanged levels of cellular metabolites leading to glucose production, in contrast to the markedly increased levels present in the catabolic model of streptozotocin treated animals. Our in vivo flux

analysis strategy provides unprecedented elucidation of upper gluconeogenic metabolism within a single experiment, coupled with statistical analysis that augments our ability to assess flux regulatory mechanisms modulating hepatic glucose production.

6.2 Materials

Biochemicals were obtained from Sigma Chemicals (St. Louis, MO) unless otherwise specified. [U-^{13}C]-glycerol and [6,6-^{2}H]-glucose were obtained from Cambridge Isotope Laboratories (Andover, MA). The custom synthesized glycerol tracer [U-^{13}C,^{2}H$_5$]glycerol (99+ At% 13C, 98+ At% 2H) was purchased from Omicron Biochemicals (South Bend, IN). The isotopic purity was of the tracer validated by GC/MS. ALZET Pumps model 2001D (Durect, CA) were implanted according to the manufacturer's instructions and described previously (Chapter 5).

6.2.1 Animals

Male C57BL/6 mice were obtained from Taconic (Germantown, NY). Male LIRKO animals and their IRlox counterparts on a mixed background were kindly donated by C. Ronald Kahn. Animals were housed at MIT in a facility approved by the American Association for Accreditation of Laboratory Animal Care. All animals received humane care in compliance with institutional guidelines. Mice had free access to water and chow *ad libitum* before the study, and were fasted overnight prior to pump implant. Mice were approximately 10 weeks old and 25-35 g body weight at their time of the experiment.

6.3 Experimental Methods

6.3.1 ALZET Pump Implant

ALZET Pumps model 2001D were implanted as recommended by the manufacturer and described previously (Chapter 5). The pump cargo in these experiments included 2M [U-^{13}C, D$_5$]-glycerol and 2M [6,6-^{2}H]glucose dissolved in saline solution. These concentrations were sufficient to administer tracer through the extent of the infusion experiment. Each mouse was simultaneously injected a bolus of deuterated water saline solution to reach 10% total body water enrichment, and fed 10% deuterated water *ad libitum*. Mice were fasted through the extent of the infusion for 24 hours.

6.3.2 Assays

Plasma glucose and lactate were assayed by the glucose oxidase method and lactate oxidase method in the YSI 2700 STAT Plus Glucose/Lactate Analyzer (YSI Inc, Yellow Springs OH). Insulin concentrations were determined by ELISA using mouse-insulin antibody (Linco Research, St. Charles, MO).

6.3.3 Directed liver metabolite profiling

Livers of IRlox, LIRKO, streptozotocin–treated and BL6 mice were donated by S. Biddinger, harvested and frozen at -80°C for further analysis. After defrosting, 100 mg of frozen liver was homogenized using a Tissue-Tearor stator-homogenizer in 2 volumes of PBS, centrifuged at 5000g x 2 min and collected the supernatant for further analysis. After methanol-chloroform extraction (2:1, 0.7mL methanol:0.38 mL chloroform), we dried the polar fraction and subjected it to TMS derivatizations with 10 μg ribitol standard as described

previously [156]. To derivatize the metabolites, we added 50 μL. of methoxyamine hydrochloride (20 mg/ml pyridine) to each sample and incubated for 90 min at 30°C. Then we added 80 mL of MSTFA + 1% TMCS (Pierce, Rockford, IL) to each sample and incubated at 37°C for 30 min. Samples were analyzed in a Saturn 2000 Gas Chromatography Mass Spectrometry instrument (Varian Inc, Walnut Creek, CA) as described previously [156, 207, 208]. One microliter of sample was injected onto a 30-m CP-SIL 8 CB low-bleed column (Varian, Walnut Creek, CA). The GC oven temperature was held at a 70°C for 5 min after sample injection, before increasing at a rate of 5°C/min to a final temperature of 265°C. This final temperature was held for 1 min for a total run time of 45 min. Peaks were identified with a local library and manually integrated for quantitation relative to ribitol standard, mg wet liver and control condition.

6.3.4 Pyruvate Tolerance Test

Tests were performed as described previously [209, 210]. Briefly, 10 week old male mice (n=3) were fasted overnight, and injected a 2g/kg intraperitoneal bolus of sodium pyruvate in normal saline. Blood glucose levels were followed every 30 minutes by tail vein bleeding in restrained animals using a OneTouch 2 Glucose Meter (LifeScan, Milpitas, CA).

6.3.5 Derivatization of glucose, glycerol

Glucose labeling patterns were determined by GC-MS analysis of aldonitrile pentapropionate, methyloxime pentapropionate and di-O-isopropylidene propionate derivatives of glucose from plasma [166] and as described previously (Chapter 4). Glycerol labeling patterns were determined from the glycerol aldonitrile propionate derivative at m/z 173 as described previously (Chapter 5).

6.3.6 Isotopomer Enrichment Analysis

Gas Chromatography-Mass Spectrometry (GC/MS) analysis for isotopomer enrichment of plasma glucose was performed as described previously (Chapter 4). We included in our analysis aldonitrile pentapropionate glucose fragments at m/z 173, 259 and 370, methyloxime pentapropionate glucose fragment at m/z 145 and di-O-isopropylidene propionate glucose at m/z 301. The aldonitrile pentapropionate glucose fragment at m/z 284 was excluded from the analysis due to poor data quality. For glycerol enrichment we included in our analysis aldonitrile propionate glycerol fragment at m/z 173. All mass isotopomer values were expressed as fractional abundances, whereby the sum of all mass isotopomers equals one.

Rate of appearance of glycerol was calculated using equation 2.28 and 2.29 for the total and endogenous appearance of glycerol respectively. The value used for enrichment was the uncorrected M+5 enrichment abundance corresponding to the fully labeled [U-^{13}C, D$_5$]-glycerol molecule (see Appendix B). Gluconeogenic uptake of glycerol was calculated as the absolute flux of glycerol determined from computational analysis using METRAN.

6.3.7 Cholesterol, Fatty Acid Secretion experiments

Mouse hepatocytes were prepared for primary culture by nonrecirculating, two-step collagenase perfusion, as adapted from Seglen [165] and described previously (Chapter 4). The protocol was modified to eliminate Percoll gradient separation of hepatocytes, such that the dispersed cells were only filtered at 4°C through 100 and 70 µm cell filters. The cells were counted with a hemacytometer, and 1.5x10^6 cells were plated onto 10-cm^2 rat collagen I–coated 6-well plates plates (4-8 ug/cm^2, Fisher Scientific Co.). Cells were cultured for 3 hr at 37C in a 5% CO$_2$ atmosphere and Advanced DMEM (Gibco) containing 5%FBS and

antibiotic cocktail (penicillin/streptomycin 10,000 U) [211]. The cells were then washed twice with warm PBS to remove debris and cultured with DMEM containing antibiotic cocktail and 0.5 mM sodium [^{13}C$_2$]acetate (Cambridge Isotopes, Cambridge, MA). After incubation for the times indicated, the medium was removed and stored at -80C for further analysis. Supernatants were collected and cells were harvested by treatment with 0.5 mL Trypsin-EDTA solution for 15 min, followed by collection and storage at -80C. The enrichment and synthesis of cholesterol and fatty acids were measured by isotopomer analysis using gas chromatography-mass spectrometry as previously described [74, 141]. The data are expressed as micrograms of compound relative to internal standard per million cells. The internal standard for cholesterol measurement was 2 μg epicoprostanol, and for fatty acid measurement was 20 μg triheptadecanoic acid.

Estimation of D and g(t) parameters was performed by Isotopomer Spectral Analysis (ISA) as described in Section 3.2.2 and Figure 3.1. The model used here assumes that the flux of the precursors to the lipogenic acetylCoA pool is constant during the time course of ^{13}C incubation. ISA uses equations for the probability of appearance of each isotopomer based on test values for D and g(t). These probabilities are compared to the fractional abundance determined for each palmitate or cholesterol isotopomer to obtain the best-fit solution. The fit is obtained by weighted nonlinear regression with the weights proportional to the inverse of the standard deviation of the isotopomer measurement.

6.3.8 Computation methods

The generalized algorithm for MFA was incorporated into Matlab based-flux analysis package METRAN and described in Section 2.3.4. Briefly at convergence, nonlinear statistical techniques were applied to obtain accurate 95% confidence intervals of fluxes by evaluating

the sensitivity of the objective function with respect to fluxes using elementary metabolite unit theory as described previously [13, 102]. Flux validation was accomplished by a statistical test for the goodness-of-fit based on chi-square test for model adequacy, and a normality test for the weighted residuals [105]. To ensure that a global optimum was found, flux estimation was repeated at least four times starting with random initial values to residual sum of squares accepting the proposed model with the 95% confidence interval. Sensitivity analysis was employed to determine the most important measurements for estimation of individual fluxes as described previously [13]. All computations were performed with Matlab 6.5 and Matlab Optimization Toolbox (Mathworks, Natick, MA).

The gluconeogenesis network model used for flux calculations was described previously (Chapter 4, Figure 4.3 and Table 4.1). In short, the network model is comprised of 24 reactions utilizing 26 metabolites, with 5 substrates (oxaloacetate, glycerol, glycogen, water, and NADH from endogenous sources), 3 products (glucose, CO_2, and a metabolic sink for NADH), and 18 balanced intracellular metabolites. Stereospecific atom transitions were assigned for all reactions in the model based on current knowledge.

6.3.9 Statistics

All data were analyzed using a Student's t test (Microsoft Excel) for single comparisons between means from experimental groups. In cases where multiple groups were all compared to a single group, the Dunnett's test for multiple comparisons was applied. Area under the curve was calculated by the trapezoid rule. $P < 0.05$ was considered statistically significant for all group comparisons.

6.4 Results

6.4.1 Study cohort characteristics

The basal metabolic parameters of the mouse cohorts studied are presented in Table 6.1. 10 week-old male mice showed non-significant differences in body weight, with LIRKO mice weighing 29.1±1.0g and control animals weighing 27.4±0.3g. The LIRKO mouse preserves normal weight and food intake despite high circulating levels of leptin [14, 212]. Liver weights in the LIRKO cohort were significantly smaller in absolute weight and relative to body weight, consistent with previous reports of decreased liver size due to absence of glycogen deposition [15]. Visually, LIRKO livers were noticeably smaller and darker than their IRlox counterparts, and had not yet developed hyperplastic nodules or lesions observed in their later stages of development.

With regards to the glucose production phenotype, circulating plasma levels of glucose in the LIRKO cohort were 158±6 mg/dL and for the control counterpart animals 196±11 mg/dL. Both plasma glucose values are hyperglycemic compared to reports in fasted C57BL/6 animals (80-120 mg/dL). However, plasma glucose values for the LIRKO cohort were significantly lower than controls in our protocol. Low fasting plasma glucose values in LIRKO mice were observed in previous reports (IRLox glucose 112±6, LIRKO glucose 88±6, $p < 0.05$) where LIRKO animals were subject to catheterization stress under the euglycemic-hyperinsulinemic clamp procedure to establish baseline hepatic glucose production [15]. As a precursor of gluconeogenesis, lactate levels in the LIRKO cohort are 38±4 mg/dL and 48±3 in the IRlox cohort. Both of these values are within the expected range for mouse plasma lactate values of 0-50mg/dL [213]. The unchanged lactate levels indicate preserved relative availability of this significant gluconeogenic precursor in plasma for use in hepatic gluconeogenesis.

LIRKO animals had circulating insulin levels of 1.83±0.18 ng/mL compared to their IRlox counterparts at 0.43±0.17. Therefore, the LIRKO cohort shows insulin plasma levels as much as four times higher than the IRlox cohort and is significantly hyperinsulinemic. This feature is consistent with the predicted phenotype of the LIRKO animal developing plasma hyperinsulinemia in an attempt to ameliorate hepatic glucose production, with secondary development of extrahepatic insulin resistance over time. The values reported in Fisher et al. reflect higher insulin amounts at 4.91 ng/mL for fasting LIRKO animals and 0.49 ng/mL for IRlox animals [15]. Comparison of these values suggests that insulin levels correspond with fasting physiology at 2 months, although the assays used are from different manufacturers. Our results are consistent with observed increases up to tenfold in the amount of circulating insulin in this model of liver insulin resistance.

In this section, we established the basal metabolic parameters of our mice cohorts undergoing in vivo flux analysis as reflecting LIRKO physiology as previously described. From the collection of results, we can establish that this cohort corresponds to a fasting physiology scenario in both LIRKO and IRlox animals as designed experimentally, and we observed values of glucose consistent with hyperglycemia in both groups. Despite our attempts at minimizing stress induction in these animals through handling and implantation of subcutaneous pumps, the values in Table 6.1 represent the metabolic status of the mouse cohorts after 24 hours post pump implant.

Table 6.1 Study Cohort Characteristics (* = p<0.05, **p<0.001)

Chemistry	*Controls (n=6)*	*LIRKO (n=6)*
Weight		
Body weight (g)	27.4±0.3	29.1±1.0
Liver weight (g)	1.243±0.016	0.922±0.038**
Liver weight (%bw)	4.5	3.2**
Serum		
Glucose (mg/dL)	196±11	158±6*
Lactate (mg/dL)	48±3	38±4
Insulin (ng/mL)	0.43±0.17	1.83±0.18**

*Body weights were measured prior to surgical implant. The mice did not lose significant amounts of weight after surgical recovery. Mice were fed ad-libitum prior to the surgical procedure, and fasted through the extent of the tracer infusion. Liver weight was measured after tracer infusion and dissection during tissue collection. Plasma glucose, lactate and insulin were measured from frozen plasma after cardiac puncture following the infusion protocol.

6.4.2 In vivo flux analysis of hepatic glucose production in the LIRKO model

Hepatic glucose production and gluconeogenesis in the basal state

We applied our in vivo flux analysis methodology as described in Chapter 5 for analysis in both mouse cohorts. We measured hepatic glucose production, fractional gluconeogenesis as well as substrate sources contributing to the production of de novo glucose. The purpose of this experiment was to assess the in vivo flux distribution of gluconeogenesis through a combined multi-labeled tracer strategy incorporating [U-^{13}C, D$_5$]-glycerol, [6,6-D$_2$]-glucose and deuterated water. In this way, we maximize the enrichment information obtained from the plasma glucose molecule as described in Chapters 3 and 5 in assessing the sources of glucose carbon and hydrogens. In addition, the tracers provide complementary information regarding specific aspects of glucose metabolism: [6,6-D$_2$] glucose permits assessment of net hepatic glucose production, deuterated water allows the calculation of fractional gluconeogenesis, and [U-^{13}C,D$_5$] glycerol permits accurate calculation of the contribution of glycerol to *de novo* glucose productions as well as estimation of reaction reversibilities such as transketolase and phosphomannose isomerase presence.

The main difference between our method and the clamp methodology involves the ability to minimally disturb insulin levels in the animal, in a manner akin to the basal portion of the infusion protocol (Chapter 3). In addition, the stress of the pump implant maybe less than that of catheter implant given the subcutaneous nature of the procedure and its short duration and subsequent recuperation. Lastly, the ease of implantation of the subcutaneous pumps opens the possibilities for widespread usage of this model of infusion in laboratories without the surgical expertise to perform mouse catheterizations. The paradigm studied is different than that of infusion protocols in that our infusion extends over 24 hours, compared to 60-120

minutes typical of infusion protocols. The implant procedure for ALZET pumps was well tolerated by all animals. Pump flow rate achieves steady state within 20% of pump lifetime (per manufacturer), in this case a minimum of 4 hours. We confirmed the presence of the dosed $[U-^{13}C, D_5]$-glycerol as M+5 enrichment of 28.5% of total plasma glycerol concentration (Appendix B), in line with observed values in vivo in fasted BL6 mice (Chapter 5) and with predetermined enrichment from in vitro experiments. (Chapter 4, Chapter 5, Antoniewicz, 2006). In addition, plasma glucose enrichment showed an enrichment signal of approximately 40% over natural abundance, indicating adequate incorporation of glycerol into plasma glucose. As in our previous animal experiments, the relative turnover of the glycerol pool is such that we would expect the pump infusion protocol to lead to higher concentrations of glycerol appearing in plasma.

A critical parameter of interest in assessing the glucose phenotype of the LIRKO animal is hepatic glucose production. Analysis of glucose isotopomer M2 enrichment in plasma glucose by dilution through calculation from equation 2.29 shows hepatic glucose production values of 34±6mg/kg/min for IRlox animals and 26±4mg/kg/min for LIRKO animals as shown in Figure 6.1 This change constitutes a significant decrease of 20% relative to wild type and is consistent in magnitude with the trend observed in Fisher et al. for decreased glucose production in LIRKO relative to IRlox in the basal state [15]. Our measured values for hepatic glucose production are higher than those previously reported in the basal portion of the euglycemic-hyperinsulinemic clamp (IRlox 22.9± 6.3 mg/kg/min, LIRKO 18.9±1.8 mg/kg/min, no significant difference) [15]. Differences in our experimental setup that could account for increased hepatic glucose production include the use of glycerol as our chosen tracer, therefore increasing the amount of gluconeogenic precursor available over the length of

the infusion relative to a single glucose dilution measurement using labeled [U-^{13}C]-glucose in previous experiments, [14, 15].

Estimation of net gluconeogenic flux from incorporation of deuterated water into the glucose molecule coupled with the aforementioned HGP dilution calculations permitted the analysis of absolute glucose production by either gluconeogenesis or glycogenolysis. These changes are represented as stacked bars in Figure 6.1. Analysis of absolute gluconeogenesis glucose production revealed no significant changes, ranging from 24.5±2.5 in the IRlox cohort to 20.0±1.7 mg/kg/min in the LIRKO cohort. In turn the contribution of glycogenolysis in the LIRKO cohort was also preserved compared to the control animals. In summary, although HGP decreased 20% in the LIRKO cohort compared to IRlox, the fractional contribution of gluconeogenesis and glycogenolysis to HGP was approximately 75% and 25% in both groups. Given the smaller size of the LIRKO livers, we asked the question whether the hepatic glucose output per unit mass of liver would reflect the same trend as total body output. We tested the hypothesis that glucose output per gram of liver in the LIRKO liver is significantly elevated due to the high levels of gluconeogenic enzymes, endowing the organ with large capacity to process gluconeogenic substrate into glucose. Figure 6.1B shows the renormalized glucose production values to grams of liver weight. Interestingly, we observe no significant difference in HGP on a liver weight basis, with the IRlox production of 0.75±0.06 mg/g/min and LIRKO production of 0.82±0.04 mg/g/min. Thus, glucose production per gram of liver in the transgenic animal is identical to the wild type animal. This finding demonstrates that large differences in gluconeogenic enzyme levels can occur without significant changes in flux distribution.

Our methodology allows us to determine parameters relevant to glucose metabolism when using glycerol as a tracer. In particular, we wished to assess whether the transgenic

phenotype has underlying differences in usage of glycerol use as a gluconeogenic substrate. Figure 6.2A presents the glycerol uptake rate distribution between gluconeogenic and non-gluconeogenic sources. First, we note that the rate of glycerol uptake at isotopic steady state equals the rate of appearance of glycerol. LIRKO mice show rates of glycerol uptake of 4.1±0.8 mg/kg/min, compared to 3.2±0.3 in the IRlox cohort. Glucose production accounts for 66% of glycerol uptake in the LIRKO cohort, and 60% in the IRlox cohort, indicating no changes in the usage of glycerol for production of glucose between transgenic strains. Figure 6.2B shows the rate of appearance of glycerol as a substrate calculated directly using Equation 2.29 and the enrichment of the M5 isotopomer in the glycerol aldonitrile propionate derivative. Similarly at isotopic steady state, the rate of glycerol appearance equals the rate of total glycerol uptake presented in Figure 6.2A. We find the endogenous rate of appearance (Ra) of glycerol in the IRlox cohort is 2.2±0.3 mg/kg/min, and Ra glycerol in the LIRKO cohort to be 3.1±0.8 mg/kg/min. As in Figure 6.2A, there are no significant differences in the rate of appearance of glycerol between cohorts, or the makeup of these rates of appearance with respect to endogenous or pump sources of glycerol. Endogenous appearance of glycerol constitutes approximately 70% of total glycerol appearance in both cohorts (IRlox 69±3%, LIRKO 74±3%, no significant difference). Glycerol dosed through the subcutaneous pump accounts for approximately 1.0 mg/kg/min of total glycerol appearance, and as expected does not change between mouse strains. Thus, the exogenous glycerol infusion rate is a fixed parameter given by the pump flow rate and substrate concentration.

The combination of endogenous versus pump glycerol rate of appearance in the context of glucose production from glycerol is presented in Figure 6.3 for clarity. In the IRlox mouse, endogenous glycerol uptake into gluconeogenesis accounts for 1.45 mg/kg/min while pump glycerol uptake into gluconeogenesis accounts for 0.66 mg/kg/min. Endogenous uptake

of glycerol into other metabolic pathways accounts for 0.76 mg/kg/min and pump glycerol uptake into other metabolic pathways accounts for 0.35 mg/kg/min of the total 3.2 mg/kg/min for glycerol uptake. Similarly in the LIRKO strain, endogenous glycerol uptake into gluconeogenesis accounts for 1.82 mg/kg/min while pump glycerol uptake into gluconeogenesis accounts for 0.63 mg/kg/min. Endogenous uptake of glycerol into other metabolic pathways accounts for 1.21 mg/kg/min and pump glycerol uptake into other metabolic pathways accounts for 0.41 mg/kg/min of the total 4.1 mg/kg/min for glycerol uptake. There are no significant differences between the partitioned components of glycerol uptake between mouse strains. Partitioning of substrate and end product usage reveals that the changes accounting for the increased uptake of glycerol in the LIRKO strain occur due to endogenous glycerol appearance, as the contribution of pump glycerol to total glycerol uptake remains quantitatively intact at approximately 1.0 mg/kg/min in both mouse strains.

In this section, we established the basal parameters of glucose production of the LIRKO model through dilution of [6,6-D$_2$]glucose tracer dosed subcutaneously., and showed correspondence with previous research estimating these parameters during the basal portion of a euglycemic-hyperinsulinemic clamp despite a shift in the model analyzed. In the next section, we probe the contribution of different substrates to this glucose production in order to assess causes of the observed similarities between the transgenic animal and its wild type counterpart.
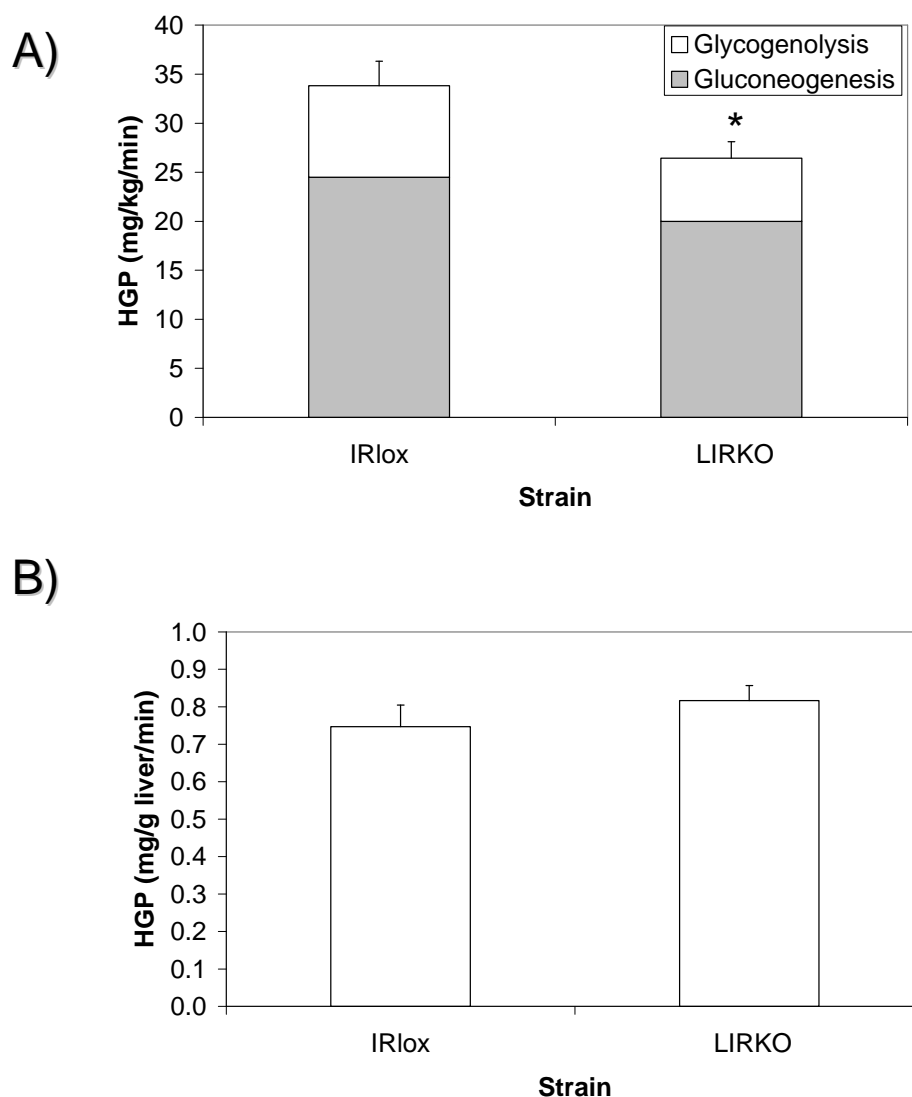
Figure 6.1: Hepatic glucose production (HGP) and gluconeogenesis glucose production (GGP) in the basal state after 24 hour combined tracer infusion. See experimental methods section 6.3.8. HGP (total bar) was estimated by dilution of $[6,6\text{-}D_2]$-glucose, and gluconeogenesis (gray bar) estimated by METRAN. (*=$p<0.05$). B) Hepatic glucose production in the studied mouse cohorts normalized to g liver weight. Liver weight was measured in mg immediately after the infusion experiment. Data are presented as mean±SEM (n=6).

A)

B)
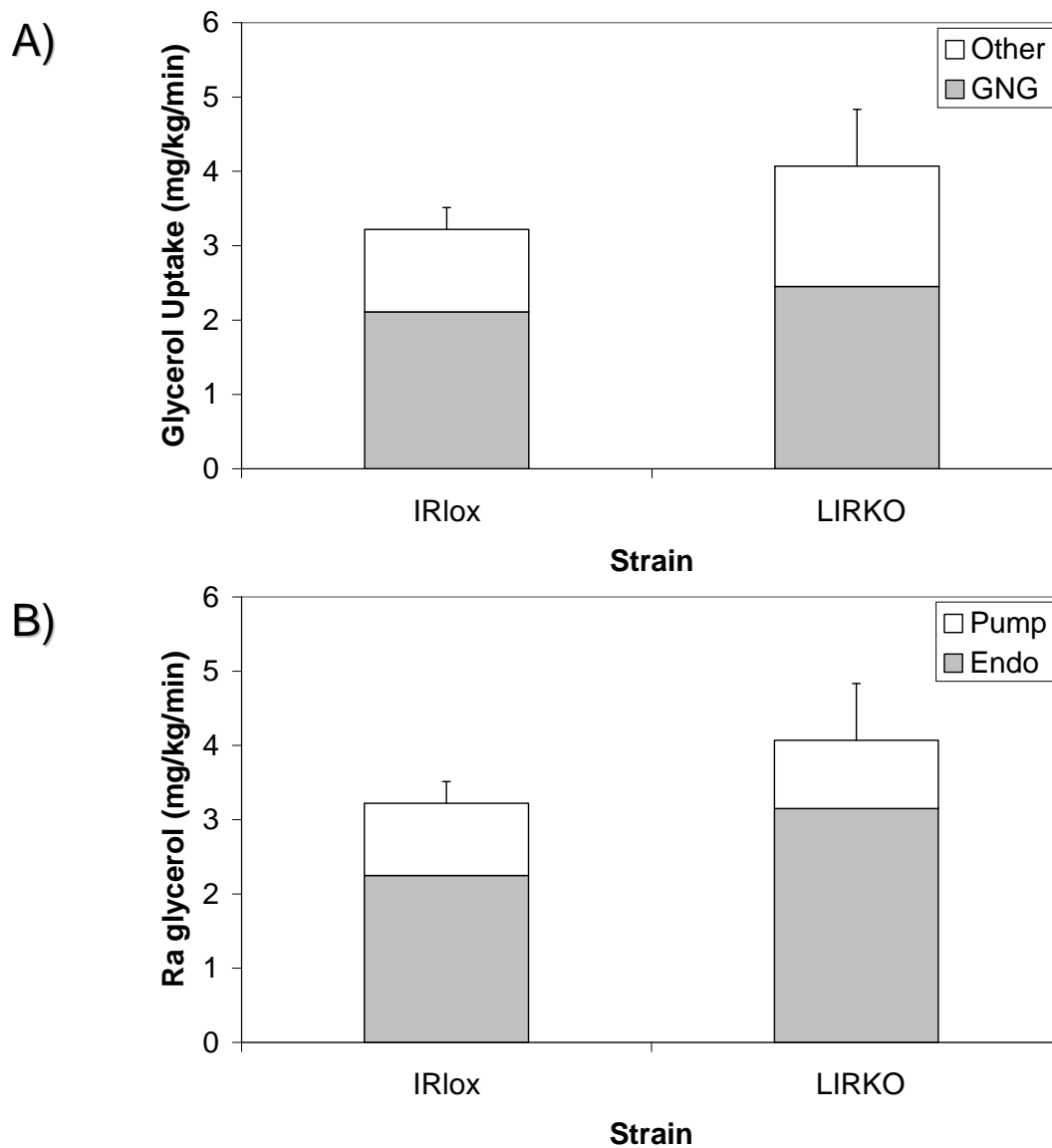
Figure 6.2: Glycerol uptake in the basal state after 24 hour combined tracer infusion. See experimental methods section 6.3.6 A) Glycerol rate of uptake broken down by gluconeogenic versus non-gluconeogenic use of glycerol. GNG = gluconeogenic B) Glycerol rate of appearance broken down by source of glycerol. Endo = endogenous. Data are presented as mean±SEM (n=6).
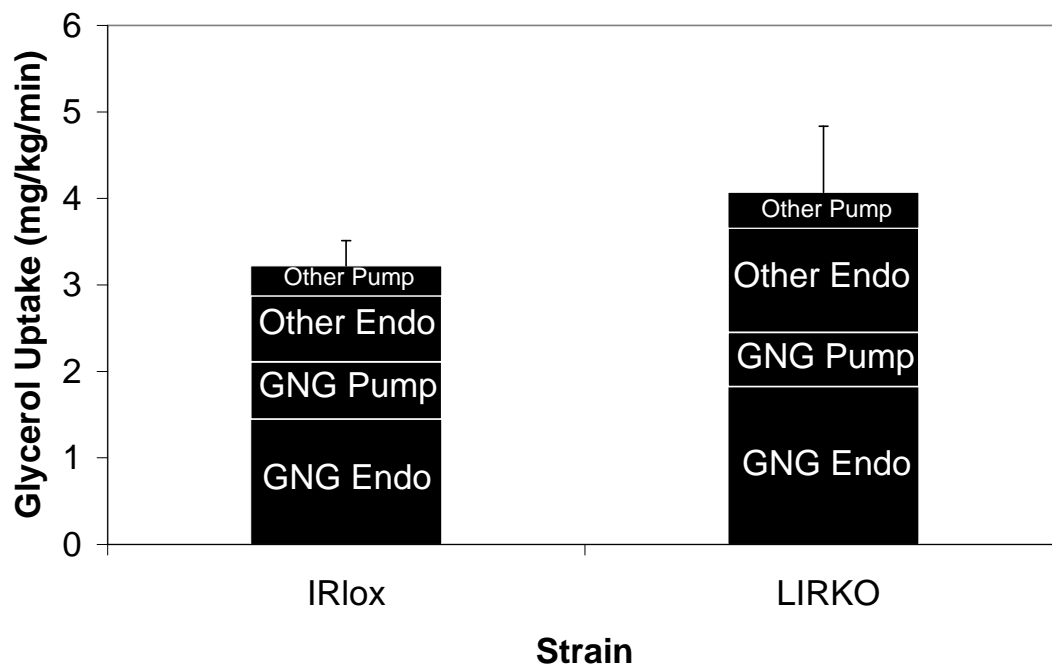
Figure 6.3: Partitioning of glycerol uptake in the basal state. See methods section 6.3.6. Glycerol uptake data is broken down by gluconeogenic versus other uses of glycerol, endogenous versus pump sources of glycerol. GNG = gluconeogenic, Endo = endogenous. Data are presented as mean±SEM (n=6).

Normalized flux distributions for hepatic glucose production reveal preserved metabolic

phenotype in the LIRKO mouse

Since LIRKO mice have been shown to express markedly elevated levels of gluconeogenic enzymes, we investigated in further detail the metabolic flux distribution of hepatic glucose production through in vivo flux analysis [14]. Previous work in our group has shown that flux regulation may not correspond with observed levels of gene transcript or metabolite levels in genetically-perturbed simple eukaryotic systems [214]. Therefore, we sought to assess whether we could explain the observed patterns in glucose production by differential fluxes in the use of gluconeogenic substrates. As described in Chapter 5, we performed in vivo flux analysis using a unique $[U\text{-}^{13}C,D_5]$ glycerol tracer aimed at establishing two additional pieces of information to the glucose production profile: the contribution of glycerol to the overall production of glucose in vivo, as well as any reaction reversibilities that exchange deuterium. Two glycerol subunits incorporate into a single glucose molecule which in turn manifests as enrichment in higher mass isotopomers that allow us to distinguish the incorporation of this gluconeogenic precursor into the glucose molecule as well as loss of deuterium enrichment through analysis of multiple glucose fragments presented in Chapter 4.

The resulting enrichment pattern of plasma glucose after 24 hours of combined, multi-labeled tracer infusion is presented in Figure 6.4. We present uncorrected aldonitrile pentapropionate glucose fragments at m/z 173 and 370 as representative of the patterns observed. Because the resulting glucose molecule potentially incorporates ^{13}C and ^2H, standard correction methods cannot be applied to eliminate natural abundance contributions. The quality of the data was adequate for observation of glucose enrichment at the aforementioned fragments and in addition we observed reproducible enrichment in aldonitrile pentapropionate glucose fragments at m/z 259, methyloxime pentapropionate glucose m/z 145 and di-

isopropyledene pentapropionate fragment m/z 301. The aldonitrile pentapropionate glucose fragments at m/z 245 presented poor quality data in terms of reproducibility and intervening mass spectra. As observed in Figure 6.4, the enrichment patterns for the both LIRKO and IRlox cohorts differ significantly from predicted natural abundance enrichment as shown by the white bars. Second, the standard errors for these enrichment values where at most between 0.5-0.7% for M0, reflecting the reproducible nature of glucose enrichment in a complex biological system. Furthermore, the patterns between these cohorts reflect very similar enrichment patterns in all observed glucose fragments. This is in contrast to a cohort of streptozotocin treated animals, where the enrichment pattern error in the estimation of M0 was between 1-2% (JA, YN, MA, unpublished observations). The similarity in enrichment patterns between strains suggests that the underlying metabolic processes contributing to the formation of enriched glucose from glycerol and deuterated water lead to a similar enrichment pattern, and that the resulting flux distributions are likely similar.

Qualitatively we can interpret the isotopomer data in Figure 6.4 in the following way. The observed increase in the M1 isotopomer of aldonitrile pentapropionate glucose fragment at m/z 173 over natural abundance primarily corresponds to deuterium enrichment at C5 from deuterated water. This value is used to calculate the fractional gluconeogenesis values in our computational methodology. This same fragment also includes C6 of the glucose molecule, which is bound to the deuterium atoms from the dosed [6,6-D$_2$] glucose molecule. Therefore, the enrichment in the M2 isotopomer over natural abundance in this glucose fragment primarily represents dilution of glucose used for calculation of hepatic glucose output with 2.29. Glycerol can incorporate one or two molecules into a single glucose molecule, with one subunit being much more likely based on the expected plasma glucose enrichment of 30%. Therefore, higher mass isotopomers (M3, M4, M5) in the glucose fragment at m/z 173 as well

as in glucose fragment at m/z 370 primarily represent enrichment from $[U-^{13}C,D_5]$-glycerol used for estimating the contribution of glycerol to glucose production and reaction reversibilities from the sequential loss of deuteriums in reactions such as mannose phosphate isomerase. These qualitative interpretations overlap in that there may be enrichment from other species in higher mass isotopomers, which are incorporated in our metabolic model in the METRAN framework. Lastly, because the presented data is uncorrected for natural abundance, there may be contributions from derivatizing agents not mentioned here but accounted for in the computational framework of METRAN.

To further address the observations for glucose enrichment, we present in Figure 6.5 the calculated flux distributions for hepatic gluconeogenic fluxes from METRAN, normalized to 100% of hepatic glucose output in each condition. Net fluxes are presented with their corresponding standard deviations. Fractional gluconeogenesis, as defined by percent contribution of gluconeogenic flux to total glucose output, does not change between IRlox (72.4±6.4%) and LIRKO (75.6±7.3%) animals, and corresponds with the results in the absolute gluconeogenesis values presented in Figure 6.1. These values are also similar to fractional gluconeogenesis estimates using our methodology in fasted BL6 mice after 6 hours (Chapter 5), suggesting that the underlying physiology of fasting in these models remains similar in both systems studied despite mouse strain differences and the underlying transgenic manipulation to ablate the insulin receptor in LIRKO. This result is consistent with the fasting conditions chosen for the infusion protocol, and further shows the metabolic state of the LIRKO mouse displays absence of insulin effects. Similarly, fractional glycogenolysis flux does not differ between mouse cohorts, with LIRKO livers showing 24±2% contribution from glycogen to total glucose production and control livers showing 28±2% respectively. This result is surprising considering the histological evidence of decreased glycogen deposition in

the LIRKO liver, and may point to differences between glycogen flux and amount measurements. Our flux analysis results represent a time average of fractional gluconeogenesis over several hours prior to the measurement of enrichment, because the turnover of circulating plasma glucose pool and glycogen stores in the liver occurs over a time scale of several hours.

Functional comparison of substrate usage in LIRKO animals is another result obtained from our in vivo flux analysis methodology. We observed previously that at least one gluconeogenic substrate (lactate) remains at similar plasma levels in LIRKO and IRlox animals. However, the over expression of gluconeogenic enzymes in the LIRKO liver could be expected to change the distribution of substrates used by preferentially drawing metabolic flux from the oxaloacetate pool in the presence of simultaneous PEPCK and G6Pase upregulation. Similarly secondary effects of peripheral insulin resistance may cause differential gluconeogenic substrate availability from muscle in the form of alanine from proteolysis. Consistent with the observed patterns for isotopomer enrichment, the calculated metabolic flux distributions for upper gluconeogenesis in the LIRKO liver remain unchanged in comparison to their IRlox counterparts. We observe that precursors from the oxaloacetate pool (lactate, pyruvate, alanine) remain the principal sources of glucose production by metabolic flux analysis, contributing 128/144 of triose phosphates in the wild-type animals and 132/152 of triose phosphates in the LIRKO mouse. The usage of these gluconeogenic substrates dominates the metabolic flux distribution for glucose production, despite significant usage of dosed glycerol as evidenced through incorporation into glucose. Specifically, glycerol flux contributes 15/144 and 15/152 of triose phosphates in the IRlox and LIRKO flux distributions for upper gluconeogenesis, respectively. This result is consistent with our previous in vivo work in fasted BL6 mice (Chapter 5) and different from the metabolic paradigm presented through in vitro

experiments (Chapter 4) therefore stressing the importance of performing in vivo flux analysis in order to characterize transgenic hepatic physiology.

In summary, in vivo flux analysis shows how the LIRKO ablation of the insulin receptor does not affect the functional usage of gluconeogenic substrates in the liver as determined my metabolic flux relative to total glucose output. As a corollary to this result, we can propose that regulation of glucose production does not occur by metabolic flux regulation in the studied metabolic network for upper gluconeogenesis. In turn, at least two possible points for regulation would be consistent with a preserved flux distribution in the LIRKO model: glucose-6-phosphatase demand on glucose production, and supply of gluconeogenic substrates from peripheral insulin-sensitive tissues such as muscle and adipose tissue. These are not mutually exclusive, and represent part of the direct and indirect effects of glucose action in the LIRKO model. In the following section, we present additional manipulation of the hepatic glucose production pathway aimed at addressing possible distinctions between these proposed mechanisms.
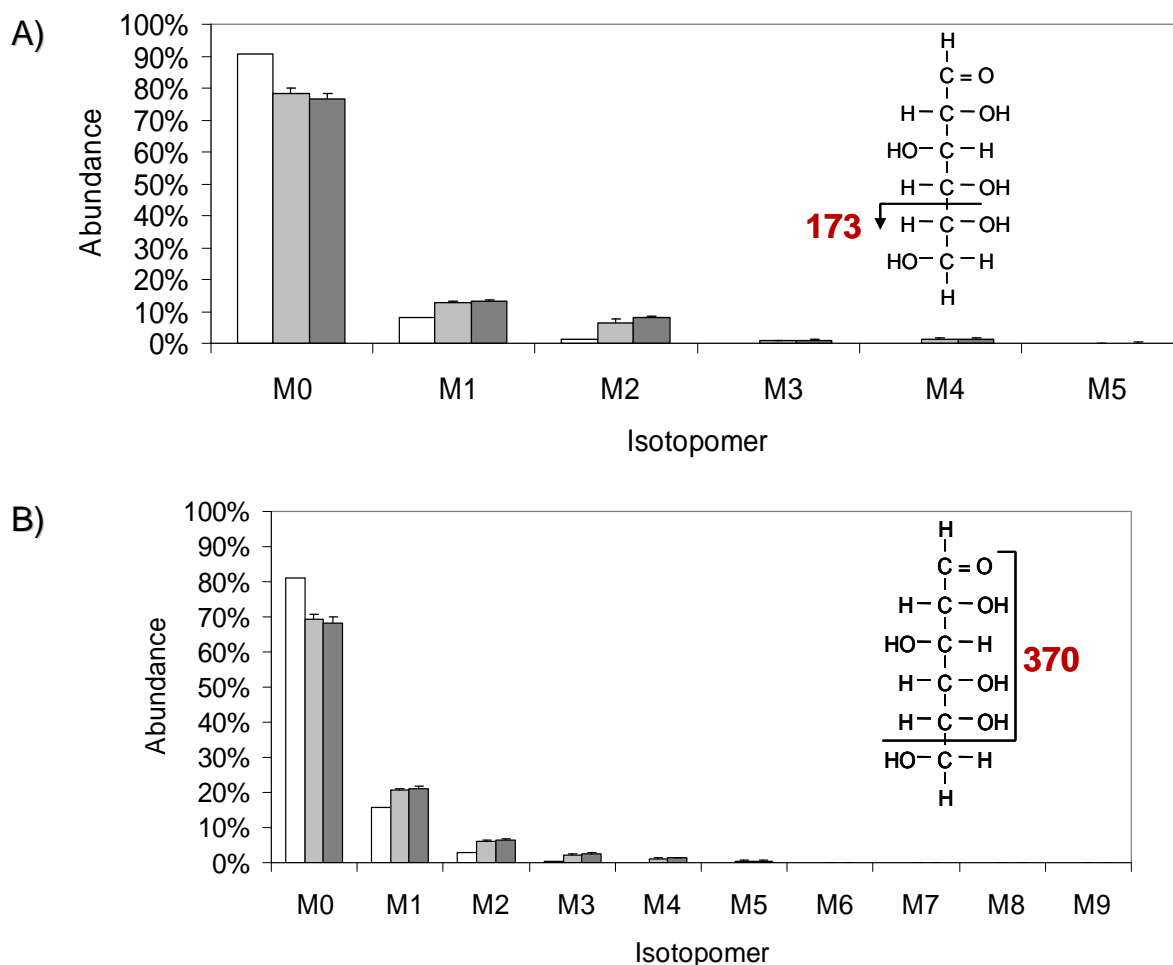
Figure 6.4: Uncorrected mass isotopomer distributions for glucose aldonitrile pentapropionate fragments at m/z 173 and 370. Treatment groups include theoretical abundance (white), IRlox (light gray), LIRKO (dark gray) after 24 hours infusion of simultaneous dosing of [U-^{13}C,D$_5$]-glycerol, [6,6-D$_2$]glucose and 10% deuterated water. Data are presented as mean±SEM (n=6).

IRlox Mouse (WT)

Glucose

$\uparrow$

100

G6P $\xleftarrow{28\pm2}$ Glycogen

$\uparrow$

72±6

DHAP $\xleftarrow{56\pm7}$ GAP

16±3   128±13

Glycerol   Lactate
Pyruvate
Amino Acids

LIRKO Mouse

Glucose

$\uparrow$

100

G6P $\xleftarrow{24\pm2}$ Glycogen

$\uparrow$

76±7

DHAP $\xleftarrow{56\pm6}$ GAP

20±3   132±14

Glycerol   Lactate
Pyruvate
Amino Acids
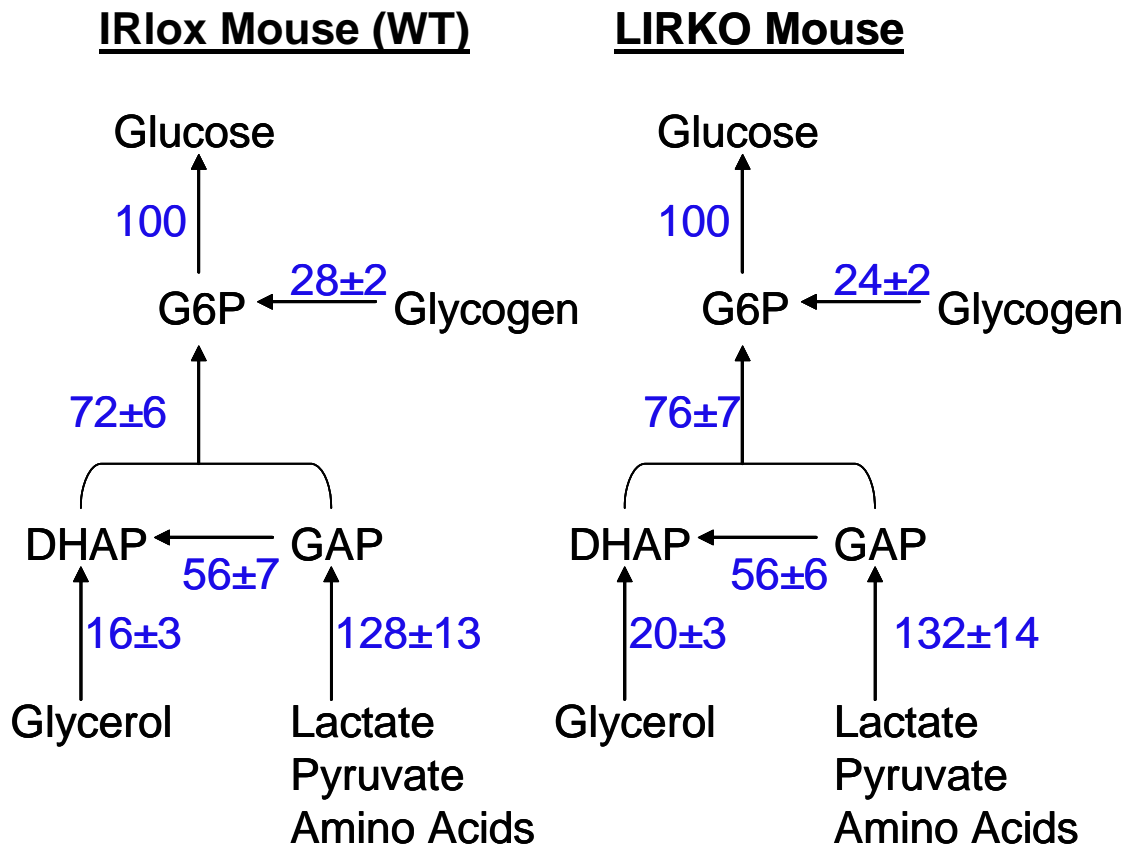
Figure 6.5: Normalized flux distributions for hepatic glucose production reveal unchanged metabolic phenotype. Mice (n=6) were infused a combination of tracers through miniosmotic ALZET pumps including 2M [6,6-D_2]-glucose, 2M [U-^{13}C, D_5]-glycerol, and 10% deuterated water (IP and fed). Gluconeogenesis net fluxes, reversibilities and confidence intervals were determined by METRAN. Fluxes are presented as mean +/- 68% confidence interval.

6.4.3 Experimental manipulation of glucose production

<u>Acute availability of gluconeogenic substrate uncovers the LIRKO gluconeogenic phenotype</u>

Given that flux estimations constitute a weighted average over several hours prior to sampling time in plasma glucose, we sought to test whether the gluconeogenic phenotype of the LIRKO liver could be elicited by acute increases in substrate availability. For this purpose, we turned to a pyruvate tolerance test, a physiological assessment of hepatic glucose production after an acute bolus of substrate [209, 210]. Administration of a 2g/kg bolus of sodium pyruvate causes a sustained increase in plasma glucose of the LIRKO mouse and significantly increases plasma glucose at 60 minutes post injection (Figure 6.6). We observe delayed uptake of glucose in peripheral tissues at 120 minutes when compared to decreasing levels of plasma glucose in the wild-type animals at the 60 minute timepoint. The area under the curve for LIRKO pyruvate tolerance is significantly increased over the IRlox animals. However, it is not clear from these results whether the increase occurs due to primary, central increase in hepatic glucose output due to substrate availability represented by the initial rise of the glucose production curve, or due to secondary muscle insulin resistance inhibiting glucose uptake of the newly synthesized glucose in the subsequent decrease phase. Under acute availability of pyruvate, the LIRKO mouse displays an elevated glucose response consistent with either increased hepatic glucose output or peripheral resistance.
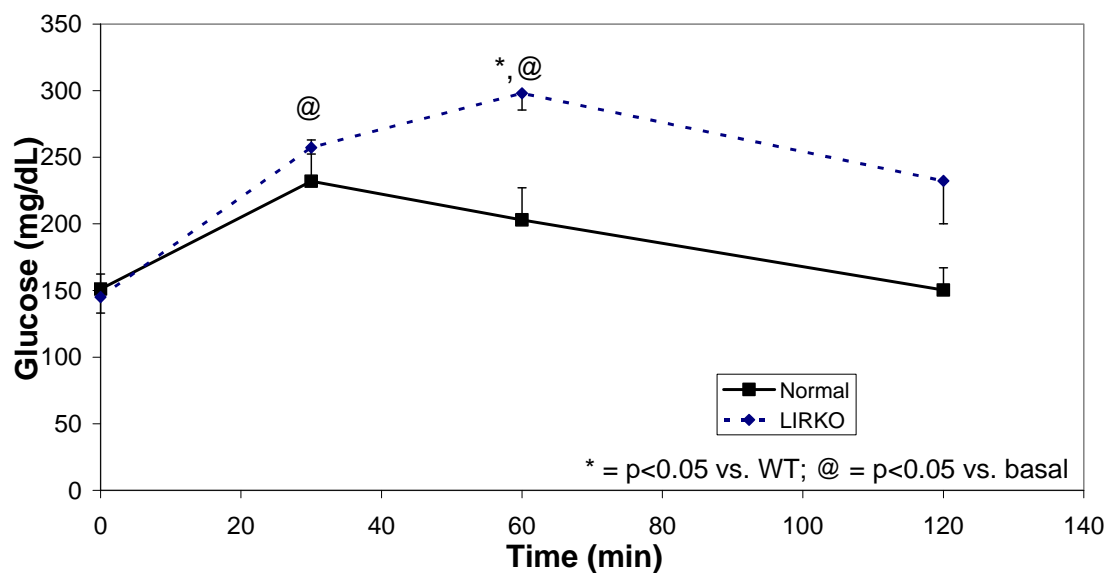
Figure 6.6: Pyruvate tolerance test unmasks the gluconeogenic phenotype of LIRKO metabolism. Mice (n=3) were injected a 2g/kg intraperitoneal bolus of sodium pyruvate (Sigma) and followed blood glucose by tail bleeding with a OneTouch Ultra2 glucometer. * = p<0.05 vs. WT; @ = p<0.05 vs. basal. AUC(LIRKO) = 30275, AUC(IRlox) =22870 , p<0.05.

Directed hepatic metabolite profiling highlights differences between LIRKO and STZ models

A static flux picture in the LIRKO mouse liver can correspond to unchanged metabolite concentrations leading to the production of glucose. On the other hand, increased levels of gluconeogenic enzymes as observed in LIRKO livers would endow this pathway with larger metabolic capacity, and in turn lower levels of intermediary metabolites leading to the production of glucose. To test the hypothesis that LIRKO mice have lower levels of metabolites, we performed directed metabolite profiling [215] of liver tissue to observe potential differences in the metabolite profile due to lack of insulin receptor. Specifically, we asked the question whether we could observe accumulation of involved metabolites suggesting single enzyme defects that could account for the resulting changes in glucose production observed through in vivo flux analysis. We processed frozen LIRKO livers from fasted animals paired with IRlox livers of the same age, as well as four livers from streptozotocin treated wild type mice and their untreated counterparts. After homogenization in PBS, we prepared the polar fraction through Folch extraction [216], added ribitol as a reaction standard and performed TMS derivatizations to inject the resulting volatile compounds into a GC-MS for quantitation of amino acids, organic acids and glucose intermediates. The amounts were normalized to mg wet liver, %ribitol amount and control condition for the experimental group. Figure 6.7 presents the resulting chromatograms from streptozotocin-treated livers and LIRKO livers, from which 16 metabolites were detected across all experimental conditions. We observe qualitative differences in our metabolite detection method, with glucose being the most abundant peak observed and the phosphorylated intermediates of glucose metabolism being found in the smallest detectable amounts. Given the large amount of glucose detected, the likely source of the observed glucose peak is extracellular glucose from plasma.
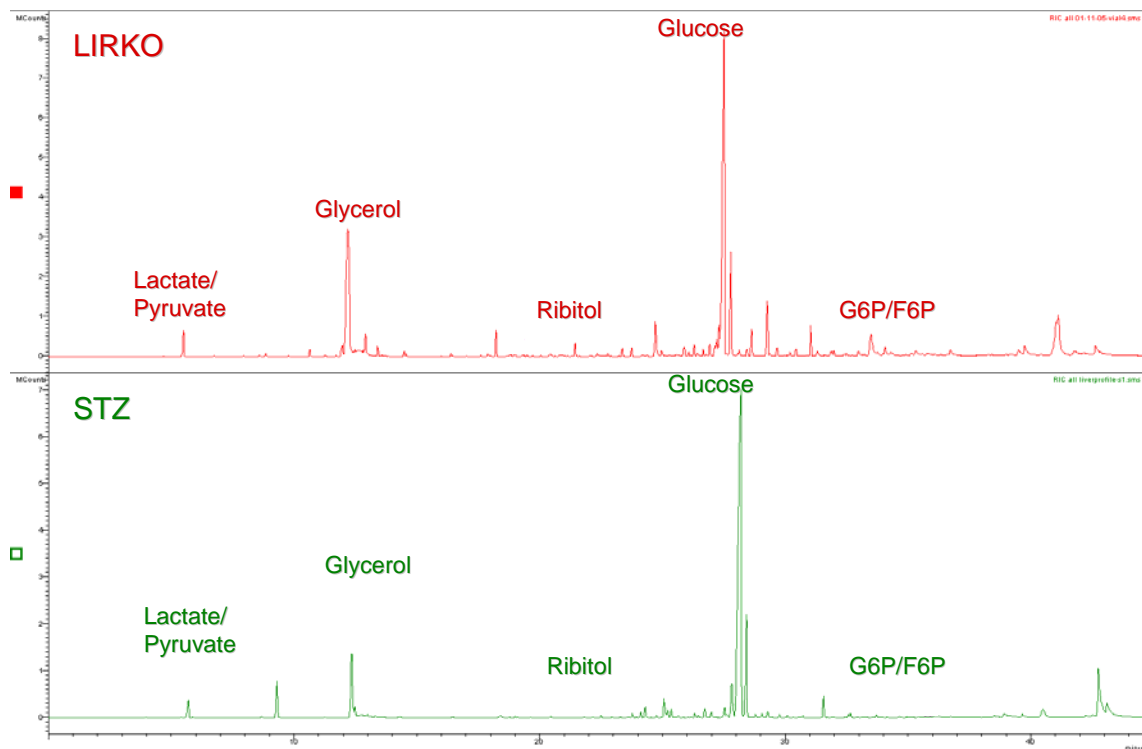
Figure 6.7: TMS liver metabolite profile for sample LIRKO, STZ liver. Data were collected by electron impact ionization on a Saturn 2000 ion-trap GC-MS system (Varian Inc, Walnut Creek CA). We identified 16 metabolites encompassing intermediary metabolism in classes including amino acids, organic acids and glucose metabolites.

The normalized ratios of metabolite levels in LIRKO livers are shown in Figure 6.8, with the corresponding intermediary metabolism map presenting the relative levels of metabolites leading to glucose production. Comparisons of metabolite levels did not yield significant differences between LIRKO and control liver. Indeed the only two metabolites for which we detect non-significant trends ($p < 0.1$) are cysteine and fructose-6-phosphate. The dynamic range of metabolite concentrations vary over multiple orders of magnitude [156]. To reconstruct a static picture of hepatic metabolite levels, we present the relative levels of metabolites, and note that the majority of the metabolite levels detected decreased in the LIRKO livers when compared to its wild-type counterpart. Exceptions include succinate corresponding to the mitochondrial compartment and malate (cytosolic and mitochondrial) in the pathway towards glucose production. We note that all amino acid levels measured in the LIRKO levels decreased, including glucogenic amino alanine, aspartate, cysteine, glutamate and glycine. On the other hand, glucogenic amino acid serine is the only detected amino acid for which the levels were increased in LIRKO livers. Glucose levels are increased in LIRKO livers as expected from our previous analysis, and phosphorylated intermediates glucose-6-phosphate and fructose-6-phosphate show decreased levels in LIRKO livers. Crossover difference in metabolite levels may indicate active regulatory sites where enzyme control is exerting an effect of a downstream metabolite [217].

We wished to test the ability of our directed metabolite profiling protocol to detect significant differences in hepatic metabolites with more acute deregulation in the glucose production phenotype. Thus, we performed a similar analysis on the livers of streptozotocin-treated mice, a common model of diabetes due to beta cell failure. The relative levels of metabolites are presented in Figure 6.9. In contrast to the previously observed results, metabolite levels in livers of streptozotocin-treated animals show increased levels for nearly all

detected metabolites leading to glucose production, stressing the catabolic nature of this model of diabetes. The ratio of detected glucose is higher than that observed for LIRKO animals, consistent with the high levels of glucose observed in this model of diabetes. Metabolites with significantly increased levels detected include aspartate, cysteine, glucose-6-phosphate, glutamate, glycine, glycerol, lactate, serine and succinate. Interestingly and unlike the LIRKO liver, the detected glucogenic amino acid levels in STZ livers were increased, with the exception of alanine which remains unchanged. Metabolite levels in STZ livers remain elevated for all metabolites observed, with the exception of alanine for which we could not detect significant differences.

One potential explanation for changes in hepatic glucose production in the LIRKO liver involves single enzyme effects that account for the observed changes in basal hepatic glucose production. In particular, we were interested in assessing the possibility that glucose-6-phosphatase could modulate the demand for hepatic glucose to match body glucose demand. To this end, we present a crossover plot from the normalized metabolite levels comparing LIRKO and STZ livers in their metabolite levels in Figure 6.10 [218]. In the presence of gluconeogenesis inhibitor mercaptopicolinic acid, previous research observed accumulation of oxaloacetate and crossover to decreased metabolite levels of PEP corresponding with enzyme inhibition at PEPCK [217]. Unlike the qualitative map representations in Figures 6.8 and 6.9, a crossover plot reveals quantitative differences in metabolite levels that imply active regulation at the level of pathway enzymes. Specifically, we observe that streptozotocin-treated livers remain above unity when compared to the levels of metabolite measured in their respective control livers, consistent with the observations in the metabolic map in Figure 6.8. The minimum normalized amount of metabolite is present at citrate, and this level is not significantly different from the control condition. Thus, we find no clear cut evidence of single

enzyme inhibition or modulation of hepatic glucose production in streptozotocin treated-livers, consistent with extrahepatic effects increasing the availability of gluconeogenic precursors from protein catabolism. We observe a decrease in the levels from F6P (9.08) to G6P (2.91) without crossover to decreased metabolite levels. This decrease in metabolite levels could be consistent with enzyme inhibition at glucose-6-phosphatase since the detected glucose corresponds to extracellular plasma glucose.

On the other hand, LIRKO crossover analysis reflects a more intricate pattern of crossover in the levels of several metabolites (Figure 6.10). As observed in the metabolic maps presented in Figure 6.7, metabolites in the LIRKO liver remain at levels lower than those in the IRlox counterpart. Three metabolites along the glucose production pathway crossover to positive abundance in the LIRKO liver: succinate (1.79), malate (1.44) and glucose (1.24). Interestingly, the first two of these metabolites are known to be present in mitochondria, where compartmentation effects could explain the low amounts detected by GC-MS. We observe the value of glucose to be slightly hyperglycemic to the IRlox counterpart, and closer to the normal level of glucose than the streptozotocin-treated liver glucose. The crossover evident for glucose is preceded by decreased levels of glucose-6-phosphate, fructose-6-phosphate and glycerol, suggesting active regulation at the glucose-6-phosphatase junction modulating demand for glucose despite decreased hepatocyte metabolite levels. This data could be improved by improving metabolic pathway coverage with GC-MS, or alternatively complementing the presented values with more sensitive technologies for metabolite detection such as chemical ionization GC-MS or liquid chromatography-mass spectrometry (LC-MS).

In summary, directed metabolite profiling provides evidence for regulation of glucose output at the level of glucose-6-phosphatase in STZ livers, which is in turn consistent with the static flux distribution observed through in vivo flux analysis for hepatic glucose output. These

analyses are useful as adjunct to genomic and proteomic profiling [219-221]. From the outset, decreased levels of intermediary metabolites would be expected in the face of excess gluconeogenic capacity. However, the small magnitude of metabolite level changes suggests the LIRKO liver operates metabolically nearby the initial metabolic state without a transgenic ablation. The observed metabolite levels suggest a system operating under maximum capacity in part due to increased gluconeogenic enzyme levels and partly due to lack of metabolite input. In comparison, the streptozotocin-treated animals display a catabolic metabolic phenotype with striking differences to the LIRKO animal. Both phenotypes manifest hyperglycemia, however the main difference between these models is the excessive presence of insulin in the former compared to the absence of insulin in the latter. The streptozotocin-treated mouse does not develop significant insulin resistance over the days post-treatment, and muscle is expected to act as source of gluconeogenic precursors in near absence of insulin presence. This manifests in metabolic profiling as increased levels of nearly all intervening metabolites despite presumably increased levels of gluconeogenic enzymes due to counter regulatory hormone action. It would be interesting to observe the flux distribution of streptozotocin-treated animals as a comparison to these phenotypes; we can expect increased hepatic glucose output fluxes corresponding to the increased availability of gluconeogenic precursor.

Figure 6.8: Directed liver metabolite profile of LIRKO livers shows unchanged metabolite levels contributing to excess glucose production. 100 mg frozen liver (n=3) was homogenized in 2 volumes of PBS using a hand-held Tissue Tearor Homogenizer. Samples were centrifuged to remove solids. After extraction with methanol:chloroform solution (2:1), the polar fraction was dried and analyzed for metabolite amounts using TMS derivatization of the polar metabolites and Gas Chromatography-Mass Spectrometry. Dashed boxes represent represents increased metabolite levels over control condition; solid boxes represent decreased metabolite levels over control condition. Data are presented as log ratios normalized per mg wet liver, mg ribitol and control condition.

STZ

☐ = exp > control; ☐ = exp < control

Metabolite	Ratio STZ/WT	P value
Aspartate	5.66	0.03
Alanine	0.98	0.99
Citrate	1.13	0.81
Cysteine	3.27	0.00
F6P	9.08	0.06
Fumarate	7.56	0.31
Glucose	1.66	0.36
G6P	2.91	0.02
Glutamine	1.38	0.61
Glutamate	3.38	0.00
Glycine	2.48	0.03
Glycerol	1.95	0.02
Lactate	2.05	0.01
Malate	2.18	0.11
Serine	2.38	0.03
Succinate	2.31	0.04
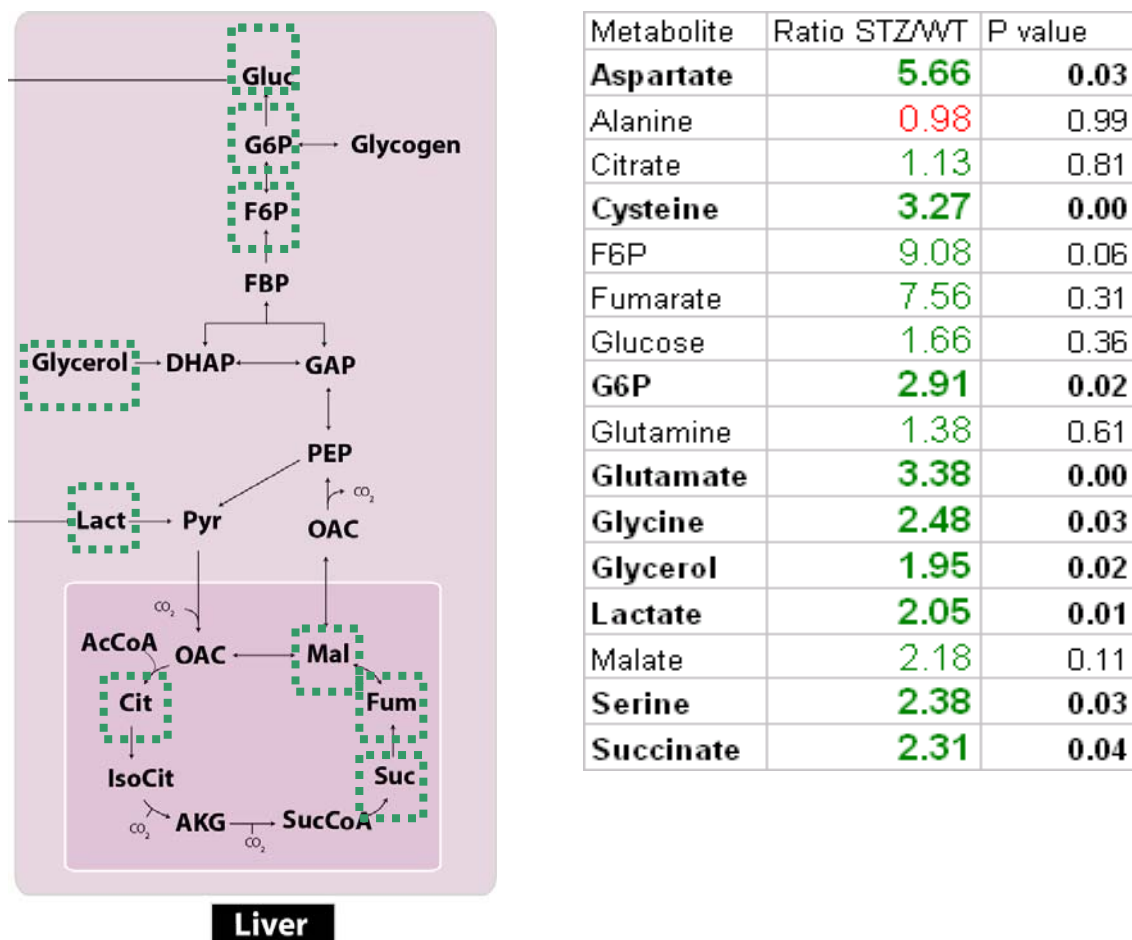
Figure 6.9 Directed liver metabolite profile of STZ livers show high metabolite levels contributing to excess glucose production. 100 mg frozen liver (n=4) was homogenized in 2 volumes of PBS using a hand-held Tissue-Tearor Homogenizer. Samples were centrifuged to remove solids. After extraction with methanol:chloroform solution (2:1), the polar fraction was dried and analyzed for metabolite amounts using TMS derivatization and Gas Chromatography-Mass Spectrometry. Dashed boxes represent represents increased metabolite levels over control condition; solid boxes represent decreased metabolite levels over control condition. Data are presented as log ratios normalized per mg wet liver, mg ribitol and control condition.
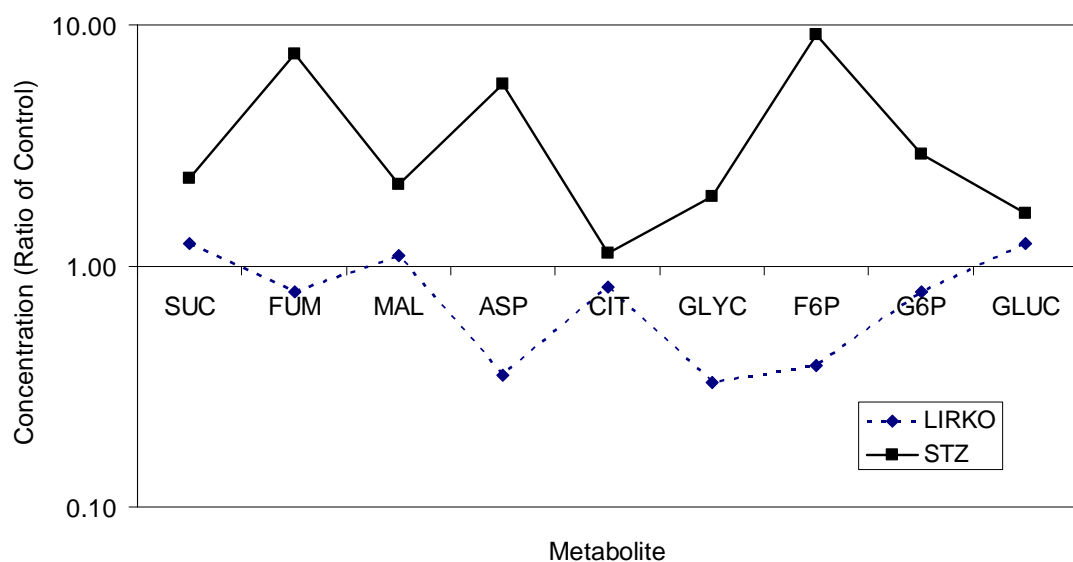
Figure 6.10: Crossover analysis of metabolites that contribute to glucose production. in LIRKO and STZ livers. Normalized metabolite levels relative to % ribitol, g wet liver weight and control conditions are presented along their relative position in the glucose production metabolic pathway.

6.4.4. Decreased lipogenic biosynthesis as a consequence of hepatic insulin resistance

Insulin has multiple metabolic effects on the liver, including modulation of lipid biosynthesis and secretion. As part of the biosynthetic program induced by insulin action, much research has documented increases in fatty acid and cholesterol biosynthetic pathways. The effects of insulin action on cholesterol synthesis are postulated to be mediated through the action of master regulator transcription factor SREBP-1c, which coordinately upregulates cholesterol gene expression leading to increased *de novo* production in the liver [222, 223]. In assessing a complete metabolic picture of the LIRKO animal, we sought to study lipogenesis through the use of stable isotope tracers through the classic methodology of isotopomer spectral analysis [224, 225]. This methodology uses the degrees of freedom acquired through measurement of cholesterol and fatty acid isotopomers to calculate biosynthetic parameters describing the dilution of the metabolite and its fractional synthetic rate as discussed in Chapter 3. We isolated LIRKO and IRlox hepatocytes simultaneously and cultured in the presence of [U-^{13}C] acetate, which contributes to the synthesis of cholesterol and fatty acids through incorporation into AcetylCoA as discussed in Chapter 3. This classic method for estimating biosynthesis has been used to estimate contributions of glutamine to lipid synthesis, as well as the effects of HMG-CoA synthase inhibitors on cholesterol metabolism in patients [74, 141].

Using this analysis, we observed biosynthetic effects on lipid metabolism due to the transgenic ablation of the insulin receptor in vitro. As seen in Figure 6.11A, the fractional synthesis of cholesterol is significantly changed in the LIRKO hepatocyte compared to the IRlox counterpart as measured by stable isotope incorporation through mass spectrometry. In particular, cholesterol synthesis as 24 and 48 hours post introduction of label shows

significantly decreased fractional synthesis at timescales when the cholesterol pool in hepatocytes has turned over at least once. We measured palmitate enrichment in order to sample plasma triglyceride fatty acids as shown in Figure 6.11B. As with cholesterol, we observe significantly decreased fractional synthesis of fatty acids in LIRKO hepatocytes when measured by area under the curve. We profiled oleate and stearate enrichment from $[U-^{13}C]$-acetate and saw similar patterns towards decreased synthesis. The measurement of fractional synthesis is independent of the amount of cholesterol detected in the hepatocytes, indeed, net cholesterol amounts were increased in LIRKO hepatocytes relative to their IRlox counterparts. These results highlight the importance of integrating biosynthesis measurements from different metabolic pathways to gain a global perspective on the effects of hepatic insulin ablation, liver insulin resistance and its role in the progression to Type 2 Diabetes.

Reconstruction of lipid metabolism in LIRKO hepatocytes underscores the importance of assessing multiple aspects affected by a genetic alteration such as hepatic insulin receptor ablation. Remarkably, we observe different metabolic phenotypes in related pathways of metabolism under a single transgenic modification, pointing to the multiplicity of actions of insulin and hypothesized dichotomies of effect between glucose and lipid metabolism [53, 54]. Detailed analysis of individual steps in lipid biosynthesis can further elucidate enzymatic targets under the regulation of insulin that contribute to the development of abnormal lipid profiles in Type 2 Diabetes, such as stearyl-CoA desaturase 1, fatty acid synthase, and transcription factors such as SREBP-1c [226, 227].

A)
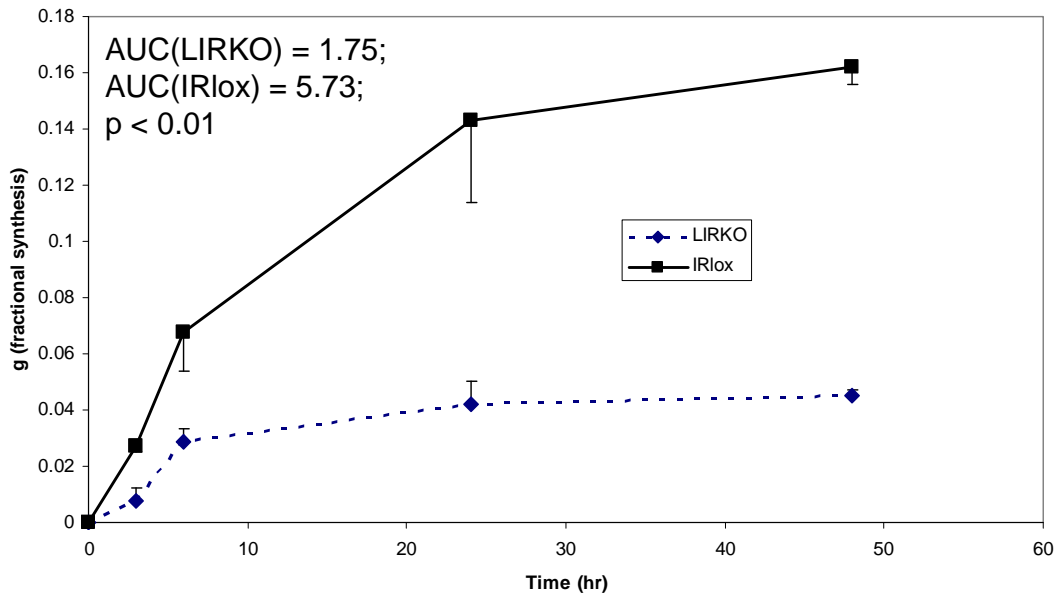
B)
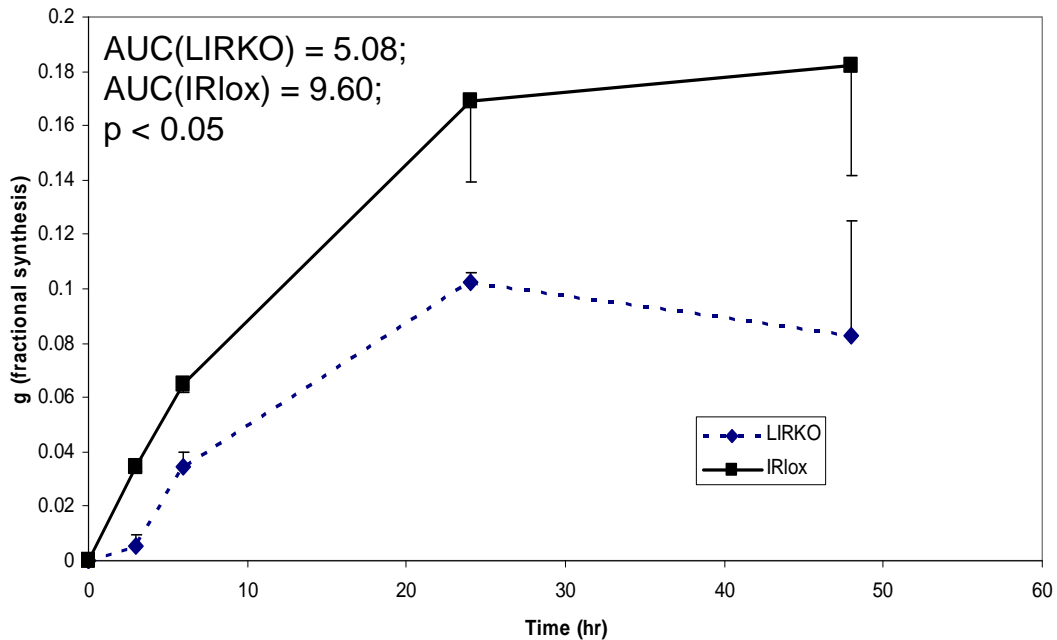
Figure 6.11: Significantly decreased lipid synthesis on LIRKO hepatocytes. IRlox, = squares, solid line, LIRKO = diamonds, dashed line A) Timecourse of cholesterol fractional synthesis in LIRKO and IRlox hepatocytes. B) Timecourse of palmitate fractional synthesis in LIRKO and IRlox hepatocytes. Data are presented as mean±SEM (n=2).

6.5 Discussion

In the previous results, we present an application of the in vivo flux analysis methodology presented in Chapter 5 for hepatic glucose production in the case of the liver-insulin-receptor knockout (LIRKO) mouse, a model of Type 2 Diabetes engineered to lack the insulin receptor in liver tissue via Cre-LoxP recombination under the control of the albumin promoter.

The LIRKO mouse is a unique, transient model in which to assess the role of extrahepatic influences on HGP in the context of complete hepatic insulin resistance. In the presence of high dose insulin (17-24 ng/mL) during the euglycemic-hyperinsulinemic clamp, previous studies have established the transgenic's inability to suppress HGP [15]. This finding can be interpreted as a lack of indirect-HGP suppressing effects of insulin in the transgenic animal. The marked glucose turnover differences observed for the LIRKO animal during the clamp study suggest profound insulin resistance in muscle that can be partially ameliorated by dosing of streptozotocin to lower circulating insulin levels. In our results, we further explored the basal phenotype of these animals through a combined, multi-tracer strategy to reconstruct hepatic metabolic fluxes in vivo such as hepatic glucose production, fractional gluconeogenesis and substrate contributions to overall glucose production. The paradigm studied here is intrinsically different to that of the euglycemic-hyperinsulinemic clamp in that insulin levels are allowed to remain at basal levels. In addition, the time scale of administration of tracer is longer than that of the basal portion of the clamp protocol, with the former estimation occurring in minutes while our method estimates glucose production over hours. Lastly, the addition of glycerol as a tracer for clearly elucidating the contribution of lipolysis to gluconeogenesis constitutes an interesting probe for the choice of metabolites contributing to glucose production (Chapter 4).

The basal parameters for the cohorts in our in vivo flux analysis study are similar to those presented previously [14, 15]. However, the glucose levels for our animal cohorts were hyperglycemic despite the fasting conditions prior to the pump implant procedure (IRlox 151 mg/dL, LIRKO 145 mg/dL) and after the combined, multi-labeled tracer infusion (IRlox 196 mg/dL, LIRKO 158 mg/dL). This result was common to our infusion experiment and pyruvate tolerance test, indicating that there may be factors such as animal handling influencing release of glycogen under stress condition or incomplete depletion of glycogen stores. The lower plasma glucose values in the LIRKO cohort have been observed by Fisher et al [15] and are attributed to the decreased glycogen stores present in the liver due to counterregulatory hormone action. The similarity of lactate levels between models shown in Table 6.1 (IRlox 48±3 mg/dL, LIRKO 38±4 mg/dL) suggests that the availability of gluconeogenic precursors in the LIRKO liver is similar to that in the wild-type animal. However, glucogenic amino acids levels in the LIRKO liver were consistently found decreased through directed hepatic metabolite profiling (Figure 6.8). This is consistent with similar red cell glycolysis and muscle glycogenolysis production in muscle yielding lactate. Amino acids derived from muscle proteolysis may be affected by the hepatic insulin receptor modification, and specific tracer amino acid tracer studies could assess the circulating levels of individual amino acids as well as their metabolic flux into glucose.

We find net hepatic glucose production in the LIRKO animal to significantly decrease 20% from the wild type animal under our experimental conditions (Figure 6.1A). These changes occur by simultaneously decreasing net gluconeogenesis (IRlox .24.5 mg/kg/min, LIRKO 20.0 mg/kg/min, no significant difference) and glycogenolysis (IRlox 9.3 mg/kg/min, LIRKO 6.4 mg/kg/min, no significant difference) without affecting the proportion of each pathway contributing to total glucose production. The reduced net hepatic glucose production cannot

be explained by changes in the production of glucose per gram of liver in LIRKO (Figure 6.1B). The results of these basal hepatic glucose production measurements suggest that the LIRKO animal has decreased its metabolic demand of glucose in liver as an adaptive process to return plasma glucose values to near normal levels. Glucose consumption by the body produces a constant demand for gluconeogenesis in the liver. Of this total demand, approximately 65% is encompassed by non-insulin sensitive tissues such as the brain, red blood cells and the renal medulla [39, 42]. The remaining amount of glucose demand is primarily encompassed by muscle, which can alter its glucose consumption depending on insulin levels to account for up to 70% of an oral glucose load [203]. Our results, together with glucose turnover values in the euglycemic-hyperinsulinemic clamp study, suggest decreased muscle glucose consumption in LIRKO animals to maintain steady state by matching the decreased HGP.

As a test to assess the importance of muscle in normalizing the plasma glucose phenotype of the LIRKO mouse, we propose that future studies measure 2-deoxyglucose uptake in vivo to assess the role of muscle glucose uptake on the glucose phenotype of the LIRKO mouse. Ex vivo analysis of glucose uptake in soleus muscle showed no differences in glucose uptake between LIRKO and control animals, and both muscle tissues increased their glucose uptake 3-fold in the presence of insulin [14]. In vivo studies could assess muscle glucose uptake for LIRKO animals under basal glucose uptake and hormonal treatment with insulin to test the hypothesis that muscle glucose utilization in LIRKO matches the decreased HGP detected in this study.

Our study tested the hypothesis that usage of glycerol as gluconeogenic substrate in LIRKO decreases due to the high PEPCK levels present (Figure 6.2). In other words, we hypothesized that livers with high PEPCK activity would preferentially use substrates from the

oxaloacetate pool over glycerol for glucose production. Our findings did not support this hypothesis, as we observed no changes in the fraction of gluconeogenesis derived from glycerol (Figure 6.2). Our additional observations of unchanged fractional conversion of glycerol to glucose (Figure 6.2A), unchanged rate of appearance of glycerol and unaffected distribution of endogenous and total glycerol appearance (Figure 6.2B) further confirm the preservation of plasma glycerol availability in the LIRKO mouse and point to the muscle as the likely source that accommodates changes in hepatic glucose production due to substrate availability. As the other product of triglyceride breakdown, unchanged levels of free fatty acid in LIRKO mice when compared to wild type have been reported to indicate that lipolysis effects from adipose tissue between transgenic and wild-type animal are similar [15].

Could there be effects from administering glycerol on the observed hepatic glucose flux distributions? The glycerol uptake and appearance rate data suggest this is not the case in the performed experiments. ALZET pumps contribute approximately 1.0 mg/kg/min of glycerol for both strain cohorts (Figure 6.3). This result indicates that glycerol delivery to the subcutaneous space is independent of mouse strain and strictly dependent on pump parameters such as the predetermined flow rate and substrate concentration as designed by the experimenter. The fixed glycerol flow rate from the miniosmotic pump contributes between 26-31% of total glycerol rate of appearance, in line with the amounts observed for plasma glycerol enrichment in preliminary cellular and animal experiments (Chapter 4, Chapter 5). The flow rate of glycerol does not impact the observed metabolic flux phenotypes, as the flux analysis results show marginal changes in the relative usage of glycerol as a gluconeogenic substrate (IRlox 16±3%, LIRKO 20±3%, Figure 6.5). The use of glycerol as a stable isotope tracer thus involves a tradeoff of perturbing the metabolic pathway of hepatic glucose production and the ability to detect label incorporation necessary for in vivo flux analysis

through enrichment of the glucose molecule. We successfully negotiated this balance to observe a robust metabolic flux phenotype for hepatic glucose production from glycerol in the absence of hepatic insulin signaling.

To our best knowledge, we are the first group to report the role of gluconeogenesis, glycogenolysis and gluconeogenic substrate usage in the LIRKO mouse. Our analysis finds the LIRKO glucose flux phenotype consistent with fasting physiology in terms of the measured fractional gluconeogenesis values of 76% in the LIRKO cohort versus 72% in the control cohort (Figure 6.5). These results agree with the preserved rates of absolute gluconeogenesis glucose production and glycogenolysis glucose production in Figure 6.1. In light of the absence of insulin signaling in the LIRKO liver, the physiology observed is consistent with the action of glucagon and counterregulatory hormones in a fasting state. In order to observe upper gluconeogenesis flux redistribution in the LIRKO model, a significant stimulus would be necessary such as clamp-levels of hyperinsulinemia, somatostatin treatment or a refeeding paradigm. For instance, in the presence of refeeding conditions, previous researchers have observed selective substrate usage differences in the PPARα-knockout mouse increasing glycerol usage over lactate for hepatic gluconeogenesis [115]. Our method requires the addition of 30% additional glycerol to the existing circulating pool (Chapter 5), yet we observe no differences in the flux distributions due to glycerol presence indicating the robustness of the metabolic steady state achieved after ablation of the liver insulin receptor.

The similar glucose isotopomer distributions (Figure 6.4) and relative flux distributions for upper gluconeogenesis (Figure 6.5) from our in vivo flux analysis for LIRKO and IRlox contrast our expected notion of the LIRKO animal as a purely gluconeogenic phenotype. Genetic and protein screening of liver tissue in this transgenic model indicates increased presence of target gluconeogenic enzymes G6Pase and PEPCK that purport a gluconeogenic

phenotype, yet the mice display only slight hyperglycemia upon fasting compared to their normal littermates [14]. Our in vivo flux analysis partially explains the conserved metabolic phenotype by demonstrating a preserved flux distribution with respect to hepatic glucose production. These results indicate that, under our experimental conditions, there is no differential flux regulation in the observed upper gluconeogenic pathway to change hepatic glucose production. Two possible regulatory schemes would be consistent with a preserved flux distribution in the LIRKO model while accounting for decreased HGP: (1) decreased glucose-6-phosphatase demand on glucose production, or (2) decreased supply of gluconeogenic substrates from peripheral insulin-sensitive tissues such as muscle. The first scheme would predict high levels of late stage intermediates prior to the glucose-6-phosphatase reaction. This was not observed in the crossover plot in Figure 6.9 for LIRKO livers. The second scheme predicts low levels of gluconeogenic intermediates in the LIRKO liver. Our metabolite profiling results in Figure 6.8 suggest a possible widespread depletion of gluconeogenic intermediates, but we would need better compound detection to clearly assess such a pattern. In addition to improved metabolite detection, future studies on the second hypothesis could focus on the role of muscle proteolysis in providing different glucogenic amino acid substrates to the liver using stable isotopes.

The pyruvate tolerance test also addresses the role of gluconeogenesis substrate supply in causing the observed decreased HGP in LIRKO (Figure 6.6). Our data in the form of the pyruvate tolerance test support the concept that decreased substrate availability accounts for the observed differences in hepatic glucose output. Acute dosing of pyruvate uncovers the gluconeogenic phenotype of the LIRKO liver in a transient manner, only to revert to its basal state with a delay of 30-60 minutes with respect to the IRlox counterpart. The likely source for this increase in plasma glucose is excess gluconeogenic capacity associated with increased levels

of PEPCK and G6Pase gene expression. We posit that this increased capacity can coexist with a static flux distribution as the substrate bolus traverses the metabolic network without perturbing net fluxes for the gluconeogenic pathway over a span of hours. In other words, peripheral insulin resistance due to prolonged hyperinsulinemia cuts the supply of gluconeogenic precursors in these animals to in turn decrease hepatic glucose production concomitantly.

The studies presented here are entirely at metabolic and isotopic steady state to enable in vivo metabolic flux analysis (Chapter 2). To better characterize the short term regulation of hepatic glucose production in LIRKO, it would be interesting to extend the presented in vivo flux analysis tools for the analysis of a transient system such as the pyruvate tolerance test. Such an extension would require computational tools for reconstruction of kinetic models given the expected changes in metabolite concentrations and enrichment throughout the course of the experiment [87, 89, 103, 228]. The analysis of metabolic fluxes in the pyruvate tolerance test would be particularly revealing in distinguishing potential effects of glucose-6-phosphatase flux modulation in the face of decreased gluconeogenic substrate availability, and provide a bridge for analysis between the acute effects of HGP observed in the euglycemic-hyperinsulinemic clamp studies and the more chronic study presented here.

Previous studies documented decreased glycogen levels in LIRKO livers [14]. Despite expected low glycogen levels our 24 hour study revealed unchanged fluxes for hepatic glycogenolysis when compared to the IRlox distribution (Figure 6.5). This observation suggests a need to study glycogen synthesis and breakdown kinetics in LIRKO. Both studies investigated overnight fasted mice with presumably low levels of glycogen. The surgical stress associated with the ALZET pump implant may also stimulate glycogenolysis through the action of epinephrine on glycogen phosphorylase via a cAMP mediated mechanism [62]. A

possibility to account for the similarities in glycogenolysis flux with decreased glycogen depots include increased hepatic glucose cycling in LIRKO, which our in vivo flux analysis does not measure directly [137, 229-231]. The contribution of glycogen cycling to glucose production can account for up to 10-30% of hepatic glucose output during fasting [137, 232]. In our studies, the magnitude of the observed net differences in glycogenolysis (IRlox 9.3±3.9 mg/kg/min, LIRKO 6.4±2.2 mg/kg/min) suggests that glycogen cycling cannot account for the full normalization of the glycogenolysis flux distribution observed in LIRKO. Therefore, we propose that the LIRKO liver may have similar glycogen breakdown rates than its wild type mouse counterpart but a different basal amount of glycogen, and these processes would be regulated separately. Insulin acts through Akt to phosphorylate GSK3 and decrease its activity towards glycogen synthase, thereby increasing glycogen synthesis [54, 233]. Ablation of the insulin receptor can be expected to decrease glycogen synthesis through GSK3 activation. In this transgenic model, the resulting glycogen level and breakdown rates in LIRKO would be balanced by glucose effects to inhibit glycogen phosphorylase and glucagon action to activate glycogen phosphorylase, respectively [62]. The complexity of these interactions would benefit from more detailed flux measurements to elucidate the resulting metabolic effect of hormonal and signaling pathway crosstalk contributing to the resulting glycogen levels.

The enzymes that catalyze thermodynamically irreversible steps of gluconeogenesis have been an intense subject of study as potential targets to decrease hepatic glucose production in Type 2 Diabetes. Of these, molecular evidence links PEPCK expression to an insulin response-element [204, 234], motivating its reference as master regulator of gluconeogenic output and hepatic glucose output in the fasted state. However, recent *ex vivo* evidence through NMR analysis supports the notion that PEPCK, by virtue of its location within the metabolic network and flux control calculations, is not rate controlling with regards to

gluconeogenesis, but instead acts as a gate keeper of TCA cycle flux into gluconeogenesis [33]. We assessed possible single enzyme changes that account for decreased hepatic glucose production in LIRKO through crossover analysis in Figure 6.10 as performed previously [217]. Should G6Pase be limiting reaction for metabolic throughput of glucose production, we would expect accumulation of substrates prior to the limiting reaction with crossover into decreased levels of metabolite in subsequent reactions. The metabolite pattern in STZ-treated animals is suggestive of this relationship with significant accumulation of F6P in the STZ liver relative to its control counterpart (Figure 6.10). We cannot rule out effects at PEPCK as our directed metabolite profile did not assess levels of metabolites such as PEP, 2-phosphoglycerate and 3-phosphoglycerate, especially in the context of increased PEPCK transcription [14]. More accurate determination of these intermediary metabolites would help clarify potential regulation of glucose production by PEPCK in the LIRKO liver.

As a counterpoint to the glucose production metabolism in the LIRKO model, the analysis of hepatic cholesterol and fatty acid synthesis highlights the multiplicity of metabolic effects of insulin in the liver (Figure 6.11). Recent research understands this separation of effects through the separation of insulin receptor substrate protein isoforms. IRS-1 is thought to mediate the glucose metabolism effects of insulin, while IRS-2 mediates the lipid metabolism effects of the insulin signal [53]. LIRKO livers and hepatocytes are known to show decreased mRNA levels of cholesterol transcription regulator SREBP-1c, fatty acid synthase and stearyl-CoA desaturase-1 (S. Biddinger, submitted). In terms of flux regulation, these results present a different paradigm from that of hepatic glucose production, namely biosynthesis of cholesterol and lipids follows the traditional biological dogma whereupon changes in gene expression proportionally affects the reaction rates leading to substrate accumulation. A possible explanation for this effect could involve the topology of the metabolic network studied. On

the one hand hepatic glucose production has inputs from multiple pools converging at this pathway (e.g. glycerol, lactate, alanine) with various regulatory checkpoints (e.g. PEPCK, G6Pase) and metabolite-enzyme interactions. On the other hand, cholesterol and fatty acid synthesis presents a linear metabolic pathway such that the transmission of signal from gene expression through enzyme levels and metabolic fluxes is preserved without modulation from metabolite enzyme interactions [214]. Our in vitro studies also reflect homogeneous substrate concentrations, which are adequate for lipid biosynthesis estimation.

Detailed flux analysis of hepatic metabolism has the potential to become a tool of clinical import in the manner of gene, protein and metabolite measurements. Flux measurement is particularly relevant when examining metabolic diseases involving highly interconnected pathways, where enzyme-metabolite interactions complicate the expected genetic response to a metabolic disturbance [235]. Comprehensive in vivo flux profiling of hepatic glucose metabolism has the potential to improve existing clinical techniques for metabolic measurement such as the euglycemic-hyperinsulinemic clamp [197], by augmenting the amount of information about hepatic glucose and lipid metabolism obtained from a single experiment. Furthermore, we demonstrate the ability to measure fractional gluconeogenesis without elaborate chemical transformations required for more established methodologies [144]. Our analysis for fractional gluconeogenesis requires derivatizations on the glucose molecule that are easily accessible to laboratory researchers, as well as simple analysis for enrichment through GC-MS. One important contribution of this work is to confirm basal values for hepatic glucose production, fractional gluconeogenesis and gluconeogenic substrate contribution without the use of catheterized animals or acute infusion, thereby facilitating comprehensive metabolic evaluation of transgenic phenotypes. The ability to estimate statistical certainty around fluxes in vivo further strengthens our confidence regarding the relevance of flux

observation in humans, where experiments are limited by subject availability and tracer cost [151]. Clinical measurement of metabolic fluxes would cast light on the most immediate metabolic phenotype integrating signals at the genetic, protein and metabolite level when changes in the preceding levels may not be observable [133]. We hope this work illustrates the significance of comprehensive flux measurement in the toolkit of researchers interested in disorders of metabolism.

In conclusion, our data support the finding that under our experimental conditions, the functional metabolic phenotype of the LIRKO mouse with respect to glucose metabolism is one of a fasting physiology. In addition, the relative flux distribution for LIRKO glucose production is surprisingly similar to that of wild-type mice despite differences in net hepatic glucose production in the basal state. The presented in vivo flux analysis through a combined, multi-tracer infusion strategy demonstrates that the functional usage patterns for gluconeogenic substrates between LIRKO mice and their wild-type counterparts are essentially unchanged for upper gluconeogenesis, despite significant genetic differences propitiating a gluconeogenic metabolic program in the LIRKO liver. This pattern is of particular interest for the usage of glycerol as a lipolytic gluconeogenic substrate, which our methodology provides as a gluconeogenic substrate without observing significant changes in the upper gluconeogenesis flux distribution. Through manipulation of glucose production in a pyruvate tolerance test, we find evidence for regulation of glucose production by pyruvate availability suggesting indirect effects of insulin on gluconeogenic substrate availability. In addition, directed metabolite profiling of glucose production in LIRKO is consistent with modulation of glucose production through decreased levels of gluconeogenic precursors, reflecting indirect effects of insulin ablation on substrate availability. This is in contrast to the STZ liver, where metabolite crossover patterns suggest accumulation of metabolites prior to the G6Pase reaction. Thus

our analysis suggests a role for indirect effects of insulin on HGP through decreased gluconeogenic substrate availability in the absence of flux modulation of upper gluconeogenesis. Extension of the results obtained here to human insulin resistance must be laced with caution as this transgenic model develops adaptive changes to cope with the excess hepatic glucose production. Lastly, the combined, multi-labeled tracer method proposed has the potential to become a clinical tool to measure hepatic glucose production in a single GC-MS study.

CHAPTER 7: Conclusions and Recommendations

7.1 Conclusions

Flux deregulation is unique and fundamental to the development of metabolic diseases, where flux is the currency by which genetic, proteomic and metabolomic phenotypes converge to manifest pathologic changes. Through the work on this thesis, we have implemented in vitro and in vivo tools to fulfill the promise of comprehensive, simultaneous in vivo flux analysis as physiological measurements to complete the characterization of insulin resistance development in Type 2 Diabetes. We hope that the tools developed facilitate the incorporation of sophisticated data-driven analysis to reconstruct metabolic fluxes in mammalian metabolism, and allow comprehensive flux elucidation become part of the pathophysiology of metabolic disease.

In Chapter 4, we put forth the hypothesis that glucose-6-phosphatase is a key modulator of cellular glucose production in the presence of glycerol. The application of comprehensive flux elucidation from glucose mass isotopomers allowed us to document the effects of three perturbations to gluconeogenic metabolism: cellular system studied, glycerol substrate availability and hormonal cues such as insulin and glucagon in the upper gluconeogenic flux distribution of cellular systems capable of de novo glucose production. We found that the presence of glycerol as a substrate has important effects in redistributing the demand of glucose around the glucose-6-phosphatase node, even in the presence of hormonal cues such insulin and glucagon. In addition, we found that with regard to flux modulation of glucose production, each in vitro model studied showcases important aspects of hepatic glucose production in vivo. Hepatoma cells respond

to hormonal queues with physiological amounts of insulin by modulating usage of glycerol for glucose production, but these cells lack the glucagon receptor and consequently the ability to upregulate glucose production from a basal state. In addition, the absolute production of glucose in this model is modest at best, and the gluconeogenic phenotype is transient. Primary rat hepatocytes behave physiologically, and as such are a prime candidate to reproduce cellular physiology of hepatic glucose production in vitro. Modulation of glucose production in these cells is mediated by the contribution of gluconeogenesis in the presence of hormones. In the presence of glycerol, the effect on gluconeogenesis is overwhelmed by the preference of glycerol as a substrate, but we still observe modulation of gluconeogenic flux by insulin and glucagon action.

Perhaps most interestingly, upper gluconeogenesis metabolism in vitro redistributes fluxes around the glucose-6-phosphatase junction in order to accommodate changes in glucose production, suggesting for an important role of glucose-6-phosphatase in regulating the hepatic glucose production in vitro at the flux level. Further studies could involve specific tracer in the form of deuterated glucose to probe glucose-6-phosphatase action and the role of glucose cycling in modulating hepatic metabolism in the absence of insulin receptor. Alternatively, studying the insulin response in cellular models of glucose production can help elucidate the functional form of glucose production regulation in the presence of insulin, revealing whether this control is exerted in a linear fashion proportional to the concentration of insulin present or if cooperativity effects reveal added regulation.

In Chapter 5, we show that a combined, multi-labeled tracer strategy using [U-^{13}C, D$_5$]-glycerol can provide accurate flux reconstructions of upper gluconeogenesis metabolic fluxes in vitro and in vivo. The transition from in vitro detailed flux analysis to in vivo flux analysis of hepatic glucose production required adapting the use of a unique glycerol tracer in order to capture increased signal given limited accessibility of metabolic intermediates. We expanded our in

vitro work to include multiple ^{13}C and ^{2}H tracers in a combined, multi-labeled tracer strategy to augment the isotopic enrichment of glucose. Through the use of a computational reconstruction of upper gluconeogenesis, we establish three parameters of importance to the hepatic glucose production phenotype: hepatic glucose output, fractional (and absolute) gluconeogenesis, and glycerol contribution to hepatic glucose production as opposed to oxaloacetate contribution. Consequently, we observe the physiological transition from fasting to feeding by changes in fractional gluconeogenesis and differential substrate uptake. Through the use of a miniosmotic pump, we were able to dose glycerol over a period of 24 hours and establish enrichment in plasma glucose at appreciable levels for mass spectrometry detection. We characterized and optimized concentrations, length of infusion and enrichment of both glycerol and glucose in vivo in order to confirm assumptions of isotopic steady state necessary for flux calculations. Ultimately, we are able to reconstruct hepatic glucose production metabolic fluxes to a degree heretofore unavailable in literature, along with confidence intervals to distinguish flux variation among substrate usage and reversibilities. This methodology has the potential to augment the information on metabolic fluxes obtained from a single experiment, improve the flux distributions obtained from euglycemic-hyperinsulinemic clamp experiments as well as lay the foundation for clinical fluxomics in the near future.

In Chapter 6, we show through in vivo flux analysis that liver insulin resistance can manifest a preserved glucose production metabolic flux phenotype. We further hypothesize that observed decreases in hepatic glucose production stem from decreased gluconeogenic substrate availability in the LIRKO mouse. As a pathophysiologic application of the developed in vivo flux analysis methodology, we chose to study hepatic insulin resistance in the liver insulin receptor knockout (LIRKO) mouse through the use of Cre-LoxP technology targeting the insulin receptor by Cre recombinase expression under control of the albumin promoter. The mild

hyperglycemia observed in these animals had been attributed to a combination of increased counterregulatory hormone action in the absence of insulin signaling, coupled with marked peripheral insulin resistance leading to decreased levels of gluconeogenic substrate availability. Through the use of in vivo flux analysis, we detail how metabolic fluxes in this animal remain fixed with respect to the normal phenotype in a poignant confirmation of the mild hyperglycemia observed in this tissue specific model of Type 2 Diabetes. This flux distribution is accompanied by global decreases in amounts of metabolites present in the LIRKO liver, relative to the wild-type counterpart and to streptozotocin treated animals. Acute availability of substrates unmasks the gluconeogenic phenotype of the LIRKO animal to indicate metabolic capacity of the gluconeogenic pathway in the presence of pyruvate. These results suggest a role for decreased availability of substrate as a regulatory mechanism modulating the decreased hepatic glucose production by the LIRKO animal.

7.2 Recommendations

The recommendations from this work fall in three broad categories, those with primary methodological impetus and those with basic biological impetus. Within the biological recommendations proposed, we distinguish those with basic and clinical research implications that could be applied in humans. Subsequent to the development of new methodologies for detailed flux calculation in vivo, we can envision the new tools raising questions regarding the biology of the metabolic systems studied to be examined in greater detail. The following section details several alternatives with clear impact stemming from the development and application of the aforementioned techniques.

7.2.1 Methodological Recommendations

We describe the methodological recommendations as outlined below for further development of in vivo flux analysis strategies with immediate impact.

Development of in vivo flux analysis in the context the euglycemic-hyperinsulinemic clamp Previous studies have shown how incorporation of [U-^{13}C]-glycerol in the regime for euglycemic-hyperinsulinemic clamp studies can maximize the information obtained regarding hepatic glucose biosynthesis [14, 236]. This analysis depends on the ability of researchers to clearly interpret the results of incorporation from glycerol into the carbon skeleton of the glucose molecule as detailed in Chapter 3. Through the use of comprehensive models that capture atom transitions for both ^{13}C and ^{2}H labeling, our methodology allows reconstruction of metabolic fluxes from enrichment patterns that would not be observable directly within limits of statistical certainty. This information would be particularly important in transitioning to clinical protocols in humans, where investigators are limited in the amount of observations possible for a given subject.

Application of multi-labeled tracers for the analysis of metabolic pathways other than glucose production Our application of [U-^{13}C,D$_5$]-glycerol in vitro and in vivo paves the way for continued analysis of metabolic fluxes in vivo using deuterated tracers in addition to the existing methodologies for ^{13}C flux measurement [133, 155]. In particular the use of deuterium tracers would open possibilities for metabolic analysis of metabolic pathways such as glycogen synthesis, lipid synthesis and protein synthesis, all of which incorporate hydrogen from the aqueous environment in addition to their constitutive monomers [133].

Flux analysis of bolus tracer dosing in the context of the pyruvate tolerance test. As shown in Chapter 6, the pyruvate tolerance test can uncover differences in gluconeogenic substrate usage the would elude observation by in vivo flux analysis The intrinsic difficulty in reconstructing metabolism in these circumstances stems from the rapidly changing metabolic conditions caused by the dosage of tracer, thereby invalidating the assumption of metabolic steady state. At the same time, the enrichment from tracer in these conditions operates in a timescale similar to that of the metabolic changes, necessitating an understanding of the kinetic parameters operating in the system at hand. Researchers have advanced the uncovering of these parameters for glucose metabolism through the use of the minimal model [91, 237]. Cybernetic models could be used to estimate kinetic parameters globally given a complete set of transient data [238].

Relaxation of metabolic and isotopic steady state assumptions for in vivo flux analysis As described in Chapter 2, the limitations of our modeling approach require the use of metabolic and isotopic steady state in order to reconstruct metabolic fluxes for upper gluconeogenesis. Relaxing the isotopic steady state assumption, we could look to use instationary analysis of metabolic flux allows the resolution of metabolic fluxes, pool sizes and their respective confidence intervals by following the transient process of isotopic tracer enrichment in metabolic systems. Relaxing the metabolic steady state assumption would allow to look at active regulatory systems such as Transient analysis will be increasingly important in translating the developed methodology to the clinical context, where fulfilling isotopic steady assumptions may be difficult, expensive or toxic given the pool size of a particular metabolite in the whole body. Incorporation of this analytical framework into the experimental guidelines presented in Chapter 2 will substantiate a comprehensive analysis of metabolism in vivo for mammalian systems.

<u>Assessment of glucose enrichment from glucuronate-conjugates</u> The glucuronate probe has been applied for the estimation of glucose metabolic fluxes by dosing acetaminophen in patients and observing enrichment in the resulting uridine diphosphate (UDP)-glucuronate metabolites [232, 239]. One particular advantage of this technique involves the collection of the conjugated glucose molecule in urine as a byproduct of acetaminophen metabolism, in contrast to the serum analysis of our presented methodology in Chapters 5 and 6. When acetaminophen is administered in conjunction with labeled $[1\text{-}^2H_1]$-galactose by infusion, researchers can measure the rate of appearance of UDP-glucose in serum through non-invasive incorporation of label into urinary acetaminophen. Addition of UDP-glucose enrichment values to our computational framework enables the reconstruction of the contribution of fractional gluconeogenesis to the UDP-glucose and UDP glucuronate pool in liver, an important substrate for conjugation of nonpolar drugs for excretion from the body [62, 232]. The reconstruction of hepatic glucose production and toxin metabolism pathways in vivo would be the relevant paradigm to study in clinical contexts such as in patients undergoing extensive pharmacotherapy for treatment of metabolic syndrome, or alternatively in HIV patients with upregulation of UDP-glucuronyltransferase levels secondary to AZT treatment, and the resulting increased drug clearance and resistance [62].

7.2.2 Biological Recommendations

The biological implications of the tracer work presented in this thesis closely follow the development of metabolic disease through flux measurement. Within the field of Type 2 Diabetes, insulin resistance is the hallmark feature of disease. Diabetes researchers have a detailed understanding of the molecular mechanisms that surround the onset of insulin resistance, but the detailed metabolic phenotype of this condition in the liver now beginning to be elucidated.

In vivo metabolic flux analysis of insulin-treated LIRKO animals The study conducted in Chapter 6 details the effects of complete hepatic insulin resistance in the basal metabolic flux distribution of upper gluconeogenesis. Fisher et al found marked differences in these animals in the context of the euglycemic-hyperinsulinemic clamp, the gold standard to evaluate insulin resistance in the context of high insulin concentrations [15]. We attempted a pilot experiment using extended release insulin pellet treatment in IRlox animals undergoing our combined, multi-tracer labeling strategy and confirmed elevated insulin levels beyond those of LIRKO animals. Analysis of these samples for glucose enrichment will yield further answers regarding the ability of the developed methodology to capture physiologic changes due to hormone presence in vivo.

Glucose cycling effects in hepatic insulin resistance An interesting metabolic effect associated with Type 2 Diabetes metabolism is glucose cycling [230, 231, 240-242]. This refers to the process whereby plasma glucose is incorporated into the liver through the action of glucokinase, only to be released immediately thereafter by action of enzyme glucose-6-phosphatase. Several studies have linked glucose cycling to the process of insulin release in the beta cell, leading to speculation regarding possible physiological roles in other tissues [240, 241]. In particular, Hellerstein and colleagues utilized a triple tracer approach in humans to assess the hepatic glucose production fluxes, glycogen cycling from UDP-glucose to plasma glucose, as well as glucose-6-phosphate/plasma glucose cycling as described previously [232]. The researchers found evidence glucose-6-phosphatase/glucose cycling activity of 0.44 mg/kg/min after an 11h fast. They also found non-zero glycogen input into plasma glucose in fasting humans, suggestive of UDP-glycogen/glucose cycling activity during fasting of 0.27 mg/kg/min, and evidence of cycling between glycogen/UDP-glycogen of 0.64 mg/kg/min. These values represent fractions of total

hepatic glucose output of approximately 2.2 mg/kg/min measured through tracer dilution. Furthermore, these cycles decreased significantly from 11 hours fasting to 60 hours fasting indicating the role of glycogen availability in increasing the activity of these cycles. Studying glucose cycling with our experimental framework requires careful forward experiment simulations to design the best tracer possible to calculate this flux, as well as optimization of the in vivo flux methodology to probe to metabolic intermediate that yield information regarding this pathway.

Gluconeogenic enzyme regulation of metabolic flux Recent work highlights the hypothesis that PEPCK does not regulate gluconeogenic flux in transgenic perfused livers with PEPCK ablation as measured by flux control coefficient [33]. This work points to PEPCK as a regulator of carbon flux from the TCA cycle into gluconeogenesis by correlation analysis, thereby highlighting the importance of other gluconeogenic enzymes in modulating hepatic glucose production. These results are consistent with our observed flux results, and would correspond to increased correlation of glucose-6-phosphatase and fructose-1,6-bisphosphatase activity with hepatic glucose production. Work with glucose-6-phosphatase inhibitors leads to increased accumulation of glucose in the form of liver glycogen. On the other hand, animal studies and early clinical trials of fructose-1,6-bisphosphatase inhibitors show clear effects regarding plasma glucose lowering, but no long-term benefit to patients have been established [181, 243]

Flux physiology of non-alcoholic fatty liver disease (NAFLD) In vivo flux analysis would contribute significantly to the understanding of the mechanisms whereby essential amino acid supplementation protects mice against the development of non-alcoholic fatty liver disease (NAFLD) and non-alcoholic steatohepatitis (NASH). In collaboration with Ajinomoto Inc, we have explored the effects of significant essential amino acid supplementation in a mouse model of NAFLD induced through 8

weeks of standard high-fat diet. Given the size of the cholesterol and fatty acid phenotypes studied, we adapted our in vivo protocol to use only deuterated water as tracer over the last 7 days of treatment. Diet-induced phenotypes can be obscured by stress conditions such as surgical pump implantation, and there is a significant body of literature analyzing lipid flux deregulation in animals using deuterated water in vivo. Using this enrichment, information, we can simultaneously trace metabolic pathways critical to the development of insulin resistance such as hepatic glucose production, fatty acid synthesis and triglyceride synthesis. The comprehensive evaluation of metabolic fluxes in vivo will establish the relevance of flux deregulation in the pathophysiology of this disease.

Integrated flux analysis of hepatic glucose production, lipid synthesis and atherogenesis Another interesting extension of the work presented regards the effects of hepatic insulin resistance in the phenotype of lipid metabolism and atherogenesis. In particular, current work looks to understand the effects of atherogenic, cholesterol rich diets in the LIRKO mouse model, with striking results that suggest a strong link between total hepatic insulin resistance and the cardiovascular effects of Type 2 Diabetes (S. Biddinger, submitted). Flux analysis of cholesterol and fatty acid metabolism would have integral roles in assessing the overall metabolic phenotype of the diseased hepatocyte. Our ISA calculations showing decreased cholesterol and fatty acid synthesis in LIRKO hepatocytes in Chapter 5 would be augmented by detailed flux analysis of intermediated leading to the synthesis of fatty acids, in particular central carbon metabolism intermediaries such as citrate, alpha-ketoglutarate, fumarate, lactate and pyruvate. In turn, this information would allow detailed reconstruction of metabolic fluxes linking glucose metabolism and lipid metabolism, two axes thought to be differentially regulated by insulin through branching of pathways between IRS-1 for glucose metabolism and IRS-2 for lipogenic metabolism under the control of SREBP-1c [53]. The

manifestation of differential metabolic regulation through these metabolic axes would be a potential therapeutic target for palliating the cardiovascular consequences of Type 2 Diabetes.

7.2.3 Translational Recommendations

In the translational research context, our developed in vivo flux analysis methodologies make use of detailed isotopomer data unlike commonly accepted tracer dilution methods described in Chapter 3. This data is complementary in the context of metabolic diseases, as it monitors the usage of metabolites independent of the amounts of concentrations present in the sampled pool such as blood or urine. Here, we present several areas in which the use of comprehensive flux estimation through isotopomer data incorporation could have significant impact in the clinical translational research arena.

<u>Clinical management of hepatic insulin resistance</u> The analysis of hepatic metabolic fluxes, in particular those relevant to glucose production, can serve as a clinical indication for the initiation of treatment with hepatic insulin sensitizers such as metformin. Current treatment standards recommend the initiation of metformin monotherapy along with lifestyle interventions for patients with insulin resistance or Type 2 Diabetes who have poorly controlled fasting glucose [244]. Should Hemoglobin A1C levels fail to maintain below 7%, the clinical scenario calls for the addition of a second oral hypoglycemic. Our in vivo flux analysis strategy would delineate the extent of hepatic insulin resistance in patients currently treated with metformin. Therefore, this test would help clinicians assess whether higher dosage of metformin or concurrent treatment with a thiazolidenedione, targeting hepatic and muscle insulin resistance, would be the preferred

therapeutic strategy over addition of sulfonylurea therapy, targeting increased pancreatic insulin secretion as described in Chapter 2.

Progression of insulin sensitivity following bariatric surgery Similarly to the above described recommendation, the progression of hepatic insulin resistance would be of particular interest in patients following bariatric surgery for weight loss. Diabetic patients who undergo bariatric surgery for weight loss experience rapid improvements in their glycemic management due to reduced glycemic load as a consequence of decreased caloric intake, as well as rapid weight loss causing improved insulin sensitivity. In addition, case reports describe anatomic changes following Roux-en-Y gastric bypass surgery that cause beta cell hyperfunction and hypoglycemic event in addition to marked improvements of plasma glucose levels [245]. Bariatric surgery patients are treated with metformin as an adjunct to improve insulin resistance, as this agent is not associated with the blood glucose fluctuations of sulfonylureas or thiazolidenediones. As with the clinical management of insulin resistance, the developed in vivo flux analysis strategies could contribute to the management of this special patient population in deciding whether hepatic insulin resistance is an adequate target for treatment with metformin, evaluation of new pharmacotherapeutic agents that improve hepatic insulin resistance or even discontinuation of metformin therapy upon weight normalization.

Clinical metabolomics/fluxomics Recent efforts in NMR and LC-MS technologies aim to comprehensively measure the full complement of metabolites in human plasma at very accurate levels for the diagnosis and progression of disease [21, 246, 247]. These efforts have focused on cardiovascular diseases due to the acuity of the changes observed as well as the role of cellular necrosis and rupture in releasing TCA cycle metabolites normally not found in plasma during acute myocardial injury. On the other hand, the changes expected to occur in the development of insulin

resistance and Type 2 diabetes would be more subtle, and require either longitudinal comparison of cohorts with insulin resistance versus overt Type 2 Diabetes or alternatively analysis under stress conditions such as the euglycemic-hyperinsulinemic clamp. Once a detection platform has been established for amounts of plasma metabolites of interest, enrichment through stable isotope tracer dosing should follow immediately for detection and calculation of fluxes from isotopomer data with the presented computational and experimental framework in Chapters 5 and 6. Careful consideration must be exerted when evaluating plasma metabolome profiles in a clinical trial setting, to avoid use of peaks representing drug biomarkers as part of the recognition algorithm [98].

References

1. Stephanopoulos, G. and J. Kelleher, *Biochemistry. How to make a superior cell.* Science, 2001. **292**(5524): p. 2024-5.
2. Stephanopoulos, G., *Metabolic Engineering.* 1998, San Diego, California, USA: Academic Press.
3. Wolfe, R.R., J.R. Allsop, and J.F. Burke, *Glucose metabolism in man: responses to intravenous glucose infusion.* Metabolism, 1979. **28**(3): p. 210-20.
4. Krebs, H.A., E. Salvin, and W.A. Johnson, *The formation of citric and alpha-ketoglutaric acids in the mammalian body.* Biochem J, 1938. **32**(1): p. 113-7.
5. Hems, R., M. Stubbs, and H.A. Krebs, *Restricted permeability of rat liver for glutamate and succinate.* Biochem J, 1968. **107**(6): p. 807-815.
6. Veech, R.L., et al., *Disequilibrium in the triose phosphate isomerase system in rat liver.* Biochem J, 1969. **115**(4): p. 837-42.
7. Heinrich, R. and T.A. Rapoport, *Linear theory of enzymatic chains; its application for the analysis of the crossover theorem and of the glycolysis of human erythrocytes.* Acta Biol Med Ger, 1973. **31**(4): p. 479-94.
8. Kacser, H. and J.A. Burns, *The control of flux.* Symp Soc Exp Biol, 1973. **27**: p. 65-104.
9. Heinrich, R. and T.A. Rapoport, *A linear steady-state treatment of enzymatic chains. General properties, control and effector strength.* Eur J Biochem, 1974. **42**(1): p. 89-95.
10. Heinrich, R. and T.A. Rapoport, *A linear steady-state treatment of enzymatic chains. Critique of the crossover theorem and a general procedure to identify interaction sites with an effector.* Eur J Biochem, 1974. **42**(1): p. 97-105.
11. Bailey, J.E., *Mathematical modeling and analysis in biochemical engineering: past accomplishments and future opportunities.* Biotechnol Prog, 1998. **14**(1): p. 8-20.
12. Alper, H., K. Miyaoku, and G. Stephanopoulos, *Construction of lycopene-overproducing E. coli strains by combining systematic and combinatorial gene knockout targets.* Nat Biotechnol, 2005. **23**(5): p. 612-6.
13. Antoniewicz, M., *Comprehensive Analysis of Metabolic Pathways through the Combined Use of Stable Isotope Tracers*, in *Chemical Engineering.* 2006, Massachusetts Institute of Technology: Cambridge, MA, USA.
14. Michael, M.D., et al., *Loss of insulin signaling in hepatocytes leads to severe insulin resistance and progressive hepatic dysfunction.* Mol Cell, 2000. **6**(1): p. 87-97.
15. Fisher, S.J. and C.R. Kahn, *Insulin signaling is required for insulin's direct and indirect action on hepatic glucose production.* J Clin Invest, 2003. **111**(4): p. 463-8.
16. Stedman, T.L., *Stedman's medical dictionary.* 28th ed. 2006, Philadelphia: Lippincott Williams & Wilkins. 1 v. (various pagings).
17. Jackson, D.A., R.H. Symons, and P. Berg, *Biochemical method for inserting new genetic information into DNA of Simian Virus 40: circular SV40 DNA molecules containing lambda phage genes and the galactose operon of Escherichia coli.* Proc Natl Acad Sci U S A, 1972. **69**(10): p. 2904-9.
18. Bergman, R.N., *Pathogenesis and prediction of diabetes mellitus: lessons from integrative physiology.* Mt Sinai J Med, 2002. **69**(5): p. 280-90.

19.   Twigger, S.N., et al., *Integrative genomics: in silico coupling of rat physiology and complex traits with mouse and human data.* Genome Res, 2004. **14**(4): p. 651-60.

20.   Mootha, V.K., et al., *Integrated analysis of protein composition, tissue diversity, and gene regulation in mouse mitochondria.* Cell, 2003. **115**(5): p. 629-40.

21.   Brindle, J.T., et al., *Rapid and noninvasive diagnosis of the presence and severity of coronary heart disease using 1H-NMR-based metabonomics.* Nat Med, 2002. **8**(12): p. 1439-44.

22.   Ginsburg, G.S., M.P. Donahue, and L.K. Newby, *Prospects for personalized cardiovascular medicine: the impact of genomics.* J Am Coll Cardiol, 2005. **46**(9): p. 1615-27.

23.   Pocai, A., et al., *A brain-liver circuit regulates glucose homeostasis.* Cell Metab, 2005. **1**(1): p. 53-61.

24.   Pocai, A., et al., *Hypothalamic K(ATP) channels control hepatic glucose production.* Nature, 2005. **434**(7036): p. 1026-31.

25.   Obici, S. and L. Rossetti, *Minireview: nutrient sensing and the regulation of insulin action and energy balance.* Endocrinology, 2003. **144**(12): p. 5172-8.

26.   Massillon, D., et al., *Carbon flux via the pentose phosphate pathway regulates the hepatic expression of the glucose-6-phosphatase and phosphoenolpyruvate carboxykinase genes in conscious rats.* J Biol Chem, 1998. **273**(1): p. 228-34.

27.   Barzilai, N. and L. Rossetti, *Role of glucokinase and glucose-6-phosphatase in the acute and chronic regulation of hepatic glucose fluxes by insulin.* J Biol Chem, 1993. **268**(33): p. 25019-25.

28.   Barnett, A.H., et al., *Diabetes in identical twins. A study of 200 pairs.* Diabetologia, 1981. **20**(2): p. 87-93.

29.   Mootha, V.K., et al., *PGC-1alpha-responsive genes involved in oxidative phosphorylation are coordinately downregulated in human diabetes.* Nat Genet, 2003. **34**(3): p. 267-73.

30.   Patti, M.E., et al., *Coordinated reduction of genes of oxidative metabolism in humans with insulin resistance and diabetes: Potential role of PGC1 and NRF1.* Proc Natl Acad Sci U S A, 2003. **100**(14): p. 8466-71.

31.   Petersen, K.F., et al., *Impaired mitochondrial activity in the insulin-resistant offspring of patients with type 2 diabetes.* N Engl J Med, 2004. **350**(7): p. 664-71.

32.   Petersen, K.F., S. Dufour, and G.I. Shulman, *Decreased insulin-stimulated ATP synthesis and phosphate transport in muscle of insulin-resistant offspring of type 2 diabetic parents.* PLoS Med, 2005. **2**(9): p. e233.

33.   Burgess, S.C., et al., *Cytosolic phosphoenolpyruvate carboxykinase does not solely control the rate of hepatic gluconeogenesis in the intact mouse liver.* Cell Metab, 2007. **5**(4): p. 313-20.

34.   Vastrik, I., et al., *Reactome: a knowledge base of biologic pathways and processes.* Genome Biol, 2007. **8**(3): p. R39.

35.   (CDC), C.f.D.C.a.P., *Behavioral Risk Factor Surveillance System Survey Data.* 2007, U.S. Department of Health and Human Services, Centers for Disease Control and Prevention.

36.   Eckel, R.H., S.M. Grundy, and P.Z. Zimmet, *The metabolic syndrome.* Lancet, 2005. **365**(9468): p. 1415-28.

37.   *Effect of intensive blood-glucose control with metformin on complications in overweight patients with type 2 diabetes (UKPDS 34). UK Prospective Diabetes Study (UKPDS) Group.* Lancet, 1998. **352**(9131): p. 854-65.

38.   *Intensive blood-glucose control with sulphonylureas or insulin compared with conventional treatment and risk of complications in patients with type 2 diabetes (UKPDS 33). UK Prospective Diabetes Study (UKPDS) Group.* Lancet, 1998. **352**(9131): p. 837-53.

39.   Greenspan, F.S. and D.G. Gardner, *Basic & clinical endocrinology.* 7th ed. 2004, New York: Lange Medical Books/McGraw-Hill. xvi, 976.

40.   *Classification and diagnosis of diabetes mellitus and other categories of glucose intolerance. National Diabetes Data Group.* Diabetes, 1979. **28**(12): p. 1039-57.

41.   Ito, C., K. Mito, and H. Hara, *Review of criteria for diagnosis of diabetes mellitus based on results of follow-up study.* Diabetes, 1983. **32**(4): p. 343-51.

42.   Berne, R.M. and M.N. Levy, *Physiology.* 3rd ed. 1993, St. Louis: Mosby Year Book. xiv, 1071.

43.   Nissen, S.E. and K. Wolski, *Effect of rosiglitazone on the risk of myocardial infarction and death from cardiovascular causes.* N Engl J Med, 2007. **356**(24): p. 2457-71.

44.   Gagnon, J., et al., *The Trp64Arg mutation of the beta3 adrenergic receptor gene has no effect on obesity phenotypes in the Quebec Family Study and Swedish Obese Subjects cohorts.* J Clin Invest, 1996. **98**(9): p. 2086-93.

45.   Walston, J., et al., *Time of onset of non-insulin-dependent diabetes mellitus and genetic variation in the beta 3-adrenergic-receptor gene.* N Engl J Med, 1995. **333**(6): p. 343-7.

46.   Widen, E., et al., *Association of a polymorphism in the beta 3-adrenergic-receptor gene with features of the insulin resistance syndrome in Finns.* N Engl J Med, 1995. **333**(6): p. 348-51.

47.   Petersen, K.F., et al., *The role of skeletal muscle insulin resistance in the pathogenesis of the metabolic syndrome.* Proc Natl Acad Sci U S A, 2007. **104**(31): p. 12587-94.

48.   Hadigan, C., et al., *Depot-specific regulation of glucose uptake and insulin sensitivity in HIV-lipodystrophy.* Am J Physiol Endocrinol Metab, 2006. **290**(2): p. E289-98.

49.   Reaven, G.M., *Banting lecture 1988. Role of insulin resistance in human disease.* Diabetes, 1988. **37**(12): p. 1595-607.

50.   Cai, D., et al., *Local and systemic insulin resistance resulting from hepatic activation of IKK-beta and NF-kappaB.* Nat Med, 2005. **11**(2): p. 183-90.

51.   Shoelson, S.E., J. Lee, and A.B. Goldfine, *Inflammation and insulin resistance.* J Clin Invest, 2006. **116**(7): p. 1793-801.

52.   Kahn, C.R., et al., *Direct demonstration that receptor crosslinking or aggregation is important in insulin action.* Proc Natl Acad Sci U S A, 1978. **75**(9): p. 4209-13.

53.   Taniguchi, C.M., K. Ueki, and R. Kahn, *Complementary roles of IRS-1 and IRS-2 in the hepatic regulation of metabolism.* J Clin Invest, 2005. **115**(3): p. 718-27.

54.   Taniguchi, C.M., B. Emanuelli, and C.R. Kahn, *Critical nodes in signalling pathways: insights into insulin action.* Nat Rev Mol Cell Biol, 2006. **7**(2): p. 85-96.

55.   Altomonte, J., et al., *Inhibition of Foxo1 function is associated with improved fasting glycemia in diabetic mice.* Am J Physiol Endocrinol Metab, 2003. **285**(4): p. E718-28.

56.   Puigserver, P., et al., *Insulin-regulated hepatic gluconeogenesis through FOXO1-PGC-1alpha interaction.* Nature, 2003. **423**(6939): p. 550-5.

57.   Ishibashi, K., T. Fujioka, and M. Ui, *Insulin increased cAMP phosphodiesterase activity antagonizing metabolic actions of glucagon in rat hepatocytes cultured with herbimycin A.* Eur J Pharmacol, 2000. **409**(2): p. 109-21.

58.   Exton, J.H., et al., *Mechanisms of hormonal regulation of liver metabolism.* Adv Cyclic Nucleotide Res, 1981. **14**: p. 491-505.

59.   Trinh, K.Y., et al., *Perturbation of fuel homeostasis caused by overexpression of the glucose-6-phosphatase catalytic subunit in liver of normal rats.* J Biol Chem, 1998. **273**(47): p. 31615-20.

60.   Barthel, A. and D. Schmoll, *Novel concepts in insulin regulation of hepatic gluconeogenesis.* Am J Physiol Endocrinol Metab, 2003. **285**(4): p. E685-92.

61.   Wolfe, R.R., D.L. Chinkes, and R.R. Wolfe, *Isotope tracers in metabolic research : principles and practice of kinetic analysis.* 2nd ed. 2005, Hoboken, N.J.: Wiley-Liss. vii, 474.

62.   Berg, J.M., et al., *Biochemistry.* 5th ed. 2002, New York: W.H. Freeman. 1 v. (various pagings).

63.   Felipe, A., X. Remesar, and M. Pastor-Anglada, *L-lactate uptake by rat liver. Effect of food deprivation and substrate availability.* Biochem J, 1991. **273(Pt 1)**: p. 195-8.

64.   Halestrap, A.P. and D. Meredith, *The SLC16 gene family-from monocarboxylate transporters (MCTs) to aromatic amino acid transporters and beyond.* Pflugers Arch, 2004. **447**(5): p. 619-28.

65.   Wolfe, R.R., et al., *Isotopic determination of amino acid-urea interactions in exercise in humans.* J Appl Physiol, 1984. **56**(1): p. 221-9.

66.   Christensen, H.N., *Role of amino acid transport and countertransport in nutrition and metabolism.* Physiol Rev, 1990. **70**(1): p. 43-77.

67.   Ruiz, B., et al., *Amino acid uptake by liver of genetically obese Zucker rats.* Biochem J, 1991. **280 (Pt 2)**: p. 367-72.

68.   Bortz, W.M., et al., *Glycerol turnover and oxidation in man.* J Clin Invest, 1972. **51**(6): p. 1537-46.

69.   Wolfe, R.R., et al., *Effect of short-term fasting on lipolytic responsiveness in normal and obese human subjects.* Am J Physiol, 1987. **252**(2 Pt 1): p. E189-96.

70.   Ross, B.D., R. Hems, and H.A. Krebs, *The rate of gluconeogenesis from various precursors in the perfused rat liver.* Biochem J, 1967. **102**(3): p. 942-951.

71.   Joost, H.G. and B. Thorens, *The extended GLUT-family of sugar/polyol transport facilitators: nomenclature, sequence characteristics, and potential function of its novel members (review).* Mol Membr Biol, 2001. **18**(4): p. 247-56.

72.   De Bari, L., et al., *Partial reconstruction of in vitro gluconeogenesis arising from mitochondrial l-lactate uptake/metabolism and oxaloacetate export via novel L-lactate translocators.* Biochem J, 2004. **380**(Pt 1): p. 231-42.

73.   Cohen, S.M., S. Ogawa, and R.G. Shulman, *13C NMR studies of gluconeogenesis in rat liver cells: utilization of labeled glycerol by cells from euthyroid and hyperthyroid rats.* Proc Natl Acad Sci U S A, 1979. **76**(4): p. 1603-9.

74.   Yoo, H., G. Stephanopoulos, and J.K. Kelleher, *Quantifying carbon sources for de novo lipogenesis in wild-type and IRS-1 knockout brown adipocytes.* J Lipid Res, 2004. **45**(7): p. 1324-32.

75.   Leturque, A., et al., *The role of GLUT2 in dietary sugar handling.* J Physiol Biochem, 2005. **61**(4): p. 529-37.

76.   Jin, E.S., et al., *Increased hepatic fructose 2,6-bisphosphate after an oral glucose load does not affect gluconeogenesis.* J Biol Chem, 2003. **278**(31): p. 28427-33.

77.   Sweet, I.R. and F.M. Matschinsky, *Mathematical model of beta-cell glucose metabolism and insulin release. I. Glucokinase as glucosensor hypothesis.* Am J Physiol, 1995. **268**(4 Pt 1): p. E775-88.

78.   Massillon, D., et al., *Quantitation of hepatic glucose fluxes and pathways of hepatic glycogen synthesis in conscious mice.* Am J Physiol, 1995. **269**(6 Pt 1): p. E1037-43.

79.   Alper, H. and G. Stephanopoulos, *Global transcription machinery engineering: a new approach for improving cellular phenotype.* Metab Eng, 2007. **9**(3): p. 258-67.

80.   Malaisse, W.J., et al., *Phosphoglucoisomerase-catalyzed interconversion of hexose phosphates. Study by 13C NMR of proton and deuteron exchange.* Mol Cell Biochem, 1991. **103**(2): p. 131-40.

81.   Malaisse, W.J., et al., *Phosphoglucoisomerase-catalyzed interconversion of hexose phosphates: isotopic discrimination between hydrogen and deuterium.* Mol Cell Biochem, 1990. **93**(2): p. 153-65.

82.   Voet, D. and J.G. Voet, *Biochemistry.* 3rd ed. 2004, New York: J. Wiley & Sons.

83.   Edwards, J.S., R.U. Ibarra, and B.O. Palsson, *In silico predictions of Escherichia coli metabolic capabilities are consistent with experimental data.* Nat Biotechnol, 2001. **19**(2): p. 125-30.

84.   Stafford, D.E., et al., *Optimizing bioconversion pathways through systems analysis and metabolic engineering.* Proc Natl Acad Sci U S A, 2002. **99**(4): p. 1801-6.

85.   Kelleher, J.K., *Flux estimation using isotopic tracers: common ground for metabolic physiology and metabolic engineering.* Metab Eng, 2001. **3**(2): p. 100-10.

86.   Kelleher, J.K., *Probing metabolic pathways with isotopic tracers: insights from mammalian metabolic physiology.* Metab Eng, 2004. **6**(1): p. 1-5.

87.   Young, J.D., et al., *An elementary metabolite unit (EMU) based method of isotopically nonstationary flux analysis.* Biotechnol Bioeng, 2007.

88. Bassingthwaighte, J.B., *Toward modeling the human physionome.* Adv Exp Med Biol, 1995. **382**: p. 331-9.

89. Cobelli, C. and A. Ruggeri, *Optimal design of sampling schedules for studying glucose kinetics with tracers.* Am J Physiol, 1989. **257**(3 Pt 1): p. E444-50.

90. Landaw, E.M. and J.J. DiStefano, 3rd, *Multiexponential, multicompartmental, and noncompartmental modeling. II. Data analysis and statistical considerations.* Am J Physiol, 1984. **246**(5 Pt 2): p. R665-77.

91. Bergman, R.N., L.S. Phillips, and C. Cobelli, *Physiologic evaluation of factors controlling glucose tolerance in man: measurement of insulin sensitivity and beta-cell glucose sensitivity from the response to intravenous glucose.* J Clin Invest, 1981. **68**(6): p. 1456-67.

92. Calvin, M. and A.A. Benson, *The Path of Carbon in Photosynthesis.* Science, 1948. **107**(2784): p. 476-480.

93. Yanagimachi, K.S., et al., *Application of radiolabeled tracers to biocatalytic flux analysis.* Eur J Biochem, 2001. **268**(18): p. 4950-60.

94. Wong, M.S., et al., *Metabolic and transcriptional patterns accompanying glutamine depletion and repletion in mouse hepatoma cells: a model for physiological regulatory networks.* Physiol Genomics, 2004. **16**(2): p. 247-55.

95. Bier, D.M., *Stable isotopes in biosciences, their measurement and models for amino acid metabolism.* Eur J Pediatr, 1997. **156 Suppl 1**: p. S2-8.

96. Raamsdonk, L.M., et al., *A functional genomics strategy that uses metabolome data to reveal the phenotype of silent mutations.* Nat Biotechnol, 2001. **19**(1): p. 45-50.

97. Soga, T., et al., *Quantitative metabolome analysis using capillary electrophoresis mass spectrometry.* J Proteome Res, 2003. **2**(5): p. 488-94.

98. Kirschenlohr, H.L., et al., *Proton NMR analysis of plasma is a weak predictor of coronary artery disease.* Nat Med, 2006. **12**(6): p. 705-10.

99. Lee, K., et al., *Profiling of dynamic changes in hypermetabolic livers.* Biotechnol Bioeng, 2003. **83**(4): p. 400-15.

100. Zupke, C., A.J. Sinskey, and G. Stephanopoulos, *Intracellular flux analysis applied to the effect of dissolved oxygen on hybridomas.* Appl Microbiol Biotechnol, 1995. **44**(1-2): p. 27-36.

101. Klapa, M.I., et al., *Metabolite and isotopomer balancing in the analysis of metabolic cycles: I. Theory.* Biotechnol Bioeng, 1999. **62**(4): p. 375-391.

102. Antoniewicz, M.R., J.K. Kelleher, and G. Stephanopoulos, *Elementary metabolite units (EMU): a novel framework for modeling isotopic distributions.* Metab Eng, 2007. **9**(1): p. 68-86.

103. Selivanov, V.A., et al., *An optimized algorithm for flux estimation from isotopomer distribution in glucose metabolites.* Bioinformatics, 2004. **20**(18): p. 3387-97.

104. Wiechert, W. and K. Noh, *From stationary to instationary metabolic flux analysis.* Adv Biochem Eng Biotechnol, 2005. **92**: p. 145-72.

105. Antoniewicz, M.R., J.K. Kelleher, and G. Stephanopoulos, *Determination of confidence intervals of metabolic fluxes estimated from stable isotope measurements.* Metab Eng, 2006. **8**(4): p. 324-37.

106. McCabe, B.J. and S.F. Previs, *Using isotope tracers to study metabolism: application in mouse models.* Metab Eng, 2004. **6**(1): p. 25-35.

107. Baker, N., et al., *Turnover and fate of plasma free fatty acids in briefly-fasted lymphoma-bearing mice.* Lipids, 1989. **24**(12): p. 1028-34.

108. Brunengraber, D.Z., et al., *Gas chromatography-mass spectrometry assay of the (18)o enrichment of water as trimethyl phosphate.* Anal Biochem, 2002. **306**(2): p. 278-82.

109. Messmer, B.T., et al., *In vivo measurements document the dynamic cellular kinetics of chronic lymphocytic leukemia B cells.* J Clin Invest, 2005. **115**(3): p. 755-64.

110.   Kim, J.K., et al., *Redistribution of substrates to adipose tissue promotes obesity in mice with selective insulin resistance in muscle.* J Clin Invest, 2000. **105**(12): p. 1791-7.

111.   Landau, B.R., et al., *Use of 2H2O for estimating rates of gluconeogenesis. Application to the fasted state.* J Clin Invest, 1995. **95**(1): p. 172-8.

112.   Katz, J., *On the determination of turnover in vivo with tracers.* Am J Physiol, 1992. **263**(3 Pt 1): p. E417-24.

113.   Yoshida, S., et al., *Effect of intracerebroventricular injection of tumor necrosis factor alpha on gut mucosal protein turnover in mice fed enterally.* J Surg Res, 1999. **87**(1): p. 73-6.

114.   Lam, T.K., et al., *Regulation of blood glucose by hypothalamic pyruvate metabolism.* Science, 2005. **309**(5736): p. 943-7.

115.   Xu, J., et al., *Peroxisome proliferator-activated receptor alpha (PPARalpha) influences substrate utilization for hepatic glucose production.* J Biol Chem, 2002. **277**(52): p. 50237-44.

116.   Xu, J., et al., *PPAR{alpha} deficiency diminishes insulin-responsiveness of gluconeogenic/glycolytic/pentose gene expression and substrate cycle flux.* Endocrinology, 2003.

117.   Xu, J., et al., *Peroxisomal proliferator-activated receptor alpha deficiency diminishes insulin-responsiveness of gluconeogenic/glycolytic/pentose gene expression and substrate cycle flux.* Endocrinology, 2004. **145**(3): p. 1087-95.

118.   Ahluwalia, N., et al., *Inhibited aortic aneurysm formation in BLT1-deficient mice.* J Immunol, 2007. **179**(1): p. 691-7.

119.   Kurland, I.J., et al., *Loss of [13C]glycerol carbon via the pentose cycle. Implications for gluconeogenesis measurement by mass isotoper distribution analysis.* J Biol Chem, 2000. **275**(47): p. 36787-93.

120.   Previs, S.F., G.W. Cline, and G.I. Shulman, *A critical evaluation of mass isotopomer distribution analysis of gluconeogenesis in vivo.* Am J Physiol, 1999. **277**(1 Pt 1): p. E154-60.

121.   Weidemann, M.J., et al., *Gluconeogenesis from propionate in kidney and liver of the vitamin B12-deficient rat.* Biochem J, 1970. **117**(1): p. 177-81.

122.   Pilkis, S.J., et al., *Hormonal control of cyclic 3':5'-AMP levels and gluconeogenesis in isolated hepatocytes from fed rats.* J Biol Chem, 1975. **250**(16): p. 6328-36.

123.   Pilkis, S.J., J.P. Riou, and T.H. Claus, *Hormonal control of [14C]glucose synthesis from [U-14C]dihydroxyacetone and glycerol in isolated rat hepatocytes.* J Biol Chem, 1976. **251**(24): p. 7841-52.

124.   Johnson, M.E., et al., *The regulation of gluconeogenesis in isolated rat liver cells by glucagon, insulin, dibutyryl cyclic adenosine monophosphate, and fatty acids.* J Biol Chem, 1972. **247**(10): p. 3229-35.

125.   Cohen, S.M., et al., *P nuclear magnetic resonance studies of isolated rat liver cells.* Nature, 1978. **273**(5663): p. 554-6.

126.   Cohen, S.M., et al., *A comparison of 13C nuclear magnetic resonance and 14C tracer studies of hepatic metabolism.* J Biol Chem, 1981. **256**(7): p. 3428-32.

127.   Chance, E.M., et al., *Mathematical analysis of isotope labeling in the citric acid cycle with applications to 13C NMR studies in perfused rat hearts.* J Biol Chem, 1983. **258**(22): p. 13785-94.

128.   Malloy, C.R., A.D. Sherry, and F.M. Jeffrey, *Carbon flux through citric acid cycle pathways in perfused heart by 13C NMR spectroscopy.* FEBS Lett, 1987. **212**(1): p. 58-62.

129.   Malloy, C.R., A.D. Sherry, and F.M. Jeffrey, *Evaluation of carbon flux and substrate selection through alternate pathways involving the citric acid cycle of the heart by 13C NMR spectroscopy.* J Biol Chem, 1988. **263**(15): p. 6964-71.

130.   Kalderon, B., A. Gopher, and A. Lapidot, *Metabolic pathways leading to liver glycogen repletion in vivo, studied by GC-MS and NMR.* FEBS Lett, 1986. **204**(1): p. 29-32.

131.   Kalderon, B., et al., *Estimation of glucose carbon recycling in children with glycogen storage disease: A 13C NMR study using [U-13C]glucose.* Proc Natl Acad Sci U S A, 1989. **86**(12): p. 4690-4.

132.   Kelleher, J.K. and T.M. Masterson, *Model equations for condensation biosynthesis using stable isotopes and radioisotopes.* Am J Physiol, 1992. **262**(1 Pt 1): p. E118-25.

133. Hellerstein, M.K., *New stable isotope-mass spectrometric techniques for measuring fluxes through intact metabolic pathways in mammalian systems: introduction of moving pictures into functional genomics and biochemical phenotyping.* Metab Eng, 2004. **6**(1): p. 85-100.

134. Katz, J., et al., *Studies of glycogen synthesis and the Krebs cycle by mass isotopomer analysis with [U-13C]glucose in rats.* J Biol Chem, 1989. **264**(22): p. 12994-3004.

135. Jung, H.R., et al., *Metabolic adaptations to dietary fat malabsorption in chylomicron-deficient mice.* Biochem J, 1999. **343 Pt 2**: p. 473-8.

136. Neese, R.A., et al., *Gluconeogenesis and intrahepatic triose phosphate flux in response to fasting or substrate loads. Application of the mass isotopomer distribution analysis technique with testing of assumptions and potential problems.* J Biol Chem, 1995. **270**(24): p. 14452-66.

137. Hellerstein, M.K., et al., *Hepatic glucose-6-phosphatase flux and glucose phosphorylation, cycling, irreversible disposal, and net balance in vivo in rats. Measurement using the secreted glucuronate technique.* Metabolism, 1997. **46**(12): p. 1390-8.

138. Previs, S.F., et al., *Limitations of the mass isotopomer distribution analysis of glucose to study gluconeogenesis. Substrate cycling between glycerol and triose phosphates in liver.* J Biol Chem, 1995. **270**(34): p. 19806-15.

139. Previs, S.F., et al., *Limitations of the mass isotopomer distribution analysis of glucose to study gluconeogenesis. Heterogeneity of glucose labeling in incubated hepatocytes.* J Biol Chem, 1998. **273**(27): p. 16853-9.

140. Landau, B.R., et al., *A limitation in the use of mass isotopomer distributions to measure gluconeogenesis in fasting humans.* Am J Physiol, 1995. **269**(1 Pt 1): p. E18-26.

141. Lindenthal, B., et al., *Isotopomer spectral analysis of intermediates of cholesterol synthesis in human subjects and hepatic cells.* Am J Physiol Endocrinol Metab, 2002. **282**(6): p. E1222-30.

142. Lifson, N., *Theory of use of the turnover rates of body water for measuring energy and material balance.* J Theor Biol, 1966. **12**(1): p. 46-74.

143. Rognstad, R., *Estimation of gluconeogenesis and glycogenolysis in vivo using tritiated water.* Biochem J, 1991. **279 (Pt 3)**: p. 911.

144. Landau, B.R., et al., *Contributions of gluconeogenesis to glucose production in the fasted state.* J Clin Invest, 1996. **98**(2): p. 378-85.

145. Allick, G., et al., *Measurement of gluconeogenesis by deuterated water: the effect of equilibration time and fasting period.* Am J Physiol Endocrinol Metab, 2006. **290**(6): p. E1212-7.

146. Rothman, D.L., et al., *Quantitation of hepatic glycogenolysis and gluconeogenesis in fasting humans with 13C NMR.* Science, 1991. **254**(5031): p. 573-6.

147. Hundal, R.S., et al., *Mechanism by which metformin reduces glucose production in type 2 diabetes.* Diabetes, 2000. **49**(12): p. 2063-9.

148. Basu, R., et al., *Obesity and type 2 diabetes impair insulin-induced suppression of glycogenolysis as well as gluconeogenesis.* Diabetes, 2005. **54**(7): p. 1942-8.

149. Jones, J.G., et al., *Measurement of gluconeogenesis and pyruvate recycling in the rat liver: a simple analysis of glucose and glutamate isotopomers during metabolism of [1,2,3-(13)C3]propionate.* FEBS Lett, 1997. **412**(1): p. 131-7.

150. Jones, J.G., et al., *13C NMR measurements of human gluconeogenic fluxes after ingestion of [U-13C]propionate, phenylacetate, and acetaminophen.* Am J Physiol, 1998. **275**(5 Pt 1): p. E843-52.

151. Jones, J.G., et al., *An integrated (2)H and (13)C NMR study of gluconeogenesis and TCA cycle flux in humans.* Am J Physiol Endocrinol Metab, 2001. **281**(4): p. E848-56.

152. Burgess, S.C., et al., *Analysis of gluconeogenic pathways in vivo by distribution of 2H in plasma glucose: comparison of nuclear magnetic resonance and mass spectrometry.* Anal Biochem, 2003. **318**(2): p. 321-4.

153. Hausler, N., et al., *Effects of insulin and cytosolic redox state on glucose production pathways in the isolated perfused mouse liver measured by integrated 2H and 13C NMR.* Biochem J, 2006. **394**(Pt 2): p. 465-73.

154. Xu, J., et al., *Lipin deficiency impairs diurnal metabolic fuel switching.* Diabetes, 2006. **55**(12): p. 3429-38.

155. Sauer, U., *Metabolic networks in motion: 13C-based flux analysis.* Molecular Systems Biology, 2006. **2**: p. 62.

156. Wong, M., *Integrated Characterization of Cellular Physiology Underlying Hepatic Metabolism*, in *Chemical Engineering*. 2006, Massachusetts Institute of Technology: Cambridge, MA. p. 208.

157. Baba, H., X.J. Zhang, and R.R. Wolfe, *Glycerol gluconeogenesis in fasting humans.* Nutrition, 1995. **11**(2): p. 149-53.

158. Diraison, F., et al., *Non-invasive tracing of liver intermediary metabolism in normal subjects and in moderately hyperglycaemic NIDDM subjects. Evidence against increased gluconeogenesis and hepatic fatty acid oxidation in NIDDM.* Diabetologia, 1998. **41**(2): p. 212-20.

159. Diraison, F., et al., *Noninvasive tracing of human liver metabolism: comparison of phenylacetate and apoB-100 to sample glutamine.* Am J Physiol, 1999. **277**(3 Pt 1): p. E529-36.

160. Antoniewicz, M.R., et al., *Metabolic flux analysis in a nonstationary system: Fed-batch fermentation of a high yielding strain of E. coli producing 1,3-propanediol.* Metab Eng, 2007. **9**(3): p. 277-92.

161. Block, G.D., et al., *Population expansion, clonal growth, and specific differentiation patterns in primary cultures of hepatocytes induced by HGF/SF, EGF and TGF alpha in a chemically defined (HGM) medium.* J Cell Biol, 1996. **132**(6): p. 1133-49.

162. Fukuhara, A., et al., *Visfatin: a protein secreted by visceral fat that mimics the effects of insulin.* Science, 2005. **307**(5708): p. 426-30.

163. Berry, M.N. and D.S. Friend, *High-yield preparation of isolated rat liver parenchymal cells: a biochemical and fine structural study.* J Cell Biol, 1969. **43**(3): p. 506-20.

164. Berry, M.N., et al., *Isolated hepatocytes : preparation, properties and applications Michael N. Berry, Anthony M. Edwards, Gregory J. Barritt ; with contributions by Marlene B. Grivell ... et al.* Laboratory techniques in biochemistry and molecular biology ; v. 21. 1991, Amsterdam ; New York: Elsevier. xx, 460.

165. Seglen, P.O., *Preparation of isolated rat liver cells.* Methods Cell Biol, 1976. **13**: p. 29-83.

166. Hachey, D.L., et al., *Quantitation of monosaccharide isotopic enrichment in physiologic fluids by electron ionization or negative chemical ionization GC/MS using di-O-isopropylidene derivatives.* Anal Chem, 1999. **71**(20): p. 4734-9.

167. Nurjhan, N., A. Consoli, and J. Gerich, *Increased lipolysis and its consequences on gluconeogenesis in non-insulin-dependent diabetes mellitus.* J Clin Invest, 1992. **89**(1): p. 169-75.

168. Seeholzer, S.H., *Phosphoglucose isomerase: a ketol isomerase with aldol C2-epimerase activity.* Proc Natl Acad Sci U S A, 1993. **90**(4): p. 1237-41.

169. Glantz, S.A. and B.K. Slinker, *Primer of applied regression & analysis of variance.* 2nd ed. 2001, New York: McGraw-Hill Medical Pub. Division. xxvii, 949.

170. Chen, C., et al., *An integrated functional genomics screening program reveals a role for BMP-9 in glucose homeostasis.* Nat Biotechnol, 2003. **21**(3): p. 294-301.

171. Deschatrette, J., *Dedifferentiated variants of a rat hepatoma: partial reversion induced by cell aggregation.* Cell, 1980. **22**(2 Pt 2): p. 501-11.

172. She, P., et al., *Mechanisms by which liver-specific PEPCK knockout mice preserve euglycemia during starvation.* Diabetes, 2003. **52**(7): p. 1649-54.

173. Mojena, M., et al., *Effect of sulfonylureas on hepatic glycogen metabolism: activation of glycogen phosphorylase.* Metabolism, 1989. **38**(5): p. 466-70.

174.   Lechuga, C.G., et al., *Decreased responsiveness of gluconeogenesis to the modulation by sulfonylureas in hepatocytes isolated from obese (fa/fa) Zucker rats.* Life Sci, 2001. **68**(14): p. 1617-28.

175.   Lochhead, P.A., et al., *5-aminoimidazole-4-carboxamide riboside mimics the effects of insulin on the expression of the 2 key gluconeogenic genes PEPCK and glucose-6-phosphatase.* Diabetes, 2000. **49**(6): p. 896-903.

176.   Greenaway, T.M., et al., *Increased gluconeogenesis in hepatocytes from GTG-obese mice is insensitive to inhibition by insulin.* Int J Obes Relat Metab Disord, 1992. **16**(12): p. 985-90.

177.   Si, Y., J. Yoon, and K. Lee, *Flux profile and modularity analysis of time-dependent metabolic changes of de novo adipocyte formation.* Am J Physiol Endocrinol Metab, 2007. **292**(6): p. E1637-46.

178.   Fernandez, C.A. and C. Des Rosiers, *Modeling of liver citric acid cycle and gluconeogenesis based on 13C mass isotopomer distribution analysis of intermediates.* J Biol Chem, 1995. **270**(17): p. 10037-42.

179.   Jahoor, F., E.J. Peters, and R.R. Wolfe, *The relationship between gluconeogenic substrate supply and glucose production in humans.* Am J Physiol, 1990. **258**(2 Pt 1): p. E288-96.

180.   van Dijk, T.H., et al., *Acute inhibition of hepatic glucose-6-phosphatase does not affect gluconeogenesis but directs gluconeogenic flux toward glycogen in fasted rats. A pharmacological study with the chlorogenic acid derivative S4048.* J Biol Chem, 2001. **276**(28): p. 25727-35.

181.   van Poelje, P.D., et al., *Inhibition of fructose 1,6-bisphosphatase reduces excessive endogenous glucose production and attenuates hyperglycemia in zucker diabetic Fatty rats.* Diabetes, 2006. **55**(6): p. 1747-54.

182.   Granner, D., et al., *Inhibition of transcription of the phosphoenolpyruvate carboxykinase gene by insulin.* Nature, 1983. **305**(5934): p. 549-51.

183.   Kruszynska, Y.T. and J.M. Olefsky, *Cellular and molecular mechanisms of non-insulin dependent diabetes mellitus.* J Investig Med, 1996. **44**(8): p. 413-28.

184.   Karam, J.H., *Reversible insulin resistance in non-insulin-dependent diabetes mellitus.* Horm Metab Res, 1996. **28**(9): p. 440-4.

185.   Simonson, D.C., Rossetti L., Giaccari, A., and DeFronzo, R.A., in *International Textbook of Diabetes Mellitus*, K.G.M.M. Alberti, Zimmet, P., DeFronzo, R.A., and Kenn, H., Editor. 1997, John Wiley & Sons, Ltd. p. 713-744.

186.   Yki-Jarvinen, H., *Glucose toxicity.* Endocr Rev, 1992. **13**(3): p. 415-31.

187.   Malloy, C.R., A.D. Sherry, and F.M. Jeffrey, *Analysis of tricarboxylic acid cycle of the heart using 13C isotope isomers.* Am J Physiol, 1990. **259**(3 Pt 2): p. H987-95.

188.   Chace, D.H. and F.P. Abramson, *Selective detection of carbon-13, nitrogen-15, and deuterium labeled metabolites by capillary gas chromatography-chemical reaction interface/mass spectrometry.* Anal Chem, 1989. **61**(24): p. 2724-30.

189.   Kay, L.E., et al., *Four-dimensional heteronuclear triple-resonance NMR spectroscopy of interleukin-1 beta in solution.* Science, 1990. **249**(4967): p. 411-4.

190.   Langstrom, B., et al., *Design of tracer molecules with emphasis on stereochemistry, position of label and multiple isotopic labeling. An important aspect in studies of biologic function using positron emission tomography.* Acta Radiol Suppl, 1991. **376**: p. 31-5.

191.   Landau, B.R., *Quantifying the contribution of gluconeogenesis to glucose production in fasted human subjects using stable isotopes.* Proc Nutr Soc, 1999. **58**(4): p. 963-72.

192.   Glantz, S.A., *Primer of biostatistics.* 6th ed. 2005, New York: McGraw-Hill Medical Pub. Division. xx, 520.

193.   Tigas, S., A. Sunehag, and M.W. Haymond, *Metabolic adaptation to feeding and fasting during lactation in humans.* J Clin Endocrinol Metab, 2002. **87**(1): p. 302-7.

194.   Lyon, J.B., Jr. and P.F. Fenton, *Muscle and liver glycogen of mouse strains susceptible or resistant to nutritionally induced obesity.* Am J Physiol, 1956. **187**(3): p. 514-6.

195. Walker, A.P., F. Muscatelli, and A.P. Monaco, *Isolation of the human Xp21 glycerol kinase gene by positional cloning.* Hum Mol Genet, 1993. **2**(2): p. 107-14.

196. Strausberg, R.L., et al., *Generation and initial analysis of more than 15,000 full-length human and mouse cDNA sequences.* Proc Natl Acad Sci U S A, 2002. **99**(26): p. 16899-903.

197. DeFronzo, R.A., J.D. Tobin, and R. Andres, *Glucose clamp technique: a method for quantifying insulin secretion and resistance.* Am J Physiol, 1979. **237**(3): p. E214-23.

198. Pelkonen, R., E.A. Nikkila, and M. Kekki, *Metabolism of glycerol in diabetes mellitus.* Diabetologia, 1967. **3**(1): p. 1-8.

199. Reuser, A.J., et al., *Biochemical, immunological, and cell genetic studies in glycogenosis type II.* Am J Hum Genet, 1978. **30**(2): p. 132-43.

200. Sindelar, D.K., et al., *A comparison of the effects of selective increases in peripheral or portal insulin on hepatic glucose production in the conscious dog.* Diabetes, 1996. **45**(11): p. 1594-604.

201. Mittelman, S.D. and R.N. Bergman, *Inhibition of lipolysis causes suppression of endogenous glucose production independent of changes in insulin.* Am J Physiol Endocrinol Metab, 2000. **279**(3): p. E630-7.

202. Edgerton, D.S., et al., *Insulin's direct effects on the liver dominate the control of hepatic glucose production.* J Clin Invest, 2006. **116**(2): p. 521-7.

203. Biddinger, S.B. and C.R. Kahn, *From mice to men: insights into the insulin resistance syndromes.* Annu Rev Physiol, 2006. **68**: p. 123-58.

204. Sasaki, K., et al., *Multihormonal regulation of phosphoenolpyruvate carboxykinase gene transcription. The dominant role of insulin.* J Biol Chem, 1984. **259**(24): p. 15242-51.

205. Massillon, D., et al., *Glucose regulates in vivo glucose-6-phosphatase gene expression in the liver of diabetic rats.* J Biol Chem, 1996. **271**(17): p. 9871-4.

206. Barrett, E.J., *Insulin's effect on glucose production: direct or indirect?* J Clin Invest, 2003. **111**(4): p. 434-5.

207. Klapa, M.I., J.C. Aon, and G. Stephanopoulos, *Systematic quantification of complex metabolic flux networks using stable isotopes and mass spectrometry.* Eur J Biochem, 2003. **270**(17): p. 3525-42.

208. Klapa, M.I., J.C. Aon, and G. Stephanopoulos, *Ion-trap mass spectrometry used in combination with gas chromatography for high-resolution metabolic flux determination.* Biotechniques, 2003. **34**(4): p. 832-6, 838, 840 passim.

209. Miyake, K., et al., *Hyperinsulinemia, glucose intolerance, and dyslipidemia induced by acute inhibition of phosphoinositide 3-kinase signaling in the liver.* J Clin Invest, 2002. **110**(10): p. 1483-91.

210. Taniguchi, C.M., et al., *Divergent regulation of hepatic glucose and lipid metabolism by phosphoinositide 3-kinase via Akt and PKClambda/zeta.* Cell Metab, 2006. **3**(5): p. 343-53.

211. Horton, J.D., et al., *Disruption of LDL receptor gene in transgenic SREBP-1a mice unmasks hyperlipidemia resulting from production of lipid-rich VLDL.* J Clin Invest, 1999. **103**(7): p. 1067-76.

212. Cohen, S.E., et al., *High circulating leptin receptors with normal leptin sensitivity in liver-specific insulin receptor knock-out (LIRKO) mice.* J Biol Chem, 2007. **282**(32): p. 23672-8.

213. Suckow, M.A., P. Danneman, and C. Brayton, *The laboratory mouse.* Laboratory animal pocket reference series. 2000, Boca Raton, Fla,: CRC Press. 168.

214. Moxley, J.F. and Massachusetts Institute of Technology. Dept. of Chemical Engineering., *Linking genetic regulation and the metabolic state.* 2007. p. 276.

215. Fiehn, O., et al., *Identification of uncommon plant metabolites based on calculation of elemental compositions using gas chromatography and quadrupole mass spectrometry.* Anal Chem, 2000. **72**(15): p. 3573-80.

216. Folch, J., et al., *Preparation of lipide extracts from brain tissue.* J Biol Chem, 1951. **191**(2): p. 833-41.

217.   Yang, L., et al., *Metabolomic assays of the concentration and mass isotopomer distribution of gluconeogenic and citric acid cycle intermediates.* Metabolomics, 2006. **2**(2): p. 85-94.

218.   Chance, B., *Phosphorylation efficiency of the intact cell. II. Crossover phenomena in bakers' yeast.* J Biol Chem, 1959. **234**: p. 3036-40.

219.   Cho, W.C., et al., *Potential biomarkers found by protein profiling may provide insight for the macrovascular pathogenesis of diabetes mellitus.* Dis Markers, 2006. **22**(3): p. 153-66.

220.   Kim, S.W., et al., *Time-dependent plasma protein changes in streptozotocin-induced diabetic rats before and after fungal polysaccharide treatments.* J Proteome Res, 2006. **5**(11): p. 2966-76.

221.   Yechoor, V.K., et al., *Coordinated patterns of gene expression for substrate and energy metabolism in skeletal muscle of diabetic mice.* Proc Natl Acad Sci U S A, 2002. **99**(16): p. 10587-92.

222.   Wang, X., et al., *SREBP-1, a membrane-bound transcription factor released by sterol-regulated proteolysis.* Cell, 1994. **77**(1): p. 53-62.

223.   Foufelle, F. and P. Ferre, *New perspectives in the regulation of hepatic glycolytic and lipogenic genes by insulin and glucose: a role for the transcription factor sterol regulatory element binding protein-1c.* Biochem J, 2002. **366**(Pt 2): p. 377-91.

224.   Kelleher, J.K., et al., *Isotopomer spectral analysis of cholesterol synthesis: applications in human hepatoma cells.* Am J Physiol, 1994. **266**(3 Pt 1): p. E384-95.

225.   Kharroubi, A.T., et al., *Isotopomer spectral analysis of triglyceride fatty acid synthesis in 3T3-L1 cells.* Am J Physiol, 1992. **263**(4 Pt 1): p. E667-75.

226.   Biddinger, S.B., et al., *Effects of diet and genetic background on sterol regulatory element-binding protein-1c, stearoyl-CoA desaturase 1, and the development of the metabolic syndrome.* Diabetes, 2005. **54**(5): p. 1314-23.

227.   Biddinger, S.B., et al., *Leptin suppresses stearoyl-CoA desaturase 1 by mechanisms independent of insulin and sterol regulatory element-binding protein-1c.* Diabetes, 2006. **55**(7): p. 2032-41.

228.   Cobelli, C. and D.M. Foster, *Compartmental models: theory and practice using the SAAM II software system.* Adv Exp Med Biol, 1998. **445**: p. 79-101.

229.   Efendic, S., A. Wajngot, and M. Vranic, *Increased activity of the glucose cycle in the liver: early characteristic of type 2 diabetes.* Proc Natl Acad Sci U S A, 1985. **82**(9): p. 2965-9.

230.   Landau, B.R., *Measuring glucose and fructose-6-phosphate cycling in liver in vivo.* Metabolism, 1993. **42**(4): p. 457-62.

231.   Efendic, S., S. Karlander, and M. Vranic, *Mild type II diabetes markedly increases glucose cycling in the postabsorptive state and during glucose infusion irrespective of obesity.* J Clin Invest, 1988. **81**(6): p. 1953-61.

232.   Hellerstein, M.K., et al., *Hepatic gluconeogenic fluxes and glycogen turnover during fasting in humans. A stable isotope study.* J Clin Invest, 1997. **100**(5): p. 1305-19.

233.   Cross, D.A., et al., *Inhibition of glycogen synthase kinase-3 by insulin mediated by protein kinase B.* Nature, 1995. **378**(6559): p. 785-9.

234.   Magnuson, M.A., P.G. Quinn, and D.K. Granner, *Multihormonal regulation of phosphoenolpyruvate carboxykinase-chloramphenicol acetyltransferase fusion genes. Insulin's effects oppose those of cAMP and dexamethasone.* J Biol Chem, 1987. **262**(31): p. 14917-20.

235.   Ideker, T., T. Galitski, and L. Hood, *A new approach to decoding life: systems biology.* Annu Rev Genomics Hum Genet, 2001. **2**: p. 343-72.

236.   Hazey, J.W., et al., *Tracing gluconeogenesis with deuterated water: measurement of low deuterium enrichments on carbons 6 and 2 of glucose.* Anal Biochem, 1997. **248**(1): p. 158-67.

237.   Bergman, R.N., *Lilly lecture 1989. Toward physiological understanding of glucose tolerance. Minimal-model approach.* Diabetes, 1989. **38**(12): p. 1512-27.

238.   Young, J.D. and D. Ramkrishna, *On the matching and proportional laws of cybernetic models.* Biotechnol Prog, 2007. **23**(1): p. 83-99.

239.	Hellerstein, M.K., D.J. Greenblatt, and H.N. Munro, *Glycoconjugates as noninvasive probes of intrahepatic metabolism: pathways of glucose entry into compartmentalized hepatic UDP-glucose pools during glycogen accumulation.* Proc Natl Acad Sci U S A, 1986. **83**(18): p. 7044-8.

240.	Lu, D., et al., *13C NMR isotopomer analysis reveals a connection between pyruvate cycling and glucose-stimulated insulin secretion (GSIS).* Proc Natl Acad Sci U S A, 2002. **99**(5): p. 2708-13.

241.	Khan, A., et al., *Evidence for the presence of glucose cycling in pancreatic islets of the ob/ob mouse.* J Biol Chem, 1989. **264**(17): p. 9732-3.

242.	Wolfe, R.R., et al., *Effect of severe burn injury on substrate cycling by glucose and fatty acids.* N Engl J Med, 1987. **317**(7): p. 403-8.

243.	Erion, M.D., et al., *MB06322 (CS-917): A potent and selective inhibitor of fructose 1,6-bisphosphatase for controlling gluconeogenesis in type 2 diabetes.* Proc Natl Acad Sci U S A, 2005. **102**(22): p. 7970-5.

244.	Nathan, D.M., et al., *Management of hyperglycemia in type 2 diabetes: A consensus algorithm for the initiation and adjustment of therapy: a consensus statement from the American Diabetes Association and the European Association for the Study of Diabetes.* Diabetes Care, 2006. **29**(8): p. 1963-72.

245.	Service, G.J., et al., *Hyperinsulinemic hypoglycemia with nesidioblastosis after gastric-bypass surgery.* N Engl J Med, 2005. **353**(3): p. 249-54.

246.	Sabatine, M.S., et al., *Metabolomic identification of novel biomarkers of myocardial ischemia.* Circulation, 2005. **112**(25): p. 3868-75.

247.	Styczynski, M.P., et al., *Systematic identification of conserved metabolites in GC/MS data for metabolomics and biomarker discovery.* Anal Chem, 2007. **79**(3): p. 966-73.

Appendix A: Cellular Experiments, Enrichment Data Overview

All data presented are uncorrected isotopomer spectra for glucose derivatives of the indicated mass to charge (m/z) ratio, unless otherwise noted. Percentages correspond to the percent abundance of each isotopomer relative to the total glucose fragment signal. Theory represents theoretical natural abundance calculated a priori given the structure of the unlabeled glucose derivative.

Color code: Yellow: Aldonitrile pentaacetate glucose fragments, high quality data.
Green = High Quality Data   Blue = Manual correction required
Tan = Qualitative data   Pink = Poor quality data

Attached Mouse Hepatocyte Experiment Details:

Experiment Date	9/11/2004	Fed/Fasted Animal	Fed
Incubation Time	20 hr	Tracers	1 mM [U-^{13}C]-glycerol
Conditions	Basal		1 mM [D$_5$]-glycerol
Replicates	3		10% D$_2$O

m/z	[U13C]-Glycerol			[D5]-Glycerol			10% D2O			Theory
	1	2	3	4	5	6	7	8	9	
287	54.8%	60.6%	58.3%	59.6%	57.5%	57.6%	54.3%	53.8%	53.4%	85.1%
288	9.4%	10.0%	9.7%	16.1%	16.5%	16.5%	32.7%	32.9%	33.2%	12.6%
289	3.3%	3.1%	3.1%	13.4%	14.4%	14.4%	10.4%	10.6%	10.7%	2.1%
290	20.4%	16.7%	17.8%	6.5%	6.9%	6.8%	2.2%	2.3%	2.3%	0.2%
291	2.9%	2.3%	2.5%	3.1%	3.3%	3.3%	0.4%	0.4%	0.4%	0.0%
292	1.4%	1.1%	1.2%	1.1%	1.2%	1.1%	0.0%	0.0%	0.0%	0.0%
293	7.2%	5.7%	6.7%	0.2%	0.2%	0.2%	0.0%	0.0%	0.0%	0.0%
294	0.6%	0.5%	0.6%	0.0%	0.0%	0.0%	0.0%	0.0%	0.0%	0.0%
295	0.1%	0.1%	0.1%	0.0%	0.0%	0.0%				0.0%
296	0.0%	0.0%	0.0%	0.0%	0.0%	0.0%				0.0%
314	54.3%	60.2%	57.9%	74.9%	74.3%	74.3%	62.8%	62.4%	62.4%	84.6%
315	9.6%	10.3%	10.0%	19.4%	19.9%	19.8%	28.9%	29.2%	29.2%	12.8%
316	11.7%	10.0%	10.5%	4.9%	5.0%	5.0%	7.1%	7.2%	7.2%	2.3%
317	13.6%	11.0%	11.7%	0.8%	0.8%	0.8%	1.2%	1.2%	1.2%	0.3%
318	2.5%	2.0%	2.2%	0.1%	0.1%	0.1%	0.1%	0.0%	0.1%	0.0%
319	7.5%	5.9%	6.9%	0.0%	0.0%	0.0%	0.0%	0.0%	0.0%	0.0%
320	0.7%	0.5%	0.6%	0.0%	0.0%	0.0%	0.0%	0.0%	0.0%	0.0%
321	0.1%	0.1%	0.1%	0.0%	0.0%	0.0%	0.0%	0.0%	0.0%	0.0%

Attached Mouse Hepatocyte Experiment Details:

Experiment Date	9/13/2004	Fed/Fasted Animal	Fed
Incubation Time	8 hr	Tracers	1 mM [U-^{13}C]-glycerol
Conditions	Basal		5 mM [U-^{13}C]-glutamine
Replicates	3		2 mM [U-^{13}C]-acetate

m/z	[U13C]-Glycerol			[U13C]-Glutamine			[U13C]-Acetate			Unabeled		Theory
	1	2	3	4	5	6	7	8	9	10	11	
287	47.5%	50.6%	46.6%	29.1%	26.2%	30.2%	82.5%	82.6%	83.3%	84.9%	85.0%	85.1%
288	8.3%	8.7%	8.1%	8.5%	8.3%	8.5%	13.8%	13.9%	13.5%	12.6%	12.7%	12.6%
289	3.4%	3.4%	3.3%	12.2%	12.7%	11.9%	3.1%	3.1%	2.8%	2.1%	2.1%	2.1%
290	24.2%	23.0%	25.2%	23.6%	24.1%	22.7%	0.5%	0.4%	0.4%	0.3%	0.2%	0.2%
291	3.5%	3.3%	3.6%	7.9%	8.4%	7.9%	0.1%	0.1%	0.0%	0.0%	0.0%	0.0%
292	1.8%	1.6%	1.8%	9.2%	10.0%	9.2%	0.0%	0.0%	0.0%	0.0%	0.0%	0.0%
293	10.4%	8.6%	10.4%	8.7%	9.4%	8.7%	0.0%	0.0%	0.0%	0.0%	0.0%	0.0%
294	0.8%	0.7%	0.8%	0.8%	0.9%	0.8%	0.0%	0.0%	0.0%	0.0%	0.0%	0.0%
295	0.1%	0.1%	0.2%	0.1%	0.2%	0.1%	0.0%	0.0%	0.0%	0.0%	0.0%	0.0%
296	0.0%	0.0%	0.0%	0.0%	0.0%	0.0%	0.0%	0.0%	0.0%	0.0%	0.0%	0.0%
314	47.6%	50.5%	46.4%	30.3%	27.6%	31.6%	83.2%	83.0%	83.4%	84.9%	85.0%	84.6%
315	8.6%	9.1%	8.5%	12.1%	12.1%	11.9%	13.3%	13.3%	13.1%	12.6%	12.5%	12.8%
316	13.3%	12.8%	13.7%	20.7%	21.2%	20.1%	3.1%	3.3%	3.2%	2.3%	2.3%	2.3%
317	15.8%	15.1%	16.5%	16.1%	16.7%	15.8%	0.3%	0.4%	0.4%	0.2%	0.2%	0.3%
318	3.0%	2.8%	3.2%	10.2%	11.0%	10.1%	0.0%	0.0%	0.0%	0.0%	0.0%	0.0%
319	10.5%	8.6%	10.6%	9.4%	10.2%	9.3%	0.0%	0.0%	0.0%	0.0%	0.0%	0.0%
320	1.0%	0.8%	1.0%	1.0%	1.0%	1.0%	0.0%	0.0%	0.0%	0.0%	0.0%	0.0%
321	0.2%	0.2%	0.2%	0.2%	0.2%	0.2%	0.0%	0.0%	0.0%	0.0%	0.0%	0.0%

Attached Mouse Hepatocyte Experiment Details (9/30/2004)

Experiment Date	9/30/2004	Fed/Fasted Animal	Fed
Incubation Time	2,5,8 hr	Tracers	1 mM [U-^{13}C]-glycerol
Conditions	Basal		1 mM [D$_5$]-glycerol
Replicates	3		10% D$_2$O
			5 mM [U-^{13}C]-glutamine
			2 mM [U-^{13}C]-acetate

m/z	[U13C]-Glycerol			[D5]-Glycerol			10% D2O			Theory
	2 hr	5 hr	8 hr	2 hr	5 hr	8 hr	2 hr	5 hr	8 hr	
287	42.5%	41.8%	48.8%	43.1%	42.2%	45.8%	56.9%	54.7%	53.7%	85.1%
288	7.3%	7.3%	8.5%	17.4%	18.0%	18.6%	31.2%	32.5%	33.0%	12.6%
289	3.0%	3.2%	3.3%	20.2%	20.8%	19.5%	9.6%	10.2%	10.6%	2.1%
290	29.5%	30.7%	26.2%	11.1%	11.1%	9.6%	2.1%	2.2%	2.3%	0.2%
291	4.0%	4.1%	3.5%	5.7%	5.4%	4.4%	0.2%	0.4%	0.3%	0.0%
292	1.8%	1.8%	1.4%	2.2%	2.1%	1.6%	0.0%	0.0%	0.0%	0.0%
293	10.9%	10.1%	7.6%	0.3%	0.5%	0.4%	0.0%	0.0%	0.0%	0.0%
294	0.9%	0.9%	0.6%	0.0%	0.1%	0.1%	0.0%	0.0%	0.0%	0.0%
295	0.1%	0.1%	0.1%	0.0%	0.0%	0.0%	0.0%	0.0%	0.0%	0.0%
296	0.0%	0.0%	0.0%	0.0%	0.0%	0.0%	0.0%	0.0%	0.0%	0.0%
314	43.1%	42.3%	49.4%	65.2%	64.5%	67.0%	65.0%	63.0%	62.6%	84.6%
315	7.5%	7.6%	8.8%	25.3%	25.8%	24.4%	27.4%	28.8%	29.1%	12.8%
316	14.0%	14.8%	13.2%	8.0%	8.1%	7.2%	6.5%	6.9%	7.1%	2.3%
317	19.7%	20.5%	17.3%	1.4%	1.4%	1.2%	1.0%	1.1%	1.1%	0.3%
318	3.3%	3.4%	2.8%	0.1%	0.1%	0.1%	0.1%	0.2%	0.1%	0.0%
319	11.1%	10.3%	7.7%	0.0%	0.0%	0.0%	0.0%	0.0%	0.0%	0.0%
320	1.0%	0.9%	0.7%	0.0%	0.0%	0.0%	0.0%	0.0%	0.0%	0.0%
321	0.2%	0.2%	0.1%	0.0%	0.0%	0.0%	0.0%	0.0%	0.0%	0.0%
gluc370 (M0)	41.6%	40.2%	47.3%	62.5%	62.1%	64.3%	62.0%	60.5%	60.1%	80.9%
gluc371 (M1)	9.3%	9.4%	10.6%	26.9%	27.2%	25.9%	29.1%	29.8%	30.3%	15.9%
gluc372 (M2)	14.0%	14.6%	13.1%	8.8%	8.8%	7.9%	7.6%	8.0%	7.9%	2.8%
gluc373 (M3)	19.2%	20.1%	17.1%	1.7%	1.8%	1.6%	1.3%	1.5%	1.5%	0.4%
gluc374 (M4)	4.1%	4.3%	3.4%	0.2%	0.3%	0.3%	0.1%	0.2%	0.2%	0.0%
gluc375 (M5)	10.5%	10.0%	7.4%	0.0%	0.0%	0.0%	0.0%	0.0%	0.0%	0.0%
gluc376 (M6)	1.4%	1.4%	1.0%	0.0%	0.0%	0.0%	0.0%	0.0%	0.0%	0.0%
gluc377 (M7)	0.1%	0.3%	0.1%	0.0%	0.0%	0.0%	0.0%	0.0%	0.0%	0.0%
gluc378 (M8)	0.0%	0.0%	0.0%	0.0%	0.0%	0.0%	0.0%	0.0%	0.0%	0.0%
gluc379 (M9)	0.0%	0.0%	0.0%	0.0%	0.0%	0.0%	0.0%	0.0%	0.0%	0.0%
gluc284 (M0)	43.0%	42.4%	49.7%	65.9%	65.2%	67.7%	70.4%	69.3%	69.0%	85.0%
gluc285 (M1)	18.5%	19.4%	18.7%	24.8%	25.6%	24.2%	23.7%	24.9%	25.1%	12.8%
gluc286 (M2)	6.9%	6.9%	6.1%	7.7%	7.7%	6.8%	5.0%	4.9%	4.9%	1.9%
gluc287 (M3)	18.9%	19.5%	16.4%	1.4%	1.5%	1.1%	0.9%	0.8%	0.9%	0.2%
gluc288 (M4)	12.7%	11.8%	9.0%	0.1%	0.1%	0.2%	0.0%	0.1%	0.1%	0.0%
gluc289 (M5)				0.0%	0.0%	0.0%	0.0%	0.0%	0.0%	0.0%

Attached Mouse Hepatocyte Experiment Details (9/30/2004 continued)

Experiment Date	9/30/2004	Fed/Fasted Animal	Fed
Incubation Time	2,5,8 hr	Tracers	1 mM [U-^{13}C]-glycerol
Conditions	Basal		1 mM [D$_5$]-glycerol
Replicates	3		10% D$_2$O
			5 mM [U-^{13}C]-glutamine
			2 mM [U-^{13}C]-acetate

m/z	[U13C]-Acetate 2 hr	5 hr	8 hr	[U13C]-Gln 2 hr	5 hr	8 hr	Unlabeled 2 hr	5 hr	8 hr	Theory
287	84.5%	84.0%	82.9%	43.9%	29.7%	23.5%	85.2%	84.5%	83.9%	85.1%
288	12.9%	13.0%	13.8%	9.9%	8.2%	7.7%	12.6%	13.0%	13.5%	12.6%
289	2.4%	2.6%	2.9%	11.0%	13.2%	13.8%	2.1%	2.2%	2.3%	2.1%
290	0.2%	0.3%	0.4%	20.2%	23.6%	24.3%	0.2%	0.2%	0.3%	0.2%
291	0.0%	0.0%	0.0%	5.0%	7.6%	9.1%	0.0%	0.0%	0.0%	0.0%
292	0.0%	0.0%	0.0%	5.0%	9.1%	11.1%	0.0%	0.0%	0.0%	0.0%
293	0.0%	0.0%	0.0%	4.6%	7.9%	9.4%	0.0%	0.0%	0.0%	0.0%
294	0.0%	0.0%	0.0%	0.4%	0.8%	0.9%	0.0%	0.0%	0.0%	0.0%
295	0.0%	0.0%	0.0%	0.0%	0.1%	0.1%	0.0%	0.0%	0.0%	0.0%
296	0.0%	0.0%	0.0%	0.0%	0.0%	0.0%	0.0%	0.0%	0.0%	0.0%
314	85.0%	84.3%	83.7%	45.5%	30.7%	25.4%	85.2%	84.9%	84.6%	84.6%
315	12.5%	12.8%	13.2%	13.2%	12.8%	12.5%	12.6%	12.8%	13.0%	12.8%
316	2.3%	2.7%	2.9%	18.2%	21.3%	21.8%	2.1%	2.1%	2.2%	2.3%
317	0.1%	0.2%	0.3%	12.1%	15.6%	17.1%	0.1%	0.1%	0.1%	0.3%
318	0.0%	0.0%	0.0%	5.7%	10.1%	12.0%	0.0%	0.0%	0.0%	0.0%
319	0.0%	0.0%	0.0%	4.9%	8.5%	9.9%	0.0%	0.0%	0.0%	0.0%
320	0.0%	0.0%	0.0%	0.4%	0.9%	1.0%	0.0%	0.0%	0.0%	0.0%
321	0.0%	0.0%	0.0%	0.1%	0.2%	0.2%	0.0%	0.0%	0.0%	0.0%
gluc370 (M0)	80.5%	80.3%	79.8%	43.3%	29.6%	24.2%	81.1%			80.9%
gluc371 (M1)	15.9%	16.1%	16.2%	14.8%	13.8%	13.1%	16.0%			15.9%
gluc372 (M2)	3.2%	3.2%	3.5%	17.9%	20.7%	21.4%	2.7%			2.8%
gluc373 (M3)	0.4%	0.4%	0.5%	12.2%	15.7%	17.4%	0.2%			0.4%
gluc374 (M4)	0.0%	0.0%	0.0%	6.2%	10.3%	12.3%	0.0%			0.0%
gluc375 (M5)	0.0%	0.0%	0.0%	5.0%	8.5%	10.0%	0.0%			0.0%
gluc376 (M6)	0.0%	0.0%	0.0%	0.6%	1.2%	1.4%	0.0%			0.0%
gluc377 (M7)	0.0%	0.0%	0.0%	0.0%	0.1%	0.2%	0.0%			0.0%
gluc378 (M8)	0.0%	0.0%	0.0%	0.0%	0.0%	0.0%	0.0%			0.0%
gluc379 (M9)	0.0%	0.0%	0.0%	0.0%	0.0%	0.0%	0.0%			0.0%
gluc284 (M0)	84.6%	84.4%	83.9%	49.1%	36.7%	31.6%	85.0%			85.0%
gluc285 (M1)	13.0%	13.0%	13.5%	21.4%	22.1%	21.9%	12.6%			12.8%
gluc286 (M2)	2.2%	2.2%	2.4%	10.4%	13.5%	15.1%	2.1%			1.9%
gluc287 (M3)	0.2%	0.3%	0.3%	13.2%	18.4%	20.5%	0.2%			0.2%
gluc288 (M4)	0.1%	0.1%	0.1%	6.0%	9.3%	10.9%	0.0%			0.0%
gluc289 (M5)	0.0%	0.0%	0.0%				0.0%			0.0%

Attached Mouse Hepatocyte Experiment Details (9/30/2004 continued)

Experiment Date	9/30/2004	Fed/Fasted Animal	Fed
Incubation Time	2,5,8 hr	Tracers	1 mM [U-^{13}C]-glycerol
Conditions	Basal		1 mM [D$_5$]-glycerol
Replicates	3		10% D$_2$O
			5 mM [U-^{13}C]-glutamine
			2 mM [U-^{13}C]-acetate

m/z	[U13C]-Glycerol			[D5]-Glycerol			10% D2O			Theory
	2 hr	5 hr	8 hr	2 hr	5 hr	8 hr	2 hr	5 hr	8 hr	
gluc259 (M0)	64.4%	64.6%	68.4%	62.4%	62.0%	64.6%	69.1%	68.0%	67.3%	86.2%
gluc260 (M1)	9.7%	9.5%	9.9%	13.2%	13.7%	13.9%	24.7%	25.6%	26.2%	11.8%
gluc261 (M2)	2.3%	2.2%	2.2%	18.2%	18.3%	16.4%	5.3%	5.4%	5.6%	1.8%
gluc262 (M3)	21.0%	21.2%	17.4%	5.1%	5.0%	4.3%	0.8%	0.9%	0.9%	0.2%
gluc263 (M4)	2.4%	2.2%	1.9%	1.0%	1.0%	0.8%	0.1%	0.1%	0.1%	0.0%
gluc264 (M5)	0.3%	0.3%	0.2%	0.1%	0.0%	0.0%	0.0%	0.0%	0.0%	0.0%
gluc265 (M6)	0.0%	0.0%	0.0%	0.0%	0.0%	0.0%	0.0%	0.0%	0.0%	0.0%
gluc173 (M0)	66.4%	66.4%	71.1%	69.3%	69.0%	71.3%	76.5%	75.7%	75.0%	90.6%
gluc174 (M1)	6.8%	6.7%	6.9%	8.3%	8.4%	8.6%	19.7%	20.7%	21.1%	8.3%
gluc175 (M2)	24.8%	25.0%	20.4%	19.7%	19.8%	17.6%	3.3%	3.2%	3.4%	1.1%
gluc176 (M3)	1.7%	1.7%	1.4%	2.5%	2.5%	2.2%	0.4%	0.4%	0.4%	0.1%
gluc177 (M4)	0.3%	0.2%	0.2%	0.3%	0.3%	0.2%	0.1%	0.0%	0.0%	0.0%
gluc178 (M5)	0.0%	0.0%	0.0%	0.0%	0.0%	0.0%	0.0%	0.0%	0.0%	0.0%
gluc301 (M0)							56.3%	54.1%	53.1%	84.2%
gluc302 (M1)							31.5%	32.8%	33.2%	13.4%
gluc303 (M2)							9.8%	10.5%	10.9%	2.2%
gluc304 (M3)							2.2%	2.3%	2.4%	0.2%
gluc305 (M4)							0.2%	0.4%	0.4%	0.0%
gluc306 (M5)							0.0%	0.0%	0.0%	0.0%
gluc307 (M6)							0.0%	0.0%	0.0%	0.0%
gluc308 (M7)							0.0%	0.0%	0.0%	0.0%
gluc309 (M8)							0.0%	0.0%	0.0%	0.0%
gluc310 (M9)							0.0%	0.0%	0.0%	0.0%
gluc311 (M10)							0.0%	0.0%	0.0%	0.0%
gluc312 (M11)							0.0%	0.0%	0.0%	0.0%
gluc313 (M12)							0.0%	0.0%	0.0%	0.0%
gluc145 (M0)							81.1%	80.2%	79.8%	92.5%
gluc146 (M1)							16.6%	17.6%	17.9%	6.7%
gluc147 (M2)							2.1%	2.1%	2.1%	0.8%
gluc148 (M3)							0.2%	0.2%	0.2%	0.0%
gluc149 (M4)							0.0%	0.0%	0.0%	0.0%

Mouse Hepatocyte Experiment Details

Experiment Date	12/13/2005	Fed/Fasted Animal	Fed	
Incubation Time	30 min	Tracers	1 mM [2-^{13}C]-glycerol	1 mM [U-^{13}C]-glycerol
Conditions	Basal		1 mM [D$_5$]-glycerol	10% D$_2$O
Replicates	3		1 mM [U-^{13}C, D$_5$]-glycerol (100% ,25%)	1 mM [U-^{13}C, D$_5$]-glycerol + 10% D$_2$O (100%, 25%)

	[2-13C]glycerol			[U-13C]glycerol			[D5]glycerol			
m/z	1	2	3	4	5	6	7	8	9	Theory
gluc370 (M0)	38.5%	38.5%	38.6%	39.6%	39.6%	39.6%	56.6%	56.7%	56.4%	80.9%
gluc371 (M1)	39.6%	39.5%	39.5%	9.1%	9.0%	9.0%	29.3%	29.2%	29.4%	15.9%
gluc372 (M2)	18.3%	18.3%	18.3%	14.1%	14.4%	14.2%	11.1%	11.1%	11.2%	2.8%
gluc373 (M3)	3.1%	3.1%	3.1%	22.0%	21.9%	22.0%	2.5%	2.5%	2.6%	0.4%
gluc374 (M4)	0.5%	0.5%	0.5%	4.4%	4.4%	4.4%	0.5%	0.5%	0.5%	0.0%
gluc375 (M5)	0.0%	0.0%	0.0%	9.3%	9.4%	9.4%	0.0%	0.0%	0.0%	0.0%
gluc376 (M6)	0.0%	0.0%	0.0%	1.3%	1.2%	1.3%	0.0%	0.0%	0.0%	0.0%
gluc377 (M7)	0.0%	0.0%	0.0%	0.2%	0.2%	0.2%	0.0%	0.0%	0.0%	0.0%
gluc378 (M8)	0.0%	0.0%	0.0%	0.0%	0.0%	0.0%	0.0%	0.0%	0.0%	0.0%
gluc379 (M9)	0.0%	0.0%	0.0%	0.0%	0.0%	0.0%	0.0%	0.0%	0.0%	0.0%
gluc284 (M0)	53.6%	53.6%	53.2%	41.5%	41.4%	41.3%	60.1%	59.7%	59.5%	85.0%
gluc285 (M1)	39.9%	39.8%	40.1%	18.6%	18.6%	18.6%	28.1%	28.3%	28.3%	12.8%
gluc286 (M2)	5.6%	5.8%	5.9%	6.2%	6.1%	6.3%	9.8%	9.8%	9.9%	1.9%
gluc287 (M3)	0.8%	0.9%	0.8%	21.2%	21.2%	21.3%	1.9%	1.9%	2.0%	0.2%
gluc288 (M4)	0.0%	0.0%	0.0%	11.1%	11.4%	11.2%	0.2%	0.3%	0.2%	0.0%
gluc289 (M5)	0.0%	0.0%	0.0%	1.3%	1.3%	1.2%	0.0%	0.0%	0.0%	0.0%
gluc259 (M0)	61.4%	61.2%	61.1%	65.4%	65.3%	65.3%	60.1%	59.9%	60.0%	86.2%
gluc260 (M1)	33.7%	33.7%	33.7%	9.5%	9.6%	9.6%	15.8%	15.8%	15.7%	11.8%
gluc261 (M2)	4.2%	4.3%	4.4%	2.3%	2.3%	2.3%	17.2%	17.3%	17.3%	1.8%
gluc262 (M3)	0.7%	0.7%	0.7%	20.3%	20.5%	20.6%	5.8%	5.9%	5.8%	0.2%
gluc263 (M4)	0.0%	0.0%	0.0%	2.1%	2.0%	2.0%	1.0%	0.9%	0.9%	0.0%
gluc264 (M5)	0.0%	0.0%	0.0%	0.3%	0.3%	0.3%	0.1%	0.1%	0.1%	0.0%
gluc265 (M6)	0.0%	0.0%	0.0%	0.0%	0.0%	0.0%	0.0%	0.0%	0.0%	0.0%
gluc173 (M0)	64.6%	64.6%	64.5%	67.6%	67.5%	67.5%	69.4%	69.1%	69.2%	90.6%
gluc174 (M1)	32.2%	32.3%	32.3%	6.6%	6.6%	6.6%	8.9%	9.0%	9.0%	8.3%
gluc175 (M2)	2.7%	2.8%	2.7%	23.9%	24.0%	24.0%	19.0%	19.2%	19.1%	1.1%
gluc176 (M3)	0.4%	0.4%	0.4%	1.7%	1.7%	1.7%	2.4%	2.4%	2.4%	0.1%
gluc177 (M4)	0.0%	0.0%	0.0%	0.2%	0.3%	0.2%	0.3%	0.3%	0.3%	0.0%
gluc178 (M5)	0.0%	0.0%	0.0%	0.0%	0.0%	0.0%	0.0%	0.0%	0.0%	0.0%
gluc301 (M0)	42.4%	39.9%	39.9%	41.0%	41.4%	40.9%	39.2%	39.0%	39.2%	84.2%
gluc302 (M1)	38.4%	39.8%	39.7%	7.5%	7.6%	7.5%	18.8%	18.9%	18.9%	13.4%
gluc303 (M2)	16.6%	17.4%	17.5%	3.2%	3.2%	3.2%	20.9%	21.0%	20.9%	2.2%
gluc304 (M3)	2.4%	2.5%	2.5%	32.0%	31.7%	32.0%	12.4%	12.4%	12.3%	0.2%
gluc305 (M4)	0.2%	0.4%	0.4%	4.5%	4.5%	4.5%	5.7%	5.7%	5.7%	0.0%
gluc306 (M5)	0.0%	0.0%	0.0%	1.6%	1.6%	1.6%	2.4%	2.3%	2.3%	0.0%
gluc307 (M6)	0.0%	0.0%	0.0%	9.2%	9.0%	9.2%	0.6%	0.6%	0.6%	0.0%
gluc308 (M7)	0.0%	0.0%	0.0%	0.9%	0.9%	0.9%	0.1%	0.1%	0.1%	0.0%
gluc309 (M8)	0.0%	0.0%	0.0%	0.2%	0.1%	0.1%	0.0%	0.0%	0.0%	0.0%
gluc310 (M9)	0.0%	0.0%	0.0%	0.0%	0.0%	0.0%	0.0%	0.0%	0.0%	0.0%
gluc311 (M10)	0.0%	0.0%	0.0%	0.0%	0.0%	0.0%	0.0%	0.0%	0.0%	0.0%
gluc312 (M11)	0.0%	0.0%	0.0%	0.0%	0.0%	0.0%	0.0%	0.0%	0.0%	0.0%
gluc313 (M12)	0.0%	0.0%	0.0%	0.0%	0.0%	0.0%	0.0%	0.0%	0.0%	0.0%
gluc145 (M0)	58.4%	58.5%	58.6%	60.2%	60.2%	60.1%	62.6%	62.5%	62.8%	92.5%
gluc146 (M1)	38.5%	38.5%	38.6%	6.5%	6.5%	6.5%	21.9%	22.0%	22.0%	6.7%
gluc147 (M2)	2.6%	2.5%	2.6%	31.2%	31.2%	31.2%	14.4%	14.4%	14.1%	0.8%
gluc148 (M3)	0.3%	0.3%	0.3%	2.1%	2.1%	2.1%	1.2%	1.2%	1.1%	0.0%
gluc149 (M4)	0.2%	0.2%	0.0%	0.1%	0.1%	0.2%	0.0%	0.0%	0.0%	0.0%
glycerol173 (M0)	4.0%	3.0%	4.3%	2.6%	2.9%	2.6%	2.1%	2.2%	2.0%	90.6%
glycerol174 (M1)	87.9%	88.8%	87.5%	0.0%	0.0%	0.0%	0.6%	0.6%	0.5%	8.3%
glycerol175 (M2)	6.7%	6.8%	6.7%	90.2%	89.9%	90.3%	0.4%	0.2%	0.2%	1.1%
glycerol176 (M3)	1.2%	1.3%	1.2%	6.1%	6.1%	6.1%	87.8%	87.7%	88.0%	0.1%
glycerol177 (M4)	0.1%	0.1%	0.2%	1.0%	1.0%	0.9%	7.8%	7.8%	7.9%	0.0%
glycerol178 (M5)	0.0%	0.0%	0.0%	0.1%	0.1%	0.1%	1.2%	1.3%	1.3%	0.0%
glycerol179 (M6)	0.0%	0.0%	0.0%	0.0%	0.0%	0.0%	0.1%	0.1%	0.1%	0.0%
glycerol180 (M7)	0.0%	0.0%	0.0%	0.0%	0.0%	0.0%	0.1%	0.1%	0.1%	0.0%

Mouse Hepatocyte Experiment Details (12/13/2005 continued)

Experiment Date	12/13/2005	Fed/Fasted	Fed	
Incubation Time	30 min	Tracers	1 mM [2-^{13}C]-glycerol	1 mM [U-^{13}C]-glycerol
Conditions	Basal		1 mM [D$_5$]-glycerol	10% D$_2$O
Replicates	3		1 mM [U-^{13}C, D$_5$]-glycerol (100% ,25%)	1 mM [U-^{13}C, D$_5$]-glycerol + 10% D$_2$O (100%, 25%)

m/z	[U-13C,D5]glycerol 10	11	12	25% [U-13C,D5]glycerol 13	14	15	10% D2O 16	17	18	Theory
gluc370 (M0)	37.4%	36.8%	37.2%	69.4%	69.6%	69.6%	58.5%	58.3%	58.4%	80.9%
gluc371 (M1)	11.4%	11.2%	11.2%	15.2%	15.1%	15.1%	31.1%	31.2%	31.1%	15.9%
gluc372 (M2)	11.4%	11.3%	11.3%	6.4%	6.5%	6.5%	8.5%	8.6%	8.6%	2.8%
gluc373 (M3)	10.7%	10.7%	10.7%	3.6%	3.6%	3.6%	1.7%	1.7%	1.7%	0.4%
gluc374 (M4)	11.6%	11.9%	11.8%	3.2%	3.2%	3.2%	0.2%	0.3%	0.2%	0.0%
gluc375 (M5)	9.0%	9.2%	9.1%	1.6%	1.5%	1.5%	0.0%	0.0%	0.0%	0.0%
gluc376 (M6)	5.6%	5.7%	5.7%	0.5%	0.4%	0.4%	0.0%	0.0%	0.0%	0.0%
gluc377 (M7)	2.4%	2.5%	2.5%	0.1%	0.1%	0.1%	0.0%	0.0%	0.0%	0.0%
gluc378 (M8)	0.6%	0.6%	0.6%	0.0%	0.0%	0.0%	0.0%	0.0%	0.0%	0.0%
gluc379 (M9)	0.1%	0.1%	0.1%	0.0%	0.0%	0.0%	0.0%	0.0%	0.0%	0.0%
gluc284 (M0)	39.3%	39.1%	39.1%	72.5%	72.7%	72.6%	68.4%	68.2%	68.1%	85.0%
gluc285 (M1)	20.5%	20.5%	20.5%	16.6%	16.6%	16.6%	25.7%	25.8%	26.0%	12.8%
gluc286 (M2)	6.7%	6.8%	6.7%	3.7%	3.7%	3.7%	5.1%	5.4%	5.2%	1.9%
gluc287 (M3)	8.6%	8.7%	8.6%	2.7%	2.6%	2.7%	0.8%	0.7%	0.7%	0.2%
gluc288 (M4)	14.7%	14.8%	14.9%	3.1%	3.0%	3.0%	0.0%	0.0%	0.0%	0.0%
gluc289 (M5)	10.2%	10.1%	10.3%	1.4%	1.4%	1.4%	0.0%	0.0%	0.0%	0.0%
gluc259 (M0)	55.6%	55.3%	55.6%	80.1%	80.0%	80.1%	64.4%	64.3%	64.4%	86.2%
gluc260 (M1)	14.9%	14.8%	14.8%	12.5%	12.5%	12.3%	28.1%	28.1%	28.2%	11.8%
gluc261 (M2)	4.5%	4.6%	4.6%	2.1%	2.1%	2.1%	6.4%	6.4%	6.3%	1.8%
gluc262 (M3)	2.2%	2.2%	2.2%	0.4%	0.4%	0.4%	1.0%	1.1%	1.0%	0.2%
gluc263 (M4)	2.1%	2.2%	2.1%	0.3%	0.3%	0.3%	0.0%	0.0%	0.1%	0.0%
gluc264 (M5)	15.8%	16.0%	15.8%	3.7%	3.7%	3.7%	0.0%	0.0%	0.0%	0.0%
gluc265 (M6)	4.9%	5.0%	4.9%	1.0%	1.0%	1.0%	0.0%	0.0%	0.0%	0.0%
gluc173 (M0)	67.1%	66.8%	67.0%	85.8%	85.8%	85.8%	72.3%	72.2%	72.3%	90.6%
gluc174 (M1)	7.4%	7.5%	7.4%	8.0%	7.9%	8.0%	23.4%	23.5%	23.4%	8.3%
gluc175 (M2)	1.4%	1.4%	1.4%	1.1%	1.2%	1.1%	3.8%	3.8%	3.8%	1.1%
gluc176 (M3)	1.8%	1.9%	1.8%	0.4%	0.5%	0.4%	0.4%	0.4%	0.4%	0.1%
gluc177 (M4)	20.1%	20.3%	20.2%	4.2%	4.2%	4.2%	0.0%	0.0%	0.0%	0.0%
gluc178 (M5)	2.1%	2.1%	2.1%	0.5%	0.5%	0.5%	0.0%	0.0%	0.0%	0.0%
gluc301 (M0)	35.2%	35.0%	35.4%	71.2%	71.1%	71.2%	50.2%	50.4%	50.2%	84.2%
gluc302 (M1)	9.8%	9.7%	9.9%	13.0%	13.1%	13.1%	34.7%	34.5%	34.6%	13.4%
gluc303 (M2)	2.5%	2.5%	2.5%	2.5%	2.6%	2.5%	11.9%	11.9%	11.9%	2.2%
gluc304 (M3)	3.0%	3.0%	3.0%	1.3%	1.3%	1.3%	2.7%	2.7%	2.7%	0.2%
gluc305 (M4)	8.7%	8.8%	8.7%	2.8%	2.9%	2.8%	0.5%	0.5%	0.5%	0.0%
gluc306 (M5)	17.9%	18.0%	17.8%	6.1%	6.0%	6.0%	0.1%	0.0%	0.1%	0.0%
gluc307 (M6)	8.4%	8.4%	8.4%	2.3%	2.3%	2.3%	0.0%	0.0%	0.0%	0.0%
gluc308 (M7)	2.2%	2.1%	2.1%	0.4%	0.4%	0.4%	0.0%	0.0%	0.0%	0.0%
gluc309 (M8)	1.9%	2.0%	1.9%	0.1%	0.1%	0.1%	0.0%	0.0%	0.0%	0.0%
gluc310 (M9)	3.9%	3.9%	3.9%	0.2%	0.2%	0.2%	0.0%	0.0%	0.0%	0.0%
gluc311 (M10)	4.1%	4.2%	4.1%	0.2%	0.2%	0.2%	0.0%	0.0%	0.0%	0.0%
gluc312 (M11)	2.0%	2.0%	2.0%	0.1%	0.1%	0.0%	0.0%	0.0%	0.0%	0.0%
gluc313 (M12)	0.5%	0.5%	0.5%	0.0%	0.0%	0.0%	0.0%	0.0%	0.0%	0.0%
gluc145 (M0)	48.7%	49.2%	48.9%	82.5%	82.3%	82.4%	79.1%	78.8%	78.9%	92.5%
gluc146 (M1)	8.7%	8.8%	8.8%	7.7%	7.7%	7.7%	18.5%	18.8%	18.7%	6.7%
gluc147 (M2)	10.9%	11.0%	10.9%	3.0%	3.0%	2.9%	2.2%	2.2%	2.2%	0.8%
gluc148 (M3)	19.1%	19.1%	19.1%	4.2%	4.2%	4.1%	0.2%	0.2%	0.2%	0.0%
gluc149 (M4)	12.6%	12.0%	12.3%	2.7%	2.8%	2.8%	0.0%	0.0%	0.0%	0.0%
glycerol173 (M0	2.4%	2.4%	2.0%	67.6%	68.5%	67.7%	90.5%	90.5%	90.4%	90.6%
glycerol174 (M1	0.4%	0.4%	0.4%	6.1%	6.2%	6.1%	8.2%	8.2%	8.2%	8.3%
glycerol175 (M2	0.2%	0.2%	0.2%	0.9%	0.9%	0.9%	1.2%	1.2%	1.2%	1.1%
glycerol176 (M3	0.3%	0.3%	0.3%	0.1%	0.1%	0.1%	0.1%	0.1%	0.1%	0.1%
glycerol177 (M4	2.1%	2.1%	2.1%	0.7%	0.6%	0.7%	0.1%	0.1%	0.1%	0.0%
glycerol178 (M5	87.8%	87.8%	88.2%	22.8%	22.0%	22.6%	0.0%	0.0%	0.0%	0.0%
glycerol179 (M6	5.8%	5.8%	5.9%	1.5%	1.5%	1.5%	0.0%	0.0%	0.0%	0.0%
glycerol180 (M7	1.0%	1.0%	1.0%	0.3%	0.3%	0.3%	0.0%	0.0%	0.0%	0.0%

Mouse Hepatocyte Experiment Details (12/13/2005 continued)

Experiment Date	12/13/2005	Fed/Fasted Animal	Fed	
Incubation Time	30 min	Tracers	1 mM [2-^{13}C]-glycerol	1 mM [U-^{13}C]-glycerol
Conditions	Basal		1 mM [D$_5$]-glycerol	10% D$_2$O
Replicates	3		1 mM [U-^{13}C, D$_5$]-glycerol (100% ,25%)	1 mM [U-^{13}C, D$_5$]-glycerol + 10% D$_2$O (100%, 25%)

m/z	[U-13C,D5]glycerol + 10% D2O			25% [U-13C,D5]glycerol + 10% D2O			unlabeled	unlabeled	[6,6-D]Fruct	Theory
	19	20	21	22	23	24	25	26	27	
gluc370 (M0)	28.8%	28.8%	28.9%	50.4%	50.4%	50.3%	81.2%	81.2%	78.2%	80.9%
gluc371 (M1)	18.1%	18.4%	18.3%	27.8%	27.7%	27.7%	15.6%	15.6%	17.9%	15.9%
gluc372 (M2)	11.7%	11.8%	11.7%	10.4%	10.4%	10.4%	2.9%	2.9%	3.4%	2.8%
gluc373 (M3)	10.4%	10.4%	10.4%	4.8%	4.8%	4.9%	0.4%	0.4%	0.5%	0.4%
gluc374 (M4)	11.6%	11.4%	11.5%	3.6%	3.6%	3.7%	0.0%	0.0%	0.0%	0.0%
gluc375 (M5)	9.4%	9.4%	9.3%	2.1%	2.2%	2.1%	0.0%	0.0%	0.0%	0.0%
gluc376 (M6)	6.0%	5.8%	5.9%	0.7%	0.7%	0.8%	0.0%	0.0%	0.0%	0.0%
gluc377 (M7)	3.1%	3.0%	3.0%	0.2%	0.2%	0.2%	0.0%	0.0%	0.0%	0.0%
gluc378 (M8)	1.0%	0.9%	1.0%	0.0%	0.0%	0.0%	0.0%	0.0%	0.0%	0.0%
gluc379 (M9)	0.1%	0.1%	0.2%	0.0%	0.0%	0.0%	0.0%	0.0%	0.0%	0.0%
gluc284 (M0)	34.5%	34.3%	34.3%	58.5%	58.4%	58.4%	85.1%	85.1%	82.2%	85.0%
gluc285 (M1)	24.2%	24.4%	24.2%	26.5%	26.6%	26.5%	12.6%	12.6%	15.2%	12.8%
gluc286 (M2)	9.8%	9.8%	9.8%	7.0%	7.1%	7.0%	2.0%	2.1%	2.4%	1.9%
gluc287 (M3)	7.9%	7.9%	7.8%	3.0%	3.0%	3.1%	0.2%	0.2%	0.2%	0.2%
gluc288 (M4)	13.0%	13.1%	13.2%	3.2%	3.1%	3.2%	0.0%	0.0%	0.0%	0.0%
gluc289 (M5)	10.7%	10.6%	10.7%	1.8%	1.8%	1.8%	0.0%	0.0%	0.0%	0.0%
gluc259 (M0)	43.6%	43.8%	43.6%	60.5%	60.4%	60.5%	86.5%	86.3%	75.6%	86.2%
gluc260 (M1)	24.8%	24.9%	24.9%	27.0%	27.1%	27.0%	11.4%	11.6%	10.5%	11.8%
gluc261 (M2)	8.3%	8.2%	8.2%	6.3%	6.3%	6.3%	1.9%	1.9%	12.1%	1.8%
gluc262 (M3)	2.9%	2.9%	2.9%	1.2%	1.2%	1.2%	0.2%	0.2%	1.6%	0.2%
gluc263 (M4)	1.9%	1.9%	1.8%	0.4%	0.4%	0.4%	0.0%	0.0%	0.2%	0.0%
gluc264 (M5)	12.2%	12.1%	12.3%	3.2%	3.2%	3.2%	0.0%	0.0%	0.0%	0.0%
gluc265 (M6)	6.3%	6.3%	6.3%	1.5%	1.5%	1.5%	0.0%	0.0%	0.0%	0.0%
gluc173 (M0)	54.2%	54.2%	54.2%	68.7%	68.7%	68.7%	90.7%	90.7%	79.6%	90.6%
gluc174 (M1)	20.0%	20.0%	20.0%	22.1%	22.2%	22.2%	8.1%	8.1%	7.5%	8.3%
gluc175 (M2)	3.8%	3.8%	3.8%	3.6%	3.6%	3.6%	1.1%	1.1%	11.7%	1.1%
gluc176 (M3)	1.8%	1.8%	1.8%	0.8%	0.8%	0.8%	0.1%	0.1%	1.0%	0.1%
gluc177 (M4)	16.6%	16.5%	16.5%	3.9%	3.9%	3.9%	0.0%	0.0%	0.1%	0.0%
gluc178 (M5)	3.7%	3.8%	3.8%	0.9%	0.9%	0.9%	0.0%	0.1%	0.0%	0.0%
gluc301 (M0)	21.8%	21.8%	22.0%	42.6%	42.4%	42.5%	84.4%	84.1%	68.0%	84.2%
gluc302 (M1)	18.4%	18.4%	18.4%	30.1%	30.2%	30.1%	13.2%	13.4%	14.1%	13.4%
gluc303 (M2)	8.0%	8.1%	8.1%	10.8%	10.9%	10.8%	2.2%	2.4%	14.3%	2.2%
gluc304 (M3)	3.7%	3.7%	3.7%	3.2%	3.2%	3.2%	0.2%	0.1%	2.7%	0.2%
gluc305 (M4)	6.2%	6.3%	6.2%	2.6%	2.6%	2.6%	0.0%	0.0%	0.9%	0.0%
gluc306 (M5)	14.0%	14.0%	14.0%	5.1%	5.1%	5.1%	0.0%	0.0%	0.1%	0.0%
gluc307 (M6)	11.4%	11.4%	11.4%	3.6%	3.6%	3.6%	0.0%	0.0%	0.0%	0.0%
gluc308 (M7)	4.6%	4.6%	4.6%	1.2%	1.3%	1.2%	0.0%	0.0%	0.0%	0.0%
gluc309 (M8)	2.1%	2.0%	2.0%	0.3%	0.3%	0.3%	0.0%	0.0%	0.0%	0.0%
gluc310 (M9)	2.9%	2.9%	2.9%	0.2%	0.2%	0.2%	0.0%	0.0%	0.0%	0.0%
gluc311 (M10)	3.8%	3.7%	3.7%	0.2%	0.2%	0.2%	0.0%	0.0%	0.0%	0.0%
gluc312 (M11)	2.5%	2.4%	2.4%	0.1%	0.1%	0.1%	0.0%	0.0%	0.0%	0.0%
gluc313 (M12)	0.8%	0.8%	0.8%	0.0%	0.0%	0.0%	0.0%	0.0%	0.0%	0.0%
gluc145 (M0)	43.6%	43.7%	43.7%	69.7%	69.6%	69.9%	92.4%	92.5%	85.0%	92.5%
gluc146 (M1)	15.3%	15.4%	15.2%	18.2%	18.4%	18.2%	6.7%	6.7%	9.9%	6.7%
gluc147 (M2)	9.9%	9.9%	10.0%	4.2%	4.2%	4.2%	0.9%	0.8%	4.8%	0.8%
gluc148 (M3)	17.5%	17.5%	17.6%	4.5%	4.4%	4.4%	0.0%	0.0%	0.4%	0.0%
gluc149 (M4)	13.7%	13.5%	13.5%	3.4%	3.5%	3.3%	0.0%	0.0%	0.0%	0.0%
glycerol173 (M0	2.2%	2.2%	2.3%	65.5%	65.4%	65.1%	90.6%	90.7%	90.6%	90.6%
glycerol174 (M1	0.5%	0.5%	0.4%	6.1%	6.1%	6.1%	8.1%	8.0%	8.0%	8.3%
glycerol175 (M2	0.3%	0.2%	0.2%	1.0%	0.9%	0.9%	1.2%	1.2%	1.3%	1.1%
glycerol176 (M3	0.3%	0.3%	0.3%	0.2%	0.2%	0.2%	0.1%	0.1%	0.1%	0.1%
glycerol177 (M4	1.9%	2.1%	2.2%	0.8%	0.8%	0.8%	0.1%	0.0%	0.0%	0.0%
glycerol178 (M5	88.0%	88.0%	87.8%	24.6%	24.8%	25.0%	0.0%	0.0%	0.0%	0.0%
glycerol179 (M6	5.9%	5.8%	5.9%	1.7%	1.7%	1.7%	0.0%	0.0%	0.0%	0.0%
glycerol180 (M7	1.0%	1.0%	1.0%	0.3%	0.3%	0.3%	0.0%	0.0%	0.0%	0.0%

Mouse Hepatocyte Experiment Details

Experiment Date	12/16/2005	Fed/Fasted	Fasted	
Incubation Time	30 min	Tracers	1 mM [2-^{13}C]-glycerol	1 mM [U-^{13}C]-glycerol
Conditions	Basal		1 mM [D$_5$]-glycerol	10% D$_2$O
Replicates	3		1 mM [U-^{13}C, D$_5$]-glycerol (100% ,25%)	1 mM [U-^{13}C, D$_5$]-glycerol + 10% D$_2$O (100%, 25%)

m/z	[2-13C]glycerol			[U-13C]glycerol			[D5]glycerol			Theory
	1	2	3	4	5	6	7	8	9	
gluc370 (M0)	59.7%	59.8%	60.0%	58.2%	58.3%	58.4%	70.3%	70.1%	70.3%	80.9%
gluc371 (M1)	28.2%	28.1%	27.9%	11.8%	11.8%	11.8%	22.1%	22.2%	22.1%	15.9%
gluc372 (M2)	10.2%	10.2%	10.2%	10.4%	10.4%	10.4%	6.2%	6.3%	6.3%	2.8%
gluc373 (M3)	1.7%	1.7%	1.7%	11.1%	11.1%	11.0%	1.2%	1.2%	1.2%	0.4%
gluc374 (M4)	0.3%	0.3%	0.2%	2.2%	2.2%	2.2%	0.2%	0.2%	0.1%	0.0%
gluc375 (M5)	0.0%	0.0%	0.0%	5.5%	5.5%	5.4%	0.0%	0.0%	0.0%	0.0%
gluc376 (M6)	0.0%	0.0%	0.0%	0.7%	0.8%	0.7%	0.0%	0.0%	0.0%	0.0%
gluc377 (M7)	0.0%	0.0%	0.0%	0.1%	0.1%	0.1%	0.0%	0.0%	0.0%	0.0%
gluc378 (M8)	0.0%	0.0%	0.0%	0.0%	0.0%	0.0%	0.0%	0.0%	0.0%	0.0%
gluc379 (M9)	0.0%	0.0%	0.0%	0.0%	0.0%	0.0%	0.0%	0.0%	0.0%	0.0%
gluc284 (M0)	70.2%	70.4%	70.5%	60.5%	60.4%	60.6%	73.9%	73.5%	73.6%	85.0%
gluc285 (M1)	25.4%	25.3%	25.3%	17.0%	17.2%	17.1%	20.0%	20.2%	20.2%	12.8%
gluc286 (M2)	3.8%	3.8%	3.7%	4.6%	4.6%	4.5%	5.1%	5.2%	5.2%	1.9%
gluc287 (M3)	0.6%	0.6%	0.6%	10.6%	10.6%	10.5%	1.0%	1.0%	1.0%	0.2%
gluc288 (M4)	0.0%	0.0%	0.0%	6.6%	6.5%	6.5%	0.0%	0.1%	0.1%	0.0%
gluc289 (M5)	0.0%	0.0%	0.0%	0.8%	0.8%	0.7%	0.0%	0.0%	0.0%	0.0%
gluc259 (M0)	72.9%	73.1%	73.0%	72.3%	72.4%	72.5%	71.0%	70.8%	70.9%	86.2%
gluc260 (M1)	23.4%	23.2%	23.2%	10.3%	10.3%	10.3%	13.3%	13.4%	13.3%	11.8%
gluc261 (M2)	3.2%	3.2%	3.2%	2.1%	2.1%	2.1%	11.7%	11.6%	11.5%	1.8%
gluc262 (M3)	0.5%	0.5%	0.5%	13.6%	13.5%	13.4%	3.4%	3.4%	3.4%	0.2%
gluc263 (M4)	0.0%	0.1%	0.1%	1.5%	1.5%	1.5%	0.7%	0.7%	0.7%	0.0%
gluc264 (M5)	0.0%	0.0%	0.0%	0.2%	0.2%	0.3%	0.1%	0.1%	0.1%	0.0%
gluc265 (M6)	0.0%	0.0%	0.0%	0.0%	0.0%	0.1%	0.0%	0.0%	0.0%	0.0%
gluc173 (M0)	76.8%	76.9%	77.0%	75.9%	76.0%	76.0%	77.0%	77.1%	77.3%	90.6%
gluc174 (M1)	20.9%	20.8%	20.8%	7.2%	7.1%	7.1%	8.8%	8.8%	8.7%	8.3%
gluc175 (M2)	2.0%	2.0%	2.0%	15.8%	15.6%	15.6%	12.6%	12.6%	12.4%	1.1%
gluc176 (M3)	0.3%	0.3%	0.2%	1.1%	1.1%	1.1%	1.4%	1.4%	1.4%	0.1%
gluc177 (M4)	0.0%	0.0%	0.0%	0.2%	0.2%	0.2%	0.2%	0.2%	0.2%	0.0%
gluc178 (M5)	0.0%	0.0%	0.0%	0.0%	0.0%	0.0%	0.0%	0.0%	0.0%	0.0%
gluc301 (M0)	62.2%	62.1%	62.2%	60.1%	60.6%	60.3%	60.0%	58.9%	60.1%	84.2%
gluc302 (M1)	27.0%	27.0%	26.8%	10.0%	10.3%	10.0%	16.1%	16.0%	16.0%	13.4%
gluc303 (M2)	9.4%	9.5%	9.4%	2.7%	2.9%	2.7%	13.0%	13.3%	12.9%	2.2%
gluc304 (M3)	1.3%	1.3%	1.3%	17.6%	16.9%	17.5%	6.5%	6.8%	6.4%	0.2%
gluc305 (M4)	0.2%	0.1%	0.2%	2.5%	2.5%	2.5%	3.0%	3.3%	3.1%	0.0%
gluc306 (M5)	0.0%	0.0%	0.0%	0.9%	1.0%	0.9%	1.2%	1.3%	1.2%	0.0%
gluc307 (M6)	0.0%	0.0%	0.0%	5.5%	5.3%	5.5%	0.2%	0.3%	0.3%	0.0%
gluc308 (M7)	0.0%	0.0%	0.0%	0.6%	0.5%	0.5%	0.0%	0.0%	0.0%	0.0%
gluc309 (M8)	0.0%	0.0%	0.0%	0.1%	0.1%	0.1%	0.0%	0.0%	0.0%	0.0%
gluc310 (M9)	0.0%	0.0%	0.0%	0.0%	0.0%	0.0%	0.0%	0.0%	0.0%	0.0%
gluc311 (M10)	0.0%	0.0%	0.0%	0.0%	0.0%	0.0%	0.0%	0.0%	0.0%	0.0%
gluc312 (M11)	0.0%	0.0%	0.0%	0.0%	0.0%	0.0%	0.0%	0.0%	0.0%	0.0%
gluc313 (M12)	0.0%	0.0%	0.0%	0.0%	0.0%	0.0%	0.0%	0.0%	0.0%	0.0%
gluc145 (M0)	77.1%	77.2%	77.5%	75.5%	75.5%	75.7%	77.7%	77.6%	77.9%	92.5%
gluc146 (M1)	21.1%	21.0%	20.7%	6.7%	6.7%	6.7%	14.1%	14.1%	14.0%	6.7%
gluc147 (M2)	1.7%	1.6%	1.6%	16.6%	16.6%	16.5%	7.6%	7.6%	7.5%	0.8%
gluc148 (M3)	0.2%	0.2%	0.2%	1.2%	1.1%	1.2%	0.6%	0.6%	0.6%	0.0%
gluc149 (M4)	0.0%	0.0%	0.0%	0.1%	0.0%	0.0%	0.0%	0.0%	0.0%	0.0%
glycerol173 (M0)	8.6%	8.5%	8.7%	7.1%	7.0%	7.2%	4.9%	4.7%	5.0%	90.6%
glycerol174 (M1)	83.7%	83.8%	83.6%	0.0%	0.0%	0.0%	2.2%	2.1%	2.2%	8.3%
glycerol175 (M2)	6.4%	6.5%	6.5%	86.0%	86.2%	86.0%	1.2%	1.3%	1.4%	1.1%
glycerol176 (M3)	1.2%	1.2%	1.2%	5.8%	5.8%	5.8%	83.0%	83.3%	82.8%	0.1%
glycerol177 (M4)	0.1%	0.1%	0.1%	0.9%	0.9%	0.9%	7.4%	7.4%	7.3%	0.0%
glycerol178 (M5)	0.0%	0.0%	0.0%	0.1%	0.1%	0.1%	1.2%	1.2%	1.2%	0.0%
glycerol179 (M6)	0.0%	0.0%	0.0%	0.0%	0.0%	0.0%	0.0%	0.1%	0.1%	0.0%
glycerol180 (M7)	0.0%	0.0%	0.0%	0.0%	0.0%	0.0%	0.0%	0.0%	0.0%	0.0%

Mouse Hepatocyte Experiment Details (12/16/2005 continued)

Experiment Date	12/16/2005	Fed/Fasted	Fasted	
Incubation Time	30 min	Tracers	1 mM [2-^{13}C]-glycerol	1 mM [U-^{13}C]-glycerol
Conditions	Basal		1 mM [D$_5$]-glycerol	10% D$_2$O
Replicates	3		1 mM [U-^{13}C, D$_5$]-glycerol (100% ,25%)	1 mM [U-^{13}C, D$_5$]-glycerol + 10% D$_2$O (100%, 25%)

m/z	[U-13C,D5]glycerol			25% [U-13C,D5]glycerol			10% D2O			Theory
	10	11	12	13	14	15	16	17	18	
gluc370 (M0)	58.6%	58.3%	58.5%	75.1%	75.2%	75.1%	68.5%	68.0%	68.3%	80.9%
gluc371 (M1)	13.2%	13.2%	13.2%	15.3%	15.3%	15.3%	24.4%	24.7%	24.5%	15.9%
gluc372 (M2)	8.6%	8.8%	8.7%	5.1%	5.1%	5.1%	6.0%	6.1%	6.0%	2.8%
gluc373 (M3)	6.1%	6.2%	6.1%	2.2%	2.1%	2.1%	1.1%	1.1%	1.1%	0.4%
gluc374 (M4)	5.4%	5.4%	5.4%	1.5%	1.5%	1.5%	0.1%	0.1%	0.1%	0.0%
gluc375 (M5)	4.1%	4.1%	4.1%	0.6%	0.7%	0.7%	0.0%	0.0%	0.0%	0.0%
gluc376 (M6)	2.8%	2.8%	2.8%	0.1%	0.2%	0.1%	0.0%	0.0%	0.0%	0.0%
gluc377 (M7)	1.1%	1.1%	1.1%	0.0%	0.0%	0.0%	0.0%	0.0%	0.0%	0.0%
gluc378 (M8)	0.2%	0.2%	0.2%	0.0%	0.0%	0.0%	0.0%	0.0%	0.0%	0.0%
gluc379 (M9)	0.0%	0.0%	0.0%	0.0%	0.0%	0.0%	0.0%	0.0%	0.0%	0.0%
gluc284 (M0)	60.6%	60.3%	60.9%	78.3%	78.3%	78.2%	75.2%	74.7%	75.1%	85.0%
gluc285 (M1)	18.1%	18.3%	18.1%	15.1%	15.1%	15.1%	20.3%	20.7%	20.4%	12.8%
gluc286 (M2)	4.7%	4.9%	4.8%	2.9%	2.9%	2.9%	3.8%	3.9%	3.8%	1.9%
gluc287 (M3)	4.8%	4.8%	4.7%	1.6%	1.6%	1.6%	0.6%	0.6%	0.6%	0.2%
gluc288 (M4)	7.3%	7.2%	7.1%	1.5%	1.5%	1.5%	0.0%	0.0%	0.0%	0.0%
gluc289 (M5)	4.5%	4.5%	4.4%	0.6%	0.6%	0.6%	0.0%	0.0%	0.0%	0.0%
gluc259 (M0)	68.6%	68.4%	68.6%	82.5%	82.4%	82.5%	76.2%	75.4%	75.6%	86.2%
gluc260 (M1)	12.8%	12.9%	12.9%	12.0%	12.0%	12.0%	19.3%	19.8%	19.7%	11.8%
gluc261 (M2)	3.3%	3.3%	3.2%	2.0%	2.0%	2.0%	3.8%	4.0%	4.0%	1.8%
gluc262 (M3)	1.4%	1.4%	1.3%	0.3%	0.3%	0.3%	0.6%	0.6%	0.6%	0.2%
gluc263 (M4)	1.7%	1.7%	1.7%	0.4%	0.4%	0.4%	0.1%	0.1%	0.1%	0.0%
gluc264 (M5)	9.6%	9.6%	9.5%	2.3%	2.3%	2.3%	0.0%	0.0%	0.0%	0.0%
gluc265 (M6)	2.7%	2.8%	2.7%	0.5%	0.6%	0.6%	0.0%	0.0%	0.0%	0.0%
gluc173 (M0)	76.7%	76.4%	76.6%	87.6%	87.6%	87.6%	82.6%	81.9%	82.2%	90.6%
gluc174 (M1)	7.6%	7.6%	7.6%	8.0%	8.0%	8.0%	14.9%	15.5%	15.3%	8.3%
gluc175 (M2)	1.4%	1.4%	1.4%	1.2%	1.2%	1.2%	2.2%	2.3%	2.3%	1.1%
gluc176 (M3)	1.5%	1.5%	1.5%	0.4%	0.4%	0.4%	0.2%	0.2%	0.2%	0.1%
gluc177 (M4)	11.7%	11.9%	11.7%	2.6%	2.6%	2.6%	0.0%	0.0%	0.0%	0.0%
gluc178 (M5)	1.1%	1.1%	1.1%	0.3%	0.3%	0.3%	0.0%	0.0%	0.0%	0.0%
gluc301 (M0)	56.7%	57.4%	57.9%	77.3%	77.3%	77.3%	66.0%	65.0%	65.9%	84.2%
gluc302 (M1)	11.0%	11.2%	11.2%	13.1%	13.1%	13.1%	25.2%	25.8%	25.3%	13.4%
gluc303 (M2)	2.4%	2.3%	2.4%	2.4%	2.4%	2.4%	7.1%	7.5%	7.2%	2.2%
gluc304 (M3)	1.9%	2.0%	2.0%	0.9%	0.9%	0.9%	1.5%	1.6%	1.5%	0.2%
gluc305 (M4)	4.9%	4.9%	4.8%	1.6%	1.6%	1.6%	0.2%	0.2%	0.2%	0.0%
gluc306 (M5)	10.4%	10.2%	10.0%	3.4%	3.4%	3.3%	0.0%	0.0%	0.0%	0.0%
gluc307 (M6)	4.4%	4.1%	4.1%	1.1%	1.1%	1.1%	0.0%	0.0%	0.0%	0.0%
gluc308 (M7)	1.1%	1.1%	1.1%	0.1%	0.2%	0.2%	0.0%	0.0%	0.0%	0.0%
gluc309 (M8)	1.2%	1.2%	1.2%	0.0%	0.0%	0.0%	0.0%	0.0%	0.0%	0.0%
gluc310 (M9)	2.3%	2.2%	2.2%	0.0%	0.1%	0.0%	0.0%	0.0%	0.0%	0.0%
gluc311 (M10)	2.5%	2.2%	2.2%	0.0%	0.0%	0.0%	0.0%	0.0%	0.0%	0.0%
gluc312 (M11)	1.1%	1.0%	0.9%	0.0%	0.0%	0.0%	0.0%	0.0%	0.0%	0.0%
gluc313 (M12)	0.1%	0.2%	0.1%	0.0%	0.0%	0.0%	0.0%	0.0%	0.0%	0.0%
gluc145 (M0)	68.6%	68.5%	68.8%	87.2%	87.2%	87.2%	84.5%	84.5%	84.3%	92.5%
gluc146 (M1)	8.4%	8.4%	8.4%	7.4%	7.4%	7.4%	13.7%	13.7%	13.9%	6.7%
gluc147 (M2)	6.9%	6.8%	6.8%	2.1%	2.1%	2.1%	1.7%	1.6%	1.7%	0.8%
gluc148 (M3)	9.6%	9.6%	9.5%	2.0%	2.0%	2.0%	0.2%	0.1%	0.1%	0.0%
gluc149 (M4)	6.5%	6.6%	6.5%	1.3%	1.3%	1.3%	0.0%	0.0%	0.0%	0.0%
glycerol173 (M0)	4.8%	4.6%	4.8%	69.3%	69.1%	69.1%	89.7%	89.8%	89.8%	90.6%
glycerol174 (M1)	1.6%	1.5%	1.6%	6.6%	6.6%	6.6%	9.0%	8.9%	8.9%	8.3%
glycerol175 (M2)	0.9%	0.8%	0.9%	1.1%	1.1%	1.1%	1.3%	1.3%	1.3%	1.1%
glycerol176 (M3)	0.9%	0.8%	0.8%	0.3%	0.3%	0.3%	0.1%	0.1%	0.1%	0.1%
glycerol177 (M4)	2.5%	2.4%	2.6%	0.7%	0.7%	0.6%	0.0%	0.0%	0.0%	0.0%
glycerol178 (M5)	83.8%	84.2%	83.8%	20.8%	20.9%	21.0%	0.0%	0.0%	0.0%	0.0%
glycerol179 (M6)	5.6%	5.6%	5.6%	1.3%	1.3%	1.3%	0.0%	0.0%	0.0%	0.0%
glycerol180 (M7)	0.0%	0.0%	0.0%	0.0%	0.0%	0.0%	0.0%	0.0%	0.0%	0.0%

Mouse Hepatocyte Experiment Details (12/16/2005 continued)

Experiment Date	12/16/2005	Fed/Fasted Animal	Fasted	
Incubation Time	30 min	Tracers	1 mM [2-^{13}C]-glycerol	1 mM [U-^{13}C]-glycerol
Conditions	Basal		1 mM [D$_5$]-glycerol	10% D$_2$O
Replicates	3		1 mM [U-^{13}C, D$_5$]-glycerol (100% ,25%)	1 mM [U-^{13}C, D$_5$]-glycerol + 10% D$_2$O (100%, 25%)

| m/z | [U-13C,D5]glycerol + 10% D2O | | | 25% [U-13C,D5]glycerol + 10% D2O | | | unlabeled | unlabeled | [6,6-D]Fruct | |
	19	20	21	22	23	24	25	26	27	
gluc370 (M0)	54.8%	53.6%	54.8%	64.5%	64.5%	64.3%	81.2%	81.1%	78.8%	80.9%
gluc371 (M1)	17.3%	17.4%	17.3%	22.6%	22.5%	22.5%	15.6%	15.6%	17.5%	15.9%
gluc372 (M2)	8.2%	8.3%	8.1%	7.2%	7.2%	7.2%	2.9%	2.9%	3.3%	2.8%
gluc373 (M3)	5.8%	6.2%	5.8%	2.9%	2.9%	2.8%	0.3%	0.3%	0.4%	0.4%
gluc374 (M4)	5.2%	5.4%	5.2%	1.7%	1.8%	1.8%	0.0%	0.0%	0.0%	0.0%
gluc375 (M5)	4.0%	4.2%	4.0%	0.9%	0.9%	0.9%	0.0%	0.0%	0.0%	0.0%
gluc376 (M6)	2.9%	2.9%	2.8%	0.3%	0.3%	0.3%	0.0%	0.0%	0.0%	0.0%
gluc377 (M7)	1.4%	1.5%	1.5%	0.0%	0.0%	0.0%	0.0%	0.0%	0.0%	0.0%
gluc378 (M8)	0.4%	0.4%	0.4%	0.0%	0.0%	0.0%	0.0%	0.0%	0.0%	0.0%
gluc379 (M9)	0.0%	0.0%	0.0%	0.0%	0.0%	0.0%	0.0%	0.0%	0.0%	0.0%
gluc284 (M0)	58.7%	57.5%	58.7%	69.9%	70.1%	69.8%	85.0%	84.9%	82.6%	85.0%
gluc285 (M1)	20.2%	20.3%	20.1%	21.0%	20.9%	21.1%	12.7%	12.7%	14.7%	12.8%
gluc286 (M2)	6.3%	6.5%	6.3%	4.8%	4.8%	4.8%	2.0%	2.1%	2.3%	1.9%
gluc287 (M3)	4.2%	4.3%	4.2%	1.8%	1.8%	1.8%	0.3%	0.2%	0.4%	0.2%
gluc288 (M4)	6.1%	6.4%	6.2%	1.6%	1.5%	1.6%	0.0%	0.0%	0.0%	0.0%
gluc289 (M5)	4.6%	4.9%	4.6%	0.8%	0.8%	0.8%	0.0%	0.0%	0.0%	0.0%
gluc259 (M0)	64.3%	63.2%	64.2%	73.6%	73.6%	73.5%	86.3%	86.3%	77.8%	86.2%
gluc260 (M1)	16.9%	17.3%	16.9%	18.6%	18.6%	18.7%	11.6%	11.6%	10.9%	11.8%
gluc261 (M2)	4.8%	5.0%	4.8%	3.9%	3.9%	3.9%	1.9%	1.9%	9.8%	1.8%
gluc262 (M3)	1.6%	1.7%	1.6%	0.7%	0.7%	0.7%	0.2%	0.2%	1.3%	0.2%
gluc263 (M4)	1.5%	1.5%	1.5%	0.4%	0.4%	0.4%	0.0%	0.0%	0.2%	0.0%
gluc264 (M5)	7.5%	7.7%	7.5%	2.0%	2.0%	2.0%	0.0%	0.0%	0.0%	0.0%
gluc265 (M6)	3.5%	3.7%	3.5%	0.9%	0.9%	0.9%	0.0%	0.0%	0.0%	0.0%
gluc173 (M0)	72.3%	71.3%	72.2%	80.1%	80.1%	80.1%	90.7%	90.7%	82.3%	90.6%
gluc174 (M1)	12.5%	12.7%	12.5%	14.2%	14.3%	14.2%	8.1%	8.0%	7.6%	8.3%
gluc175 (M2)	2.3%	2.3%	2.3%	2.2%	2.2%	2.2%	1.1%	1.1%	9.2%	1.1%
gluc176 (M3)	1.4%	1.4%	1.4%	0.5%	0.5%	0.5%	0.1%	0.1%	0.8%	0.1%
gluc177 (M4)	9.6%	10.0%	9.6%	2.4%	2.4%	2.5%	0.0%	0.0%	0.1%	0.0%
gluc178 (M5)	2.0%	2.1%	2.1%	0.6%	0.5%	0.5%	0.0%	0.0%	0.0%	0.0%
gluc301 (M0)	52.1%	50.9%	51.9%	61.8%	62.1%	62.0%	82.7%	84.2%	70.8%	84.2%
gluc302 (M1)	16.8%	16.5%	16.5%	22.7%	22.7%	22.8%	13.7%	13.3%	13.5%	13.4%
gluc303 (M2)	5.1%	5.0%	4.9%	6.5%	6.4%	6.6%	2.8%	2.3%	12.1%	2.2%
gluc304 (M3)	2.1%	2.1%	2.0%	1.8%	1.7%	1.8%	0.1%	0.2%	2.4%	0.2%
gluc305 (M4)	3.4%	3.5%	3.4%	1.5%	1.5%	1.5%	0.1%	0.0%	1.0%	0.0%
gluc306 (M5)	7.2%	7.6%	7.4%	2.9%	2.9%	2.9%	0.5%	0.0%	0.2%	0.0%
gluc307 (M6)	5.3%	5.6%	5.4%	1.9%	1.8%	1.9%	0.1%	0.0%	0.0%	0.0%
gluc308 (M7)	2.0%	2.2%	2.1%	0.6%	0.6%	0.5%	0.0%	0.0%	0.0%	0.0%
gluc309 (M8)	1.0%	1.1%	1.1%	0.1%	0.1%	0.0%	0.0%	0.0%	0.0%	0.0%
gluc310 (M9)	1.6%	1.7%	1.7%	0.1%	0.1%	0.0%	0.0%	0.0%	0.0%	0.0%
gluc311 (M10)	2.0%	2.1%	2.1%	0.1%	0.1%	0.0%	0.0%	0.0%	0.0%	0.0%
gluc312 (M11)	1.1%	1.2%	1.2%	0.0%	0.0%	0.0%	0.0%	0.0%	0.0%	0.0%
gluc313 (M12)	0.2%	0.3%	0.3%	0.0%	0.0%	0.0%	0.0%	0.0%	0.0%	0.0%
gluc145 (M0)	66.2%	63.9%	64.5%	79.4%	79.3%	79.1%	92.4%	92.4%	86.2%	92.5%
gluc146 (M1)	12.8%	13.2%	13.1%	14.1%	14.1%	14.3%	6.7%	6.7%	9.0%	6.7%
gluc147 (M2)	6.3%	6.6%	6.5%	2.8%	2.8%	2.8%	0.9%	0.9%	4.5%	0.8%
gluc148 (M3)	8.6%	9.1%	8.8%	2.1%	2.1%	2.2%	0.0%	0.0%	0.3%	0.0%
gluc149 (M4)	6.1%	7.1%	7.1%	1.6%	1.6%	1.6%	0.0%	0.0%	0.0%	0.0%
glycerol173 (M0	4.5%	4.2%	4.2%	66.1%	66.0%	66.3%	90.7%	90.7%	90.1%	90.6%
glycerol174 (M1	1.9%	1.8%	1.8%	7.3%	7.3%	7.3%	8.1%	8.1%	8.0%	8.3%
glycerol175 (M2	0.9%	0.8%	0.8%	1.3%	1.3%	1.3%	1.2%	1.1%	1.7%	1.1%
glycerol176 (M3	0.8%	0.8%	0.8%	0.3%	0.3%	0.3%	0.1%	0.1%	0.1%	0.1%
glycerol177 (M4	2.3%	2.2%	2.2%	0.8%	0.8%	0.7%	0.0%	0.0%	0.0%	0.0%
glycerol178 (M5	84.0%	84.6%	84.6%	22.6%	22.8%	22.7%	0.0%	0.0%	0.0%	0.0%
glycerol179 (M6	5.6%	5.7%	5.6%	1.5%	1.5%	1.4%	0.0%	0.0%	0.0%	0.0%
glycerol180 (M7	0.0%	0.0%	0.0%	0.0%	0.0%	0.0%	0.0%	0.0%	0.0%	0.0%

Appendix B: Mouse Experiments, Enrichment Data Overview

All data presented are uncorrected isotopomer spectra for glucose derivatives of the indicated mass to charge (m/z) ratio, unless otherwise noted. Percentages correspond to the percent abundance of each isotopomer relative to the total glucose fragment signal. Theory represents theoretical natural abundance calculated a priori given the structure of the unlabeled glucose derivative.

Color code: Green = High Quality Data   Blue = Manual correction required
Tan = Qualitative data   Pink = Poor quality data

Mouse Experiment Details:

Experiment Date	6/23/2006	Fed/Fasted Animal	Fed prior to implant, fasted through infusion
Time Sample	24 hr	Tracers	M1: Unlabeled
Mouse Phenotype	BL6		M2: [U-^{13}C,D$_5$]-glycerol
Replicates	1		M3: 10% D$_2$O, [U-^{13}C,D$_5$]-glycerol

Date :	6/23/2006	6/23/2006	6/23/2006	Theory
Mouse# :	M1	M2	M3	
gluc370 (M0)	81.0%	75.8%	56.2%	80.9%
gluc371 (M1)	15.8%	16.9%	28.4%	15.9%
gluc372 (M2)	2.9%	4.7%	9.5%	2.8%
gluc373 (M3)	0.4%	1.4%	3.3%	0.4%
gluc374 (M4)	0.0%	0.8%	1.7%	0.0%
gluc375 (M5)	0.0%	0.3%	0.7%	0.0%
gluc376 (M6)	0.0%	0.1%	0.2%	0.0%
gluc377 (M7)	0.0%	0.0%	0.0%	0.0%
gluc378 (M8)	0.0%	0.0%	0.0%	0.0%
gluc379 (M9)	0.0%	0.0%	0.0%	0.0%
gluc284 (M0)	84.4%	79.5%	63.1%	85.0%
gluc285 (M1)	13.4%	15.5%	26.5%	12.8%
gluc286 (M2)	2.1%	3.1%	6.6%	1.9%
gluc287 (M3)	0.2%	1.1%	2.1%	0.2%
gluc288 (M4)	0.0%	0.7%	1.3%	0.0%
gluc289 (M5)	0.0%	0.2%	0.5%	0.0%
gluc259 (M0)	86.2%	82.7%	62.9%	86.2%
gluc260 (M1)	11.8%	13.2%	26.8%	11.8%
gluc261 (M2)	1.8%	2.5%	6.8%	1.8%
gluc262 (M3)	0.2%	0.5%	1.4%	0.2%
gluc263 (M4)	0.1%	0.2%	0.4%	0.0%
gluc264 (M5)	0.0%	0.8%	1.2%	0.0%
gluc265 (M6)	0.0%	0.2%	0.4%	0.0%
gluc173 (M0)	90.4%	88.0%	71.7%	90.6%
gluc174 (M1)	8.3%	9.0%	21.6%	8.3%
gluc175 (M2)	1.2%	1.7%	4.2%	1.1%
gluc176 (M3)	0.1%	0.3%	0.8%	0.1%
gluc177 (M4)	0.0%	0.9%	1.4%	0.0%
gluc178 (M5)	0.0%	0.1%	0.2%	0.0%

Mouse Experiment Details (6/23/2006 continued)

Experiment Date	6/23/2006	Fed/Fasted Animal	Fed
Time Sample	24 hr	Tracers	M1: Unlabeled
Mouse Phenotype	BL6		M2: [U-^{13}C,D$_5$]-glycerol
Replicates	1		M3: 10% D$_2$O, [U-^{13}C,D$_5$]-glycerol

Date :	6/23/2006	6/23/2006	6/23/2006	Theory
Mouse# :	M1	M2	M3	
gluc301 (M0)	83.8%	77.5%	47.5%	84.2%
gluc302 (M1)	13.7%	15.2%	31.1%	13.4%
gluc303 (M2)	2.3%	3.4%	12.0%	2.2%
gluc304 (M3)	0.2%	1.1%	3.8%	0.2%
gluc305 (M4)	0.0%	0.8%	1.8%	0.0%
gluc306 (M5)	0.0%	1.4%	2.0%	0.0%
gluc307 (M6)	0.0%	0.4%	1.2%	0.0%
gluc308 (M7)	0.0%	0.1%	0.4%	0.0%
gluc309 (M8)	0.0%	0.0%	0.1%	0.0%
gluc310 (M9)	0.0%	0.0%	0.0%	0.0%
gluc311 (M10)	0.0%	0.0%	0.0%	0.0%
gluc312 (M11)	0.0%	0.0%	0.0%	0.0%
gluc313 (M12)	0.0%	0.0%	0.0%	0.0%
gluc145 (M0)	92.2%	88.7%	74.8%	92.5%
gluc146 (M1)	6.8%	7.7%	18.5%	6.7%
gluc147 (M2)	0.9%	2.1%	3.9%	0.8%
gluc148 (M3)	0.0%	1.1%	2.0%	0.0%
gluc149 (M4)	0.0%	0.4%	0.8%	0.0%
glycerol173 (M0)	90.8%	81.8%	78.0%	90.6%
glycerol174 (M1)	8.1%	7.7%	12.1%	8.3%
glycerol175 (M2)	1.0%	1.4%	2.3%	1.1%
glycerol176 (M3)	0.1%	0.3%	0.5%	0.1%
glycerol177 (M4)	0.0%	1.6%	0.2%	0.0%
glycerol178 (M5)	0.0%	6.8%	6.4%	0.0%
glycerol179 (M6)	0.0%	0.4%	0.4%	0.0%
glycerol180 (M7)	0.0%	0.1%	0.1%	0.0%

Mouse Experiment Details

Experiment Date	8/1/2006	Fed/Fasted Animal	Fed
Time Sample	24 hr	Tracers	M1: 10% Deuterated Water
Mouse Phenotype	BL6		M2: 2M [U-^{13}C,D$_5$]-glycerol
Replicates	1		M3: 10% D$_2$O, 2M [U-^{13}C,D$_5$]-glycerol

Date :	8/1/2006	8/1/2006	8/1/2006	Theory
Mouse# :	M1	M2	M3	
gluc370 (M0)	80.4%	73.0%	70.7%	80.9%
gluc371 (M1)	16.2%	21.8%	21.7%	15.9%
gluc372 (M2)	3.0%	4.5%	5.3%	2.8%
gluc373 (M3)	0.4%	0.7%	1.4%	0.4%
gluc374 (M4)	0.0%	0.1%	0.6%	0.0%
gluc375 (M5)	0.0%	0.0%	0.2%	0.0%
gluc376 (M6)	0.0%	0.0%	0.0%	0.0%
gluc377 (M7)	0.0%	0.0%	0.0%	0.0%
gluc378 (M8)	0.0%	0.0%	0.0%	0.0%
gluc379 (M9)	0.0%	0.0%	0.0%	0.0%
gluc284 (M0)	83.6%	77.7%	75.3%	85.0%
gluc285 (M1)	14.0%	18.8%	19.5%	12.8%
gluc286 (M2)	2.2%	3.2%	3.6%	1.9%
gluc287 (M3)	0.2%	0.4%	0.9%	0.2%
gluc288 (M4)	0.0%	0.0%	0.5%	0.0%
gluc289 (M5)	0.0%	0.0%	0.2%	0.0%
gluc259 (M0)	85.5%	78.2%	76.9%	86.2%
gluc260 (M1)	12.4%	18.3%	18.4%	11.8%
gluc261 (M2)	1.9%	3.1%	3.3%	1.8%
gluc262 (M3)	0.2%	0.4%	0.5%	0.2%
gluc263 (M4)	0.0%	0.0%	0.1%	0.0%
gluc264 (M5)	0.0%	0.0%	0.6%	0.0%
gluc265 (M6)	0.0%	0.0%	0.2%	0.0%
gluc173 (M0)	89.7%	83.9%	82.9%	90.6%
gluc174 (M1)	8.7%	13.7%	13.7%	8.3%
gluc175 (M2)	1.1%	1.8%	2.0%	1.1%
gluc176 (M3)	0.1%	0.2%	0.3%	0.1%
gluc177 (M4)	0.0%	0.0%	0.7%	0.0%
gluc178 (M5)	0.0%	0.0%	0.1%	0.0%

Mouse Experiment Details (8/1/2006 continued)

Experiment Date	8/1/2006	Fed/Fasted Animal	Fed
Time Sample	24 hr	Tracers	M1: 10% Deuterated Water
Mouse Phenotype	BL6		M2: [U-^{13}C,D$_5$]-glycerol
Replicates	1		M3: 10% D$_2$O, [U-^{13}C,D$_5$]-glycerol

Date :	8/1/2006	8/1/2006	8/1/2006	Theory
Mouse# :	M1	M2	M3	
gluc301 (M0)	82.7%	70.6%	68.1%	84.2%
gluc302 (M1)	14.6%	23.4%	23.2%	13.4%
gluc303 (M2)	2.4%	5.1%	5.5%	2.2%
gluc304 (M3)	0.3%	0.8%	1.2%	0.2%
gluc305 (M4)	0.0%	0.1%	0.6%	0.0%
gluc306 (M5)	0.0%	0.0%	0.9%	0.0%
gluc307 (M6)	0.0%	0.0%	0.4%	0.0%
gluc308 (M7)	0.0%	0.0%	0.1%	0.0%
gluc309 (M8)	0.0%	0.0%	0.0%	0.0%
gluc310 (M9)	0.0%	0.0%	0.0%	0.0%
gluc311 (M10)	0.0%	0.0%	0.0%	0.0%
gluc312 (M11)	0.0%	0.0%	0.0%	0.0%
gluc313 (M12)	0.0%	0.0%	0.0%	0.0%
gluc145 (M0)	91.8%	87.1%	85.2%	92.5%
gluc146 (M1)	7.3%	11.6%	11.7%	6.7%
gluc147 (M2)	0.9%	1.3%	2.0%	0.8%
gluc148 (M3)	0.0%	0.1%	0.8%	0.0%
gluc149 (M4)	0.0%	0.0%	0.4%	0.0%
glycerol173 (M0)	90.2%	87.7%	75.1%	90.6%
glycerol174 (M1)	8.1%	10.3%	9.0%	8.3%
glycerol175 (M2)	1.5%	1.8%	1.2%	1.1%
glycerol176 (M3)	0.1%	0.1%	0.2%	0.1%
glycerol177 (M4)	0.0%	0.0%	0.5%	0.0%
glycerol178 (M5)	0.0%	0.1%	13.2%	0.0%
glycerol179 (M6)	0.0%	0.0%	0.9%	0.0%
glycerol180 (M7)	0.1%	0.0%	0.0%	0.0%

Appendix B: Mouse Experiments Enrichment

Mouse Experiment Details

Experiment Date	10/4/2006	Fed/Fasted Animal	Fasted through infusion
Time Sample	24 hr	Tracers	10% Deuterated Water (Bolus and fed)
Mouse Phenotype	LIRKO: M1, M3, M5, M7, M9, M11		2M [6,6-D2]-glucose (in pump)
	IRlox: M2, M4, M6, M8, M10, M12		2M [U-^{13}C,D$_5$]-glycerol (in pump)

Date :	10/4/2006	10/4/2006	10/4/2006	10/4/2006	10/4/2006	10/4/2006	Theory
Mouse# :	M1	M2	M3	M4	M5	M6	
gluc370 (M0)	69.4%	68.0%	69.3%	69.8%	69.8%	71.4%	80.9%
gluc371 (M1)	20.4%	21.1%	21.3%	20.6%	20.4%	20.0%	15.9%
gluc372 (M2)	6.0%	6.5%	6.1%	5.9%	5.8%	5.3%	2.8%
gluc373 (M3)	2.2%	2.4%	2.0%	2.1%	2.1%	1.8%	0.4%
gluc374 (M4)	1.3%	1.4%	1.0%	1.1%	1.2%	1.0%	0.0%
gluc375 (M5)	0.5%	0.5%	0.4%	0.4%	0.6%	0.4%	0.0%
gluc376 (M6)	0.1%	0.1%	0.1%	0.1%	0.1%	0.1%	0.0%
gluc377 (M7)	0.0%	0.0%	0.0%	0.0%	0.0%	0.0%	0.0%
gluc378 (M8)	0.0%	0.0%	0.0%	0.0%	0.0%	0.0%	0.0%
gluc379 (M9)	0.0%	0.0%	0.0%	0.0%	0.0%	0.0%	0.0%
gluc284 (M0)	73.0%	72.2%	74.4%	74.0%	74.3%	75.8%	85.0%
gluc285 (M1)	19.8%	20.1%	19.2%	19.2%	18.8%	18.1%	12.8%
gluc286 (M2)	4.1%	4.4%	4.0%	4.0%	4.0%	3.6%	1.9%
gluc287 (M3)	1.6%	1.7%	1.4%	1.4%	1.4%	1.2%	0.2%
gluc288 (M4)	1.1%	1.2%	0.8%	1.0%	1.0%	0.9%	0.0%
gluc289 (M5)	0.4%	0.4%	0.3%	0.3%	0.4%	0.4%	0.0%
gluc259 (M0)	71.6%	70.3%	72.1%	73.2%	71.5%	74.6%	86.2%
gluc260 (M1)	16.9%	17.4%	17.9%	17.1%	16.7%	16.4%	11.8%
gluc261 (M2)	8.2%	8.6%	7.2%	6.9%	8.7%	6.4%	1.8%
gluc262 (M3)	1.4%	1.5%	1.2%	1.2%	1.4%	1.0%	0.2%
gluc263 (M4)	0.3%	0.4%	0.3%	0.3%	0.4%	0.3%	0.0%
gluc264 (M5)	1.2%	1.4%	1.0%	1.1%	1.0%	1.0%	0.0%
gluc265 (M6)	0.4%	0.4%	0.3%	0.3%	0.3%	0.3%	0.0%
gluc173 (M0)	77.8%	76.7%	78.5%	79.2%	77.8%	80.7%	90.6%
gluc174 (M1)	12.5%	13.0%	13.4%	12.8%	12.3%	12.1%	8.3%
gluc175 (M2)	7.2%	7.6%	6.2%	5.9%	7.7%	5.3%	1.1%
gluc176 (M3)	0.9%	0.9%	0.7%	0.7%	0.9%	0.6%	0.1%
gluc177 (M4)	1.4%	1.6%	1.1%	1.3%	1.2%	1.1%	0.0%
gluc178 (M5)	0.1%	0.2%	0.1%	0.1%	0.1%	0.1%	0.0%

Mouse Experiment Details (10/4/2006 continued)

Experiment Date	10/4/2006	Fed/Fasted Animal	Fasted through infusion
Time Sample	24 hr	**Tracers**	10% Deuterated Water (Bolus and fed)
Mouse Phenotype	LIRKO: M1, M3, M5, M7, M9, M11		2M [6,6-D2]-glucose (in pump)
	IRlox: M2, M4, M6, M8, M10, M12		2M [U-^{13}C,D$_5$]-glycerol (in pump)

Date :	10/4/2006	10/4/2006	10/4/2006	10/4/2006	10/4/2006	10/4/2006	Theory
Mouse# :	M1	M2	M3	M4	M5	M6	
gluc301 (M0)	62.5%	60.5%	62.8%	64.5%	63.1%	67.1%	84.2%
gluc302 (M1)	20.4%	21.2%	22.0%	20.7%	19.9%	19.8%	13.4%
gluc303 (M2)	10.0%	10.6%	9.3%	8.6%	10.3%	7.9%	2.2%
gluc304 (M3)	2.4%	2.7%	2.2%	2.2%	2.4%	1.8%	0.2%
gluc305 (M4)	1.4%	1.5%	1.2%	1.2%	1.3%	1.0%	0.0%
gluc306 (M5)	2.1%	2.2%	1.6%	1.7%	1.8%	1.6%	0.0%
gluc307 (M6)	1.0%	1.0%	0.8%	0.8%	0.9%	0.7%	0.0%
gluc308 (M7)	0.3%	0.3%	0.2%	0.2%	0.2%	0.2%	0.0%
gluc309 (M8)	0.1%	0.1%	0.0%	0.1%	0.1%	0.1%	0.0%
gluc310 (M9)	0.0%	0.0%	0.0%	0.0%	0.0%	0.0%	0.0%
gluc311 (M10)	0.0%	0.0%	0.0%	0.0%	0.0%	0.0%	0.0%
gluc312 (M11)	0.0%	0.0%	0.0%	0.0%	0.0%	0.0%	0.0%
gluc313 (M12)	0.0%	0.0%	0.0%	0.0%	0.0%	0.0%	0.0%
gluc145 (M0)	83.5%	82.5%	83.9%	83.9%	84.2%	85.1%	92.5%
gluc146 (M1)	10.8%	11.5%	11.3%	11.1%	10.6%	10.5%	6.7%
gluc147 (M2)	2.8%	3.1%	2.6%	2.7%	2.6%	2.3%	0.8%
gluc148 (M3)	1.7%	1.9%	1.3%	1.5%	1.6%	1.4%	0.0%
gluc149 (M4)	1.1%	1.0%	0.9%	0.8%	1.0%	0.8%	0.0%
glycerol173 (M0)	65.9%	48.5%	75.7%	54.8%	53.4%	66.1%	90.6%
glycerol174 (M1)	8.2%	6.9%	10.5%	6.2%	7.5%	8.1%	8.3%
glycerol175 (M2)	1.0%	1.2%	1.6%	0.6%	1.3%	1.1%	1.1%
glycerol176 (M3)	0.0%	0.1%	0.1%	0.2%	0.1%	0.1%	0.1%
glycerol177 (M4)	0.9%	1.7%	0.6%	1.4%	1.2%	0.5%	0.0%
glycerol178 (M5)	22.6%	38.9%	11.2%	35.2%	34.5%	23.6%	0.0%
glycerol179 (M6)	1.3%	2.5%	0.3%	1.5%	1.9%	0.3%	0.0%
glycerol180 (M7)	0.1%	0.1%	0.0%	0.1%	0.1%	0.2%	0.0%

Mouse Experiment Details (10/4/2006 continued)

Experiment Date	10/4/2006	Fed/Fasted Animal	Fasted through infusion
Time Sample	24 hr	Tracers	10% Deuterated Water (Bolus and fed)
Mouse Phenotype	LIRKO: M1, M3, M5, M7, M9, M11		2M [6,6-D2]-glucose (in pump)
	Irlox: M2, M4, M ,M8, M10, M12		2M [U-^{13}C,D$_5$]-glycerol (in pump)

Date :	10/4/2006	10/4/2006	10/4/2006	10/4/2006	10/4/2006	10/4/2006	Theory
Mouse# :	M7	M8	M9	M10	M11	M12	
gluc370 (M0)	64.6%	69.7%	68.0%	69.5%	68.3%	67.2%	80.9%
gluc371 (M1)	22.2%	20.9%	21.5%	20.7%	21.0%	21.4%	15.9%
gluc372 (M2)	7.4%	5.8%	6.3%	6.0%	6.4%	6.6%	2.8%
gluc373 (M3)	3.1%	2.0%	2.3%	2.1%	2.4%	2.6%	0.4%
gluc374 (M4)	1.8%	1.1%	1.3%	1.1%	1.3%	1.5%	0.0%
gluc375 (M5)	0.7%	0.4%	0.5%	0.5%	0.5%	0.6%	0.0%
gluc376 (M6)	0.2%	0.1%	0.1%	0.1%	0.1%	0.2%	0.0%
gluc377 (M7)	0.0%	0.0%	0.0%	0.0%	0.0%	0.0%	0.0%
gluc378 (M8)	0.0%	0.0%	0.0%	0.0%	0.0%	0.0%	0.0%
gluc379 (M9)	0.0%	0.0%	0.0%	0.0%	0.0%	0.0%	0.0%
gluc284 (M0)	69.8%	74.4%	73.2%	74.1%	73.2%	71.9%	85.0%
gluc285 (M1)	20.8%	19.0%	19.6%	19.2%	19.4%	20.2%	12.8%
gluc286 (M2)	5.0%	3.9%	4.3%	4.0%	4.2%	4.3%	1.9%
gluc287 (M3)	2.2%	1.4%	1.6%	1.4%	1.7%	1.9%	0.2%
gluc288 (M4)	1.6%	0.9%	1.0%	1.0%	1.1%	1.3%	0.0%
gluc289 (M5)	0.6%	0.4%	0.4%	0.3%	0.4%	0.4%	0.0%
gluc259 (M0)	64.6%	72.7%	69.8%	72.7%	69.7%	69.4%	86.2%
gluc260 (M1)	18.6%	17.4%	17.8%	17.1%	17.5%	17.9%	11.8%
gluc261 (M2)	11.8%	7.1%	8.9%	7.2%	9.1%	8.8%	1.8%
gluc262 (M3)	2.0%	1.2%	1.5%	1.2%	1.5%	1.5%	0.2%
gluc263 (M4)	0.6%	0.3%	0.4%	0.3%	0.4%	0.5%	0.0%
gluc264 (M5)	1.8%	1.1%	1.2%	1.1%	1.4%	1.5%	0.0%
gluc265 (M6)	0.6%	0.3%	0.4%	0.3%	0.4%	0.4%	0.0%
gluc173 (M0)	71.8%	78.9%	76.2%	78.9%	76.3%	75.9%	90.6%
gluc174 (M1)	14.0%	13.0%	13.4%	12.8%	13.0%	13.4%	8.3%
gluc175 (M2)	10.6%	6.0%	8.0%	6.1%	8.0%	7.8%	1.1%
gluc176 (M3)	1.3%	0.7%	0.9%	0.8%	0.9%	1.0%	0.1%
gluc177 (M4)	2.1%	1.2%	1.4%	1.3%	1.6%	1.7%	0.0%
gluc178 (M5)	0.2%	0.1%	0.1%	0.1%	0.2%	0.2%	0.0%

Mouse Experiment Details (10/4/2006 continued)

Experiment Date	10/4/2006	Fed/Fasted Animal	Fasted through infusion
Time Sample	24 hr	Tracers	10% Deuterated Water (Bolus and fed)
Mouse Phenotype	LIRKO: M1, M3, M5, M7, M9, M11		2M [6,6-D2]-glucose (in pump)
	Irlox: M2, M4, M ,M8, M10, M12		2M [U-^{13}C,D$_5$]-glycerol (in pump)

Date :	10/4/2006	10/4/2006	10/4/2006	10/4/2006	10/4/2006	10/4/2006	Theory
Mouse# :	M7	M8	M9	M10	M11	M12	
gluc301 (M0)	53.8%	64.1%	59.9%	63.7%	59.9%	59.3%	84.2%
gluc302 (M1)	22.2%	21.2%	21.7%	20.9%	21.1%	21.6%	13.4%
gluc303 (M2)	13.9%	8.9%	11.2%	9.0%	11.2%	11.0%	2.2%
gluc304 (M3)	3.5%	2.1%	2.7%	2.2%	2.7%	2.8%	0.2%
gluc305 (M4)	1.9%	1.2%	1.4%	1.3%	1.5%	1.6%	0.0%
gluc306 (M5)	2.8%	1.7%	2.0%	1.8%	2.2%	2.4%	0.0%
gluc307 (M6)	1.3%	0.8%	0.9%	0.8%	1.0%	1.1%	0.0%
gluc308 (M7)	0.4%	0.2%	0.2%	0.2%	0.3%	0.3%	0.0%
gluc309 (M8)	0.1%	0.1%	0.1%	0.1%	0.1%	0.1%	0.0%
gluc310 (M9)	0.0%	0.0%	0.0%	0.0%	0.0%	0.0%	0.0%
gluc311 (M10)	0.0%	0.0%	0.0%	0.0%	0.0%	0.0%	0.0%
gluc312 (M11)	0.0%	0.0%	0.0%	0.0%	0.0%	0.0%	0.0%
gluc313 (M12)	0.0%	0.0%	0.0%	0.0%	0.0%	0.0%	0.0%
gluc145 (M0)	80.6%	84.1%	83.1%	83.7%	82.8%	82.4%	92.5%
gluc146 (M1)	12.2%	11.2%	11.5%	11.2%	11.4%	11.6%	6.7%
gluc147 (M2)	3.6%	2.5%	2.8%	2.7%	2.9%	3.1%	0.8%
gluc148 (M3)	2.3%	1.4%	1.7%	1.5%	1.8%	1.9%	0.0%
gluc149 (M4)	1.3%	0.8%	0.9%	0.8%	1.0%	1.0%	0.0%
glycerol173 (M0)	56.4%	60.0%	62.8%	53.7%	63.2%	64.4%	90.6%
glycerol174 (M1)	8.2%	8.5%	7.8%	6.8%	7.1%	7.9%	8.3%
glycerol175 (M2)	1.3%	0.9%	0.9%	0.6%	0.7%	0.9%	1.1%
glycerol176 (M3)	0.1%	0.0%	0.1%	0.2%	0.1%	0.2%	0.1%
glycerol177 (M4)	1.3%	1.0%	0.5%	0.9%	0.5%	0.6%	0.0%
glycerol178 (M5)	30.9%	28.5%	26.8%	36.7%	27.7%	25.4%	0.0%
glycerol179 (M6)	1.6%	1.1%	1.1%	1.2%	0.7%	0.7%	0.0%
glycerol180 (M7)	0.1%	0.1%	0.0%	0.2%	0.0%	0.1%	0.0%

Mouse Experiment Details

Experiment Date	3/21/2007	Fed/Fasted Animal	Fasted through infusion
Time Sample	3 hr	Tracers	M1-M2 -2M [U-^{13}C,D$_5$]-glycerol (in pump)
Mouse Phenotype	BL6		M3-M4: 2M [6,6-D2]-glucose (in pump)

Date :	3/21/2007	3/21/2007	3/21/2007	3/21/2007	Theory
Mouse# :	M1	M2	M3	M4	
gluc370 (M0)	81.0%	81.1%	81.0%	81.1%	80.9%
gluc371 (M1)	15.7%	15.6%	15.7%	15.6%	15.9%
gluc372 (M2)	2.9%	2.9%	3.0%	3.0%	2.8%
gluc373 (M3)	0.4%	0.4%	0.4%	0.4%	0.4%
gluc374 (M4)	0.0%	0.0%	0.0%	0.0%	0.0%
gluc375 (M5)	0.0%	0.0%	0.0%	0.0%	0.0%
gluc376 (M6)	0.0%	0.0%	0.0%	0.0%	0.0%
gluc377 (M7)	0.0%	0.0%	0.0%	0.0%	0.0%
gluc378 (M8)	0.0%	0.0%	0.0%	0.0%	0.0%
gluc379 (M9)	0.0%	0.0%	0.0%	0.0%	0.0%
gluc284 (M0)	84.5%	85.3%	86.1%	84.5%	85.0%
gluc285 (M1)	12.6%	12.8%	12.2%	13.1%	12.8%
gluc286 (M2)	2.1%	1.8%	1.7%	1.9%	1.9%
gluc287 (M3)	0.6%	0.1%	0.0%	0.4%	0.2%
gluc288 (M4)	0.1%	0.0%	0.0%	0.0%	0.0%
gluc289 (M5)	0.0%	0.0%	0.0%	0.0%	0.0%
gluc259 (M0)	86.7%	86.8%	87.0%	86.8%	86.2%
gluc260 (M1)	11.4%	11.4%	11.3%	11.4%	11.8%
gluc261 (M2)	1.7%	1.7%	1.7%	1.7%	1.8%
gluc262 (M3)	0.2%	0.2%	0.1%	0.2%	0.2%
gluc263 (M4)	0.0%	0.0%	0.0%	0.0%	0.0%
gluc264 (M5)	0.0%	0.0%	0.0%	0.0%	0.0%
gluc265 (M6)	0.0%	0.0%	0.0%	0.0%	0.0%
gluc173 (M0)	90.9%	90.9%	90.9%	91.0%	90.6%
gluc174 (M1)	8.0%	8.0%	8.0%	8.0%	8.3%
gluc175 (M2)	1.0%	1.0%	1.0%	1.0%	1.1%
gluc176 (M3)	0.0%	0.0%	0.0%	0.0%	0.1%
gluc177 (M4)	0.0%	0.0%	0.0%	0.0%	0.0%
gluc178 (M5)	0.0%	0.0%	0.0%	0.0%	0.0%

Mouse Experiment Details (3/21/2007 Continued)

Experiment Date	3/21/2007	Fed/Fasted Animal	Fasted through infusion
Time Sample	3 hr	Tracers	M1-M2 -2M [U-^{13}C,D$_5$]-glycerol (in pump)
Mouse Phenotype	BL6		M3-M4: 2M [6,6-D2]-glucose (in pump)

Date :	3/21/2007	3/21/2007	3/21/2007	3/21/2007	Theory
Mouse# :	M1	M2	M3	M4	
gluc301 (M0)					84.2%
gluc302 (M1)					13.4%
gluc303 (M2)					2.2%
gluc304 (M3)					0.2%
gluc305 (M4)					0.0%
gluc306 (M5)					0.0%
gluc307 (M6)					0.0%
gluc308 (M7)					0.0%
gluc309 (M8)					0.0%
gluc310 (M9)					0.0%
gluc311 (M10)					0.0%
gluc312 (M11)					0.0%
gluc313 (M12)					0.0%
gluc145 (M0)	92.7%	92.6%	92.7%	92.6%	92.5%
gluc146 (M1)	6.8%	6.8%	6.7%	6.8%	6.7%
gluc147 (M2)	0.5%	0.6%	0.6%	0.6%	0.8%
gluc148 (M3)	0.0%	0.0%	0.0%	0.0%	0.0%
gluc149 (M4)	0.0%	0.0%	0.0%	0.0%	0.0%
glycerol173 (M0)	90.1%	92.0%		90.4%	90.6%
glycerol174 (M1)	8.4%	7.3%		7.7%	8.3%
glycerol175 (M2)	1.5%	0.7%		1.7%	1.1%
glycerol176 (M3)	0.0%	0.0%		0.2%	0.1%
glycerol177 (M4)	0.0%	0.0%		0.0%	0.0%
glycerol178 (M5)	0.0%	0.0%		0.0%	0.0%
glycerol179 (M6)	0.0%	0.0%		0.0%	0.0%
glycerol180 (M7)	0.0%	0.0%		0.0%	0.0%

Mouse Experiment Details

Experiment Date	3/29/2007	Fed/Fasted Animal	Fasted through infusion
Time Sample	12 hr	Tracers	M1-M2 -2M [U-^{13}C,D$_5$]-glycerol (in pump)
Mouse Phenotype	BL6		M3-M4: 2M [6,6-D2]-glucose (in pump)

Date :	3/29/2007	3/29/2007	3/29/2007	3/29/2007	Theory
Mouse# :	M1	M2	M3	M4	
gluc370 (M0)		73.7%	81.0%	80.9%	80.9%
gluc371 (M1)		16.6%	15.9%	15.9%	15.9%
gluc372 (M2)		5.8%	2.9%	2.9%	2.8%
gluc373 (M3)		2.2%	0.2%	0.3%	0.4%
gluc374 (M4)		1.3%	0.0%	0.0%	0.0%
gluc375 (M5)		0.3%	0.0%	0.0%	0.0%
gluc376 (M6)		0.0%	0.0%	0.0%	0.0%
gluc377 (M7)		0.0%	0.0%	0.0%	0.0%
gluc378 (M8)		0.0%	0.0%	0.0%	0.0%
gluc379 (M9)		0.0%	0.0%	0.0%	0.0%
gluc284 (M0)		76.3%	83.8%	83.3%	85.0%
gluc285 (M1)		16.1%	13.7%	13.7%	12.8%
gluc286 (M2)		3.6%	2.1%	2.3%	1.9%
gluc287 (M3)		2.2%	0.3%	0.7%	0.2%
gluc288 (M4)		1.4%	0.0%	0.1%	0.0%
gluc289 (M5)		0.3%	0.0%	0.0%	0.0%
gluc259 (M0)		81.8%	77.7%	77.0%	86.2%
gluc260 (M1)		12.6%	11.1%	11.0%	11.8%
gluc261 (M2)		2.5%	9.6%	10.2%	1.8%
gluc262 (M3)		0.6%	1.4%	1.4%	0.2%
gluc263 (M4)		0.3%	0.1%	0.3%	0.0%
gluc264 (M5)		1.8%	0.0%	0.1%	0.0%
gluc265 (M6)		0.5%	0.0%	0.0%	0.0%
gluc173 (M0)		87.6%	82.6%	81.8%	90.6%
gluc174 (M1)		8.6%	7.7%	7.7%	8.3%
gluc175 (M2)		1.6%	8.8%	9.6%	1.1%
gluc176 (M3)		0.3%	0.7%	0.8%	0.1%
gluc177 (M4)		1.7%	0.1%	0.1%	0.0%
gluc178 (M5)		0.2%	0.0%	0.0%	0.0%

Note: M1 Plasma did not derivatize properly

Mouse Experiment Details

Experiment Date	4/10/2007	Fed/Fasted Animal	Fasted through infusion
Time Sample	6 hr	Tracers	M5-M6 -2M [U-^{13}C,D$_5$]-glycerol (in pump)
Mouse Phenotype	BL6		M1, M4-: 2M [6,6-D2]-glucose (in pump)
			M2-M3 -2M [U-^{13}C]-glycerol (in pump)

Date :	4/10/2007	4/10/2007	4/10/2007	4/10/2007	4/10/2007	4/10/2007	Theory
Mouse# :	M1	M2	M3	M4	M5	M6	
gluc370 (M0)	80.9%	76.5%	76.4%	80.9%	76.2%	77.3%	80.9%
gluc371 (M1)	15.8%	15.7%	15.6%	15.7%	16.0%	15.9%	15.9%
gluc372 (M2)	2.9%	4.9%	5.0%	3.0%	4.7%	4.3%	2.8%
gluc373 (M3)	0.3%	2.3%	2.4%	0.4%	1.7%	1.3%	0.4%
gluc374 (M4)	0.1%	0.4%	0.5%	0.0%	1.0%	0.8%	0.0%
gluc375 (M5)	0.0%	0.1%	0.2%	0.0%	0.4%	0.3%	0.0%
gluc376 (M6)	0.0%	0.0%	0.0%	0.0%	0.1%	0.1%	0.0%
gluc377 (M7)	0.0%	0.0%	0.0%	0.0%	0.0%	0.0%	0.0%
gluc378 (M8)	0.0%	0.0%	0.0%	0.0%	0.0%	0.0%	0.0%
gluc379 (M9)	0.0%	0.0%	0.0%	0.0%	0.0%	0.0%	0.0%
gluc284 (M0)	84.8%	80.5%	80.5%	85.0%	79.8%	81.0%	85.0%
gluc285 (M1)	13.0%	14.4%	14.3%	12.7%	14.7%	14.2%	12.8%
gluc286 (M2)	2.0%	2.7%	2.6%	2.0%	2.9%	2.7%	1.9%
gluc287 (M3)	0.2%	2.0%	2.0%	0.2%	1.2%	1.0%	0.2%
gluc288 (M4)	0.1%	0.4%	0.5%	0.1%	1.1%	0.8%	0.0%
gluc289 (M5)	0.0%	0.1%	0.1%	0.0%	0.3%	0.2%	0.0%
gluc259 (M0)	74.8%	84.0%	83.9%	85.8%	83.3%	84.1%	86.2%
gluc260 (M1)	10.5%	11.7%	11.7%	11.6%	12.3%	12.1%	11.8%
gluc261 (M2)	12.8%	2.1%	2.1%	2.3%	2.1%	2.0%	1.8%
gluc262 (M3)	1.7%	2.0%	2.1%	0.3%	0.4%	0.4%	0.2%
gluc263 (M4)	0.2%	0.2%	0.2%	0.0%	0.2%	0.1%	0.0%
gluc264 (M5)	0.0%	0.0%	0.0%	0.0%	1.4%	1.1%	0.0%
gluc265 (M6)	0.0%	0.0%	0.0%	0.0%	0.3%	0.2%	0.0%
gluc173 (M0)	79.0%	88.4%	88.4%	90.2%	88.4%	89.0%	90.6%
gluc174 (M1)	7.4%	8.2%	8.1%	8.0%	8.3%	8.2%	8.3%
gluc175 (M2)	12.5%	3.1%	3.1%	1.6%	1.4%	1.3%	1.1%
gluc176 (M3)	1.1%	0.2%	0.2%	0.1%	0.2%	0.2%	0.1%
gluc177 (M4)	0.1%	0.0%	0.1%	0.0%	1.6%	1.2%	0.0%
gluc178 (M5)	0.0%	0.0%	0.0%	0.0%	0.1%	0.1%	0.0%

Mouse Experiment Details (4/10/2007 continued)

Experiment Date	4/10/2007	Fed/Fasted Animal	Fasted through infusion
Time Sample	6 hr	Tracers	M5-M6 -2M [U-^{13}C,D$_5$]-glycerol (in pump)
Mouse Phenotype	BL6		M1, M4-: 2M [6,6-D2]-glucose (in pump)
			M2-M3 -2M [U-^{13}C]-glycerol (in pump)

Date :	4/10/2007	4/10/2007	4/10/2007	4/10/2007	4/10/2007	4/10/2007	Theory
Mouse# :	M1	M2	M3	M4	M5	M6	
gluc301 (M0)	74.8%	79.5%	79.4%	83.8%	78.5%	80.0%	84.2%
gluc302 (M1)	12.5%	13.3%	13.3%	13.3%	13.7%	13.5%	13.4%
gluc303 (M2)	10.2%	2.9%	2.9%	2.5%	2.8%	2.7%	2.2%
gluc304 (M3)	1.7%	3.6%	3.7%	0.3%	1.0%	0.8%	0.2%
gluc305 (M4)	0.4%	0.5%	0.5%	0.0%	1.1%	0.8%	0.0%
gluc306 (M5)	0.4%	0.1%	0.1%	0.0%	2.0%	1.5%	0.0%
gluc307 (M6)	0.1%	0.1%	0.1%	0.0%	0.6%	0.4%	0.0%
gluc308 (M7)	0.0%	0.0%	0.0%	0.0%	0.1%	0.1%	0.0%
gluc309 (M8)	0.0%	0.0%	0.0%	0.0%	0.0%	0.0%	0.0%
gluc310 (M9)	0.0%	0.0%	0.0%	0.0%	0.0%	0.0%	0.0%
gluc311 (M10)	0.0%	0.0%	0.0%	0.0%	0.0%	0.0%	0.0%
gluc312 (M11)	0.0%	0.0%	0.0%	0.0%	0.0%	0.0%	0.0%
gluc313 (M12)	0.0%	0.0%	0.0%	0.0%	0.0%	0.0%	0.0%
gluc145 (M0)	92.0%	89.7%	89.6%	92.3%	88.1%	89.3%	92.5%
gluc146 (M1)	6.9%	7.0%	6.9%	6.7%	7.4%	7.2%	6.7%
gluc147 (M2)	1.0%	3.1%	3.2%	0.9%	2.1%	1.8%	0.8%
gluc148 (M3)	0.1%	0.2%	0.2%	0.1%	1.6%	1.1%	0.0%
gluc149 (M4)	0.0%	0.1%	0.1%	0.0%	0.8%	0.6%	0.0%
glycerol173 (M0)	90.4%	65.2%	58.3%	90.2%	55.2%	71.9%	90.6%
glycerol174 (M1)	8.1%	6.1%	5.9%	8.3%	5.5%	6.9%	8.3%
glycerol175 (M2)	1.3%	26.5%	33.2%	1.3%	0.8%	0.8%	1.1%
glycerol176 (M3)	0.1%	1.8%	1.8%	0.0%	0.1%	0.0%	0.1%
glycerol177 (M4)	0.0%	0.3%	0.7%	0.0%	1.4%	0.2%	0.0%
glycerol178 (M5)	0.0%	0.1%	0.1%	0.1%	34.3%	20.2%	0.0%
glycerol179 (M6)	0.0%	0.0%	0.0%	0.0%	2.3%	1.5%	0.0%
glycerol180 (M7)	0.0%	0.0%	0.0%	0.0%	0.4%	0.2%	0.0%

Mouse Experiment Details

Experiment Date	6/8/2007	Fed/Fasted Animal	Fasted through infusion
Time Sample	24 hr	Tracers	5% Deuterated Water (IP Bolus and fed)
Mouse Phenotype	LIRKO : M1-M3		2M [6,6-D2]-glucose (in pump)
	IRlox: M4-M5		2M [U-^{13}C,D$_5$]-glycerol (in pump)

Date :	6/8/2007	6/8/2007	6/8/2007	6/8/2007	6/8/2007	Theory
Mouse# :	M1	M2	M3	M4	M5	
gluc370 (M0)	72.9%	72.9%	72.9%	68.3%	71.9%	80.9%
gluc371 (M1)	21.6%	21.5%	21.5%	22.1%	20.3%	15.9%
gluc372 (M2)	4.6%	4.6%	4.6%	6.2%	5.2%	2.8%
gluc373 (M3)	0.8%	0.8%	0.8%	2.0%	1.6%	0.4%
gluc374 (M4)	0.1%	0.2%	0.2%	1.0%	0.7%	0.0%
gluc375 (M5)	0.0%	0.1%	0.1%	0.3%	0.2%	0.0%
gluc376 (M6)	0.0%	0.0%	0.0%	0.1%	0.1%	0.0%
gluc377 (M7)	0.0%	0.0%	0.0%	0.0%	0.0%	0.0%
gluc378 (M8)	0.0%	0.0%	0.0%	0.0%	0.0%	0.0%
gluc379 (M9)	0.0%	0.0%	0.0%	0.0%	0.0%	0.0%
gluc284 (M0)	78.4%	78.2%	78.5%	73.8%	76.9%	85.0%
gluc285 (M1)	18.0%	18.1%	17.8%	19.9%	18.0%	12.8%
gluc286 (M2)	3.0%	3.0%	3.0%	4.0%	3.4%	1.9%
gluc287 (M3)	0.4%	0.5%	0.5%	1.3%	0.9%	0.2%
gluc288 (M4)	0.1%	0.2%	0.2%	0.8%	0.6%	0.0%
gluc289 (M5)	0.0%	0.0%	0.0%	0.2%	0.2%	0.0%
gluc259 (M0)	78.7%	77.6%	78.3%	70.6%	74.3%	86.2%
gluc260 (M1)	17.6%	17.1%	17.1%	18.2%	16.2%	11.8%
gluc261 (M2)	3.1%	4.5%	3.8%	8.0%	7.0%	1.8%
gluc262 (M3)	0.4%	0.6%	0.5%	1.3%	1.0%	0.2%
gluc263 (M4)	0.1%	0.1%	0.1%	0.3%	0.3%	0.0%
gluc264 (M5)	0.0%	0.1%	0.1%	1.2%	0.9%	0.0%
gluc265 (M6)	0.0%	0.1%	0.1%	0.4%	0.3%	0.0%
gluc173 (M0)	84.9%	83.6%	84.3%	77.4%	80.3%	90.6%
gluc174 (M1)	13.0%	12.8%	12.7%	13.5%	11.9%	8.3%
gluc175 (M2)	1.8%	3.2%	2.6%	6.8%	5.9%	1.1%
gluc176 (M3)	0.2%	0.3%	0.3%	0.7%	0.6%	0.1%
gluc177 (M4)	0.0%	0.1%	0.2%	1.5%	1.1%	0.0%
gluc178 (M5)	0.0%	0.0%	0.0%	0.1%	0.1%	0.0%

Mouse Experiment Details (6/8/2007 Continued)

Experiment Date	6/8/2007	Fed/Fasted Animal	Fasted through infusion
Time Sample	24 hr	Tracers	5% Deuterated Water (IP bolus and fed)
Mouse Phenotype	LIRKO : M1-M3		2M [6,6-D2]-glucose (in pump)
	IRlox: M4-M5		2M [U-^{13}C,D$_5$]-glycerol (in pump)

Date :	6/8/2007	6/8/2007	6/8/2007	6/8/2007	6/8/2007	Theory
Mouse# :	M1	M2	M3	M4	M5	
gluc301 (M0)	71.3%	70.6%	71.1%	61.1%	66.8%	84.2%
gluc302 (M1)	22.7%	22.0%	22.0%	22.8%	20.2%	13.4%
gluc303 (M2)	5.0%	6.1%	5.6%	10.0%	8.4%	2.2%
gluc304 (M3)	0.8%	1.0%	0.9%	2.2%	1.8%	0.2%
gluc305 (M4)	0.1%	0.2%	0.2%	1.1%	0.9%	0.0%
gluc306 (M5)	0.1%	0.1%	0.2%	1.7%	1.3%	0.0%
gluc307 (M6)	0.0%	0.1%	0.1%	0.7%	0.5%	0.0%
gluc308 (M7)	0.0%	0.0%	0.0%	0.2%	0.1%	0.0%
gluc309 (M8)	0.0%	0.0%	0.0%	0.1%	0.0%	0.0%
gluc310 (M9)	0.0%	0.0%	0.0%	0.0%	0.0%	0.0%
gluc311 (M10)	0.0%	0.0%	0.0%	0.0%	0.0%	0.0%
gluc312 (M11)	0.0%	0.0%	0.0%	0.0%	0.0%	0.0%
gluc313 (M12)	0.0%	0.0%	0.0%	0.0%	0.0%	0.0%
gluc145 (M0)	87.2%	87.2%	87.1%	83.7%	85.8%	92.5%
gluc146 (M1)	11.4%	11.2%	11.3%	12.0%	10.8%	6.7%
gluc147 (M2)	1.3%	1.3%	1.3%	2.4%	2.0%	0.8%
gluc148 (M3)	0.2%	0.2%	0.2%	1.3%	1.0%	0.0%
gluc149 (M4)	0.0%	0.1%	0.1%	0.6%	0.4%	0.0%
glycerol173 (M0)	88.9%	58.9%	80.2%	76.3%	60.4%	90.6%
glycerol174 (M1)	9.3%	6.2%	8.3%	8.6%	7.6%	8.3%
glycerol175 (M2)	1.2%	0.9%	1.2%	1.4%	1.2%	1.1%
glycerol176 (M3)	0.1%	0.1%	0.1%	0.3%	0.2%	0.1%
glycerol177 (M4)	0.0%	1.2%	0.4%	0.5%	1.1%	0.0%
glycerol178 (M5)	0.3%	30.4%	9.3%	12.1%	27.6%	0.0%
glycerol179 (M6)	0.0%	2.0%	0.6%	0.7%	1.7%	0.0%
glycerol180 (M7)	0.0%	0.3%	0.0%	0.0%	0.2%	0.0%

Mouse Experiment Details

Experiment Date	7/3/2007	Fed/Fasted Animal	Fasted through infusion
Time Sample	Delayed Infusion 6 hr	Tracers	M1-M3 - 2M [U-^{13}C,D$_5$]-glycerol (pump), 2M [6,6-D2]-glucose (pump), 5% D$_2$O (IP, fed)
Mouse Phenotype	BL6		M4-Unenriched Control

Date :	7/3/2007	7/3/2007	7/3/2007	7/3/2007	Theory
Mouse# :	M1	M2	M3	M4	
gluc370 (M0)	65.4%	65.6%	62.5%	80.9%	80.9%
gluc371 (M1)	22.8%	23.5%	23.2%	15.7%	15.9%
gluc372 (M2)	7.4%	6.9%	8.4%	3.0%	2.8%
gluc373 (M3)	2.4%	2.5%	3.2%	0.5%	0.4%
gluc374 (M4)	1.4%	1.1%	2.0%	0.0%	0.0%
gluc375 (M5)	0.7%	0.4%	0.6%	0.0%	0.0%
gluc376 (M6)	0.0%	0.0%	0.0%	0.0%	0.0%
gluc377 (M7)	0.0%	0.0%	0.0%	0.0%	0.0%
gluc378 (M8)	0.0%	0.0%	0.0%	0.0%	0.0%
gluc379 (M9)	0.0%	0.0%	0.0%	0.0%	0.0%
gluc284 (M0)	72.1%	70.5%	68.2%	85.2%	85.0%
gluc285 (M1)	21.1%	22.6%	21.8%	12.5%	12.8%
gluc286 (M2)	4.5%	4.0%	5.5%	2.1%	1.9%
gluc287 (M3)	1.3%	1.6%	2.5%	0.2%	0.2%
gluc288 (M4)	0.7%	0.9%	1.6%	0.0%	0.0%
gluc289 (M5)	0.4%	0.3%	0.4%	0.0%	0.0%
gluc259 (M0)	67.1%	66.5%	66.1%	86.3%	86.2%
gluc260 (M1)	20.3%	20.8%	19.2%	11.7%	11.8%
gluc261 (M2)	8.9%	8.7%	9.7%	1.8%	1.8%
gluc262 (M3)	1.3%	1.5%	1.6%	0.2%	0.2%
gluc263 (M4)	0.2%	0.5%	0.7%	0.0%	0.0%
gluc264 (M5)	1.5%	1.5%	2.0%	0.0%	0.0%
gluc265 (M6)	0.6%	0.5%	0.7%	0.0%	0.0%
gluc173 (M0)	74.0%	73.8%	72.3%	90.9%	90.6%
gluc174 (M1)	14.9%	15.2%	14.8%	7.9%	8.3%
gluc175 (M2)	8.0%	8.0%	9.1%	1.0%	1.1%
gluc176 (M3)	0.9%	1.1%	1.3%	0.1%	0.1%
gluc177 (M4)	1.7%	1.8%	2.5%	0.0%	0.0%
gluc178 (M5)	0.5%	0.2%	0.0%	0.0%	0.0%

Mouse Experiment Details (7/3/2007 continued)

Experiment Date	7/3/2007	Fed/Fasted Animal	Fasted through infusion
Time Sample	Delayed Infusion 6 hr	Tracers	M1-M3 - 2M [U-^{13}C,D$_5$]-glycerol (pump), 2M [6,6-D2]-glucose (pump), 5% D$_2$O (IP, fed)
Mouse Phenotype	BL6		M4-Unenriched Control

Date :	7/3/2007	7/3/2007	7/3/2007	7/3/2007	Theory
Mouse# :	M1	M2	M3	M4	
gluc301 (M0)					84.2%
gluc302 (M1)					13.4%
gluc303 (M2)					2.2%
gluc304 (M3)					0.2%
gluc305 (M4)					0.0%
gluc306 (M5)					0.0%
gluc307 (M6)					0.0%
gluc308 (M7)					0.0%
gluc309 (M8)					0.0%
gluc310 (M9)					0.0%
gluc311 (M10)					0.0%
gluc312 (M11)					0.0%
gluc313 (M12)					0.0%
gluc145 (M0)	83.2%	82.3%	83.3%	92.5%	92.5%
gluc146 (M1)	12.7%	12.6%	13.0%	6.6%	6.7%
gluc147 (M2)	1.8%	2.7%	0.8%	0.8%	0.8%
gluc148 (M3)	1.6%	1.8%	2.2%	0.1%	0.0%
gluc149 (M4)	0.8%	0.6%	0.6%	0.0%	0.0%

Curriculum Vitae

José O. Alemán

Education

Massachusetts Institute of Technology   Cambridge, MA

September 2002 – January 2008. Ph.D. candidate in Medical Physics and Medical Engineering, Bioinformatics and Integrative Genomics Track, Division of Health Sciences and Technology (joint program with Harvard Medical School).

Thesis title: Gluconeogenesis as a system: Development of in vivo flux analysis of hepatic glucose production in Type 2 Diabetes mellitus.
Advisor: Gregory Stephanopoulos, Department of Chemical Engineering.

Harvard Medical School   Boston, MA

August 2003 – June 2009. MD-PhD Student in Castle society. USMLE STEP 1 completed in June 2005. MD expected June 2009.

Cornell University   Ithaca, NY

Bachelor of Science in Chemical Engineering, Magna Cum Laude, May 27, 2001. Participated in research activities in reproductive physiology and biochemical engineering.
Advisors: Susan Suarez, Department of Biomedical Sciences, College of Veterinary Medicine; Michael L. Shuler, School of Chemical and Biomolecular Engineering.

Awards

National Science Foundation Graduate Research Fellowship (2002-2007), Bioinformatics and Integrative Genomics Training Grant, Division of Health Sciences and Technology, NIH (2003-2005), Fulbright Grant (2001-2002), Gates Millennium Scholar (2000-2006), Xerox Technical Minority Scholarship (1999-2000), Tau Beta Pi Engineering Honor Society (2000-2001).

Research Experience

Massachusetts Institute of Technology   Cambridge, MA

Advisor: Gregory Stephanopoulos, Ph.D. Department of Chemical Engineering and Division of Health Sciences and Technology.
Gluconeogenesis as a system: Development of in vivo flux analysis of hepatic glucose production in Type 2 Diabetes mellitus.

Children's Hospital   Boston, MA, USA

Advisor: Marco Ramoni, Ph.D. Children's Hospital Informatics Program.
Laboratory Rotation Research: "Placental Gene Expression Profiling in Normal Pregnancy versus Preeclampsia." (January 2003-June 2003)

Massachusetts Institute of Technology   Cambridge, MA

Advisor: Gregory Stephanopoulos, Ph.D. Department of Chemical Engineering and Division of Health Sciences and Technology.
Laboratory Rotation Research: "Analysis of Free Aminoacid Isotopomer Distribution in *Corynebacterium glutamicum*." (June 2002-September 2002)

Universidad Complutense de Madrid   Madrid, Spain

Advisors: Juan Carlos Nuño, Ph.D., Francisco Montero, Ph.D. Faculty of Chemical Sciences.

Fulbright Grant Research: "Structure of Large Metabolic Networks of known Stoichiometric Matrix." (September 2001-June 2002)

Cornell University   Ithaca, NY

Advisor: Aaron Sin, Michael L. Shuler, Ph.D. School of Chemical and Biomolecular Engineering.

"Use of Polystyrene to build Micro Cell Culture Analog Devices." (August 1999-May 2001)

Presentations and Publications

Taniguchi CM, Aleman JO, Ueki K, Luo J, Asano T, Kaneto H, Stephanopoulos G, Cantley LC, Kahn CR. The p85-alpha Regulatory Subunit of Phosphoinositide 3-Kinase Potentiates JNK-mediated Insulin Resistance. Mol Cell Biol. 2007 Apr,27(8):2830-40. PMID: 17283057

Alemán JO, Antoniewicz MR, Wong M, Kelleher JK and GN Stephanopoulos. "Flux metabolomics of glucose production reveals metabolic phenotypes in Type 2 Diabetes." Poster presented at Keystone Symposium J1: Diabetes: Molecular Genetics, Signaling Pathways and Integrated Physiology, January 15, 2007. Keystone Symposia Travel Award Winner.

Alemán JO, Antoniewicz M, Wong M, Kelleher JK, Stephanopoulos G. Flux Metabolomics of Liver Glucose Production in Type 2 Diabetes. Oral Presentation at the Minority Trainee Research Forum 2006 Conference. September 7, 2006 .Miami, Florida, USA.

Alemán JO, Antoniewicz M, Wong M, Kelleher JK, Stephanopoulos G. Gluconeogenesis as a system: Flux Metabolomics of Glucose Production in Type 2 Diabetes. Oral Presentation at the Metabolomics 2006 Conference. June 25, 2006 .Boston, Massachusetts, USA.

Alemán JO, Maynard SE, Yeo GW, Libermann T, Kohane I, Epstein FH, Sukhatme VS, Ramoni M, and Karumanchi SA. "Placental Gene Expression Profiling in Normal Pregnancy versus Preeclampsia." Poster presented at the International Conference on the Analysis of Genomic Data. May 10, 2004. Boston, Massachusetts, USA.

Alemán JO, Maynard SE, Yeo GW, Libermann T, Ramoni M, Kohane I, Epstein FH, Sukhatme VS and Karumanchi SA. "Placental Gene Expression Profiling in Normal Pregnancy versus Preeclampsia." Poster presented at the Days of Molecular Medicine 2004 Conference. March 18, 2004. Wellcome Trust Genome Campus, Cambridgeshire, UK.

Alemán JO, Maynard SE, Yeo GW, Libermann T, Ramoni, M, Kohane I, Epstein FH, Sukhatme VS and Karumanchi SA. "Placental Gene Expression Profiling in Normal Pregnancy versus Preeclampsia." Oral Presentation delivered at the New England Science Symposium. February 27, 2004. Boston, Massachusetts, USA.

Alemán, JO, Sánchez-Valdenebro, I, Nuño, JC and Montero, F. "Structural and Dynamic Effects of Transaldolase Presence on the Calvin Cycle." Manuscript report of Fulbright Grant Research, 2001-2002.

Mentoring and Outreach	Alemán, JO. "Metabolic Control Theory: Application to the Calvin Cycle." Guest Lecture as part of course Design of Metabolism: Optimization and Control of Metabolic Pathways. Universidad Complutense de Madrid. June 6, 2002. Madrid, Spain
	MIT Summer Research Program Mentor, June-August 2006. Summer research experience program directed by the MIT Graduate Student Office targeting underserved students interested in research careers. Directed research project for undergraduate student Lalisse Guillén (University of Puerto Rico-Mayaguez Campus) presented at ABRCMS 2006, Anaheim CA.
	MD-PhD student representative, Annual Biomedical Research Conference for Minority Students (ABRCMS). Held in Atlanta, GA (November 2005) and Anaheim, CA (November 2006)
Activities	Student Member, HST PhD Admissions Committee 2006, 2007. Student Member, Computational and Systems Biology Initiative, MIT. Resident Advisor, Holland International Living Center, Cornell University (1999-2001). Director of Academic Affairs for SHPE/Cornell 1999-2000.
Languages	Fluent in Spanish and English.